
# Luminescent Surface-Active Transition Metal Complexes as Probes for Sensing and Supramolecular Recognition Architectures

By

SAMUEL JOSEPH ADAMS

A thesis submitted to the University of Birmingham for the degree of DOCTOR OF PHILOSOPHY

School of Chemistry

College of Engineering and Physical Sciences

University of Birmingham

August 2015

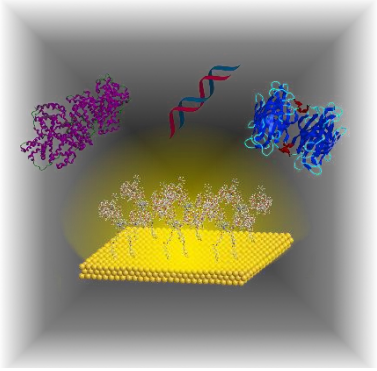

# Abstract

Surface-active luminescent transition metal complexes are synthesised, characterised and successfully attached to gold surfaces for the purposes of micropatterning and biomolecular recognition. Monolayers of ruthenium(II) and iridium(III) complexes bearing disulfide moieties display enchanced lifetimes on gold surfaces compared with aerated solution, and are micropatterned through the use of microcontact printing (μCP). The monolayers also display recognition of serum protein bovine serum albumin through surface plasmon resonance spectroscopy and time-resolved and steady state luminescence spectroscopy. Mixed monolayers of these respective complexes with commercially available surfactants are studied to provide understanding of nanoparticle systems and their involvement in protein interactions. Cyclodextrin containing transition metal complexes are synthesised and characterised for the purposes of supramolecular micropatterning. Mixed monolayers of ruthenium(II) and iridium(III) complexes bearing cyclodextrin moieties can be attached through directed assembly afforded by the μCP technique. Surface-active cyclodextrin containing transition metal complexes are synthesised and characterised for use in selective biomolecular recognition and stepwise assembly. Monolayers of ruthenium(II) and iridium(III) complexes bearing cyclodextrin and disulfide moieties are shown to be luminescent on gold surfaces, and through stepwise assembly afford a selective recognition motif for the protein streptavidin through luminescence and surface plasmon resonance studies. The results indicate the potential of these systems in reusable functional sensing systems.

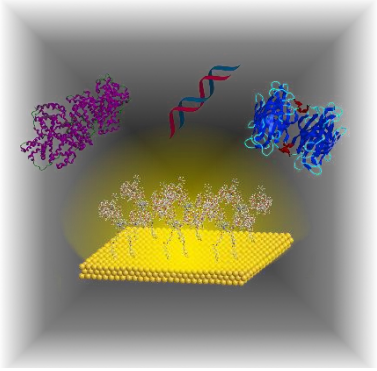

# Acknowledgements

Many thanks to Prof. Zoe Pikramenou for the opportunity to work toward my PhD and for her guidance during my time in the group. Thanks also to Prof. Jon A. Preece for many fruitful discussions and guidance as my academic adviser.

Many thanks to Dr Suleman Khan, Dr Kimberley Wright, Dr Alison Savage, Richard Horniblow, Dr Nicola J. Rogers, Sunil Claire, Chris Stepanek, Johnathon Lilley, Dr David J. Lewis and the rest for your help and support.

Also, many thanks to the analytical staff that helped me obtain all of my spectra and whose discussions were invaluable in helping me ascertain what I had actually made, in particular Dr Neil Spencer and Mr Peter Ashton.

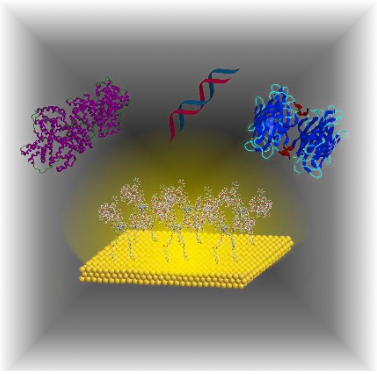

# Abbreviations

| | |
|---|---|
| µCP | Microcontact printing |
| CD | Cyclodextrin |
| bpy | Bipyridine |
| ppy | Phenylpyridine |
| biptpy | Biphenylterpyridine |
| SPR | Surface plasmon resonance |
| SAM | Self-assembled monolayer |
| EBL | Electron beam lithography |
| PDMS | Polydimethylsiloxane |
| EDTA | Ethylenediaminetetraacetic acid |
| DTPA | Diethylenetriaminepentaacetic acid |
| MLCT | Metal-to-ligand charge transfer |
| MC | Metal-centred |
| OLED | Organic light-emitting diode |
| DNA | Deoxyribose nucleic acid |
| BSA | Bovine serum albumin |
| DTC | Dithiocarbamate |
| Fc | Ferrocene |
| ECL | Electrochemiluminescent |
| TOF-SIMS | Time of flight secondary ion mass spectrometry |
| ECz | N-ethylcarbazolyl |
| TEOA | Triethanolamine |
| MV | Methylviologen |
| ITO | Indium tin oxide |

| | |
|---|---|
| $k_{CR}$ | Rate of charge recombination |
| $k_{CS}$ | Rate of charge separation |
| pI | Isoelectric point |
| FRET | Forster resonant energy transfer |
| HAS | Human serum albumin |
| XPS | X-ray photoelectron spectroscopy |
| CV | Cyclic voltammetry |
| GFP | Green fluorescent protein |
| TFA | trifluoroacetic acid |
| NMR | Nuclear magnetic resonance |
| Boc | *tert*-Butyloxycarbonyl |
| UV-vis | Ultraviolet-visible |
| COSY | Correlation spectroscopy |
| HSQC | Heteronuclear single quantum coherence |
| HMBC | Heteronuclear multiple bond correlation |
| ES(+) | Electrospray (+) |
| FBS | Fetal bovine serum |
| PEG | Poly(ethylene glycol) |
| FWHM | Full width at half maximum |
| EDC.HCl | 1-Ethyl-3-(3-dimethylaminopropyl)carbodiimide hydrochloride |
| N-EM | N-ethylmorpholine |
| NTA | Nitrilotriacetate |
| FCA | Ferrocene carboxylic acid |
| SEM | Scanning electron microscopy |
| DPN | Dip pen nanolithography |
| AFM | Atomic force microscopy |
| B-GOx | Biotinylated-glucose oxidase |
| STM | Scanning tunneling microscopy |
| I-V | Current-voltage |
| ABCN | 1,1′-Azobis(cyclohexanecarbonitrile) |
| TBDMS.Cl | *tert*-Butyldimethylsilane hydrochloride |
| DMF | Dimethylformamide |

| | |
|---|---|
| AIBN | Azobisisobutyronitrile |
| MALDI | Matrix assisted laser desorption ionisation |
| COD | 1,5-cyclooctadienyl |
| TLC | Thin layer chromatography |
| THF | tetrahydrofuran |
| NIR | near-infrared |
| UVO | Ultraviolet ozone |
| µRIU | Micro refractive index units |

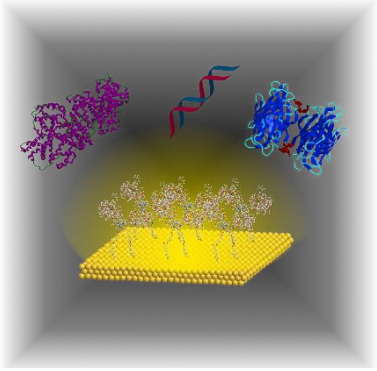

# Contents

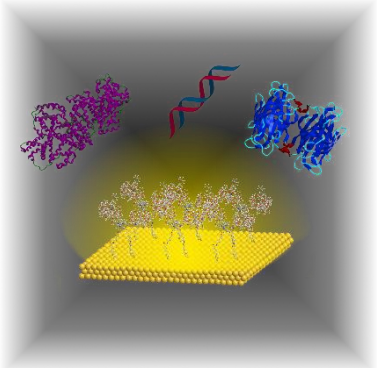

# Chapter One

## Introduction

# 1.1 General Introduction

The drive toward nanoscale devices has led to an explosion of research in the field of nanotechnology over the last thirty years. In particular, the work begun by Sagiv,[1] Nuzzo and Allara[2] into the use of self-assembled monolayers (SAMs) has driven such research into a large and multidisciplinary area.[3] The need for smaller devices is pushed in part by the proliferation in computer use during the 20th century, which have pushed 'top-down' methods of device fabrication, such as electron beam lithography (EBL) to their limits. As such, self-assembly methods such as SAMs have flourished,[3-26] due in part to their ease of fabrication and the removal of the need for 'clean lab' chemistry.

# 1.2 Use of Self-Assembly in Device Formation

The use of self-assembly in device formation allows a multitude of chemistries to be performed on many different substrates, in particular organic thiols on gold[27-29] or silver,[9, 10] as well as chemistry that can be performed on glass. An example of each of these is shown below (Figure 1.1). In the first example by Nuzzo,[5] self-assembly can be achieved by immersing a prepared gold, copper or silver substrate into a solution of an alkanethiol for a given period of time, before washing and drying under nitrogen. In the second example by Sagiv,[1] a similar process of immersing a glass substrate in a solution of an alkyltrichlorosilane results in a monolayer through condensation polymerisation after adsorbing to the surface of the glass.

Such motifs are now widely used not only on planar substrates but also in nanoparticle chemistry, with probe molecules also acting as capping agents to otherwise unstable nanoparticle cores.[30-32] The two types of nanoparticles that often utilise this particular chemistry are noble metal, and oxide nanoparticles.[32-34] Noble metal nanoparticles, such as gold,[31, 35-37] silver[37] or platinum[38] are commonly used in biological applications[39-42] or catalytic systems,[42-

[44] where their large surface areas provide more active sites for reactions to take place. Noble metal nanoparticles, particularly gold nanoparticles offer intriguing properties that can be useful in luminescence. Due to the inherently unstable nature of surface gold atoms, as well as the high ratio of surface:bulk atoms that exists in nanoparticles, the free electrons in the nanoparticle oscillate at a visible frequency to create a plasmon. Studies have shown that this plasmon will interact with dipoles in luminescent materials to enhance or quench emission.[24, 45, 46] Rogers *et al.*[31] have shown that the luminescence lifetime of a ruthenium(II) complex adsorbed to 13 nm gold nanoparticles is enhanced compared with its lifetime in solution, indicating that such systems can be useful in tracking or detection motifs. The facility of synthesis of both noble metal nanoparticles and oxide nanoparticles is offset by their lack of reusability. Because these systems are for the majority solution based, the probes are discarded after a test has been carried out, whereas a planar surface can be reused, provided it can be regenerated. The reusability of planar substrates means that costs such as production can therefore be minimised over longer periods of time, making them more attractive as sensors and other devices.

One area of research towards controlling the deposition of molecules on a planar surface is that of microcontact printing (μCP) originally outlined by Whitesides.[47, 48] In this method (Figure 1.2), surfaces are subjected to patterning with a PDMS stamp that has been 'inked' with a surface-active molecule such as an alkanethiol, before removal of the stamp and washing to reveal a patterned monolayer. Such systems have been used as chemical resists for the etching of substrates for electronic devices,[8-10, 49, 50] as well as more elaborate designs for patterned supramolecular architectures, such as the ones outlined by Reinhoudt.[11, 51-66] In these systems, cyclodextrins and adamantyl groups are used as supramolecular linkages to pattern large arrays, which allow the use of multiplex sensing.[67]

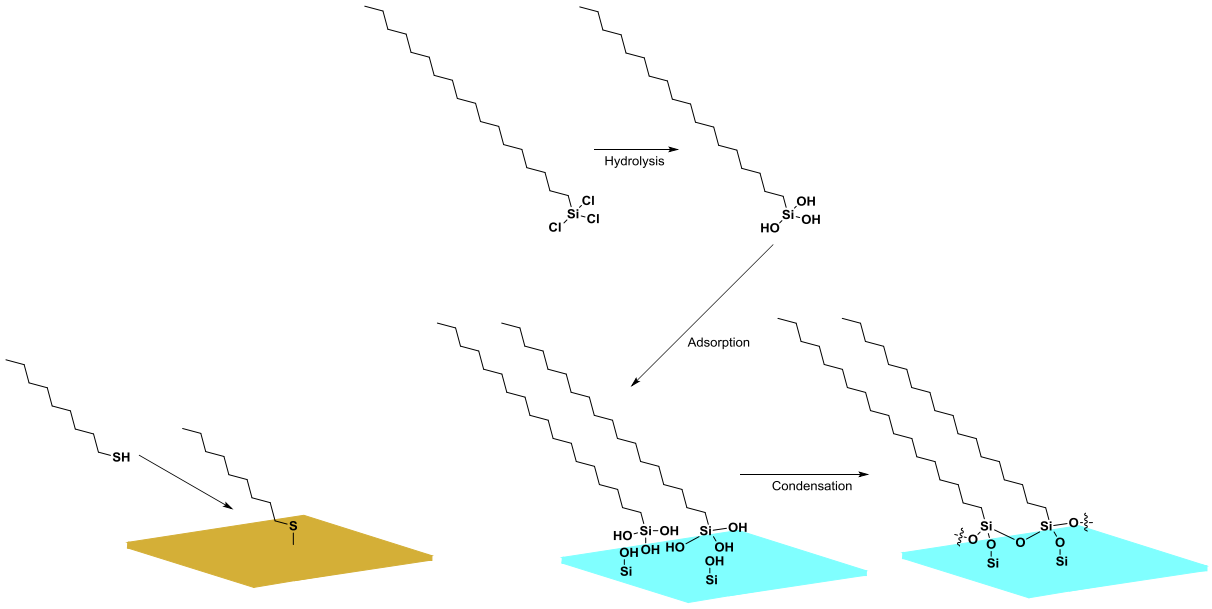


**Figure 1.1.** Examples of self-assembly on gold[5] (left) and glass[1] (right).

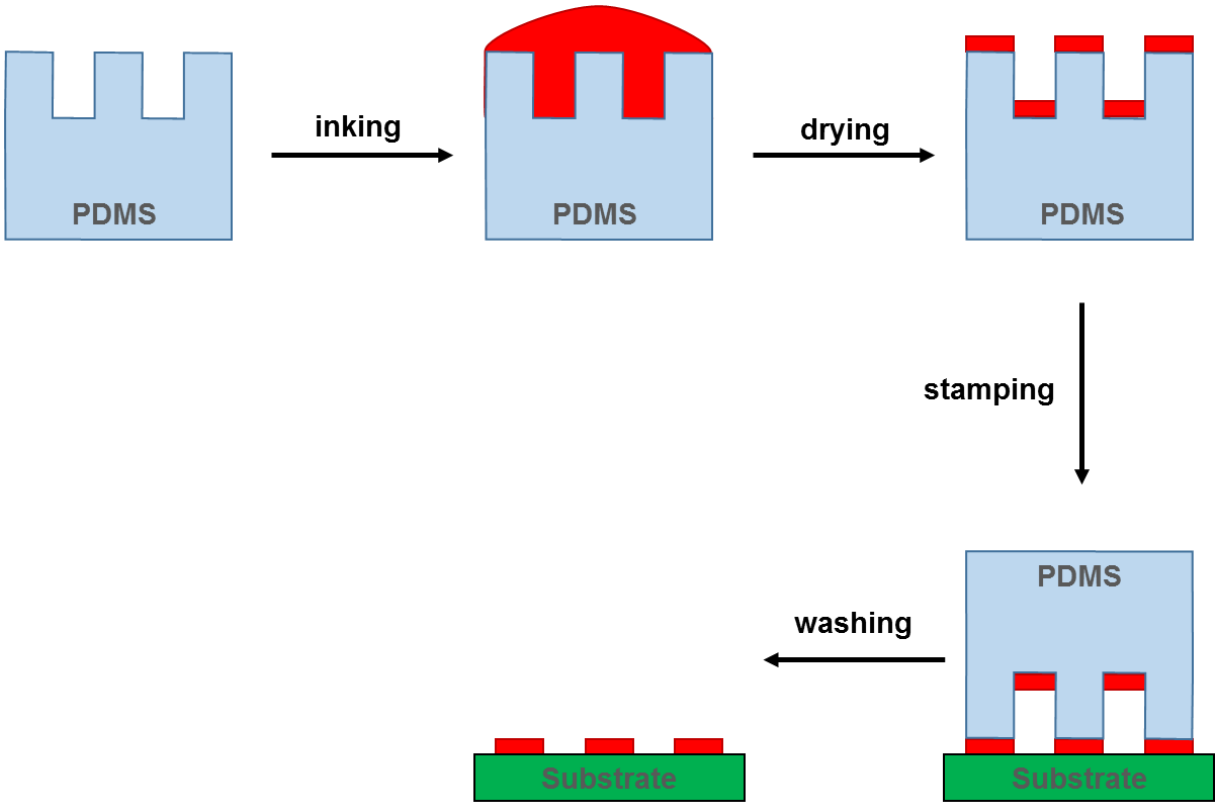


**Figure 1.2.** Microcontact printing protocol as outlined by Whitesides.[8]

## 1.3 Use of Luminescent Transition Metal Complexes

Due to the high sensitivity of luminescence based techniques, luminescent molecules offer a useful tool for studying low concentration systems such as self-assembled monolayers closely and reliably, particularly in imaging[24, 67-69] and sensing applications.[70, 71] Traditionally, fluorescent dyes have been used as the standard for surface based luminescence as they are reasonably cheap to purchase and have high luminescence quantum yields. However, their commercial potential is limited by several factors. Fluorescent dyes have small Stokes shifts (typically less than 10 nm), as absorption and decay occur to/from the same excited state. This small Stokes shift can mean the signal is attenuated either by self-quenching; absorption of light emitted by proximal molecules; or signal lost through the use of filters to distinguish emission light from excitation light. Fluorescent dyes also have short luminescence lifetimes (typically less than 10 ns), which limit their potential when examining systems that contain biological media, as biomolecules can also have fluorescence profiles due to chromophoric amino acids such as tyrosine or tryptophan. The photostability of organic fluorophores is also relatively low, as the excited states are typically reactive and form nonfluorescent photochemical products over time, causing the device to lose efficiency.

Research into the use of lanthanide complexes as sensing architectures has also been explored,[72-75] due to their attractive luminescent properties. Lanthanide complexes display sharp line band emission profiles due to f-f transitions that are caused by the highly shielded character of the f orbitals. However, f-f transitions are Laporte forbidden and generally direct excitation of the lanthanide is unfavourable. This problem can be avoided by the use of organic sensitisers which take advantage of the ‘antenna’ effect, whereby the energy from absorbed light from the chromophore is transferred to the lanthanide before emitting. Because of these energy transfer steps and relaxations, the emitted light is normally far red-shifted (greater than

100 nm) from the absorbed light. Indeed, the use of the 'antenna' effect can be very useful in sensing for chromophoric ligands such as dipicolinic acid; a highly absorptive molecule found in anthrax spores; particularly when non-absorbing complexes are used as sensors.[72, 76] Due to the Laporte forbidden transitions, lanthanide luminescence is also very long lived, with typical lifetimes ranging from microseconds to milliseconds.[77, 78] However, three problems exist for lanthanide complexes. Lanthanide ions are very toxic due to their similar size and behaviour to important elements in biological systems such as calcium. For this reason, when designing lanthanide systems involving biological applications, strongly chelating ligands such as EDTA or DTPA are favoured, and as such work has gone into attaching chromophores to these types of ligands.[74] The other problems that arise in the use of lanthanide systems, particularly in imaging is that of low luminescence quantum yield and use of organic sensitisers. Because organic sensitisers generally absorb below 350 nm, this makes them difficult to excite in conventional microscopy set ups due to the use of glass optics, which has an optical cut off of *ca.* 350 nm. Coupled with the low quantum yield of luminescence, the use of lanthanide complexes in biological sensing is possibly limited.

The photophysical properties for luminescent transition metal complexes such as $[Ru(bpy)_3]^{2+}$ (Figure 1.3) are well studied.[79] Due to their favourable properties, such as large emission Stokes shifts in the region of tens to hundreds of nanometres, their typically long lived excited states greater than 100 ns, and their reasonable luminescence quantum yields (*ca.* 1-10%), ruthenium(II) polypyridyl complexes have been particularly used in sensing applications, such as molecular probes in cell studies,[31, 80, 81] flow tracking,[82] oxygen sensing[83] and biomolecular recognition.[81, 84-87] Ruthenium(II) complexes of this type have also been employed in energy transfer systems.[88-90]

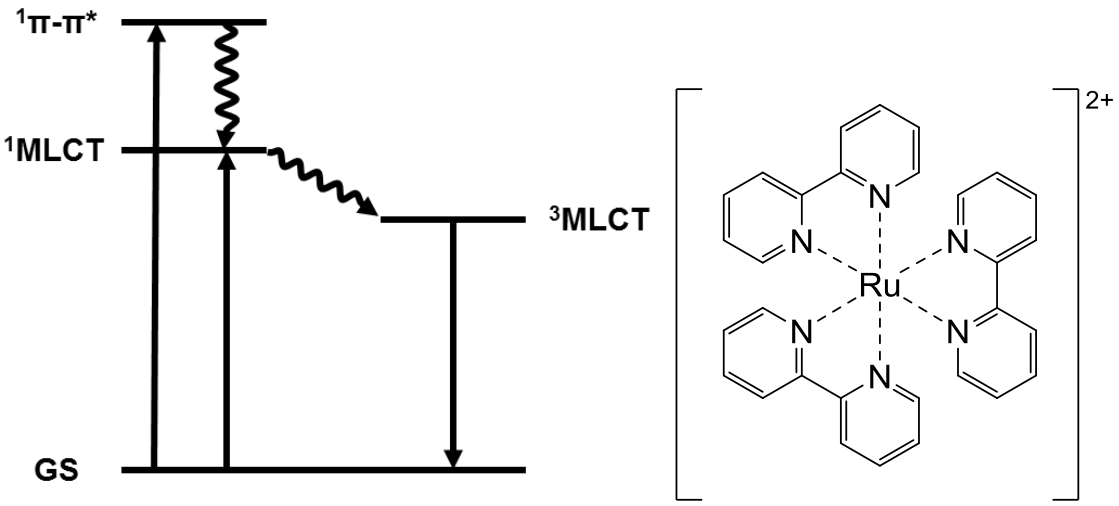


**Figure 1.3.** Jablonski diagram illustrating emission pathway for ruthenium(II) tris-bipyridyl complexes (left) and schematic illustration of $[Ru(bpy)_3]^{2+}$ (right).

Indeed, such complexes are advantageous over terpyridyl complexes due to their luminescence at room temperature, as ruthenium(II) terpyridyl complexes are typically quenched by a low lying $^3$MC state which can be populated thermally, causing the $^3$MLCT state to be deactivated.

Iridium(III) polypyridyl complexes behave somewhat differently, with the emissive state being populated through mixing of the $^3$π-π* and $^1$MLCT states caused by spin-orbit coupling.[91, 92] Because of this effect, the excited state energy of iridium(III) complexes can be manipulated drastically with small changes to the ligand system around the metal centre, and as such much effort has gone into the study of such complexes in OLED systems.[93-97] Indeed, the sensitivity of iridium(III) polypyridyl complexes to their environment means research has also focused on their use in biomolecular recognition.[98, 99]

## 1.4 Use of Supramolecular Chemistry in Device Formation

Supramolecular chemistry can provide a powerful tool in the fabrication of devices, as chemistry 'beyond the molecule' allows reversible yet stable structures to be assembled without the need for forming covalent bonds or the use of catalysts and other reagents. Many examples of the use of supramolecular entities in devices for various applications are found in the literature, from crown ethers,[100-102] curcubiturils,[103-105] cyclodextrins[106-113] and calixarenes,[100, 101, 106, 114, 115] to molecule-protein interactions.[60, 116-118] In particular, we are interested in the study and use of systems incorporating cyclodextrins as supramolecular host groups. Cyclodextrins (Figure 1.4) are cyclic sugars, made up of 5 or more glucose units, and are typically made by enzymatic degradation of starch. The three commercial derivatives of these types of molecules are α-(6 membered), β-(7 membered) and γ-(8 membered) cyclodextrins, and exist as cone shaped structures with hydrophilic exteriors and hydrophobic interiors. Because of their reasonable solubility in aqueous systems, cyclodextrins can trap hydrophobic guest molecules within their cavities, with relatively high binding constants (*ca.* $10^3$ for adamantyl or phenyl groups in β-cyclodextrins). For this reason, cyclodextrins make very good building blocks for building supramolecular systems, and indeed there are many examples of this in solution[119-122] as well as on planar substrates.[58, 123-126] In particular, the works of Reinhoudt, Huskens and Ravoo have used cyclodextrins on surfaces to create 'molecular printboards', in which a monolayer of cyclodextrin molecules is used as the first building block in a larger epitaxial system.[127, 128] One such example (Figure 1.5) shows how surfaces functionalised with β-cyclodextrins can be used as hosts to adamantyl functionalised guests to form fluorescent layers without the need for covalent bonds. One advantage to this is that the fluorescent layer can also be removed at will by washing the substrate with a solution of free β-cyclodextrin to desorb the bound material. Such motifs could be useful in systems whereby

the regeneration of the surface extends the life of a sensing surface, which is a focus of research into biomolecular recognition in particular.[129-131]

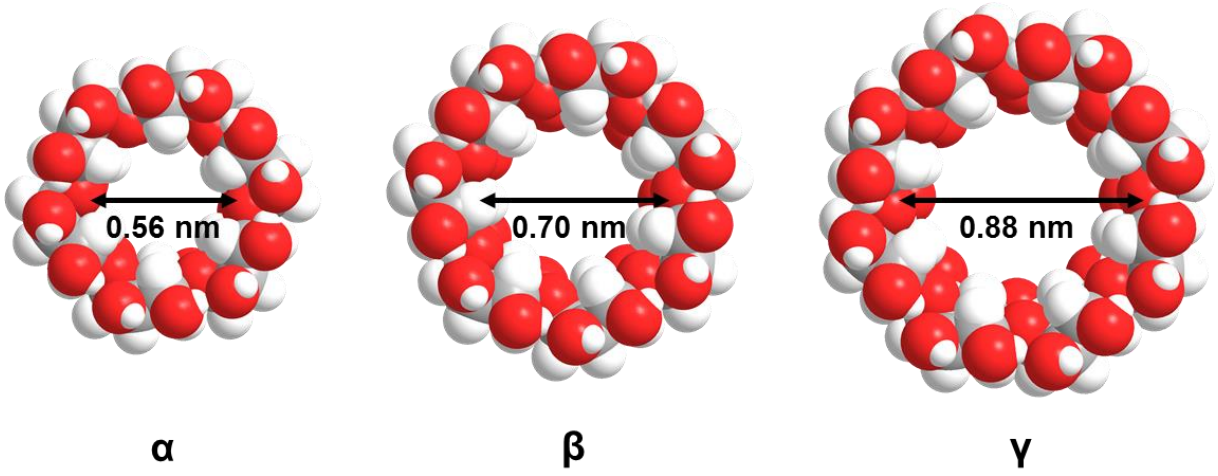


**Figure 1.4.** Structures of cyclodextrins and cavity diameters.

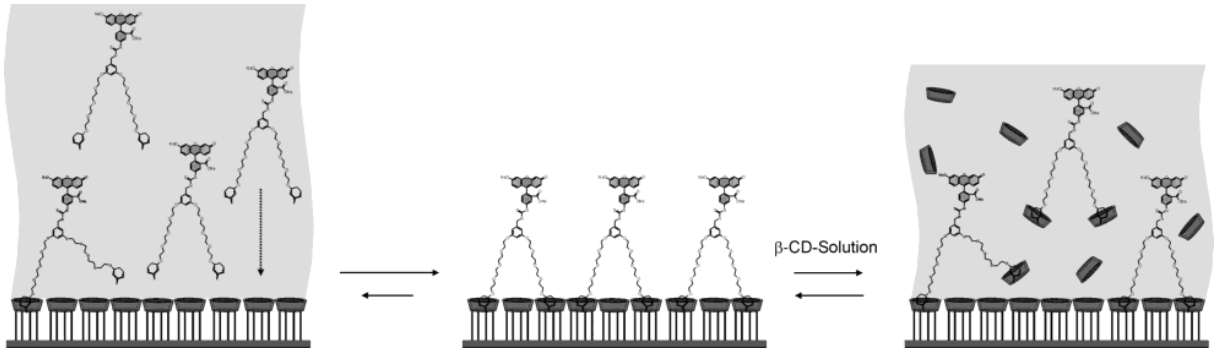


**Figure 1.5.** Schematic of 'molecular printboard' by Reinhoudt. Reprinted with permission from reference (132). Copyright 2004 American Chemical Society.

## 1.5 Thesis Outline

This thesis focuses on the development of devices based on luminescent transition metal probes. Chapter two elaborates on the synthesis and characterisation of novel surface-active transition metal complexes. The luminescent properties of the complexes are studied in solution, as well as on gold substrates, and protein recognition studies are carried out to determine their efficacy.[99]

The first part of chapter three further explores these complexes in mixed monolayer systems with commercially available surfactants, in a parallel to current work in the group focusing on similar systems on gold nanoparticles.[31] The luminescence properties of the systems are studied, and protein recognition studies are also carried out. The second part of chapter three focuses on the incorporation of cyclodextrin containing ligands into transition metal complexes for use in surface based systems. Cyclodextrin containing ruthenium(II) and iridium(III) complexes are synthesised and attached to gold substrates *via* supramolecular connections to an adamantyl terminated monolayer through immersion and the use of micro-contact printing techniques.

Chapter four expands on the use of surface-active transition metal complexes and cyclodextrin containing transition metal complexes. The synthesis and characterisation of transition metal complexes containing both cyclodextrin containing ligands and surface-active ligands is described, and the properties of the complexes in solution and at the surface are studied. Using the cyclodextrin containing ligand as a building block, a supramolecular architecture for recognising streptavidin is created and studied.

# 1.6 References


1. J. Sagiv, *J. Am. Chem. Soc.*, 1980, **102**, 92-98.
2. R. G. Nuzzo and D. L. Allara, *J. Am. Chem. Soc.*, 1983, **105**, 4481-4483.
3. J. C. Love, L. E. Estroff, J. K. Kriebel, R. G. Nuzzo and G. M. Whitesides, *Chem. Rev.*, 2005, **105**, 1103-1169.
4. C. D. Bain, E. B. Troughton, Y.-T. Tao, J. Evall, G. M. Whitesides and R. G. Nuzzo, *J. Am. Chem. Soc.*, 1989, **111**, 321-335.
5. P. E. Laibinis, G. M. Whitesides, D. L. Allara, Y.-T. Tao, A. N. Parikh and R. G. Nuzzo, *J. Am. Chem. Soc.*, 1991, **113**, 7152-7167.
6. A. Kumar, H. A. Biebuyck, N. L. Abbot and G. M. Whitesides, *J. Am. Chem. Soc.*, 1992, **114**, 9188-9189.
7. A. Kumar, H. A. Biebuyck and G. M. Whitesides, *Langmuir*, 1994, **10**, 1498-1511.
8. A. Kumar and G. M. Whitesides, *Appl. Phys. Lett.*, 1993, **63**, 2002-2004.
9. Y. Xia, X.-M. Zhao and G. M. Whitesides, *Microelectron. Eng.*, 1996, **32**, 255-268.
10. Y. Xia, N. Venkateswaran, D. Qin, J. Tien and G. M. Whitesides, *Langmuir*, 1998, **14**, 363-371.
11. J. Lahiri, E. Ostuni and G. M. Whitesides, *Langmuir*, 1999, **15**, 2055-2060.
12. M. D. Porter, T. B. Bright, D. L. Allara and C. E. D. Chidsey, *J. Am. Chem. Soc.*, 1987, **109**, 3559-3568.
13. R. G. Nuzzo, L. H. Dubois and D. L. Allara, *J. Am. Chem. Soc.*, 1990, **112**, 558-569.
14. J. M. Tour, L. Jones, D. L. Pearson, J. J. S. Lamba, T. P. Burgin, G. M. Whitesides, D. L. Allara, A. N. Parikh and S. V. Atre, *J. Am. Chem. Soc.*, 1995, **117**, 9529-9534.
15. J. J. Stapleton, P. Harder, T. A. Daniel, M. D. Reinard, Y. Yao, D. W. Price, J. M. Tour and D. L. Allara, *Langmuir*, 2003, **19**, 8245-8255.
16. C. E. D. Chidsey, C. R. Bertozzi, T. M. Putvinski and A. M. Mujsce, *J. Am. Chem. Soc.*, 1990, **112**, 4301-4306.
17. J. F. Smalley, S. W. Feldberg, C. E. D. Chidsey, M. R. Linford, M. D. Newton and Y.-P. Liu, *J. Phys. Chem.*, 1995, **99**, 13141-13149.
18. M. T. Rojas, R. Königer, J. F. Stoddart and A. E. Kaifer, *J. Am. Chem. Soc.*, 1995, **117**, 336-343.
19. R. C. Ahuja, P.-L. Caruso, D. Möbius, G. Wildburg, H. Ringsdorf, D. Philp, J. A. Preece and J. F. Stoddart, *Langmuir*, 1993, **9**, 1534-1544.
20. Y. B. Zheng, Y.-W. Yang, L. Jensen, L. Fang, B. K. Juluri, A. H. Flood, P. S. Weiss, J. F. Stoddart and T. J. Huang, *Nano Lett.*, 2009, **9**, 819-825.
21. T. J. Huang, B. Brough, C.-M. Ho, Y. Liu, A. H. Flood, P. A. Bonvallet, H.-R. Tseng, J. F. Stoddart, M. Baller and S. Magonov, *Appl. Phys. Lett.*, 2004, **85**, 5391-5393.
22. S. S. Jang, Y. H. Jang, Y.-H. Kim, W. A. Goddard, A. H. Flood, B. W. Laursen, H.-R. Tseng, J. F. Stoddart, J. O. Jeppesen, J. W. Choi, D. W. Steuerman, E. Delonno and J. R. Heath, *J. Am. Chem. Soc.*, 2005, **127**, 1563-1575.
23. J. M. Spruell, B. A. Sheriff, D. A. Rozkiewicz, W. R. Ditchel, R. D. Rohde, D. N. Reinhoudt, J. F. Stoddart and J. R. Heath, *Angew. Chem. Int. Ed.*, 2008, **47**, 9927-9932.
24. A. D'Aléo, R. M. Williams, Y. Chriqui, V. M. Iyer, P. Belser, F. Vergeer, V. Ruiz, P. R. Unwin and L. De Cola, *Open Inorg. Chem. J.*, 2007, **1**, 26-36.
25. S. Ramachandra, K. C. Schuermann, F. Edafe, P. Belser, C. A. Nijhuis, W. F. Reus, G. M. Whitesides and L. De Cola, *Inorg. Chem.*, 2011, **50**, 1581-1591.

26. J. Lehr, T. Lang, O. A. Blackburn, T. A. Barendt, S. Faulkner, J. J. Davis and P. D. Beer, *Chem. Eur. J.*, 2013, **19**, 15898-15906.
27. K. D. Schierbaum, T. Weiss, E. U. Thoden van Velzen, J. F. J. Engbersen, D. N. Reinhoudt and W. Göpel, *Science*, 1994, **265**, 1413-1415.
28. S. Flink, B. A. Boukamp, A. van den Berg, F. C. J. M. van Veggel and D. N. Reinhoudt, *J. Am. Chem. Soc.*, 1998, **120**, 4652-4657.
29. M. Liebau, J. Huskens and D. N. Reinhoudt, *Adv. Funct. Mater.*, 2001, **11**, 147-150.
30. M. Jebb, P. K. Sudeep, P. Pramod, K. G. Thomas and P. V. Kamat, *J. Phys. Chem. B*, 2007, **111**, 6839-6844.
31. N. J. Rogers, S. Claire, R. M. Harris, S. Farabi, G. Zikeli, I. B. Styles, N. J. Hodges and Z. Pikramenou, *Chem. Commun.*, 2014, **50**, 617-619.
32. D. J. Lewis, V. Dore, N. J. Rogers, T. K. Mole, G. B. Nash, P. Angeli and Z. Pikramenou, *Langmuir*, 2013, **29**, 14701-14708.
33. P. K. Jain, X. Huang, I. H. El-Sayed and M. A. El-Sayed, *Acc. Chem. Res.*, 2008, **41**, 1578-1586.
34. M. Mahmoudi, S. Sant, B. Wang, S. Laurent and T. Sen, *Adv. Drug Deliver. Rev.*, 2011, **63**, 24-46.
35. M. Brust, M. Walker, D. Bethell, D. J. Schiffrin and R. Whyman, *J. Chem. Soc. Chem. Commun.*, 1994, 801-802.
36. C. A. Mirkin, R. L. Letsinger, R. Mucic and J. J. Storhoff, *Nature*, 1996, **382**, 607-609.
37. Y. Sun and Y. Xia, *Science*, 2002, **298**, 2176-2179.
38. T. S. Ahmadi, Z. L. Wang, T. C. Green, A. Henglein and M. A. El-Sayed, *Science*, 1996, **272**, 1924-1926.
39. Q. A. Pankhurst, J. Connolly, S. K. Jones and J. Dobson, *J. Phys. D: Appl. Phys.*, 2003, **36**, R167-R181.
40. D. A. Giljohann, D. S. Seferos, W. L. Daniel, M. D. Massich, P. C. Patel and C. A. Mirkin, *Angew. Chem. Int. Ed.*, 2010, **49**, 3280-3294.
41. R. A. Sperling, P. R. Gil, F. Zhang, M. Zanella and W. J. Parak, *Chem. Soc. Rev.*, 2008, **37**, 1896-1908.
42. A.-H. Lu, E. L. Salabas and F. Schüth, *Angew. Chem. Int. Ed.*, 2007, **46**, 1222-1244.
43. D. Astruc, F. Lu and J. R. Aranzaes, *Angew. Chem. Int. Ed.*, 2005, **44**, 7852-7872.
44. M. Haruta and M. Daté, *Appl. Catal. A-Gen.*, 2001, **222**, 427-437.
45. T. L. Jennings, M. P. Singh and G. F. Strouse, *J. Am. Chem. Soc.*, 2006, **128**, 5462-5467.
46. C. J. Breshike, R. A. Riskowski and G. F. Strouse, *J. Phys. Chem. C*, 2013, **117**, 23942-23949.
47. Y. Xia, J. A. Rogers, K. E. Paul and G. M. Whitesides, *Chem. Rev.*, 1999, **99**, 1823-1848.
48. V. B. Sadhu, A. Perl, M. Péter, D. I. Rozkiewicz, G. Engbers, B. J. Ravoo, D. N. Reinhoudt and J. Huskens, *Langmuir*, 2007, **23**, 6850-6855.
49. Y. Xia, X.-M. Zhao, E. Kim and G. M. Whitesides, *Chem. Mater.*, 1995, **7**, 2332-2337.
50. Y. Xia and G. M. Whitesides, *Annu. Rev. Mater. Sci.*, 1998, **28**, 153-184.
51. C. Wendeln, O. Roling, C. Schulz, C. Hentschel and B. J. Ravoo, *Langmuir*, 2013, **29**, 2692-2699.
52. O. Crespo-Biel, B. Dordi, P. Maury, M. Péter, D. N. Reinhoudt and J. Huskens, *Chem. Mater.*, 2006, **18**, 2545-2551.
53. M. J. W. Ludden, D. N. Reinhoudt and J. Huskens, *Chem. Soc. Rev.*, 2006, **35**, 1122-1134.

54. P. Maury, M. Péter, O. Crespo-Biel, X. Y. Ling, D. N. Reinhoudt and J. Huskens, *Nanotechnology*, 2007, **18**, 044007.
55. M. J. W. Ludden, A. Mulder, K. Schulze, V. Subramaniam, R. Tampé and J. Huskens, *Chem. Eur. J.*, 2008, **14**, 2044-2051.
56. X. Y. Ling, D. N. Reinhoudt and J. Huskens, *Chem. Mater.*, 2008, **20**, 3574-3578.
57. M. J. W. Ludden, L. Xiao, J. Greve, A. Van Amerongen, M. Escalante, V. Subramaniam, D. N. Reinhoudt and J. Huskens, *J. Am. Chem. Soc.*, 2008, **130**, 6964-6973.
58. A. Perl, L. Kumprecht, T. Kraus, D. Armspach, D. Matt, D. N. Reinhoudt and J. Huskens, *Langmuir*, 2009, **25**, 1534-1539.
59. I. A. Banerjee, L. Yu and H. Matsui, *J. Am. Chem. Soc.*, 2003, **125**, 9542-9543.
60. J. Hyun, S. J. Ahn, W. K. Lee, A. Chilkoti and S. Zauscher, *Nano Lett.*, 2002, **2**, 1203-1207.
61. L. Scheres, J. ter Maat, M. Giesbers and H. Zuilhof, *Small*, 2010, **6**, 642-650.
62. L. Yan, W. T. S. Huck, X.-M. Zhao and G. M. Whitesides, *Langmuir*, 1999, **15**, 1208-1214.
63. C. Wendeln, S. Rinnen, C. Schulz, H. F. Arlinghaus and B. J. Ravoo, *Langmuir*, 2010, **26**, 15966-15971.
64. M. Escalante, Y. Zhao, M. J. W. Ludden, R. Vermeij, J. D. Olsen, E. Berenschot, C. N. Hunter, J. Huskens, V. Subramaniam and C. Otto, *J. Am. Chem. Soc.*, 2008, **130**, 8892-8893.
65. P. M. Mendes, C. L. Yeung and J. A. Preece, *Nanoscale Res. Lett.*, 2007, **2**, 373-384.
66. H. Kind, M. Geissler, H. Schmid, B. Michel, K. Kern and E. Delamarche, *Langmuir*, 2000, **16**, 6367-6373.
67. L. Basabe-Desmonts, J. Beld, R. S. Zimmerman, J. Hernando, P. Mela, M. F. García Parajó, N. F. van Hulst, A. van den Berg, D. N. Reinhoudt and M. Crego-Calama, *J. Am. Chem. Soc.*, 2004, **126**, 7293-7299.
68. T. Auletta, B. Dordi, A. Mulder, A. Sartori, S. Onclin, C. M. Bruinink, M. Péter, C. A. Nijhuis, H. Beijleveld, H. Schönherr, G. J. Vancso, A. Casnati, R. Ungaro, B. J. Ravoo, J. Huskens and D. N. Reinhoudt, *Angew. Chem. Int. Ed.*, 2004, **43**, 369-373.
69. D. A. Rozkiewicz, D. Jańczewski, W. Verboom, B. J. Ravoo and D. N. Reinhoudt, *Angew. Chem. Int. Ed.*, 2006, **45**, 5292-5296.
70. A. Vaish, W.-S. Liao, M. J. Shuster, J. M. Hinds, P. S. Weiss and A. M. Andrews, *Anal. Chem.*, 2011, **83**, 7451-7456.
71. L. Basabe-Desmonts, D. N. Reinhoudt and M. Crego-Calama, *Chem. Soc. Rev.*, 2007, **36**, 993-1017.
72. B. Eker, M. D. Yilmaz, S. Schlautmann, J. G. E. Gardeniers and J. Huskens, *Int. J. Mol. Sci.*, 2011, **12**, 7335-7351.
73. S. Khan, *PhD. Thesis - University of Birmingham*, 2014.
74. D. J. Lewis, T. M. Day, J. V. MacPherson and Z. Pikramenou, *Chem. Commun.*, 2006, 1433-1435.
75. A. Davies, D. J. Lewis, S. P. Watson, S. G. Thomas and Z. Pikramenou, *Proc. Natl. Acad. Sci.*, 2012, **109**, 1862-1867.
76. J. Lehr, J. Bennett, M. Tropiano, T. J. Sorensen, S. Faulkner, P. D. Beer and J. J. Davis, *Langmuir*, 2013, **29**, 1475-1482.
77. A. P. Bassett, S. W. Magennis, P. B. Glover, D. J. Lewis, N. Spencer, S. Parsons, R. M. Williams, L. De Cola and Z. Pikramenou, *J. Am. Chem. Soc.*, 2004, **126**, 9413-9424.
78. S. V. Eliseeva and J.-C. G. Bünzli, *Chem. Soc. Rev.*, 2010, **39**, 189-227.

79. A. Juris, V. Balzani, F. Barigelletti, S. Campagna, P. Belser and A. von Zelewsky, *Coord. Chem. Rev.*, 1988, **84**, 85-277.
80. K. K.-W. Lo, A. W.-T. Choi and W. H.-T. Law, *Dalton Trans.*, 2012, **41**, 6021-6047.
81. V. Fernández-Moreira, F. L. Thorp-Greenwood and M. P. Coogan, *Chem. Commun.*, 2010, **46**, 186-202.
82. D. J. Lewis, V. Dore, M. J. Goodwin, A. C. Savage, G. B. Nash, P. Angeli and Z. Pikramenou, *Meas. Sci. Technol.*, 2012, **23**, 084004.
83. P. Hartmann, M. J. P. Leiner and M. E. Lippitsch, *Anal. Chem.*, 1995, **67**, 88-93.
84. C. V. Kumar, J. K. Barton and N. J. Turro, *J. Am. Chem. Soc.*, 1985, **107**, 5518-5523.
85. A. E. Friedman, C. V. Kumar, N. J. Turro and J. K. Barton, *Nucleic Acids Res.*, 1991, **19**, 2595-2602.
86. J. L. Beck, R. Gupta, T. Urathamakul, N. L. Williamson, M. M. Sheil, J. R. Aldrich-Wright and S. F. Ralph, *Chem. Commun.*, 2003, 626-627.
87. P. C. A. Bruijnincx and P. J. Sadler, *Curr. Opin. Chem. Biol.*, 2008, **12**, 197-206.
88. V. Balzani, A. Juris, M. Venturi, S. Campagna and S. Serroni, *Chem. Rev.*, 1996, **96**, 759-833.
89. J. A. Faiz, R. M. Williams, M. Silva, L. De Cola and Z. Pikramenou, *J. Am. Chem. Soc.*, 2006, **128**, 4520-4521.
90. J. M. Haider, R. M. Williams, L. De Cola and Z. Pikramenou, *Angew. Chem. Int. Ed.*, 2003, **42**, 1830-1833.
91. K. A. King and R. J. Watts, *J. Am. Chem. Soc.*, 1987, **109**, 1589-1590.
92. M. G. Colombo, A. Hauser and H. U. Güdel, *Inorg. Chem.*, 1993, **32**, 3088-3092.
93. A. B. Tamayo, S. Garon, T. Sajoto, P. I. Djurovich, I. M. Tsyba, R. Bau and M. E. Thompson, *Inorg. Chem.*, 2005, **44**, 8723-8732.
94. J. D. Slinker, A. A. Gorodetsky, M. S. Lowry, J. Wang, S. Parker, R. Rohl, S. Bernhard and G. G. Malliaras, *J. Am. Chem. Soc.*, 2004, **126**, 2763-2767.
95. M. S. Lowry, J. I. Goldsmith, J. D. Slinker, R. Rohl, R. A. Pascal, G. G. Malliaras and S. Bernhard, *Chem. Mater.*, 2005, **17**, 5712-5719.
96. H. J. Bolink, E. Coronado, S. G. Santamaria, M. Sessolo, N. Evans, C. Klein, E. Baranoff, K. Kalyanasundaram, M. Grätzel and M. K. Nazeeruddin, *Chem. Commun.*, 2007, 3276-3278.
97. E. Baranoff, S. Suárez, P. Bugnon, C. Barolo, R. Buscaino, R. Scopelliti, L. Zuppiroli, M. Grätzel and M. K. Nazeeruddin, *Inorg. Chem.*, 2008, **47**, 6575-6577.
98. J. S.-Y. Lau, P.-K. Lee, K. H.-K. Tsang, C. H.-C. Ng, Y.-W. Lam, S.-H. Cheng and K. K.-W. Lo, *Inorg. Chem.*, 2009, **48**, 708-718.
99. S. J. Adams, D. J. Lewis, J. A. Preece and Z. Pikramenou, *ACS Appl. Mater. Interfaces*, 2014, **6**, 11598-11608.
100. P. D. Beer and P. A. Gale, *Angew. Chem. Int. Ed.*, 2001, **40**, 486-516.
101. N. H. Evans, H. Rahman, J. J. Davis and P. D. Beer, *Anal. Bioanal. Chem.*, 2012, **402**, 1739-1748.
102. S. Flink, F. C. J. M. van Veggel and D. N. Reinhoudt, *Adv. Mater.*, 2000, **12**, 1315-1328.
103. K. Kim, W. S. Jeon, J.-K. Kang, J. W. Lee, S. Y. Jon, T. Kim and K. Kim, *Angew. Chem. Int. Ed.*, 2003, **42**, 2293-2296.
104. I. Hwang, K. Baek, M. Jung, Y. Kim, K. M. Park, D.-W. Lee, N. Selvapalam and K. Kim, *J. Am. Chem. Soc.*, 2007, **129**, 4170-4171.
105. H. Yang, B. Yuan, X. Zhang and O. A. Scherman, *Acc. Chem. Res.*, 2014, **47**, 2106-2115.

106. X. Zhang, H. Chen and H. Zhang, *Chem. Commun.*, 2007, 1395-1405.
107. Q. Chen, H. Chen, Y. Zhao, F. Zhang, F. Yang, J. Tang and P. He, *Biosens. Bioelectron.*, 2014, **54**, 547-552.
108. E. Almirall, A. Fragoso and R. Cao, *Electrochem. Commun.*, 1999, **1**, 10-13.
109. C. Henke, C. Steinem, A. Janshoff, G. Steffan, H. Luftmann, M. Sieber and H.-J. Galla, *Anal. Chem.*, 1996, **68**, 3158-3165.
110. C. T. Mallon, R. J. Forster, A. McNally, E. Campagnoli, Z. Pikramenou and T. E. Keyes, *Langmuir*, 2007, **23**, 6997-7002.
111. T. Fukuda, Y. Maeda and H. Kitano, *Langmuir*, 1999, **15**, 1887-1890.
112. M. T. Rojas, R. Koeniger, J. F. Stoddart and A. E. Kaifer, *J. Am. Chem. Soc.*, 1995, **117**, 336-343.
113. I. Willner and B. Willner, *J. Mater. Chem.*, 1998, **8**, 2543-2556.
114. A. Ikeda, T. Hatano, S. Shinkai, T. Akiyama and S. Yamada, *J. Am. Chem. Soc.*, 2001, **123**, 4855-4856.
115. B. Genorio, T. He, A. Meden, S. Polanc, J. Jamnik and J. M. Tour, *Langmuir*, 2008, **24**, 11523-11532.
116. J. J. Davis, G. A. Orlowski, H. Rahman and P. D. Beer, *Chem. Commun.*, 2010, **46**, 54-63.
117. L. G. Fägerstam, Å. Frostell, R. Karlsson, M. Kullman, A. Larsson, M. Malmqvist and H. Butt, *J. Mol. Recognit.*, 1990, **3**, 208-214.
118. T. Hoshi, J.-i. Anzai and T. Osa, *Anal. Chem.*, 1995, **67**, 770-774.
119. N. Hayashi, R. Chen, M. Hiraoka, T. Ujihara and H. Ikezaki, *J. Agric. Food Chem.*, 2010, **58**, 8351-8356.
120. J. M. Haider, M. Chavarot, S. Weidner, I. Sadler, R. M. Williams, L. De Cola and Z. Pikramenou, *Inorg. Chem.*, 2001, **40**, 3912-3921.
121. J. A. Faiz, R. M. Williams, M. J. J. P. Silva, L. De Cola and Z. Pikramenou, *J. Am. Chem. Soc.*, 2006, **128**, 4520-4521.
122. M.-X. Zhao, M. Zhao, E.-Z. Zeng, Y. Li, J.-M. Li, Q. Cao, C.-P. Tan, L.-N. Ji and Z.-W. Mao, *J. Inorg. Biochem.*, 2014, **137**, 31-39.
123. D. Thompson and J. A. Larsson, *J. Phys. Chem. B*, 2006, **110**, 16640-16645.
124. W. C. E. Schofield and J. P. S. Badyal, *ACS Appl. Mater. Interfaces*, 2011, **3**, 2051-2056.
125. K. Khan, M. Guerrouache, B. Carbonnier, M. Lazerges, H. Perrot and M.-C. Millot, *J. Colloid Interf. Sci.*, 2007, **315**, 800-804.
126. I. Tredici, D. Merli, F. Zavarise and A. Profumo, *J. Electroanal. Chem.*, 2010, **645**, 22-27.
127. J. Huskens, *Curr. Opin. Chem. Biol.*, 2006, **10**, 537-543.
128. S. Onclin, J. Huskens, B. J. Ravoo and D. N. Reinhoudt, *Small*, 2005, **1**, 852-857.
129. P. M. Mendes, *Chem. Soc. Rev.*, 2008, **37**, 2512-2529.
130. J. Homola, *Chem. Rev.*, 2008, **108**, 462-493.
131. D. S. Turygin, M. Subat, O. A. Raitman, S. L. Selector, V. V. Arslanov, B. König and M. A. Kalinina, *Langmuir*, 2007, **23**, 2517-2524.
132. S. Onclin, A. Mulder, J. Huskens, B. J. Ravoo and D. N. Reinhoudt, *Langmuir*, 2004, **20**, 5460-5466.

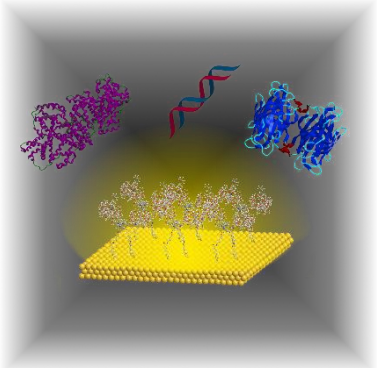

# Chapter Two

## Synthesis, Characterisation and Biomolecular Recognition Studies of 'Long-Legged' Transition Metal Complexes

# 2.1 Introduction

The advantages of appending transition metal complexes to surfaces for the purposes of device fabrication are many. In this chapter, we explore the synthesis and surface attachment of luminescent transition metal complexes, and their recognition of the serum protein bovine serum albumin (BSA), work that has been published as a journal article during the course of this PhD.[1]

## 2.1.1 Methods of Attachment of Compounds to Surfaces

As discussed in chapter 1, the advent of self-assembly at the interface has allowed chemists to easily functionalise surfaces, particularly with organic molecules that bear functional groups that react readily with the functional groups at the interface. In the case of gold (a soft metal), the obvious choice for chemistry is essentially complexation, and indeed soft to medium ligands such as sulfur[2, 3] and nitrogen donors[4] have been exploited to functionalise surfaces. One interesting property of simple surface bound molecules such as alkanethiolates is their ability to 'hop' between binding sites on the surface in order to reorganise into well packed monolayers, due to hydrophobic interactions between the alkyl chains[3] and typically, these monolayers have surface concentrations of *ca.* 1 nmol $cm^{-2}$. Work by groups such as Forster, Keyes and Constable,[4-8] has shown that the coverage of transition metal complexes on surfaces is generally lower than their organic counterparts. Figure 2.1 shows an example of one such system. A ruthenium(II) complex bearing a pyridyl based surface-active ligand is attached to the surface and examined by electrochemical methods. In this study, monolayers of the complex were found to form over 10-20 hours on platinum surfaces at a maximum coverage of 110 pmol $cm^{-2}$, approximately one tenth that of organic thiolates. Similar results have also been found for

similar bipyridyl based complexes on platinum[4] and gold,[5] and also for terpyridyl based complexes of both osmium(II) and ruthenium(II).[7, 8]

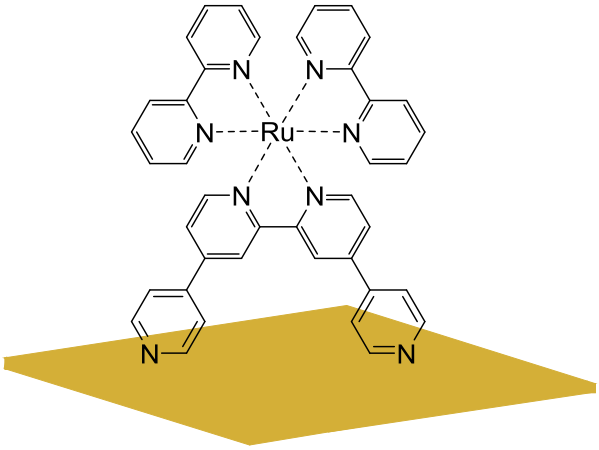


**Figure 2.1.** Schematic of $[Ru(bpy)_2Qpy]^{2+}$ complex adsorbed to a gold surface. Qpy = 2,2′:4,4″:4′,4″-quarterpyridyl.[6]

Because of the nature of the chemical bond to noble metal surfaces by ligating atoms, it is reasonable to expect exchange of surface bound materials to occur. Work by Collard *et al.*[9] studies this postulation on gold surfaces (Figure 2.2) using a mixed monolayer of a ferrocene functionalized hexadecanethiol and hexadecanethiol. Here, the ferrocene group acts as an electrochemical reporter group. It was found upon formation of the mixed monolayer that the electrochemical signal from the ferrocene terminated molecules dropped by a third when immersed in a solution of alkanethiol up to 5 days, indicating that the interactions with the gold surface can indeed be reversed. After this time it was shown that exchange of the thiols was much slower, which the group concluded was due to the presence of defects on the surface.

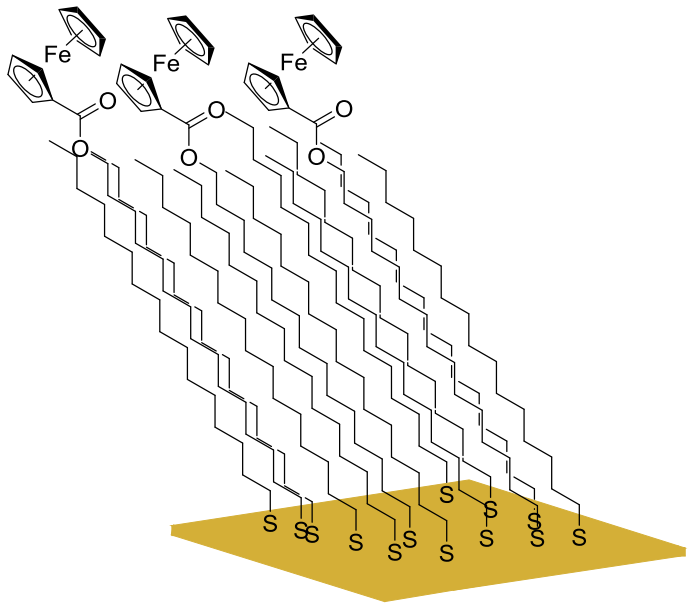


**Figure 2.2.** Schematic of one of the mixed monolayer systems studied by Collard *et al.*[9]

Thiols are widely used as anchoring groups to gold surfaces,[2, 3, 10-13] however other sulfur containing functional groups have also proven to be effective for immobilising transition metal complexes on gold surfaces. Work by Murphy *et al.*[14] (Figure 2.3) exploits the dithiocarbamate (DTC) functionality, as a surface-active moiety for terpyridyl based ruthenium(II) and osmium(II) complexes. Through electrochemical experiments it was shown that the SAMs were stable to potentials up to +1 V vs. the $Fc/Fc^{+}$ redox couple, while at +1.1 V only 10% of the coverage was lost, indicating that SAMs utilising the DTC linkage are indeed robust. A second experiment, immersing the SAMs in a solution of 2-mercaptoethanol, commonly used to remove monolayers by exchange reaction, showed only a 31% decrease in electrochemical signal, where an organic thiol monolayer would have been predicted to have been completely removed. From these experiments the group concluded that the monolayers were very resilient and thus showed potential in device formation.

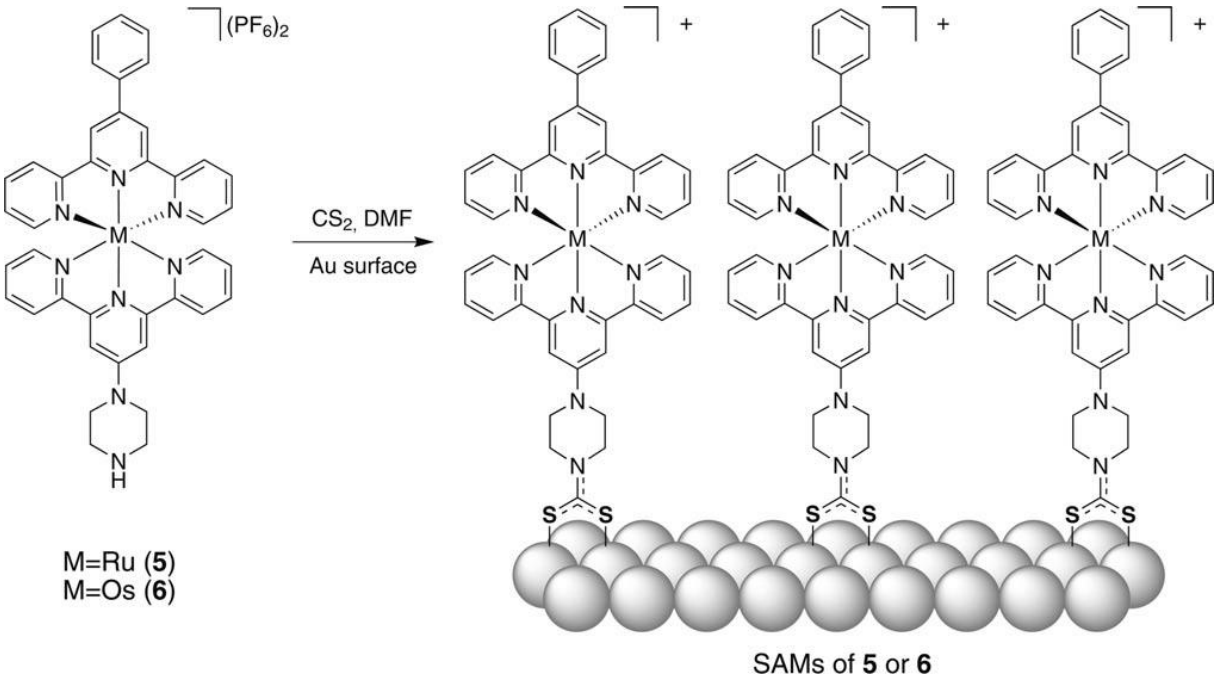


**Figure 2.3.** Schematic of formation of terpyridyl functionalised transition metal complexes adsorbed to gold surfaces outlined by Murphy *et al.* Image reproduced with permission from reference (14). Copyright 2009 John Wiley and Sons

One other functionality that can be used to tether molecules to gold surfaces is disulfides. Disulfides (Figure 2.4) have been widely used in self-assembly,[15-17] however α-lipoic acid functionality in particular is postulated to allow the formation of stronger surface binding, as the disulfide bond typically breaks upon binding to the surface, causing normal alkyl disulfides to split into two separate molecules each with one Au-S bond. α-Lipoic acid however contains a disulfide in a 5-membered ring system, so when the bond breaks upon binding to the surface, the α-lipoic acid has two Au-S bonds. Work by Zanarini *et al.*[18] (Figure 2.5) exploits this functionality in a different approach to previous examples, with a monolayer of α-lipoic acid being formed first, followed by an amide coupling on the carboxylic acid terminated surface with an amine functionalized tris-bipyridyl ruthenium(II) complex to create an electrochemiluminescent (ECL) device. Time of Flight Secondary Ion Mass Spectrometry (ToF

SIMS) of the monolayer showed uniform coverage of both α-lipoic acid and ruthenium group fragments, indicating that SAMs formed in this way are homogeneous across the substrate. The group studied the ECL properties of the monolayers and found that they were indeed luminescent when subjected to a positive voltage vs. reference. It was found that using the two-step method of surface functionalization more compact monolayers were formed compared with immersion of surfaces with preformed surface-active complexes.

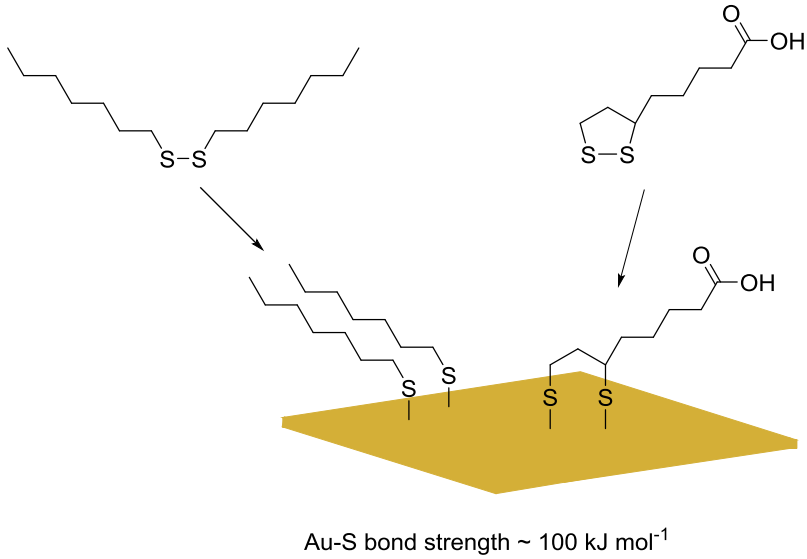


**Figure 2.4.** Schematic of surface binding of simple alkyldisulfide (left) and α-lipoic acid (right).

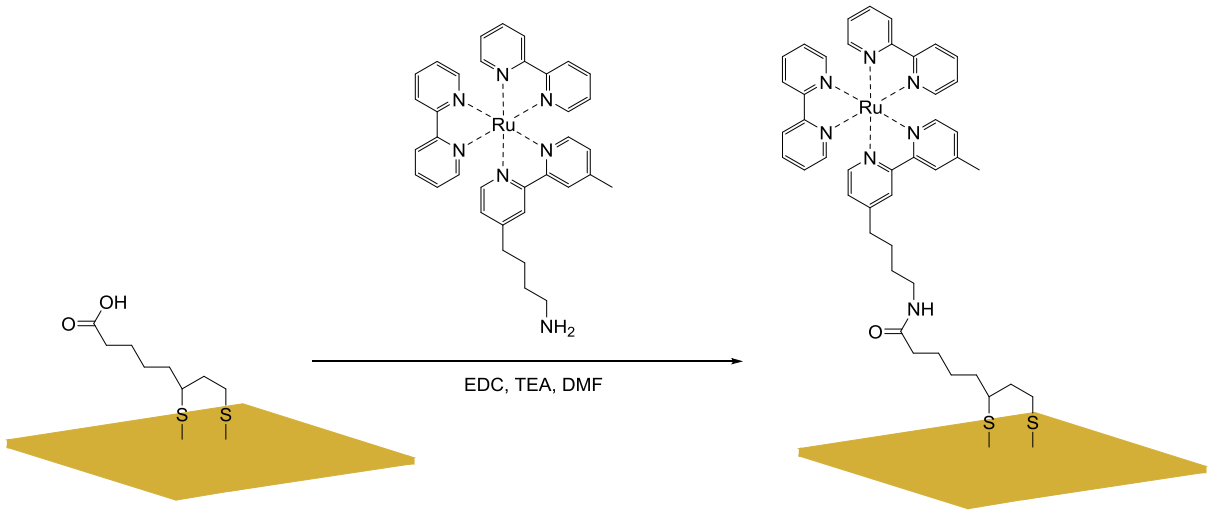


**Figure 2.5.** Schematic of ruthenium(II) complex attached to gold *via* α-lipoic acid linkage.[18]

Work by Yasutomi *et al.*[19] (Figure 2.6) shows the potential use of ruthenium(II) complexes in photodiode systems. Here, they present a helical hexadecamer peptide tethered with a lipoic acid moiety to allow attachment to a gold substrate at one end, and either an N-ethylcarbazolyl (ECz) group or a tris-bipyridyl ruthenium(II) complex at the other end. Utilising electron transfer pathways and a mixed monolayer of the two components, the group were able to switch the direction of photocurrent, either by exciting at 351 nm, causing an electron to be transferred from triethanolamine (TEOA) to the N-ethylcarbazolyl group resulting in an anodic current, or at 459 nm causing a cathodic current arising from electron transfer from the excited state of the ruthenium(II) complex to methylviologen ($MV^{2+}$). The photocurrents generated by these electron transfer pathways are enhanced by the presence of the peptides, due to their respective dipole moments, which accelerates electron transfer to or from the surface in order to complete the electrical circuit. Such a system illustrates the usefulness of ruthenium(II) complexes in device formation.

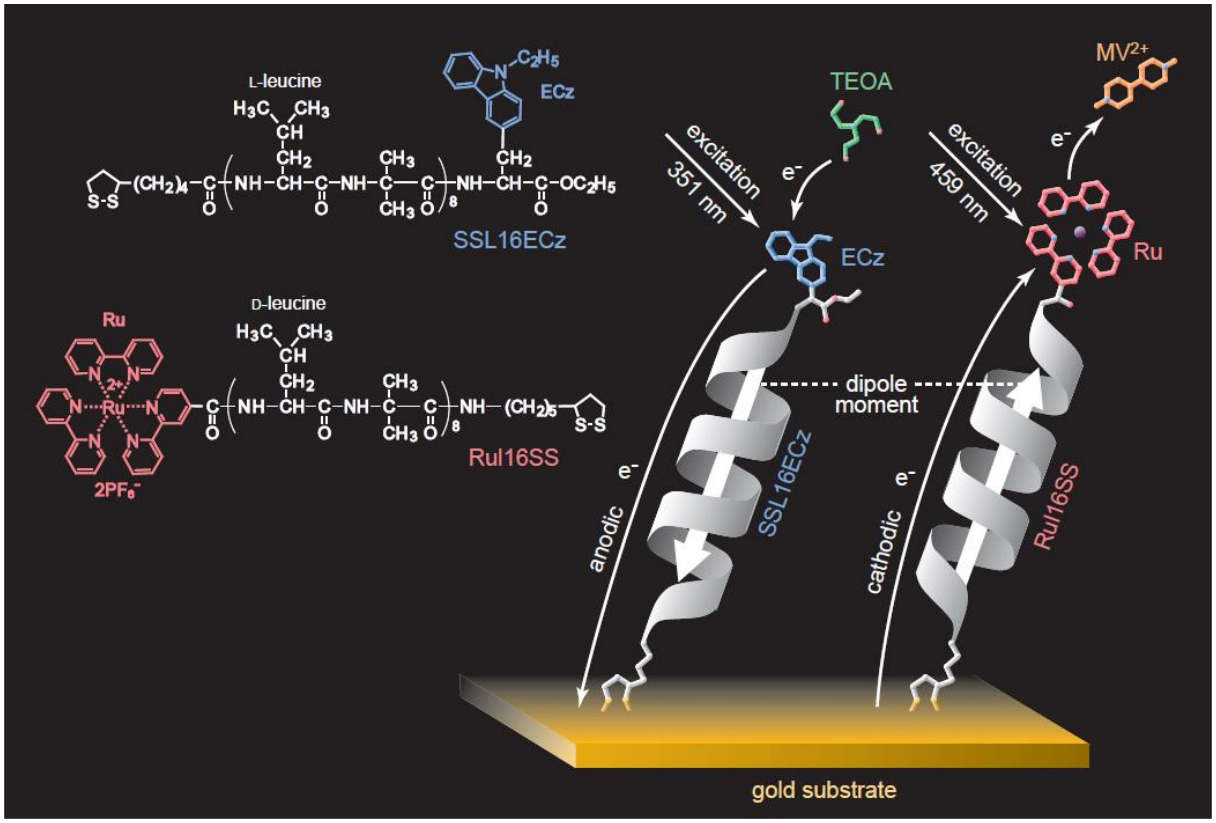


**Figure 2.6.** Schematic of photodiode system where photocurrent is switched depending on excitation wavelength. Image reproduced with permission from reference (19). Copyright 2004 American Association for the Advancement of Science.

Controlling the deposition of molecules on surfaces has many advantages, as the scope for potential device formation is increased greatly.[20, 21] In the field of electronic devices particularly, techniques such as lithography have enabled device features to come down to a nanometre scale.[22] However, these techniques can be very time consuming and expensive. One alternative to this is that of microcontact printing (μCP), developed by the group of Whitesides.[23] As discussed in chapter 1, preformed PDMS stamps can be used to pattern a variety of substrates and molecules,[21, 24, 25] and in particular, early work in this technique by Whitesides[23] focused on the use of thiols on gold surfaces. Figure 2.7 illustrates the versatility of the stamping technique for producing well defined arrays with minimal pattern defects when

stamping simple alkanethiols onto gold surfaces to form chemical resists, before etching of the surface to reveal the patterns. Indeed, the method has also been used to pattern silver substrates by chemical etching,[26] and also to perform chemistry through patterning, such as amide coupling over very short (less than 1 hour) timescales.[27]

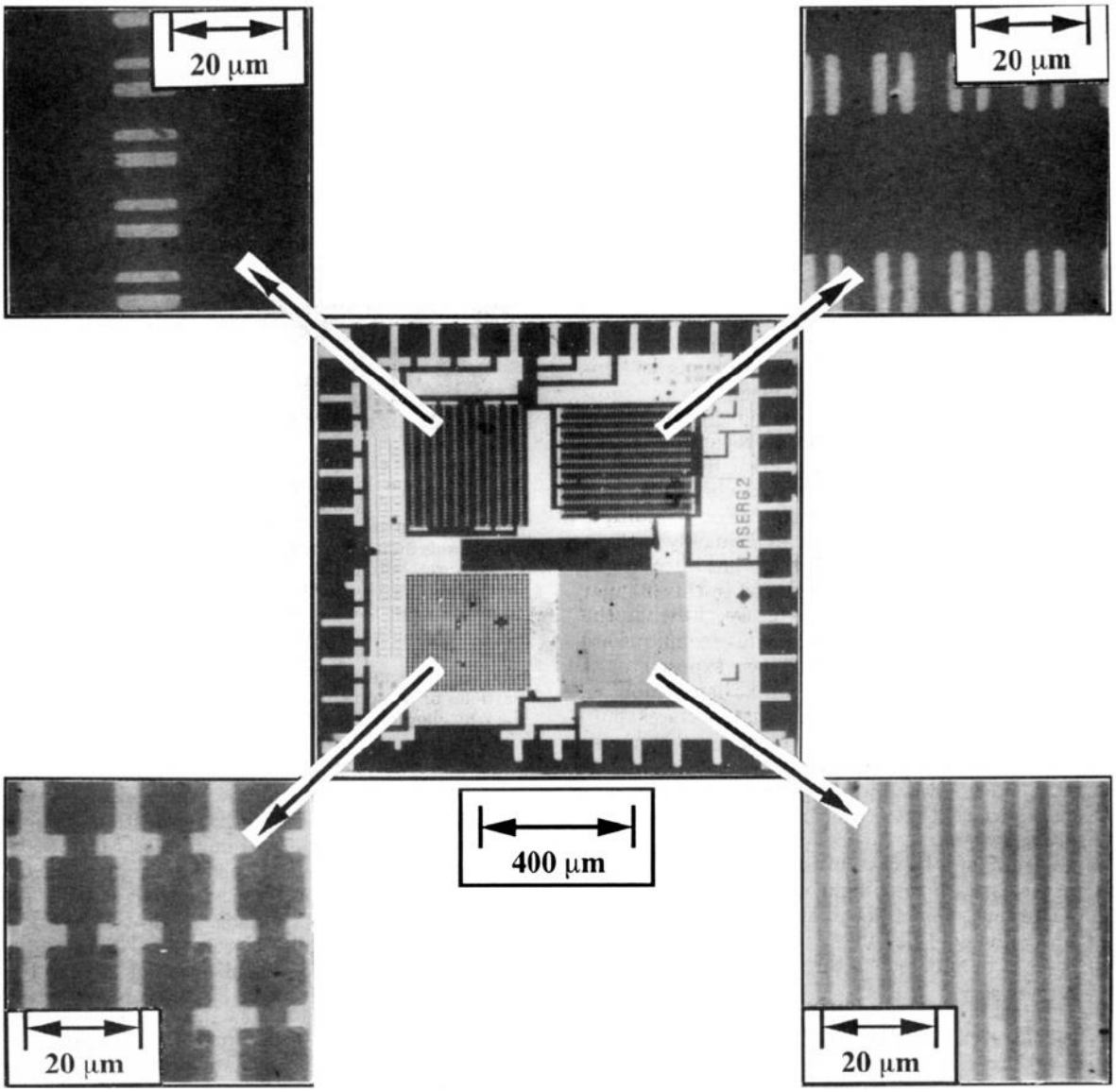


**Figure 2.7.** Scanning electron micrographs of various features that can be produced by stamping and subsequently chemically etching gold substrates. Reprinted with permission from reference (23). Copyright 1994 American Chemical Society.

However, patterning metal complexes on planar substrates is not well studied, with only few examples in the literature[28] such as the work by Rapino *et al*.[29] In this example (Figure 2.8), a reactive surface is formed by electrodepositing N-succinimidylacrylate onto gold or indium tin oxide (ITO) electrodes, causing polymerisation to occur and terminating the surface with N-succinimidyl groups. A platinum ultramicroelectrode is then brought into close proximity with the surface in a solution of an amine terminated ruthenium(II) complex, and a potential is applied so that the complexes can react with N-succinimidyl groups in the local area of the ultramicroelectrode, thus allowing patterning of the substrate. The group showed that using this method, ruthenium(II) complexes can indeed be patterned locally by drawing the complex onto the surface, thus allowing devices to be formed by this method with any molecular species displaying an amino or nucleophilic group.

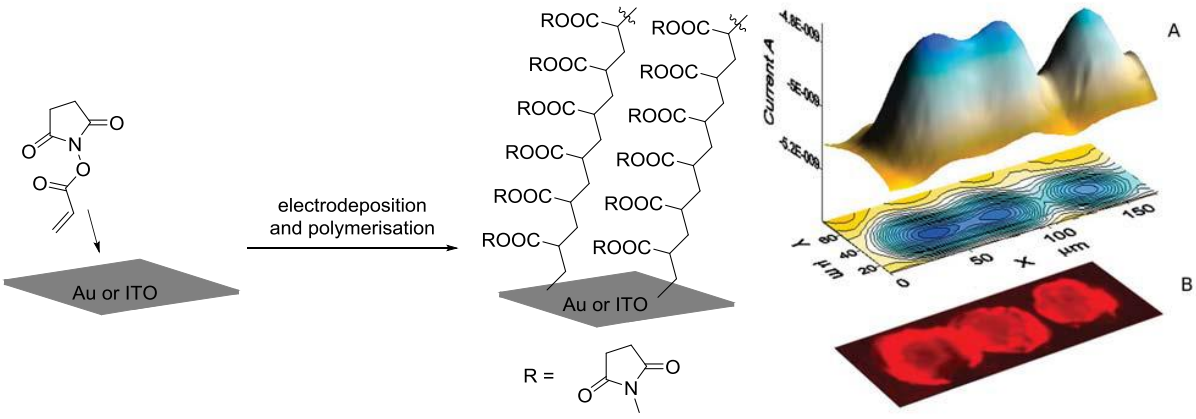


**Figure 2.8.** Left - Schematic of electrodeposition of poly-N-succinimidylacrylate onto surface for microdrawing. Right – Scanning electrochemical microscopy results (A) and luminescence microscopy image (B) of patterned ruthenium(II) complex on the surface. Reproduced from reference (29) with permission of the Royal Society of Chemistry.

### 2.1.2 Luminescence Quenching of Surface Bound Systems

One of the potential problems with functionalising conductive surfaces with luminescent metal complexes is that of quenching. Earlier work into the luminescence lifetimes of such complexes by Kuhn and Drexhage[30, 31] showed that luminescence decays were influenced greatly by their distance from metal mirrors due to interactions between the emitter and the interface. Indeed the work has since been extended to allow the prediction of energy coupling between gold nanoparticles and emitting dyes as shown by Strouse.[32] On surfaces, quenching of the excited state of ruthenium(II) complexes is shown on gold by De Cola[33, 34] and Pikramenou,[5] and electron transfer between ruthenium(II) complexes and titania surfaces is shown by Grätzel[35-38] and many others,[39-43] where quenching of the excited state is relied upon to induce photocurrent generation.

Quenching between the interface and the emitter is not the only consideration to be taken into account when examining these systems, energy or electron transfer can also happen between luminescent metal complexes. In particular, quenching of ruthenium complexes on gold nanoparticles has been shown by Kamat,[44, 45] (Figure 2.9), which was ascribed to lateral interactions between complexes, causing the excited states to be deactivated. Indeed, studies showed that lower loadings of the complexes on the nanoparticles led to less quenching being observed.[45]

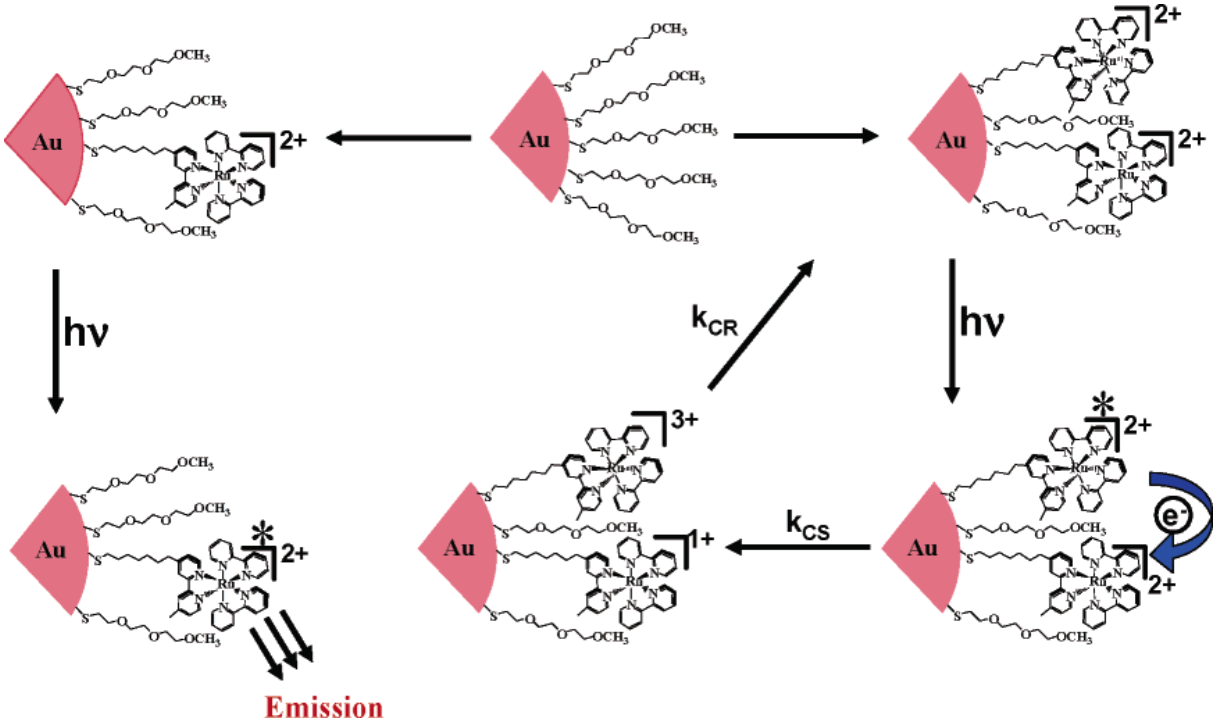


**Figure 2.9.** Schematic of lateral electron transfer between ruthenium(II) complexes on gold nanoparticles. Reprinted with permission from reference (44). Copyright 2006 American Chemical Society.

Quenching by other molecules on surfaces is also shown by Meyer *et al.*[46] In this example (Figure 2.10), ruthenium(II) complexes were adhered to silica or ITO surfaces through carboxylate groups on one of the bipyridyl ligands. Once adsorbed to the surfaces, they exhibited quenching by lateral energy or electron transfer in mixed monolayers of the ruthenium(II) complex and the analogous osmium(II) complex, phenothiazine or methylviologen quencher, as shown by a decrease in the luminescence lifetime of the ruthenium(II) complex. In the case of the phenothiazine quencher, an increase in lifetime of the quencher was also recorded. The results help to show that many factors on the surface influence the excited state properties of metal complexes, and thus great care must be taken when designing surface bound systems or devices. The influence of external factors on the properties of these complexes can, however, be exploited in sensing systems.

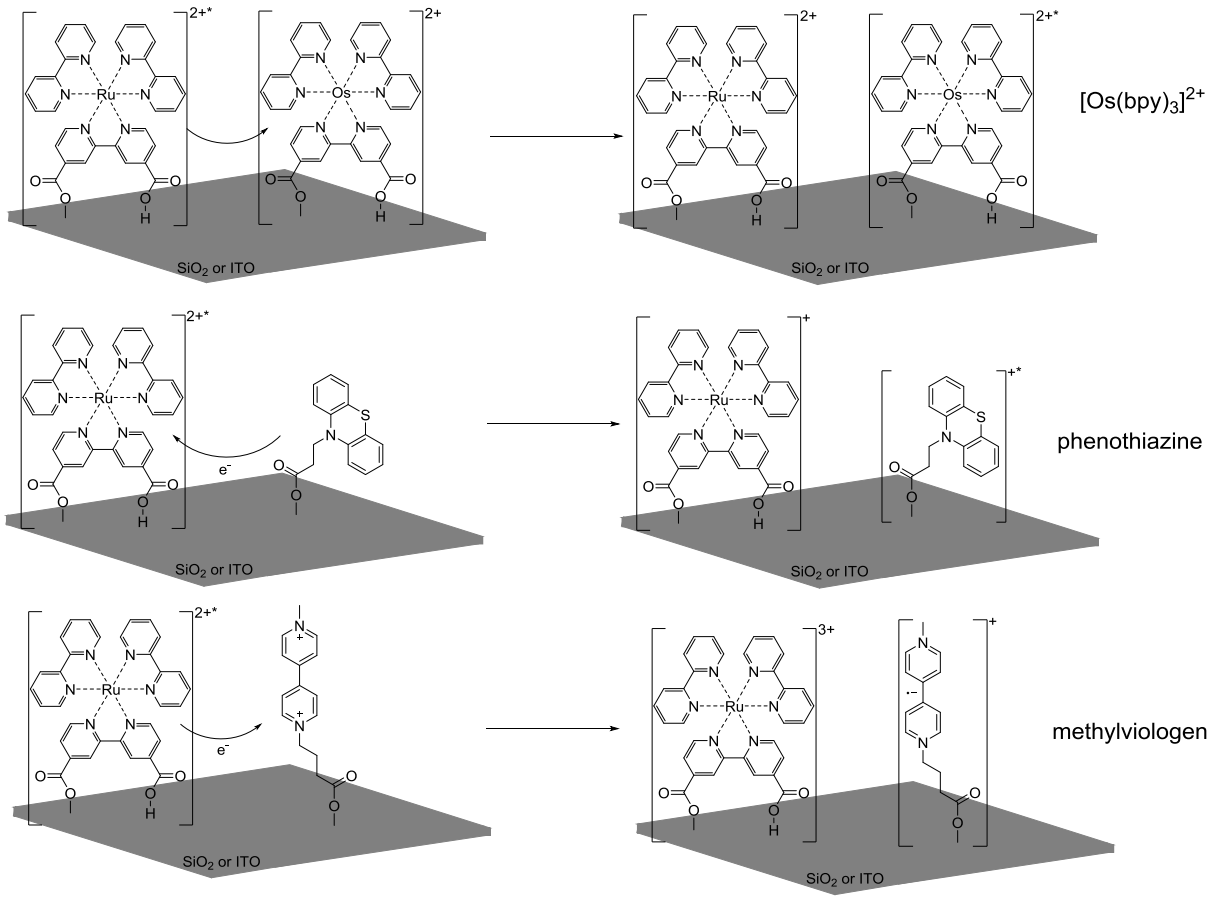


**Figure 2.10.** Schematic illustrating quenching pathways between ruthenium(II) complexes and other adsorbed molecules.[46]

## 2.1.3 Biomolecular Recognition with Transition Metal Complexes

The use of transition metal complexes as luminescent sensors is well established,[47] due to their intrinsically favourable properties such as large Stokes shifts, high photostability and relatively long lifetimes, as outlined in chapter 1. Indeed, luminescence lends itself to sensing as well, due to the high sensitivity of the techniques used to study it. Biomolecules are of particular interest for sensing as they are a wide ranging class of molecules useful in medical diagnostics.[48-50] Many of these probes are based in solution, and utilise the many accessible biomolecular recognition motifs afforded by the wide scope of binding sites.

One such recognition motif is that of ruthenium(II) polypyridyl complexes and DNA,[51-55] such as outlined by Kumar *et al.*[54] In this example, the binding of calf-thymus DNA to the complexes in Figure 2.11 is examined, and shows that upon mixing between $[Ru(phen)_3]^{2+}$ or $[Ru(dpp)_3]^{2+}$ with DNA, the emission of the complexes increased, indicating binding to the DNA. Further studies revealed that this binding was in part due to intercalation with the DNA, due to the flat aromatic structures of the ligands. The conclusion was further evidenced by the lack of emission enhancement and therefore binding from $[Ru(bpy)_3]^{2+}$, which does not contain this extended aromatic structure.

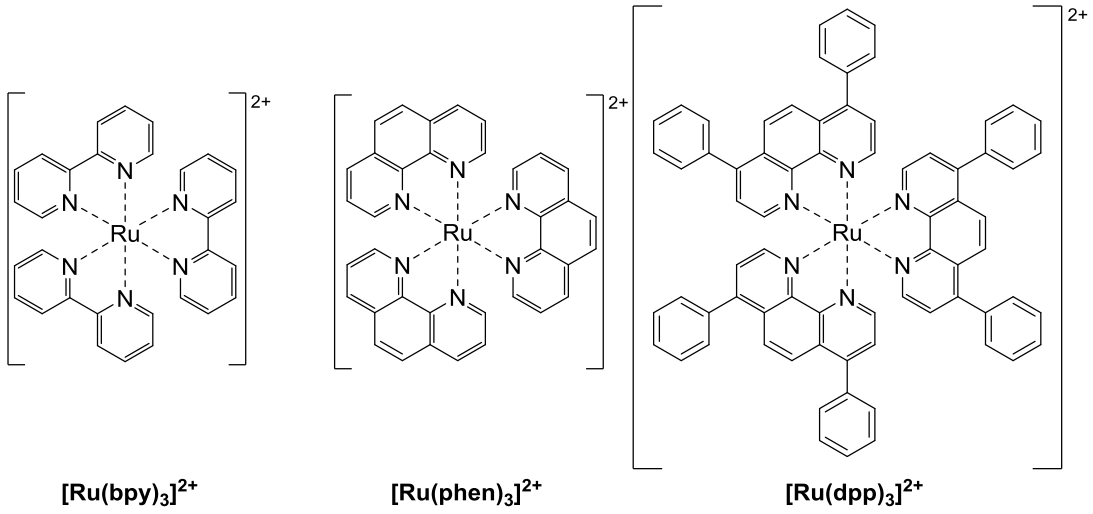


**Figure 2.11.** Schematic of ruthenium(II) complexes used in study of interaction with calf-thymus DNA.[54]

Interactions between proteins and transition metal complexes can also be studied,[48] as work by Lau *et al.*[56] shows. Here, a series of iridium(III) complexes (Figure 2.12) bearing indole functionalised bipyridyl ligands was mixed with bovine serum albumin (BSA), revealing up to a 13 fold increase in the intensity of the iridium emission band. The group rationalised that the increase in emission intensity was indeed due to binding, more specifically the increase in hydrophobicity in the environment that the emitting complexes found themselves in.

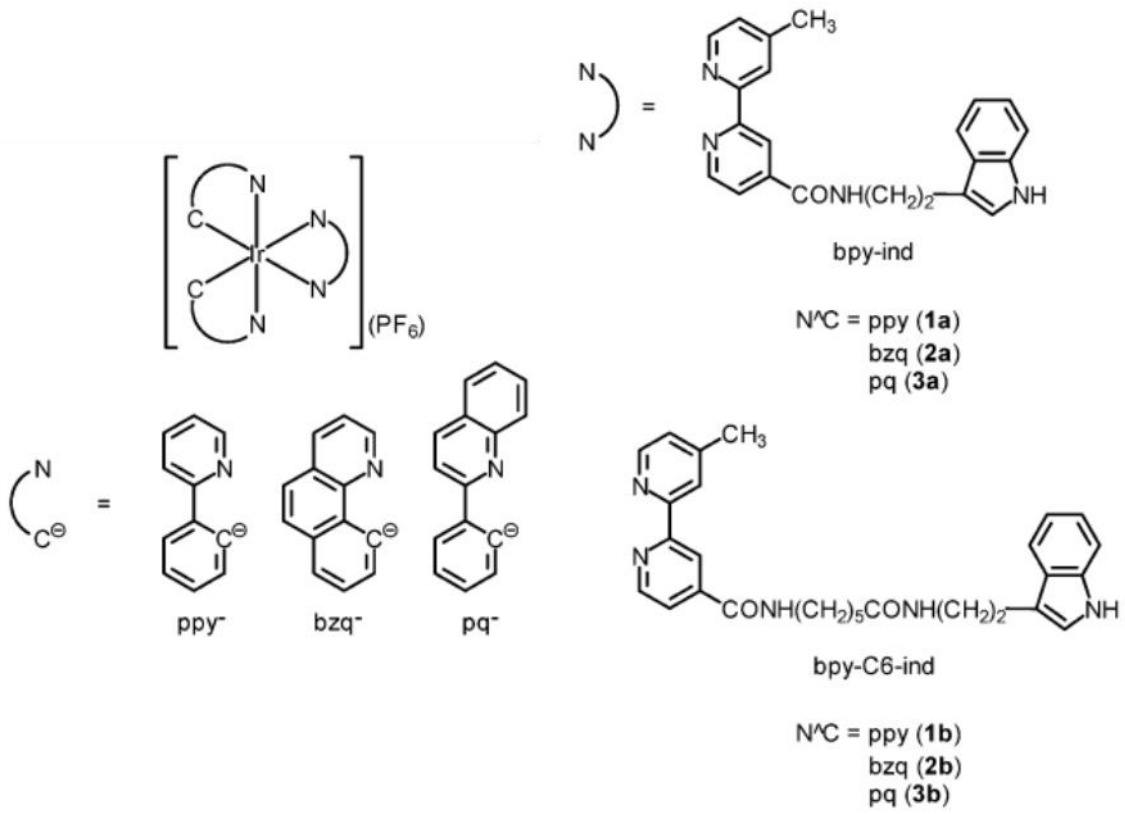


**Figure 2.12.** Schematic of synthesised iridium(III) complexes that were tested for recognition of BSA. Reprinted with permission from reference (56). Copyright 2009 American Chemical Society.

Muldoon *et al.*[57] have shown that ruthenium(II) complexes can also be synthesised with groups to recognise proteins. In this particular example, complexes in Figure 2.13 were synthesised and mixed with a range of proteins, including cytochrome c, lysozyme and myoglobin. It was found that emission quenching was observed for all complexes apart from **4** (Figure 2.13) when mixed with cytochrome *c*. More interestingly, when tested with similar proteins such as lysozyme (which has a similar pI and surface composition to that of cytochrome c), very little binding was observed.[57] This result indicated that the complexes were selective in the proteins they would bind to, meaning that the concept could be employed in effective sensors in more complex biological media.

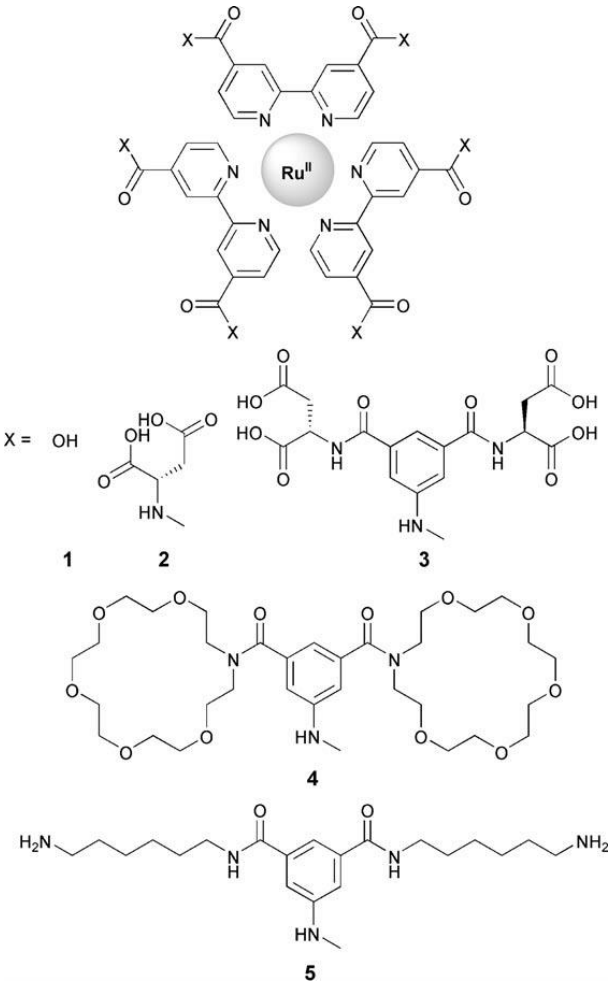


**Figure 2.13.** Schematic of synthesised ruthenium(II) complexes that were tested for recognition of cytochrome *c*. Imaged reproduced with permission from reference (57). Copyright 2009 John Wiley and Sons.

Polymers including transition metal complexes have also been employed to detect biomolecular recognition. Chung and Yam[58] reported (Figure 2.14) the use of a fluorescent polymer **PPE-SO$_3$** which exhibited FRET with platinium(II) complexes **1** and **2** when associated with the polymer through π stacking interactions in high concentrations. When this polymer was introduced to human serum albumin (HSA), the loosely bound platinum(II) complexes deaggregated from the polymer, allowing the polymer to fluoresce, indicating that binding had occurred. The results obtained by the group demonstrated the polymer-complex aggregate

allowed label free detection of HSA with high selectivity and sensitivity by monitoring the fluorescence output of the system.

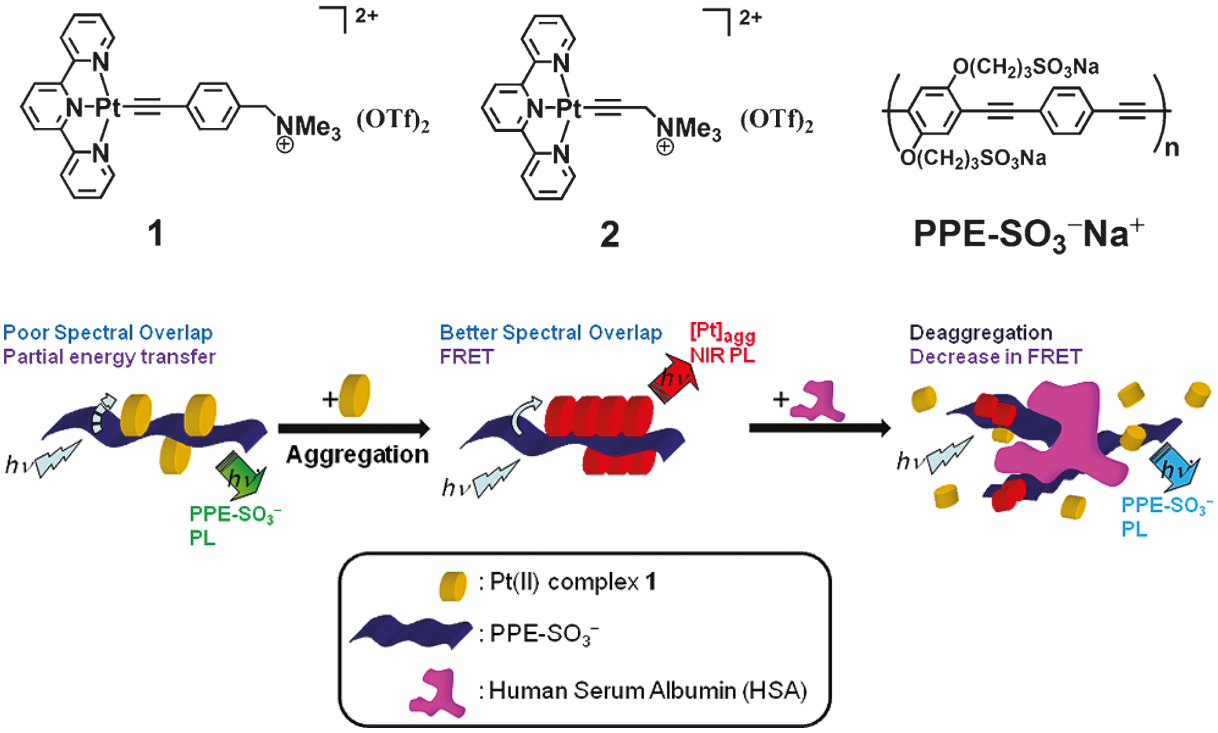


**Figure 2.14.** Top - Schematic of complexes used to quench polymer emission (**1**, **2**) and polymer used to recognise HSA. Bottom – Schematic of binding of Pt(II) complex and subsequent recognition of HSA. Reprinted with permission from reference (58). Copyright 2011 American Chemical Society.

The use of fluorescent materials in surface bound recognition systems has been studied,[59] however these systems generally do not involve the use of metal complexes, due to the problems with quenching as described earlier. Particularly for transition metal complexes, surface bound recognition typically employs electrochemical methods, due to the favourable redox behaviour of many transition metals, allowing a well-established detection method that is also environment sensitive. One example of this is the work of Blankespoor *et al.*[60] which involved the use of copper(II) and nickel (II) complexes (Figure 2.15). Here, chelating ligands were

attached to the surfaces of carbon electrodes by diazotisation of the aniline group of the ligand (step i), followed by electrodepositing the ligand (step ii). From there, the group immersed the electrodes in a solution of $CuCl_2$ to immobilise the complex (step iii). A histidine-tagged horseradish peroxidase could be chemically attached to the complex (step iv), utilising the imidazole rings of histidine as ligands. XPS and CV data confirmed monolayer coverage of the complex at a concentration of *ca*. 140 pmol $cm^{-2}$, and showed through electrochemical methods that the enzyme was indeed active on the surface of the electrodes. To further test their method for immobilisation of proteins at the surface, a second histidine-tagged green fluorescent protein (GFP) was synthesised, and tested by fluorescence microscopy, revealing immobilisation of the protein only when $Cu^{2+}$ was also present at the surface. The group concluded that such a method would be very useful in device formation, particularly to create catalytic systems utilising complex but energy efficient biological processes.

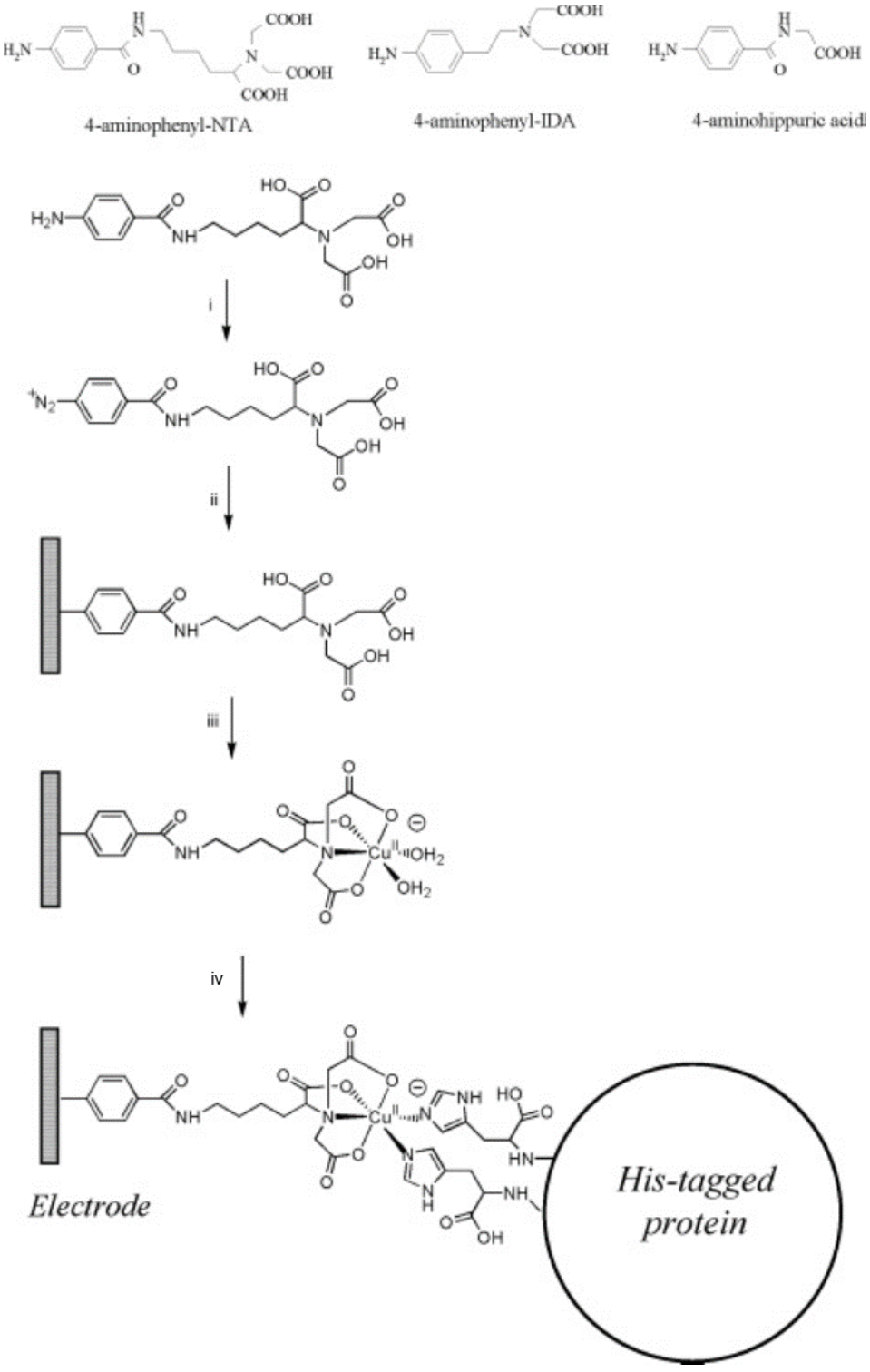


**Figure 2.15.** Schematic of attachment of copper complex to carbon electrode and subsequent protein attachment. Adapted with permission from reference (60). Copyright 2005 American Chemical Society.

The literature illustrates the many facets and pathways to device formation with transition metal complexes, from the choice of surface and surface-active group, to controlled deposition and the creation of sensors based on planar or nanoparticle scaffolds. Due to the complex interactions between the interface and the complex, careful design of complex must be employed in order to reduce or eliminate quenching at the surface.

### 2.1.4 Preliminary Work

The work in this chapter builds on previous work in the group concerning the immobilisation of transition metal complexes on gold surfaces. Figure 2.16 shows the surface-active complexes previously synthesised. The short chain complex **RubpySH** showed an expected luminescence signal in acetonitrile solution but was almost entirely quenched on platinum and gold substrates.[5] In order to try and improve the surface luminescence, a second complex with longer 'legs' (**RubpySAc**) was designed and synthesised, and showed some quenching on planar surfaces.[61] The complex was also successfully attached to gold nanoparticles and displayed very acceptable luminescence properties.[62] It was postulated that by extending the complex further from the surface through longer surface-active 'legs', that the problem of quenching could be eliminated entirely. To do this, the surface-active architecture from a terpyridyl ruthenium(II) complex **RutpySS** designed for molecular wire growth[63] was used to create a 'long-legged' luminescent ruthenium(II) complex **RubpySS** (Figure 2.17) which displayed favourable luminescence properties when attached to gold surfaces.

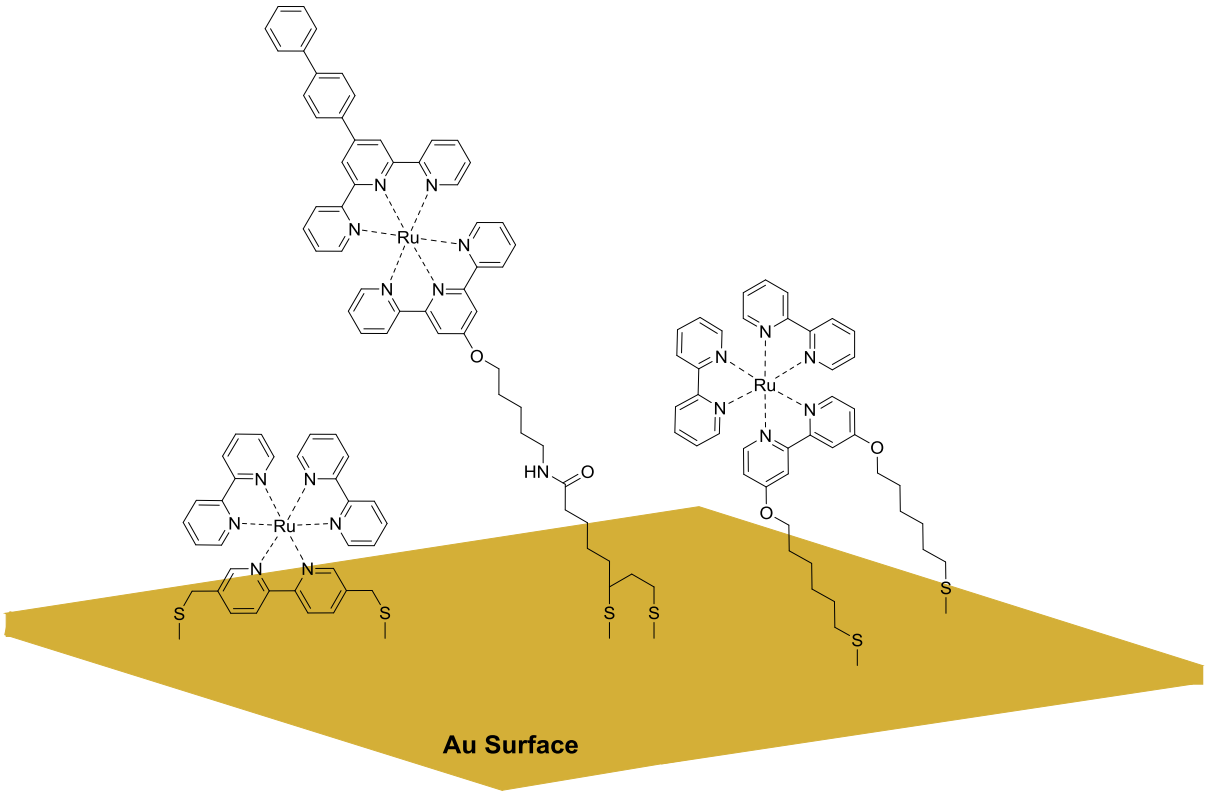


**Figure 2.16.** Schematic of previous complexes synthesised in the group, **RubpySH** (left),[5] **RutpySS** (middle)[63] and **RubpySAc** (right).[62]

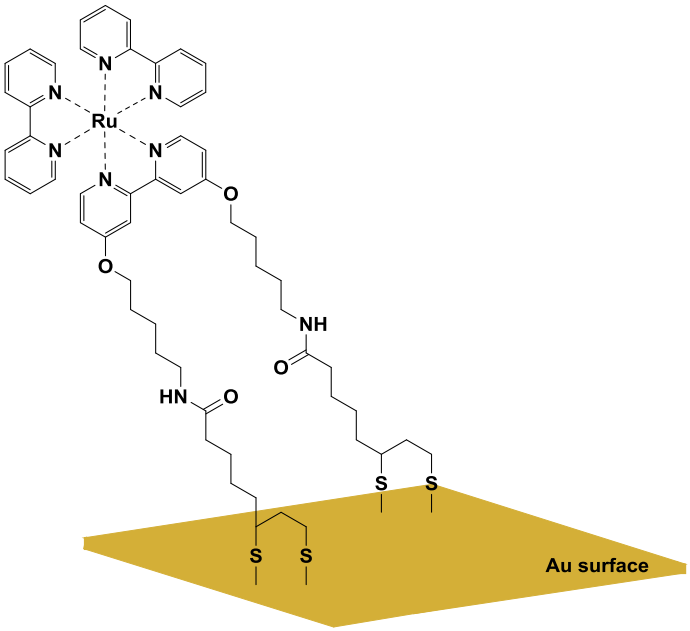


**Figure 2.17.** Schematic of **RubpySS** attached to a gold surface.

### 2.1.5 Chapter Outline

This chapter expands on the previous preliminary work carried out for **RubpySS**. The synthetic routes to the analogous osmium(II) complex **OsbpySS** will be introduced, alongside an attempted alternative synthetic route to **RubpySS**. The characterisation and photophysical properties of the precursor complexes **RubpyNH$_2$** and **OsbpyNH$_2$** will be discussed. The published work outlines the synthesis and characterisation of **RubpySS**, **OsbpySS** and the iridium(III) complex **IrbpySS**. The photophysical properties of these three complexes in solution is discussed, and the surface properties and characterisation for **RubpySS** and **IrbpySS** will be introduced. Through μCP, the micropatterning of these complexes will be shown, and the biomolecular recognition of serum protein bovine serum albumin (BSA) will be discussed.

# 2.2 Synthesis and Properties of Surface-Active Transition Metal Complexes

## 2.2.1 Attempted Synthesis of MbpySS Complexes via Alternative Synthetic Route

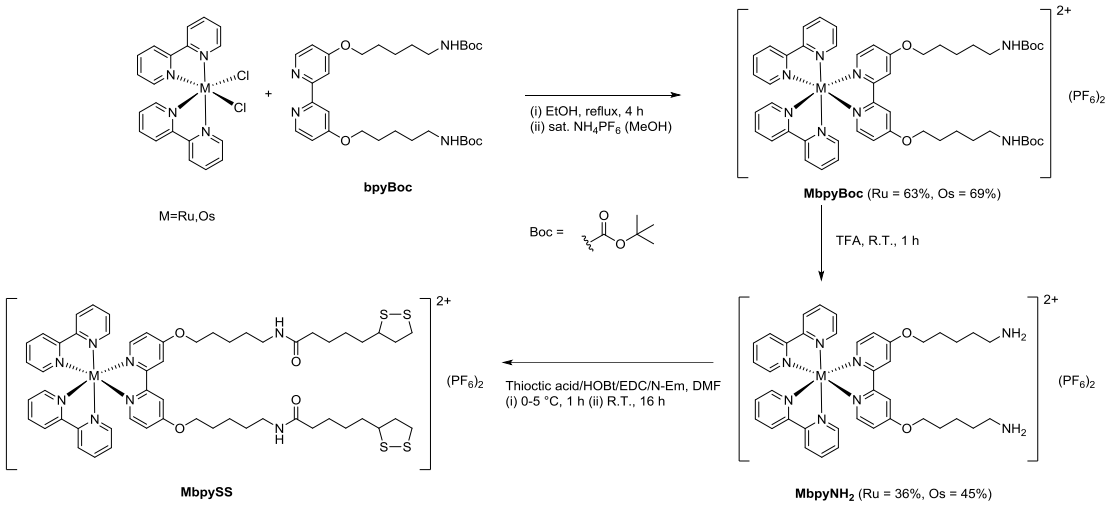


**Scheme 2.1.** Attempted synthetic route to **MbpySS**.

To extend the work carried out with **RubpySS**, we sought to synthesise a complex with the same surface-active ligand **bpySS** which had luminescence in the far red/NIR region of the spectrum. To achieve this, we wished to synthesise the analogous osmium(II) complex. However, due to osmium(II)'s affinity for soft ligands such as sulfur, we decided to design a synthesis that allowed sulfur groups to be attached after complexation. This new synthetic route is outlined in Scheme 2.1. The Boc protected bipyridyl ligand **bpyBoc**, **Ru(bpy)$_2$Cl$_2$** and **Os(bpy)$_2$Cl$_2$** were obtained by synthetic methods described previously.[1, 64] **M(bpy)$_2$Cl$_2$** was reacted with **bpyBoc** in ethanol and precipitated with ammonium hexafluorophosphate to afford **MbpyBoc**. The Boc groups were then deprotected in TFA to yield the **MbpyNH$_2$** complex.

Attempts at attaching the thioctic acid via standard amide coupling conditions were attempted, but yielded impure products.

**OsbpyBoc** and **RubpyBoc** were characterised by $^{1}H$ and $^{13}C$ NMR spectroscopy. $^{1}H$ NMR spectroscopic data for **OsbpyBoc** shows that the product is formed, as evidenced by the peaks at 8.29 ppm (H-d/d′) and 6.72 ppm (H-5), which integrate for 4 and 2 respectively, indicating complexation between the **bpyBoc** ligand and the osmium(II) complex. $^{13}C$ NMR spectroscopy indicates that the product is formed, with all peaks visible in the spectrum aside from C-13 and C-4, which is most likely attributable to the weak response from the sample. The product was deemed pure enough at this stage and was thus carried forward to the next step without further characterisation. Very similar results were also observed for **RubpyBoc** and this was also carried forward.

**OsbpyNH$_2$** and **RubpyNH$_2$** were characterised by $^{1}H$ and $^{13}C$ NMR spectroscopy and UV-Vis spectroscopy. $^{1}H$ NMR spectroscopy for **OsbpyNH$_2$** indicates that Boc deprotection is successful, with the loss of the large methyl peak at 1.23 ppm. Figure 2.18 shows the aliphatic region of the $^{1}H$ NMR spectrum, which reveals that H-11 at 2.90 ppm and 3.55 ppm (2.82-2.94 ppm in **OsbpyBoc**) is now in two separate environments. We attribute this effect to salt formation in the product at one of the terminal amine groups, which in turn gives rise to a downfield shift of the peak. The peak for the terminal amine groups centred at 6.02 ppm also has a larger integration of 5H than expected for the product (4H in product), indicating the formation of an $NH_3^+$ group on one of the legs. Very similar results are observed in the $^{1}H$ NMR spectrum of **RubpyNH$_2$** and indeed the above conclusion is further evidenced when the isolated product of **RubpyNH$_2$** is dissolved in NaOH and reprecipitated in $NH_4.PF_6$, as the integration of the peak for H-11′ decreases in magnitude. The $^{13}C$ NMR spectra for both complexes agree well with each other. A mass spectrum for **RubpyNH$_2$** was also obtained, revealing three ion

envelopes at 917 ($[M\text{-}PF_6]^+$), 1063 ($[M+H]^+$) and 1102 ($[M+K]^+$) Da, indicating that the product does form. However the yields of the Boc deprotections were very low; 45% and 36% for **OsbpyNH$_2$** and **RubpyNH$_2$**, respectively; compared with other boc deprotections with TFA (approaching quantitative yield), which is a probable result of the difficulties arising from salt formation at the terminal amine.

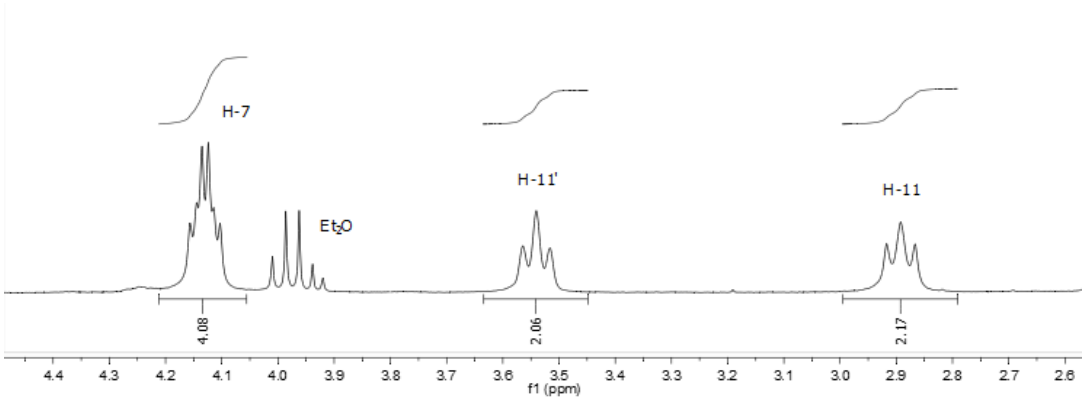


**Figure 2.18.** Aliphatic region of $^1$H NMR spectrum of OsbpyNH$_2$ in $CD_3CN$.

## 2.2.2 Photophysical Properties of Amino Functionalised Transition Metal Complexes

Despite the difficulties in moving forward with the synthesis, the photophysical properties of both **RubpyNH$_2$** and **OsbpyNH$_2$** were studied by UV-vis absorption, and steady state and time-resolved luminescence spectroscopy, with the results summarised in Table 2.1. Figure 2.19 shows the UV-vis absorption spectra of both complexes, revealing typical spectra containing π-π* transitions at 289 and 291 nm for **RubpyNH$_2$** and **OsbpyNH$_2$**, respectively, and also $^1$MLCT transitions at 461 and 488 nm for **RubpyNH$_2$** and **OsbpyNH$_2$**, respectively. The $^1$MLCT bands for both complexes are significantly redshifted from those of $[Ru(bpy)_3]^{2+}$ and $[Os(bpy)_3]^{2+}$ by 9 nm for **RubpyNH$_2$** and 7 nm for **OsbpyNH$_2$**, an effect also observed in both

**RubpySS** and **OsbpySS**.[1] Excitation spectra for both complexes (Figure 2.19) agree well with their respective absorption profiles.

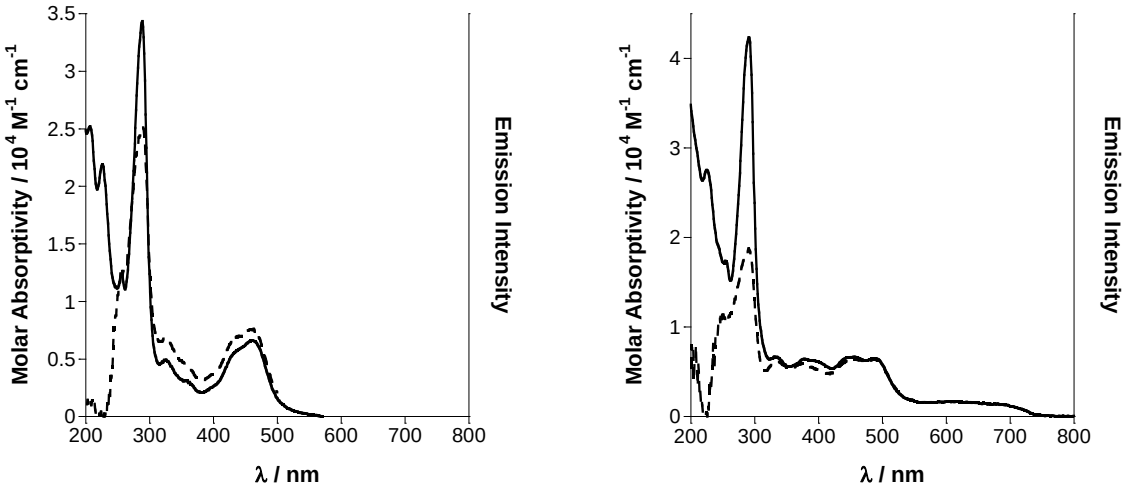


**Figure 2.19.** UV-vis absorption (solid) and steady state excitation spectra (dash) of **RubpyNH$_2$** (left) (14 μM, $\lambda_{em}$ = 640 nm) and **OsbpyNH$_2$** (right) (17 μM, $\lambda_{em}$ = 745 nm) in acetonitrile solution. Excitation spectra corrected for instrument response.

Figure 2.20 shows the emission spectra for **RubpyNH$_2$** and **OsbpyNH$_2$**, revealing typical broad $^3$MLCT emission centred at 650 and 785 nm, respectively. The emission bands are again significantly redshifted from those of $[Ru(bpy)_3]^{2+}$ and $[Os(bpy)_3]^{2+}$ by 35 and 62 nm, respectively, agreeing well with the similar complexes **RubpySS** (645 nm) and **OsbpySS** (790 nm).[1] The luminescence quantum yield of both complexes was measured by the optically dilute method,[65] with $[Ru(bpy)_3]Cl_2$ as the standard[66] and gave rise to a 1% quantum efficiency in aerated acetonitrile solution for **RubpyNH$_2$**, which increased to 4% upon deaerating the solution. This result corresponds well with similar ruthenium(II) complexes,[1, 67] with the increase in quantum yield upon deaerating attributed to the removal of oxygen which can quench the $^3$MLCT state.[68] The luminescence quantum yield results for **OsbpyNH$_2$** (Table 2.1)

are expectedly low and agree well with the similar osmium(II) complex **OsbpySS**.[1] The luminescence lifetimes of both complexes were found to be monoexponential in acetonitrile solution, with aerated lifetimes of 137 ns for **RubpyNH$_2$** and 22 ns for **OsbpyNH$_2$**. Both of these lifetimes increase upon deaerating the solution, with values of 745 and 27 ns for **RubpyNH$_2$** and **OsbpyNH$_2$**. All of the lifetimes measured for both complexes were shorter than their simpler counterparts $[Ru(bpy)_3]^{2+}$ and $[Os(bpy)_3]^{2+}$, but comparable to those of **RubpySS** and **OsbpySS**.[1]

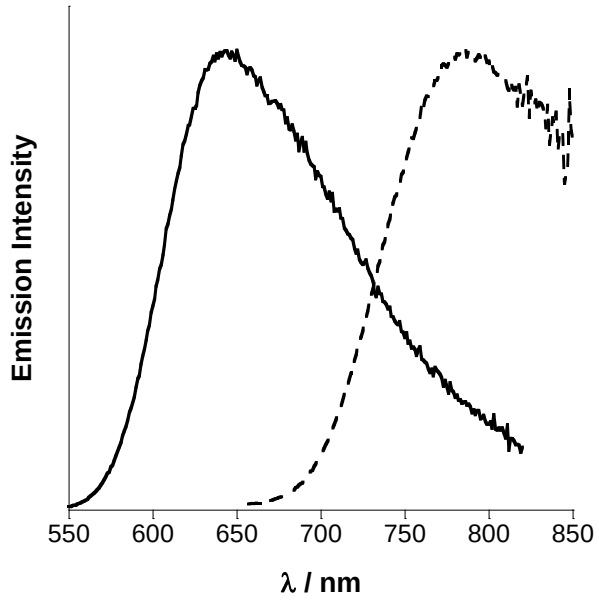


**Figure 2.20.** Steady state emission spectra of **RubpyNH$_2$** (solid) (14 μM, $\lambda_{exc}$ = 465 nm) and **OsbpyNH$_2$** (dash) (17 μM, $\lambda_{exc}$ = 488 nm) in acetonitrile solution. Spectra corrected for instrument response, intensities are not to scale.

**Table 2.1.** Summarised emission data for **RubpyNH$_2$**, **OsbpyNH$_2$** and similar complexes in acetonitrile solution.

| Complex | $\lambda_{max}$ / nm ($\varepsilon$ / $10^4$ $M^{-1}$ $cm^{-1}$) | $\lambda_{em}$ / nm | $\tau$ / ns | | $\Phi$ / % | |
|---|---|---|---|---|---|---|
| | | | aerated | deaerated | aerated | deaerated |
| **RubpyNH$_2$** | 289 (3.4) 461 (0.7) | 650 | 137 | 745 | 1 | 4 |
| **OsbpyNH$_2$** | 291 (4.2) 378 (0.6) 455 (0.7) 489 (0.7) | 785 | 22 | 27 | 0.1 | 0.1 |
| $[Ru(bpy)_3]^{2+}$ | 452 (1.3) | 615 | 172 | 840 | 1 | 10 |
| $[Os(bpy)_3]^{2+}$ | 482 (1.1) | 723 | 39 | 58 | 0.3 | 0.5 |

## 2.2.3 Synthesis of bpySS Complexes *via* Complexation with bpySS

In order to synthesise **OsbpySS**, a new route (Scheme 2.2) was formulated based on complexing **bpySS** with **Os(bpy)$_2$Cl$_2$** using a modification to a previously published method,[69] but utilising microwave irradiation to achieve the desired product, as such methods have been successfully employed to produce osmium(II) complexes before.[70] The iridium(III) complex **IrbpySS** (Scheme 2.2) was also synthesised by reacting with the μ-chloro bridged *tetrakis*-(2-phenylpyridine)iridium(III) dimer *via* a modification to a method outlined by Slinker *et al.*[71] The syntheses and characterisation of both of these complexes is elaborated below.

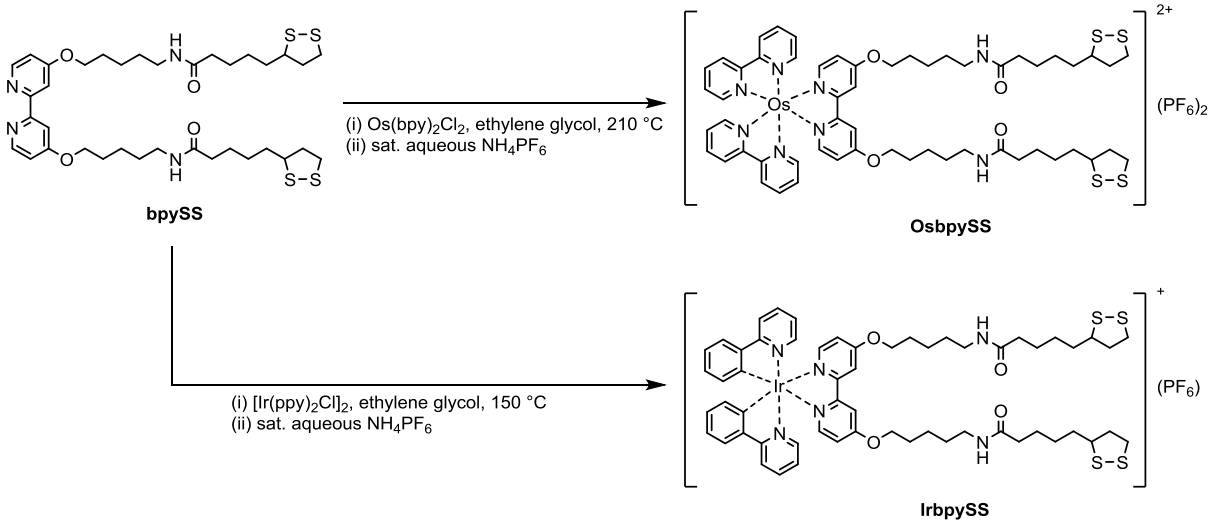


**Scheme 2.2.** Synthetic route to **OsbpySS** and **IrbpySS**.

**OsbpySS** was characterised by $^{1}H$, $^{13}C$ and 2D NMR spectroscopy, ES(+) mass spectrometry, UV-vis absorption spectroscopy and microelemental analysis. NMR assignments were confirmed by COSY, HSQC and HMBC experiments. Figure 2.21 shows the $^{1}H$ NMR spectrum of **OsbpySS**, revealing all of the expected environments. The peak integrations of the compound agree well, particularly those of H-a/a′ (7.61 ppm, 2H) and H-5 (6.85 ppm, 2H) indicating that the desired product has been formed. The $^{13}C$ NMR spectrum of **OsbpySS** also agrees well with the expected environments, and also that of **RubpySS**. ES(+) mass spectrometry reveals one adduct at 1383 Da corresponding to $(M\text{-}PF_6)^+$ and calculated elemental percentages agree well with the observed results, confirming that the product has been successfully formed.

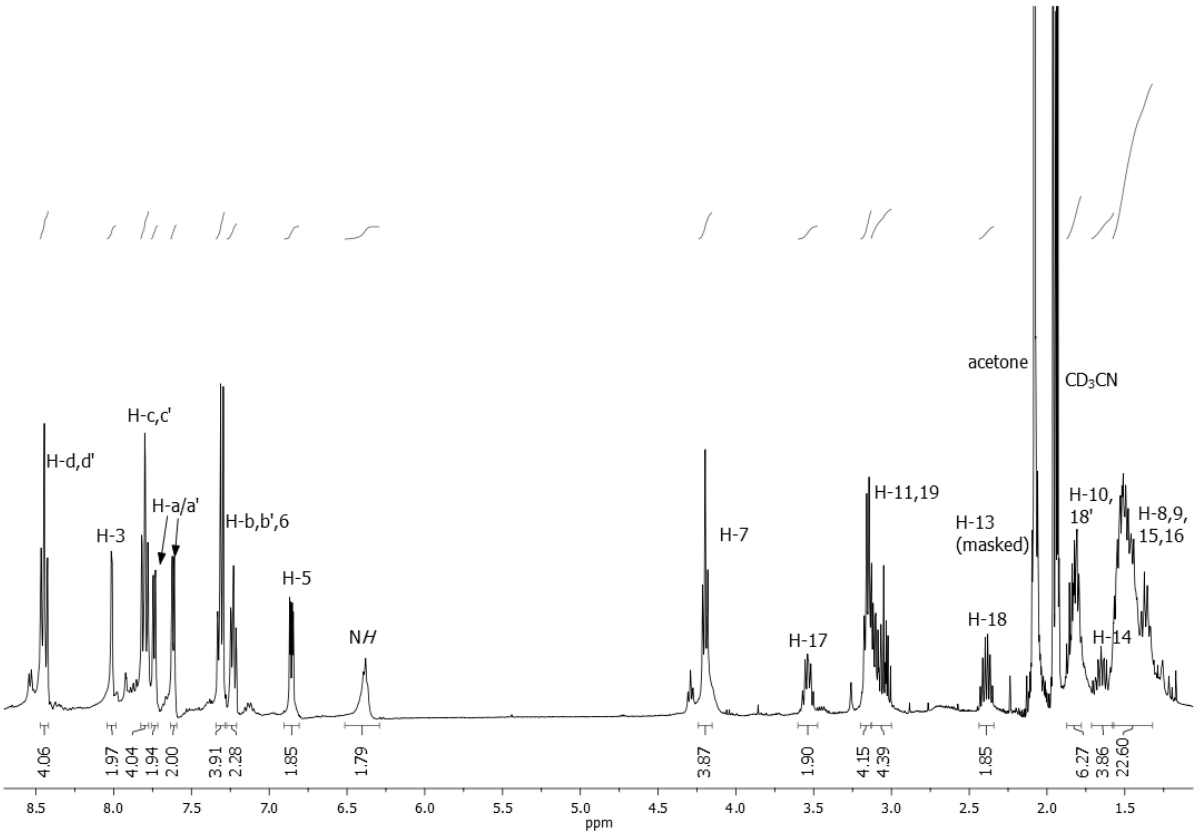


**Figure 2.21.** $^{1}$H NMR spectrum of **OsbpySS** in $CD_3CN$.

**IrbpySS** was characterised by $^{1}$H, $^{13}$C and 2D NMR spectroscopy, ES(+) mass spectrometry, UV-vis absorption spectroscopy and microelemental analysis. NMR assignments were confirmed by COSY, HSQC and HMBC experiments. Figure 2.22 shows the $^{1}$H NMR spectrum of **IrbpySS**, revealing all of the expected environments. Again, the peak integrations of the spectrum agree well, particularly those of H-3 (8.29 ppm, 2H), H-k (6.21, 2H) and H-18 (*ca.* 2.3 ppm, 2H), indicating that complexation between the dimer and **bpySS** has occurred. The $^{13}$C NMR spectrum also fits the expected environments. The ES(+) mass spectrum reveals one ion envelope at 1235 corresponding to $(M\text{-}PF_6)^+$ and microelemental analysis results agree well with calculated atomic percentages, confirming the formation of the desired product.

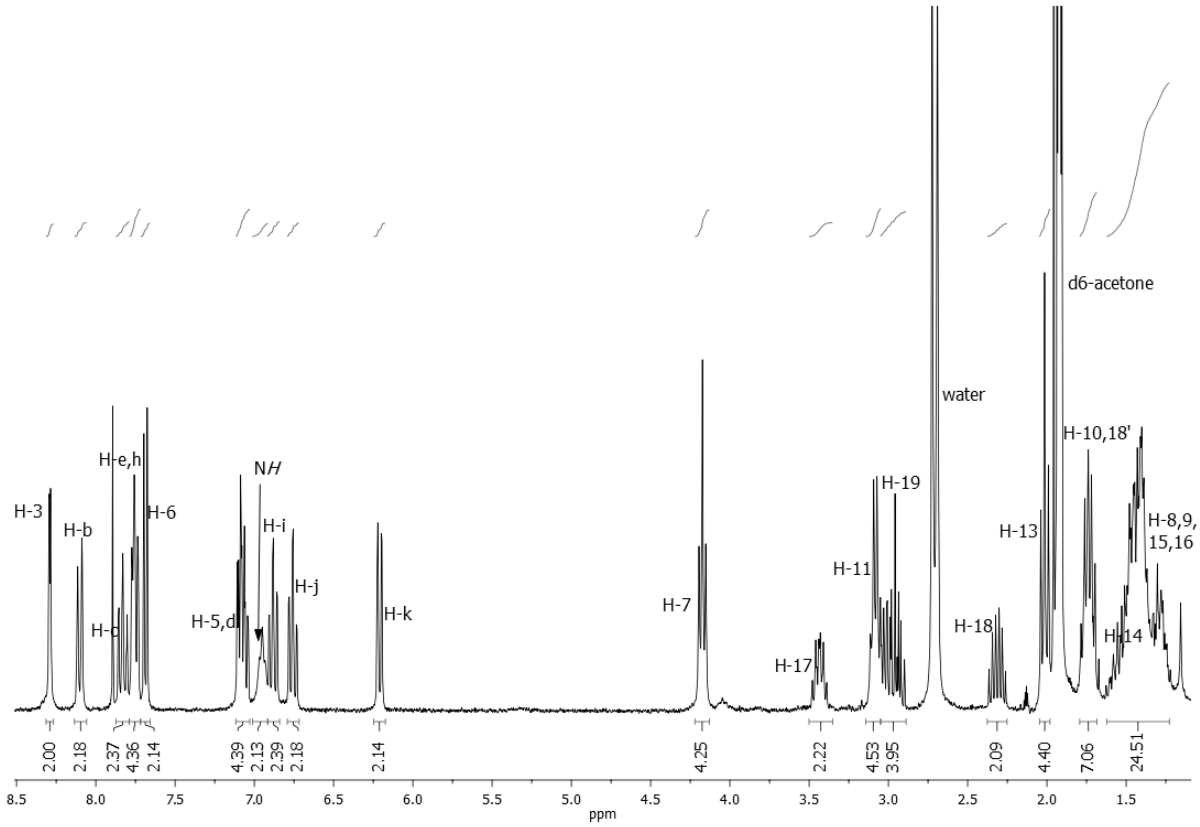


**Figure 2.22.** $^{1}$H NMR spectrum of **IrbpySS** in acetone-$d_6$.

## 2.3 Published Work

As part of this chapter, a summary of work undertaken and published in ACS Materials and Interfaces in 2014 and also shown below is as follows:

Novel transition metal complexes based on the ruthenium(II) complex **RubpySS** developed by Dr David J. Lewis were synthesised and fully characterised. The complexes contained long spacer groups between the metal centres and the disulfide moieties to mitigate the potential effects of luminescence quenching from the gold substrates. It was shown that contrary to quenching on the surface, the complexes **RubpySS** and **IrbpySS** exhibited enhanced luminescence lifetimes of 210 ns and 130 (83%), 12 (17%) ns respectively, compared with aerated acetonitrile solutions of 130 ns and 25 (68%), 80 (32%) ns respectively. Binding of the complexes to gold substrates was confirmed by kinetic ellipsometric studies, SPR spectroscopic studies and XPS studies. It was shown through the use of μ-contact printing that complexes of this type can be micropatterned on gold substrates, albeit over longer time periods than their organic counterparts, with luminescent micrographs of **RubpySS** and **IrbpySS** in various patterns shown in the manuscript. Finally, it was shown that the complexes can participate in biomolecular recognition. In solution and particularly in the case of **IrbpySS**, an 80-fold increase in luminescence intensity coupled with an increase in aqueous luminescence lifetime from 15 ns to 37 (8%), 283 (92%) ns was observed, along with a decrease in the α-helical folding of BSA as evidenced by CD spectroscopy. On gold substrates, both complexes exhibited enhancement in their luminescence lifetimes upon the addition of BSA, as well as increases in the SPR response compared with blank gold substrates.

ACS APPLIED MATERIALS & INTERFACES

Research Article

www.acsami.org



# Luminescent Gold Surfaces for Sensing and Imaging: Patterning of Transition Metal Probes

Samuel J. Adams, David J. Lewis, Jon A. Preece, and Zoe Pikramenou*

School of Chemistry, University of Birmingham, Edgbaston, Birmingham, West Midlands B15 2TT, United Kingdom

Supporting Information

**ABSTRACT:** Luminescent transition metal complexes are introduced for the microcontact printing of optoelectronic devices. Novel ruthenium(II), RubpySS, osmium(II), OsbpySS, and cyclometalated iridium(III), IrbpySS, bipyridyl complexes with long spacers between the surface-active groups and the metal were developed to reduce the distance-dependent, nonradiative quenching pathways by the gold surface. Indeed, surface-immobilized RubpySS and IrbpySS display strong red and green luminescence, respectively, on planar gold surfaces with luminescence lifetimes of 210 ns (RubpySS·Au) and 130 and 12 ns (83%, 17%) (IrbpySS·Au). The modified surfaces show enhancement of their luminescence lifetime in comparison with solutions of the respective metal complexes, supporting the strong luminescence signal observed and introducing them as ideal inorganic probes for imaging applications. Through the technique of microcontact printing, complexes were assembled in patterns defined by the stamp. Images of the red and green patterns rendered by the RubpySS·Au and IrbpySS·Au monolayers were revealed by luminescence microscopy studies. The potential of the luminescent surfaces to respond to biomolecular recognition events is demonstrated by addition of the dominant blood-pool protein, bovine serum albumin (BSA). Upon treatment of the surface with a BSA solution, the RubpySS·Au and IrbpySS·Au monolayers display a large luminescence signal increase, which can be quantified by time-resolved measurements. The interaction of BSA was also demonstrated by surface plasmon resonance (SPR) studies of the surfaces and in solution by circular dichroism spectroscopy (CD). Overall, the assembly of arrays of designed coordination complexes using a simple and direct $\mu$-contact printing method is demonstrated in this study and represents a general route toward the manufacture of micropatterned optoelectronic devices designed for sensing applications.

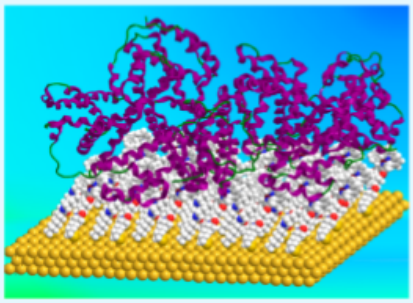

**KEYWORDS:** *imaging, optical active surfaces, printing, luminescence, recognition*

## INTRODUCTION

"Bottom-up" approaches for surface fabrication toward nanoscale devices have flourished in recent years, as "top-down" methods have begun to reach the limits of their potential.[1−5] In particular, microcontact printing ($\mu$CP), initially developed by Whitesides,[6,7] allows controlled deposition of molecules on planar substrates such as gold or glass for the fabrication of surfaces for sensing devices for the detection of analytes.[8−11] Photoactive transition metal complexes offer many attractive properties for imaging applications[12−15] including photostability and excitation and emission profiles within the visible region that are more compatible with conventional imaging techniques and larger Stokes shifts (greater than 100 nm). Luminescent thin films have been developed using noncovalent assembly of photoactive metals via Langmuir−Blodgett methods[16,17] or "layer-by-layer" approaches.[18,19] However, applications of gold surfaces modified with transition metal complexes have been dominated by electrochemical studies[20−22] due to the reported luminescence quenching of the excited state by the gold.[23−25] Despite this, the covalent attachment of metal complexes to gold is attractive as a platform to build recognition sites and develop sensing motifs.

Complexes of ruthenium(II) and in particular iridium(III) have been shown to have significant affinities for biomolecules.[26−29] Albumins especially are popular proteins for employment in immunodiagnostics and devices.[28,30−33] In this paper, we introduce the design of transition metal complexes for stable luminescent films patterned by $\mu$CP, suitable for imaging of the surface pattern and also as surface-immobilized probes for protein binding. In order to produce robust monolayers for use with $\mu$-contact printing techniques, we have designed a lipoic acid based surface attachment on a bipyridine ligand, bpySS (Scheme 1), with a long spacer chain to reduce luminescence quenching from the gold surface. We have examined the formation of monolayers of ruthenium(II), RubpySS, and cyclometalated iridium(III), IrbpySS, bipyridyl complexes on gold and analyzed their photophysical properties for promising optoelectronic device development (Scheme 1). The osmium(II), OsbpySS, monolayers on gold did not show any luminescence and were not further examined. Transition metal complexes have not been used in microcontact printing, and our method for attachment to the surface was used to test the potential formation of stable stamps that can be used in sensing applications. The patterning of

Received: April 17, 2014
Accepted: June 16, 2014
Published: June 16, 2014

**Scheme 1. Transition Metal Complexes for Surface Patterning**

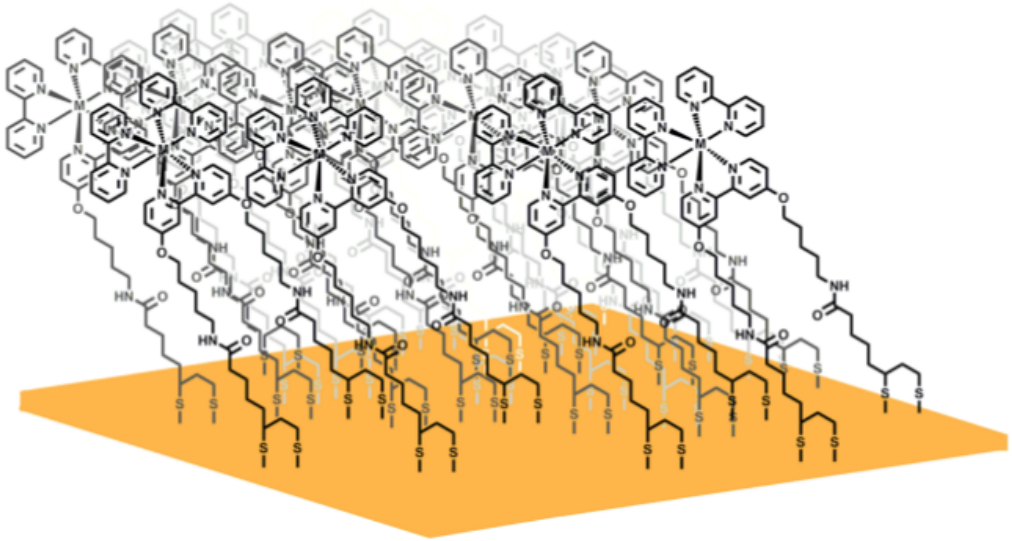

the complexes to surfaces is examined, and luminescence microscopy studies are used to reveal the pattern. The response of the luminescent surfaces to the serum protein bovine serum albumin (BSA) has also been studied.

## EXPERIMENTAL SECTION

**Materials and Methods.** Starting materials were obtained from Sigma-Aldrich, Fluka, Fisher Scientific, or Acros Chemicals and used without any further purification. Dimethylformamide (DMF) was obtained from AGTC Bioproducts Ltd. and dried with 3 or 4 Å molecular sieves before use. Gold slides (30 nm on silicon with 5 nm Ti priming layer) were purchased from Georg Albert PVD, Germany. A Sylgard 184 Elastomer Kit (Dow-Corning) was used to create the polydimethylsiloxane (PDMS) stamps. Flash column chromatography was performed using LC60A 40−63 $\mu$m silica gel. All reactions were performed under a nitrogen atmosphere unless stated otherwise. $Os(bpy)_2Cl_2$ was prepared via the method of Kober et al.[34] (0.69 g, 53%). $[Ir(ppy)_2Cl]_2$ was prepared via a method outlined by Sprouse et al.[35] (0.36 g, 51%). 4,4′-Dihydroxy-2,2′-bipyridine (**4**) was prepared by the method of Gorman et al.[36]

**Instrumentation.** $^1$H NMR spectroscopy was carried out on a Brüker AVIII300 spectrometer. $^{13}$C and 2D NMR spectroscopy was carried out on a Brüker AVIII400 spectrometer. Electrospray mass spectrometry was carried out on a Micromass LC-TOF. MALDI mass spectrometry was carried out on a Micromass MX MALDI-TOF. UV−vis spectroscopy was carried out on a Varian Cary 50 or Cary 5000 spectrophotometer. UV−vis spectra were collected using 1 cm path length quartz cuvettes. Luminescence spectroscopy was carried out by a Photon Technology International luminescence spectrometer with a 75 W xenon arc lamp as the illumination source and also on an Edinburgh Instruments FLS920 steady state and time-resolved spectrometer fitted with an Olympus IX71 inverted microscope. The detection system used incorporated R928 (visible) and R5509-72 (NIR) Hamamatsu photomultiplier tubes. The emission monochromator is fitted with two interchangeable gratings blazed at 500 and 1200 nm. F900 spectrometer analysis software was used to record the data. Luminescence lifetime experiments were carried out using an Edinburgh Instruments EPL-445 or EPL-375 laser as the excitation source. Lifetimes were fitted using Edinburgh Instruments F900 software, with errors of ±10%. Luminescence experiments were carried out using 1 cm path length quartz cuvettes with four transparent polished faces. Degassed samples were obtained by bubbling nitrogen through the cuvettes for 30−40 min. Circular dichroism experiments were carried out on a Jasco J-810 spectropolarimeter using 1 cm path length quartz cuvettes. Surface plasmon resonance studies were carried out on a Reichert SR7500DC surface plasmon resonance (SPR) system at 15 °C. Microwave reactions were performed in a CEM Discovery SP Microwave under open vessel conditions unless otherwise stated.

**Synthetic Procedures.** *4,4′-Di(5-lipoamido-1-pentoxy)-2,2′-bipyridine (bpySS).* A solution of $\alpha$-lipoic acid (0.48 g, 2.3 mmol) and 1-hydroxybenzotriazole hydrate (0.36 g, 2.7 mmol) in dry DMF (8.8 mL) was cooled to 0−5 °C, upon which 1-ethyl-3-(3-(dimethylamino)-propyl)carbodiimide (EDC) (0.41 g, 2.6 mmol) was added and stirred, maintaining this temperature until the EDC had fully dissolved (ca. 1 h). The solution was allowed to warm to room temperature and stirred for a further hour. A solution of *N*-ethylmorpholine (0.27 g, 2.4 mmol) and **6** (0.35 g, 9.8 mmol) in dry DMF (12.3 mL) was added to the reaction mixture and stirred overnight. The resulting cream precipitate was filtered, dried in air, triturated in $CHCl_3$ (150 mL), and isolated by filtration, following washings with $CHCl_3$ (2 × 10 mL) (0.41 g, 39%). Found: C, 58.9; H, 7.1; N, 7.7. Calc. for $C_{36}H_{54}N_4O_4S_4$: C, 58.8; H, 7.4; N, 7.6%. $\delta_H$ (300 MHz; $CDCl_3$) 1.35−1.65 (12 H, m, H-8,9,15), 1.61−1.78 (8 H, m, H-14,16), 1.79−1.96 (6 H, m, H-10, H-18′), 2.17 (4 H, t, $J$ = 7.4, H-13), 2.38−2.50 (2 H, dddd, $J$ = 0.8, 5.6, 6.3, 6.6, H-18), 3.04−3.10 (4 H, m, H-19), 3.20 (4 H, tt, $J$ = 6.1, 6.7, H-11), 3.50−3.61 (2 H, tdd, $J$ = 1.5, 6.5, 6.5, H-17), 4.13 (4 H, t, $J$ = 6.3, H-7), 5.48 (2 H, br s, NH), 6.82 (2 H, dd, $J$ = 5.7, 2.5, H-5), 7.95 (2 H, d, $J$ = 2.5, H-3) and 8.45 (2 H, d, $J$ = 5.7, H-6); $\delta_C$ (100 MHz; $CDCl_3$) 23.4 (C-9), 25.4 (C-14), 28.6 (C-15), 28.9 (C-8), 29.4 (C-10), 34.6 (C-16), 36.5 (C-13), 38.5 (C-19), 39.3 (C-11), 40.2 (C-18), 56.4 (C-17), 67.7 (C-7), 106.8 (C-3), 111.3 (C-5), 150.2 (C-6), 157.8 (C-2), 166.1 (C-4), and 172.7 (C-12); MS (ESI$^+$) $m/z$: 757 (M + Na)$^+$. NMR assignments were confirmed by COSY, HSQC, and HMBC.

*RubpySS.*

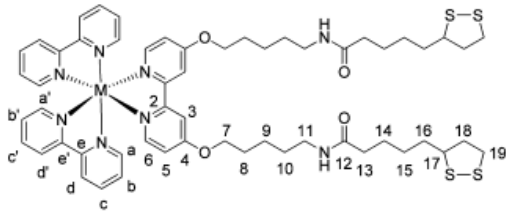

RubpySS was prepared via a modification to a method outlined by Sullivan et al.[37] A solution of bpySS (0.19 g, 0.3 mmol) and $Ru(bpy)_2Cl_2$ (0.13 g, 0.3 mmol) in ethanol (100 mL) was heated under reflux for 16 h. The red/orange solution was cooled to room temperature and concentrated *in vacuo* (~25 mL). $H_2O$ (35 mL) was added, forming a fine cream precipitate, which was filtered. A saturated methanolic solution of ammonium hexafluorophosphate (0.25 g, 1.5 mmol in 2 mL of MeOH) was added to the filtrate to give an orange precipitate. The precipitate was filtered and washed with ice cold $H_2O$ and ice cold $Et_2O$ to give the crude product as an orange/red solid. The solid was dissolved in a minimal amount of acetonitrile and the solvent removed *in vacuo* to give a red crystalline solid RubpySS (0.14 g, 65%). Found: C, 47.2; H, 4.8; N, 7.6. Calc. for $C_{56}H_{70}N_8O_4RuS_4(CH_3CN)_{0.25}$: C, 46.8; H, 4.9; N, 7.8%. $\lambda_{max}$ (MeCN)/nm ($\varepsilon$/dm$^3$ mol$^{-1}$ cm$^{-1}$) 289 (77200) and 461 (14600); $\delta_H$ (300 MHz; $CD_3CN$) 1.29−1.65 (16 H, m, H-8,9,15,16), 1.68−1.78 (4 H, m, H-14), 1.80−1.92 (6 H, m, H-10,18′), 2.11 (4 H, t, $J$ = 7.2, H-13), 2.37−2.49 (2 H, dddd, $J$ = 6.3, 6.6, H-18), 3.02−3.15 (4 H, m, H-19), 3.15−3.21 (4 H, dt, $J$ = 6.7, 6.2, H-11), 3.52−3.61 (2 H, tdd, $J$ = 2.6, 6.3, 6.5, H-17), 4.21 (4 H, t, $J$ = 6.5, H-7), 6.40 (2 H, t, $J$ = 5.1, NH), 6.92 (2 H, dd, $J$ = 6.5, 2.7, H-5), 7.43 (2 H, d, $J$ = 6.5, H-6), 7.43 (2 H, ddd, $J$ = 1.3, 5.8, 7.8, H-b/b′), 7.44 (2 H, ddd, $J$ = 1.3, 5.8, 7.8, H-b/b′), 7.73 (2 H, d, $J$ = 5.8, H-a/a′), 7.85 (2 H, d, $J$ = 5.8, H-a/a′), 8.00−8.10 (4 H, dd, $J$ = 1.3, 7.8, H-c,c′), 8.07 (2H, d, $J$ = 2.7, H-3), and 8.47−8.53 (4 H, d, $J$ = 7.8, H-d,d′); $\delta_C$ (100 MHz; $CD_3CN$) 22.6 (C-9), 25.2 (C-4), 27.8 (C-15), 28.4 (C-8), 28.9 (C-10), 34.2 (C-16), 35.6 (C-13), 38.1 (C-19), 38.2 (C-11), 40.0 (C-18), 56.4 (C-17), 69.6 (C-7), 111.3 (C-3), 114.1 (C-5), 124.0 (C-d,d′), 127.3 (C-b,b′), 137.2 (C-c,c′), 151.5 (C-a/a′), 151.7 (C-a/a′), 151.9 (C-6), 157.1 (C-2/e,e′), 157.2 (C-2/e,e′), and 166.6 (C-12); MS (ESI$^+$) $m/z$: 1294 (M-$PF_6$)$^+$, 574 (M-2($PF_6$))$^{2+}$. NMR assignments were confirmed by COSY, HSQC, and HMBC.

*OsbpySS.* OsbpySS was prepared in a modification to the method outlined by Gaudiello et al.[38] $Os(bpy)_2Cl_2$ (21.8 mg, 0.04 mmol) and bpySS (26.6 mg, 0.04 mmol) were suspended in degassed ethylene glycol (30 mL) and heated under microwave conditions (power = 300 W, $T$ = 250 °C) for 7 min. The green/brown mixture was allowed to cool to room temperature, upon which saturated aqueous ammonium hexafluorophosphate (50 mL) was added. The black precipitate was filtered and washed with copious amounts of $H_2O$ and $Et_2O$, dissolved in a minimal amount of acetone and the solvent removed *in vacuo* to give a black crystalline solid OsbpySS (47.6 mg, 78%). Found: C, 42.9; H, 4.3; N, 7.3. Calc. for $C_{56}H_{70}F_{12}N_8O_4OsP_2S_4(NH_4PF_6)_{0.25}$: C, 42.9; H, 4.6; N, 7.4%. $\lambda_{max}$ (MeCN)/nm ($\varepsilon$/dm$^3$ mol$^{-1}$ cm$^{-1}$) 292 (77300), 334 (13600), 459 (13700), and 487 (13500); $\delta_H$ (300 MHz; $CD_3CN$) 1.28−1.61 (16 H, m, H-8,9,15,16), 1.61−1.68 (4 H, m, H-14), 1.74−1.89 (6 H, m, H-10,18′), 2.04−2.12 (4 H, m, H-13), 2.32−2.47 (2 H, dddd, $J$ = 6.1, 6.3, H-18), 2.98−3.04 (4 H, m, H-19), 3.04−3.21 (4 H, td, $J$ = 6.1, 6.8, H-11), 3.49−3.60 (2 H, m, H-17), 4.19 (4 H, t, $J$ = 6.5, H-7), 6.35 (2 H, t, $J$ = 4.8, NH), 6.85 (2 H, dd, $J$ = 6.5, 2.7, H-5), 7.19−7.34 (4 H, ddd, $J$ = 1.3, 5.8, 7.8, H-b,b′), 7.23 (2 H, d, $J$ = 6.5, H-6), 7.61 (2 H, d, $J$ = 5.8, H-a/a′), 7.73 (2 H, d, $J$ = 5.8, H-a/a′), 7.79 (4 H, dd, $J$ = 7.8, 1.3, H-c,c′), 8.00 (2 H, d, $J$ = 2.7, H-3), and 8.43 (4 H, t, $J$ = 6.8, H-d,d′); $\delta_C$ (100 MHz; $CD_3CN$) 22.3 (C-9), 24.9 (C-4), 27.6 (C-15), 28.2 (C-8), 28.6 (C-10), 34.0 (C-16), 35.3 (C-13), 38.0 (C-11,19), 39.8 (C-18), 56.1 (C-17), 69.4 (C-7), 111.2 (C-3), 114.2 (C-5), 123.9 (C-d,d′), 127.6 (C-b,b′), 136.2 (C-c,c′), 150.2 (C-6/a/a′), 150.6 (C-6/a/a′), 150.9 (C-6/a/a′), 159.0 (C-2/e,e′), 159.3 (C-2/e,e′), and 165.9 (C-12); MS (ESI$^+$) $m/z$: 1383 (M-$PF_6$)$^+$. NMR assignments were confirmed by COSY, HSQC, and HMBC.

*IrbpySS.*

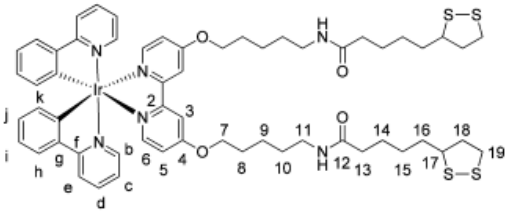

IrbpySS was synthesized via a modified method outlined by Slinker et al.[39] $[Ir(ppy)_2Cl]_2$ (66.6 mg, 0.06 mmol) and bpySS (100.8 mg, 0.14 mmol) was suspended in ethylene glycol (6.5 mL) and heated to 150 °C for 19 h. The yellow mixture was allowed to cool to room temperature, upon which $H_2O$ (150 mL) was added, and the mixture heated to 60−70 °C. Saturated aqueous ammonium hexafluorophosphate (1 g in 2.5 mL $H_2O$) was added, immediately forming a yellow precipitate, which was cooled on ice, filtered, and washed with $H_2O$. The solid was dissolved in minimal acetone and the solvent removed *in vacuo* to give IrbpySS (103.8 mg, 61%). Found: C, 50.4; H, 5.5; N, 5.9. Calc. for $C_{58}H_{70}F_6IrN_6PS_4$: C, 50.5; H, 5.1; N, 6.1%. $\lambda_{max}$ (MeCN)/nm ($\varepsilon$/dm$^3$ mol$^{-1}$ cm$^{-1}$) 224 (44800), 255 (50000), and 342sh (8200); $\delta_H$ (300 MHz; acetone-$d_6$) 1.21−1.50 (16 H, m, H-8,9,15,16), 1.50−1.61 (4 H, m, H-14), 1.66−1.81 (6 H, m, H-10,18′), 2.01 (4 H, t, $J$ = 7.1, H-13), 2.25−2.38 (2 H, dddd, $J$ = 0.9, 5.9, 6.3, 6.7, H-18), 2.90−3.05 (8 H, m, H-19), 3.09 (4 H, td, 6.5, 6.0), 3.37−3.47 (2 H, m, H-17), 4.17 (4 H, t, $J$ = 6.4, H-7), 6.21 (2 H, d, $J$ = 7.6, H-k), 6.75 (2 H, td, $J$ = 1.3, 7.5, H-j), 6.88 (2 H, td, $J$ = 1.3, 7.5, H-i), 6.95 (2 H, t, $J$ = 5.5, NH), 7.06 (2 H, dd, $J$ = 1.3, 5.8, H-d), 7.08 (2 H, dd, $J$ = 2.5, H-5), 7.69 (2 H, d, $J$ = 6.4, H-6), 7.72−7.78 (4 H, m, H-e,h), 7.83 (2 H, dd, $J$ = 1.3, 8.0, H-c), 8.10 (2 H, d, $J$ = 8.0, H-b), and 8.29 (2 H, d, $J$ = 2.5, H-3); $\delta_C$ (100 MHz; acetone-$d_6$) 23.7 (C-9), 26.3 (C-4), 28.9 (C-15), 29.3−30.4 (C-8, masked by NMR solvent), 35.4 (C-16), 36.6 (C-13), 39.1 (C-19), 39.2 (C-11), 41.0 (C-18), 57.3 (C-17), 70.4 (C-7), 112.7 (C-6), 115.2 (C-5/d), 120.6 (C-b), 123.1 (C-j), 124.4 (C-5/d), 125.8 (C-3/k), 131.1 (C-i), 132.6 (C-h), 139.3 (C-c), 145.0 (C-f), 152.0 (C-g), 152.3 (C-3/k), 154.2 (C-e), 158.5 (C-2), 168.3 (C-4), 168.8 (C-a), and 172.8 (C-12); MS (ESI$^+$) $m/z$: 1235 (M-$PF_6$)$^+$. NMR assignments were confirmed by COSY, HSQC, and HMBC.

**Surface Preparation.** Gold substrates were cleaned using a UVO cleaner (1 h) and immersed in MeCN for at least 10 min before use. Slides were immersed in a 1 mM solution of complex and 2 mM TCEP·HCl (1:1 MeCN/$H_2O$) and sealed from the outside atmosphere to prevent solvent evaporation. The slides were left immersed for a stipulated amount of time, before immersion in clean MeCN and drying under $N_2$.

**Micropatterning Surface via the Micro-Contact Printing Method.** Gold slides were cleaned by the general method described above. Stamps were made as per the method outlined by Whitesides et al.[40] from PDMS. PDMS/PDMS curing agent (9:1) was mixed for 10 min and poured onto the masters. The mixture was allowed to cure at room temperature for 1 h, and the bubbles that formed on the top of the mixture were removed manually. The mixture was then cured in the oven at 60 °C for 1 h. The PDMS stamps were peeled away from the masters and cut into shape. The stamps were then oxidized by UVO cleaner (1 h) and immersed in MeCN for 10 min. The stamps with inked by immersion in a 5 mM solution of complex and 10 mM TCEP·HCl (1:1 MeCN/$H_2O$) for 30 min before drying under $N_2$. The stamps were placed firmly (with the aid of a small weight) on the clean gold slides (~12 kPa) for 16 h before peeling the stamp away to leave the micropatterned surface. The slides were then washed by immersion in clean MeCN and dried under $N_2$.

**Procedure for SPR Studies.** Gold chips (50 nm on glass, Reichert) were cleaned in Piranha solution *(CAUTION: Piranha solution reacts violently with organic material)* for 10 min, washed with ultrahigh purity (UHQ 18 MΩ cm) water followed by ethanol, and stored in ethanol until used. During the experiments, the chips were equilibrated in the solvent system used for each experiment for at least 10 min to ensure a steady baseline. The system was then injected with the appropriate solution at an initial flow rate of 1500 $\mu$L min$^{-1}$ followed by a flow rate of 10 or 0 $\mu$L min$^{-1}$. The slides were then washed with the solvent system at a flow rate of 1500 $\mu$L min$^{-1}$.

X-ray photoelectron spectroscopy was carried out at the University of Leeds by Dr. Benjamin Johnson. The instrument is a VG ESCAlab 250 with a monochromated Al K$\alpha$ source. Experiments were performed in UHV (~$10^{-10}$ mbar). Survey scans were recorded at a pass energy of 150 eV, detailed scans at 20 eV. Offline analysis of the spectra was performed using Casa 2.3.15 XPS software.

**Scheme 2. Synthetic Route for Preparation of RubpySS, IrbpySS, and OsbpySS**

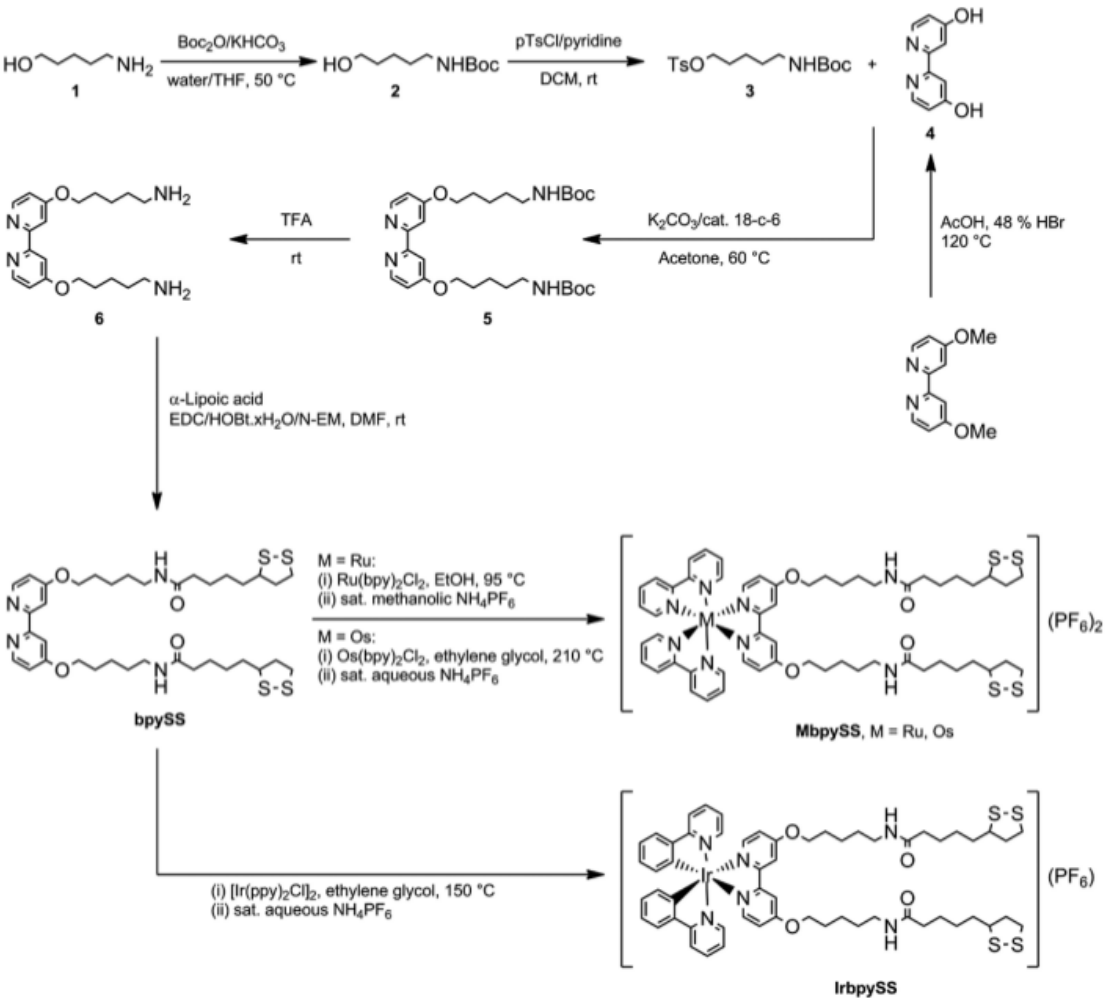


## RESULTS AND DISCUSSION

**Synthesis.** The ligand explored in this study was synthesized by appending 5-amino-1-pentanol 'legs' to dihydroxy-2,2′-bipyridine, followed by an amide coupling with α-lipoic acid to yield the surface-active bpySS ligand (Scheme 2).

The ruthenium(II) and osmium(II) complexes were synthesized by reaction of $M(bpy)_2Cl_2$ (M = Ru,Os) with the bpySS ligand followed by precipitation with $NH_4PF_6$ (Scheme 2). The cyclometalated iridium(III) complex was synthesized via reaction of the bpySS ligand with $[Ir(ppy)_2Cl]_2$, followed by precipitation with $NH_4PF_6$. All complexes were synthesized with acceptable (60−80%) yields and fully characterized by $^1H$ and $^{13}C$ NMR spectroscopy, mass spectrometry, elemental analysis, and UV−visible absorption spectroscopy (Supporting Information).

**Photophysical Properties of RubpySS, IrbpySS, and OsbpySS in Solution.** The absorption and luminescence properties of the complexes are summarized in Table 1. The absorption spectrum of RubpySS shows two characteristic absorption bands at 289 and 461 nm, corresponding to the $^1(\pi-\pi^*)$ and singlet metal-to-ligand charge transfer ($^1$MLCT) bands, respectively (Supporting Information). OsbpySS has a similar absorption spectrum, with two absorption bands at 292 and 487 nm, in agreement with similar osmium(II) complexes.[41−43] It is noteworthy that the $^1$MLCT bands of RubpySS and OsbpySS are red-shifted by 9 and 5 nm, respectively, compared to tris-bipyridyl analogues of each of the complexes, in agreement with other complexes with 4,4′-disubstituted bipyridine ligands with electron donating substituents, as evidenced by 4,4′-dimethoxy bipyridyl ruthenium(II) complexes.[41,44,45] The absorption spectrum of IrbpySS shows a peak in the UV region, centered at 255 nm, in agreement with other iridium(III) complexes with functionalized bipyridyl ligands.[46,47] The luminescence properties of the complexes are summarized in Table 1. IrbpySS has the highest energy emission state, with an emission maximum at 580 nm, comparable to similar iridium(III) complexes,[15,39,48] originating from significant mixing between the $^3\pi-\pi^*$, $^1$MLCT, and $^3$MLCT states due to spin−orbit coupling.[35,39,49] The luminescence spectra

**Table 1. Absorption and Luminescence Properties of Metal Complexes**

| complex | $\lambda_{max}$/nm ($\varepsilon$/$10^4$ $M^{-1}$ $cm^{-1}$) | $\lambda_{em}$/nm | $\tau$/ns | | $\Phi$/% | |
|---|---|---|---|---|---|---|
| | | | aerated | deaerated | aerated | deaerated |
| RubpySS | 289 (7.8), 323 (1.3), 461 (1.5) | 645 | 130 | 707 | 1 | 4 |
| OsbpySS | 292 (7.7), 317 (1.3), 487 (1.4) | 790 | 20 | 25 | 0.1 | 0.1 |
| IrbpySS | 255 (5.0), 298 (1.8) sh, 337 (0.8) sh | 580 | 25 (68%) 80 (32%) | 35 (34%) 246 (66%) | 0.5 | 3 |
| $[Ru(bpy)_3]Cl_2$ | 452 (1.3)[54] | 615[54] | 172 | 840 | 1 | 10 |
| $[Os(bpy)_3](PF_6)_2$ | 482 (1.1) | 723 | 39 | 58 | 0.3 | 0.5 |
| $[Ir(ppy)_2(dtb\text{-}bpy)](PF_6)$[a] | | 580[39] | 65[39] | 557[39] | | 24[39] |

[a]dtb-bpy = 4,4′-di-*tert*-butyl-2,2′-bipyridine.

of RubpySS and OsbpySS show $^3$MLCT based broad emission centered at 645 and 790 nm, respectively. Both spectra are significantly red-shifted from their tris-bipyridyl analogues (30 and 67 nm, respectively), suggesting that the bulky moieties have a stabilizing effect on the excited state, in agreement with other similar ruthenium(II) and osmium(II) complexes.[44,45,50,51] The range of emission profiles of the three complexes, from the yellow of iridium to the far red of ruthenium and osmium, implies their usefulness in participating as donor/acceptor photoactive units (Figure 1) in

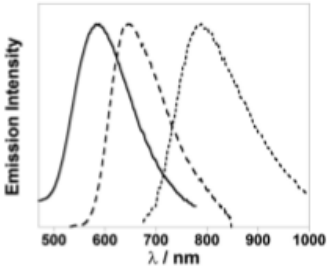


**Figure 1.** Photoluminescence emission spectra of IrbpySS (solid line, $\lambda_{exc}$ = 280 nm), RubpySS (long dash line, $\lambda_{exc}$ = 465 nm), and OsbpySS (short dash line, $\lambda_{exc}$ = 491 nm) in acetonitrile solutions. Spectra corrected for instruction response for detection. Intensities are not to scale.

energy cascades, as has been reported previously for supramolecular systems.[52,53] The complexes possess lifetimes characteristic of the nature of their excited states. The longer lifetimes of RubpySS and IrbpySS solutions in deaerated conditions demonstrate the extent of $^3O_2$ quenching of their excited states.

**Immobilization of RubpySS, IrbpySS, and OsbpySS on Gold Surfaces.** To study the surface attachment of the metal complexes on gold, ellipsometric, surface plasmon resonance, and X-ray photoelectron spectroscopy (XPS) studies were carried out. Surfaces were treated with aqueous acetonitrile (1:1) solutions of the complexes with two equivalents of a reducing agent, *tris*-(2-carboxyethyl)phosphine hydrochloride ($TCEPH^+Cl^-$) added to aid the reduction of the disulfide attachments. The time-resolved ellipsometric plots of monolayer formation on gold for RubpySS and IrbpySS show an increase in layer thickness over a period of 10 min, with full coverage achieved within 30 min (Figure 2a,b). A 24 h study confirms the stability of the RubpySS·Au monolayer (Supporting Information). The layer thickness at 30 min is 1.8 ± 0.1 nm for RubpySS·Au and 1.7 ± 0.1 nm for IrbpySS·Au. These values were compared with simplified models of the height of the complexes on planar surfaces, at a tilt angle of 40° reported for lipoic acid[55] (Figure 2d) and were found to be in good agreement (ca. 2 nm) with the experimental values obtained. These results also agree well with ellipsometric results from the growth of a palladium film formed by a layer-by-layer method.[56]

Surface plasmon resonance (SPR) spectroscopy studies were performed to examine the formation of monolayers of RubpySS·Au and IrbpySS·Au on gold substrates. SPR studies measure a change in refractive index, which is calculated from the angle of minimum intensity from a light source which is shined at a prism on the back of a gold sensor chip. This change in refractive index at the surface is due to adsorbates coming into proximity with the surface of the sensor chip. For larger adsorbates such as proteins, this change is generally high (ca. 0.4° or 4000 $\mu$RIU where RIU = refractive index unit),[57−59] with smaller adsorbates expected to have lower responses, as molecular weight can contribute to the response.[60] Adsorption kinetics for adsorbates with molecular weights as low as hexadecanethiol have been previously studied.[61] The solid lines (Figure 2c) show the kinetics of adsorption of a 1 mM RubpySS or IrbpySS solution in 1:1 acetonitrile/water. For RubpySS, we observe an increase in response units over 30 min from 0 to 0.30°, showing an association of the complex with the substrate. Subsequent washing in clean 1:1 acetonitrile/water at a flow rate of 1500 $\mu$L $min^{-1}$ followed by 10 min at a flow rate of 50 $\mu$L $min^{-1}$ shows that some complex is specifically adsorbed to the surface, with an average response of 0.20° even after solvent wash, which we expect for smaller adsorbates.[61] A similar trend is observed for IrbpySS, with the response increasing over 30 min from 0 to 0.37°. Following the wash step, the signal drops to 0.31°, also indicative of specific binding to the gold substrate. Control studies were also conducted, examining any possible adsorption of reducing agent or solvent effect (Figure 2c). The $TCEPH^+Cl^-$ control shows that there is some association during the course of the experiment, but it is only nonspecifically adsorbed, with all of the reducing agent being removed to leave 0.05° following a wash in clean solvent. The clean solvent control also shows negligible adsorption (0.05°) to the substrate within experimental error. These results confirm the stability of the monolayer as shown in the ellipsometric studies, with the same final response units recorded for RubpySS·Au (ca. 0.19°) after 30 min or 24 h (Supporting Information).

XPS analysis of the RubpySS·Au and IrbpySS·Au monolayers reveals the presence of each of the elements present in the complexes on gold. The Ru $3d_{5/2}$ and $3d_{3/2}$ photoelectron peaks present at 281.1 and 286.1 eV, respectively, while the Ir $4f_{7/2}$ and $4f_{5/2}$ peaks appear at 61.8 and 64.8 eV, respectively (Supporting Information). The RubpySS·Au monolayer was examined under two preparation routes, with and without treatment using $TCEPH^+Cl^-$. The S 2p region of the spectrum of the monolayer RubpySS·Au without the $TCEPH^+Cl^-$ treatment shows only two environments, with S $2p_{3/2}$ peaks at 161.6 and 163.1 eV corresponding to thiolate (66%) and disulfide (34%), respectively, previously assigned for thioctic acid monolayers.[55] A monolayer of RubpySS·Au treated with $TCEPH^+Cl^-$ also

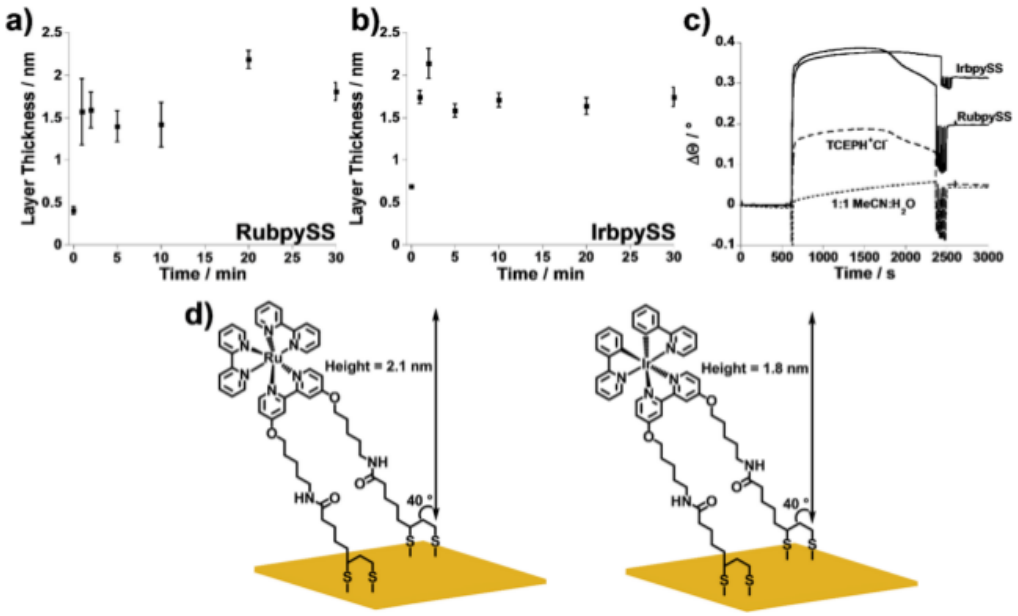


**Figure 2.** Plot of ellipsometric data for time dependence of monolayer formation of (a) RubpySS and (b) IrbpySS. (c) SPR sensorgram to monitor monolayer formation of IrbpySS (1 mM), RubpySS (1 mM), control solution ($TCEPH^+Cl^-$), dotted line (2 mM), and solvent control (1:1, $H_2O$/$CH_3CN$) on a gold substrate over 30 min. Solutions were injected across clean gold surfaces. (d) Schematic of RubpySS·Au and IrbpySS·Au adhered to gold substrates.

shows only two environments at the same peak positions with a thiolate (75%) and disulfide (25%), respectively (Figure 3).

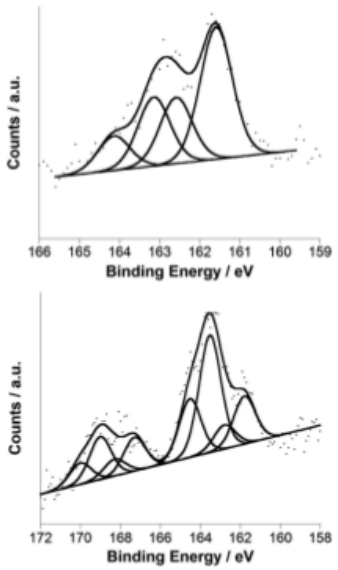


**Figure 3.** XPS S 2p spectra of RubpySS·Au (top) and IrbpySS·Au (bottom). Recorded spectra (dots) are fitted with linear backgrounds and show curve fitting components (solid lines).

These results show that the great majority of the disulfide anchors are reduced to thiolate to bind to gold and that the treatment with the reducing agent has a small effect on thiolate formation. The estimated Ru/S ratio from the peaks is 1:4 which is in agreement with the molecular formula of the complex.

The S 2p region of the spectrum of the IrbpySS·Au reveals the S $2p_{3/2}$ peaks at 161.8 and 163.5 eV with an additional peak identified as oxidized sulfur between 167 and 169 eV (Figure 3). The peaks at 161.8 and 163.5 eV are assigned to thiolate and disulfide species as previously reported.[55] The peak of the oxidized species is usually attributed to sulfonate; the peak can be fitted to two environments at 167.3 and 169.0 eV.[62] For this monolayer, 48% of the overall sulfur region exists in the disulfide form. The oxidized species account for 32% of the total sulfur. The peaks for C 1s, N 1s, and O 1s for both complexes were also observed. The formation of oxidized species has been observed previously[62] and has been shown to be eliminated by longer monolayer assembly times. Although the difference of the binding mode of the anchoring group in RubpySS·Au and IrbpySS·Au monolayers is not apparently linked to the preparation method, it is clear that in both cases the metal complex is bound to the gold surface.

Monolayer samples of RubpySS·Au and IrbpySS·Au display the characteristic charge transfer based emission at 630 and 532 nm, respectively (Figure 4). Blue-shifts of 15 and 48 nm for RubpySS·Au and IrbpySS·Au occur, respectively, from the solution spectra. A similar trend is also observed for the powder spectra of RubpySS and IrbpySS, with blue-shifts of 4 and 26 nm from the solution spectra, respectively. Neat solid iridium(III) complexes with blue-shifts similar to that observed in acetonitrile solutions have been previously reported,[15] as have those for similar ruthenium(II) complexes.[63] For the case of ruthenium-(II) complexes, these shifts are attributed to the lack of solvent influence in the stabilization of the charge transfer states and

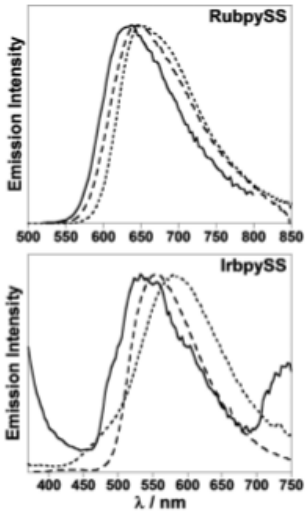


**Figure 4.** Overlays of luminescence spectra of RubpySS (top), $\lambda_{exc}$ = 465 nm, and IrbpySS (bottom), $\lambda_{exc}$ = 360 nm; monolayer (solid line), powder (long dash line), and solution in acetonitrile (short dash line). Emission spectra corrected for instrument response for detection. Intensities are not to scale.

possibly the effect of lack of free movement of the complexes. The blue shifts on the surface indicate the influence of the anchoring to the substrate, resulting in a reduction in vibronic coupling associated with excited states in the solution and thus leading to a tightening of the excited state bands which renders the transition higher in energy. The excitation spectra show similar $\lambda_{max}$ values to those of solution samples, with no discernible shifts in the bands of the spectra. OsbpySS·Au monolayers on gold surfaces were also prepared; however, luminescence from these surfaces was too weak to detect.

The luminescence lifetime of the RubpySS·Au monolayer is 210 ns (Table 2), which is considerably longer than the aerated solution (130 ns), and comparable to the powder (200 ns). This enhancement of lifetime is in contrast to previous studies that quenching of ruthenium(II) emission was observed when at small distances (within ca. 10 nm) of the surface.[23,64] The luminescence lifetime of IrbpySS·Au on the surface was calculated to be biexponential, with a long component of 130 ns (83%) and a short component of 12 ns (17%). These lifetimes are longer than those calculated in aerated solution (25, 80 ns) and again comparable to that of the powder (110, 30 ns). These results suggest that not only is there no quenching from the gold surface but also there is enhancement of luminescence compared with solutions of the complexes. The luminescence signal is also strong enough to allow luminescence microscopy images of the monolayers of the complexes to be collected (Supporting Information).

To demonstrate the usefulness of transition-metal complex systems in lab-on-chip opto-responsive devices, we used the microcontact printing method outlined by the group of Whitesides.[40] Such formed stamps from transition metal complexes can be used in sensing applications if the metal complex is firmly attached to the surface and does not wash away during cleaning steps designed to remove unbound complexes.

Poly(dimethylsiloxane) (PDMS) stamps patterned with 10 $\mu$m-wide inking areas were inked with 5 mM RubpySS or IrbpySS and 10 mM $TCEPH^+Cl^-$ for 30 min by immersion in a 1:1 acetonitrile/water solution, followed by drying and stamping

**Table 2. Photoluminescence Data for Interaction of Complexes with 10 Mol Equiv of BSA[a]**

| complex | τ/ns | |
|---|---|---|
| | before BSA addition | after BSA addition |
| RubpySS in 0.5% $CH_3CN$ in water | 210 | 84 (4%), 250 (96%) |
| IrbpySS in 0.5% $CH_3CN$ in water | 15 | 37 (8%), 283 (92%) |
| $[Ru(bpy)_3]^{2+}$ in 0.5% $CH_3CN$ in water | 393 | 387 |
| RubpySS·Au surface | 210 | 283 |
| IrbpySS·Au surface | 12 (17%), 130 (83%) | 15 (30%), 170 (70%) |

[a]Concentrations of complexes, ca. 1 $\mu$M. Surfaces immersed in 15 $\mu$M solution of BSA for 30 min.

for 16 h. Luminescence microscopy of the patterned surfaces shows emission from ruthenium iridium(III) complexes, revealing that the patterning was successful. In the image of the RubpySS·Au pattern (Figure 5), the lines show brighter spots

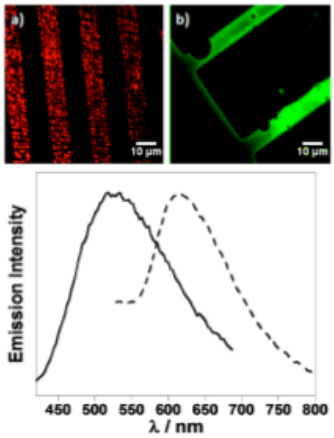


**Figure 5.** (Top) Luminescence microscope images of patterned complexes on gold substrates. (a) RubpySS·Au; (b) IrbpySS·Au. (Bottom) Steady state emission spectra of stamped surfaces. Solid line, IrbpySS·Au; dashed line, RubpySS·Au. Spectra corrected for instrument response for detection. Intensities are not to scale.

that may originate from the stamping process or the quality of the features of the stamp. The image of stamped IrbpySS (Figure 5) reveals the 10 $\mu$m wide areas and illustrates that many patterns can be utilized in order to create functional devices. Luminescence spectroscopy studies (Figure 5) of the patterned complexes confirm the distinct $^3$MLCT emission from the ruthenium(II) center and emission from the iridium(III) center.

We noted that, in order to create more robust patterns, the stamping time is considerably longer than those of simple alkanethiols. Luminescence microscopy of different substrates with stamping times up to 2 h often led to most or all of the complex being removed from the surface during the washing stage. We speculate that this could be due to lipophilic interactions with the legs of the complexes due to the innately higher concentrations of complex at the stamp surface that inhibits the gold−thiolate interaction. We believe that this observation also contributes to some defect formation in the finished patterns, as shown by the round defects in the IrbpySS pattern.

**Biomolecular Recognition Studies on Surfaces and in Solution.** The interaction of the modified gold monolayers

RubpySS·Au and IrbpySS·Au with bovine serum albumin (BSA) was studied by SPR and luminescence spectroscopy, accompanied by solution steady state and time-resolved emission spectroscopy, as well as circular dichroism spectroscopy. To monitor the changes on the gold surfaces upon BSA addition, we employed SPR studies. A solution of BSA (15 $\mu$M in water) was added to monolayers of RubpySS·Au and IrbpySS·Au, and the SPR response was recorded (Figure 6). A large change in $\Delta\Theta$ was

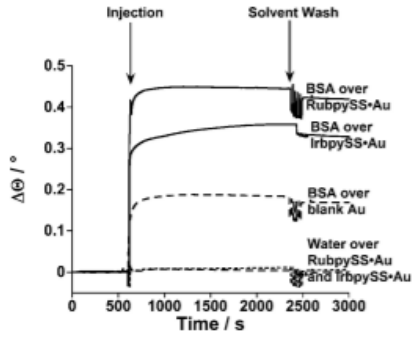


**Figure 6.** SPR sensograms of BSA injected across monolayers of RubpySS·Au or IrbpySS·Au (solid line), BSA injected across a blank gold substrate (long dash line), and a blank solution of water injected across a monolayer of RubpySS·Au or IrbpySS·Au (short dash line).

observed for both surfaces upon introduction of BSA, displaying an increase of more than double the interaction of BSA with clean gold surfaces. We speculate that this affinity is most likely due to two possible factors, (a) hydrophobic interactions in the binding pockets of BSA, such as fatty acid binding sites III and IV, which can change shape and accommodate up to six fatty acid chains through nonpolar interactions[65,66] and (b) Coulombic interactions through an increase of the net positive charge at the surface. Upon injection of water across monolayers of RubpySS·Au and IrbpySS·Au used as a control study, we observe no increase in response, confirming that the change in response is only due to specific adsorption of BSA molecules.

The interaction of the BSA was also studied by the change in the environment of the metal complex using luminescence lifetime measurements. Addition of a solution of BSA (15 $\mu$M in water) to RubpySS·Au and IrbpySS·Au monolayers was monitored by the luminescence lifetime decays (Table 2). Upon interaction with BSA, we observe a luminescence lifetime increase for IrbpySS·Au monolayers, with the major component increased from 130 to 170 ns, indicating that interactions between the complex and BSA occur when anchored to gold substrates. This change is expected on the basis of charge transfer state character of the complex, which is sensitive to changes in the environment and consequently to interactions with BSA. In solution experiments, where 10 mol equiv of BSA was added to ca. 1 $\mu$M solutions of IrbpySS or RubpySS, a similar trend is observed for IrbpySS, with an increase in luminescence lifetime from 15 ns to 37 and 283 ns. Similar results for iridium(III) complexes have also been reported where binding occurs through hydrophobic chains and indole moieties specific to the binding of BSA that lead to increased lifetimes and emission intensities due to the increased hydrophobicity of the iridium(III) environment.[67] The lifetime of RubpySS·Au monolayers increased from 210 to 283 ns upon immersion in BSA solutions, and a change in solution experiments also indicated some binding, with the lifetime changing from monoexponential in solution (210 ns) to biexponential upon addition of BSA (84, 250 ns) (Table 2). No observable change in luminescence lifetime was observed when solution samples of the control complex $[Ru(bpy)_3]Cl_2$ were examined (Table 2).

To monitor the interaction of the metal complexes with BSA in solutions independently, we studied the effect of BSA addition to the luminescence signal of the metal complex. Solutions of IrbpySS displayed a large 80-fold increase in the integrated emission intensity signal corrected for BSA absorption at 350 nm (Figure 7) with a concurrent 13 nm blue shift. The luminescence

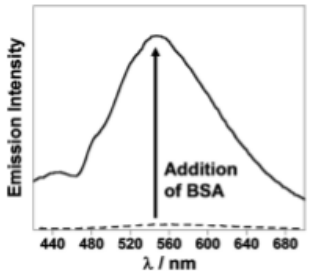


**Figure 7.** Steady state emission spectra of IrbpySS (0.7 $\mu$M) solution before (long dash line) and after (solid line) BSA (15 $\mu$M) addition. Spectra corrected for instrument response for detection. $\lambda_{exc}$ = 350 nm.

signal of RubpySS was less affected; a 90% increase was observed upon BSA addition. The signal of complex $[Ru(bpy)_3]Cl_2$ changed only by 30%.

To further demonstrate the biomolecular interactions in solution, circular dichroism spectroscopy was employed. The spectra (Figure 8) show the presence of BSA, with two negative

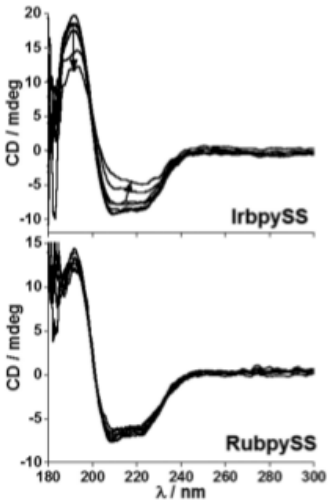


**Figure 8.** Circular dichroism spectra of BSA (0.1 $\mu$M) with the additions of IrbpySS (100 $\mu$M) (top) in 0.1, 0.4, 0.8, 4.1, 8.2, 41.0, and 82.2 equiv and RubpySS (100 $\mu$M) (bottom) in 0.1, 0.4, 0.8, 4.0, 8.1, 40.5, and 81.0 equiv.

peaks at 209 and 222 nm, as well as a positive peak at 190 nm.[68] Upon the sequential addition of a solution of IrbpySS (10 $\mu$M), a

decrease in intensity of these peaks is observed, indicating change on the structural features of the protein, attributed to interaction with IrbpySS. In contrast, we see no interaction between BSA and RubpySS (Figure 8) or $[Ru(bpy)_3^{2+}]$ (Supporting Information). We speculate that the stronger interaction of IrbpySS is assisted by the more hydrophobic nature of iridium increasing the hydrophobic interactions with BSA and allowing the complex to bind into a cavity, changing the secondary structure of the BSA.

## CONCLUSIONS

We have presented three novel luminescent transition metal complexes with surface-active moieties designed to attenuate quenching associated with luminescent thin films on planar metal surfaces. The results show that not only is quenching reduced but also the luminescence lifetimes of the complexes are enhanced when the complexes are anchored to gold surfaces. We have shown that complexes of this type can be patterned directly using a simple stamping methodology and explored the possibility of multimodal sensing applications of these surfaces using SPR and luminescence studies in the detection of bovine serum albumin. The iridium(III) monolayers show the most sensitive response upon protein binding based on luminescence detection, and they can also be used for sensing by SPR, proving the concept of multimodal detection. Future studies will invariably be focused on improving these systems with novel designs for the remaining bipyridine/phenylpyridine ligands to create complexes with specific sensing properties for antibodies and other biomolecules. The stability of these complexes to stamping makes the methodology attractive for developing surfaces in optoelectronic lab-on-chip devices, that incorporate flow systems or other platforms in which luminescence can be introduced as a very sensitive detection method together with SPR. Luminescence imaging can provide very sensitive detection in lab-on-chip devices for multianalyte binding fabricated with microcontact printing methods.

## ASSOCIATED CONTENT

### Supporting Information

Synthetic methodology of the reactions for preparation of the ligand, 2D NMR and UV−vis spectra of the complexes, additional circular dichroism spectra, control ellipsometry data, and further XPS spectra showing all the regions. This material is available free of charge via the Internet at http://pubs.acs.org/.

## AUTHOR INFORMATION

### Corresponding Author

*E-mail: z.pikramenou@bham.ac.uk.

### Notes

The authors declare no competing financial interest.

## ACKNOWLEDGMENTS

The authors would also like to thank Dr. Benjamin Johnson (University of Leeds) and Leeds EPSRC Nanoscience and Nanotechnology Facility (LENNF) for performing and fitting XPS experiments and also Prof. Paula M. Mendes and Dr. Chun Yeung for the provision of silicon masters with which to produce the PDMS stamps used in this work. We acknowledge the EPSRC, The Leverhulme Trust and the School of Chemistry, University of Birmingham for funding. Some of the spectrometers used in this research were obtained through Birmingham Science City: Innovative Uses for Advanced Materials in the Modern World (West Midlands Centre for Advanced Materials Project 2), with support from Advantage West Midlands (AWM) and partial funding from the European Regional Development Fund (ERDF).

## REFERENCES

(1) Fahrenbach, A. C.; Warren, S. C.; Incorvati, J. T.; Avestro, A.-J.; Barnes, J. C.; Stoddart, J. F.; Grzybowski, B. A. Organic Switches for Surfaces and Devices. *Adv. Mater.* **2013**, *25*, 331−348.

(2) Puigmarti-Luis, J.; Rubio-Martinez, M.; Imaz, I.; Cvetkovic, B. Z.; Abad, L.; Perez del Pino, A.; Maspoch, D.; Amabilino, D. B. Localized, Stepwise Template Growth of Functional Nanowires from an Amino Acid-Supported Framework in a Microfluidic Chip. *ACS Nano* **2014**, *8*, 818−826.

(3) Gong, Y.; Yang, S.; Zhan, L.; Ma, L.; Vajtai, R.; Ajayan, P. M. A Bottom-up Approach to Build 3d Architectures from Nanosheets for Superior Lithium Storage. *Adv. Funct. Mater.* **2014**, *24*, 125−130.

(4) Guo, X.; Ying, Y.; Tong, L. Photonic Nanowires: From Subwavelength Waveguides to Optical Sensors. *Acc. Chem. Res.* **2014**, *47*, 656−666.

(5) Love, J. C.; Estroff, L. E.; Kriebel, J. K.; Nuzzo, R. G.; Whitesides, G. M. Self-Assembled Monolayers of Thiolates on Metals as a Form of Nanotechnology. *Chem. Rev.* **2005**, *105*, 1103−1169.

(6) Perl, A.; Reinhoudt, D. N.; Huskens, J. Microcontact Printing: Limitations and Achievements. *Adv. Mater.* **2009**, *21*, 2257−2268.

(7) Xia, Y.; Rogers, J. A.; Paul, K. E.; Whitesides, G. M. Unconventional Methods for Fabricating and Patterning Nanostructures. *Chem. Rev.* **1999**, *99*, 1823−1848.

(8) Demming, A.; Osterbacka, P. R.; Han, D. J.-W. Nanotechnology in Paper Electronics. *Nanotechnology* **2014**, *25*, 090201−090201.

(9) Dorokhin, D.; Hsu, S.-H.; Tomczak, N.; Reinhoudt, D. N.; Huskens, J.; Velders, A. H.; Vancso, G. J. Fabrication and Luminescence of Designer Surface Patterns with beta-Cyclodextrin Functionalized Quantum Dots Via Multivalent Supramolecular Coupling. *ACS Nano* **2010**, *4*, 137−142.

(10) Basabe-Desmonts, L.; Reinhoudt, D. N.; Crego-Calama, M. Design of Fluorescent Materials for Chemical Sensing. *Chem. Soc. Rev.* **2007**, *36*, 993−1017.

(11) Liebau, M.; Huskens, J.; Reinhoudt, D. N. Microcontact Printing with Heavyweight Inks. *Adv. Funct. Mater.* **2001**, *11*, 147−150.

(12) Rogers, N.; Claire, S.; Harris, R.; Farabi, S.; Zikeli, G.; Styles, I.; Hodges, N.; Pikramenou, Z. High Coating of Ru(II) Complexes on Gold Nanoparticles for Single Particle Luminescence Imaging in Cells. *Chem. Commun.* **2014**, *50*, 617−619.

(13) Rapino, S.; Valenti, G.; Marcu, R.; Giorgio, M.; Marcaccio, M.; Paolucci, F. Microdrawing and Highlighting a Reactive Surface. *J. Mater. Chem.* **2010**, *20*, 7272−7275.

(14) Zanarini, S.; Rampazzo, E.; Della Ciana, L.; Marcaccio, M.; Marzocchi, E.; Montalti, M.; Paolucci, F.; Prodi, L. $Ru(bpy)_3$ Covalently Doped Silica Nanoparticles as Multicenter Tunable Structures for Electrochemiluminescence Amplification. *J. Am. Chem. Soc.* **2009**, *131*, 2260−2267.

(15) Tamayo, A. B.; Garon, S.; Sajoto, T.; Djurovich, P. I.; Tsyba, I. M.; Bau, R.; Thompson, M. E. Cationic Bis-Cyclometalated Iridium(III) Diimine Complexes and Their Use in Efficient Blue, Green, and Red Electrochemiluminescent Devices. *Inorg. Chem.* **2005**, *44*, 8723−8732.

(16) Zhang, J.; Chu, B. W.-K.; Zhu, N.; Yam, V. W.-W. Synthesis, Characterization, Langmuir-Blodgett Film-Forming Property, and Second-Order Nonlinear Optical Study of Rhenium(I) and Ruthenium-(II) Diimine Complexes. *Organometallics* **2007**, *26*, 5423−5429.

(17) Chu, B. W.-K.; Yam, V. W.-W. Sensitive Single-Layered Oxygen-Sensing Systems: Polypyridyl Ruthenium(II) Complexes Covalently Attached or Deposited as Langmuir-Blodgett Monolayer on Glass Surfaces. *Langmuir* **2006**, *22*, 7437−7443.

(18) Krass, H.; Plummer, E. A.; Haider, J. M.; Barker, P. R.; Alcock, N. W.; Pikramenou, Z.; Hannon, M. J.; Kurth, D. G. Immobilization of II-Assembled Metallo-Supramolecular Arrays in Thin Films: From

Crystal-Engineered Structures to Processable Materials. *Angew. Chem., Int. Ed.* **2001**, *40*, 3862−3865.
(19) Hoertz, P. G.; Mallouk, T. E. Light-to-Chemical Energy Converstion in Lamellar Solids and Thin Films. *Inorg. Chem.* **2005**, *44*, 6828−6840.
(20) Piper, D. J. E.; Barbante, G. J.; Brack, N.; Pigram, P. J.; Hogan, C. F. Highly Stable Ecl Active Films Formed by the Electrografting of a Diazotized Ruthenium Complex Generated *in Situ* from the Amine. *Langmuir* **2011**, *27*, 474−480.
(21) Zanarini, S.; Rampazzo, E.; Bich, D.; Canteri, R.; Della Ciana, L.; Marcaccio, M.; Marzocchi, E.; Montalti, M.; Panciatichi, C.; Pederzolli, C.; Paolucci, F.; Prodi, L.; Vanzetti, L. Synthesis and Electrochemiluminescence of a Ru(bpy)$_3$-Labeled Coupling Adduct Produced on a Self-Assembled Monolayer. *J. Phys. Chem. C* **2008**, *112*, 2949−2957.
(22) Bayly, S. R.; Gray, T. M.; Chmielewski, M. J.; Davis, J. J.; Beer, P. D. Anion Templated Surface Assembly of a Redox-Active Sensory Rotaxane. *Chem. Commun.* **2007**, 2234−2236.
(23) Ramachandra, S.; Schuermann, K. C.; Edafe, F.; Belser, P.; Nijhuis, C. A.; Reus, W. F.; Whitesides, G. M.; De Cola, L. Luminescent Ruthenium Tripod Complexes: Properties in Solution and on Conductive Surfaces. *Inorg. Chem.* **2011**, *50*, 1581−1591.
(24) Contreras-Carballada, P.; Edafe, F.; Tichelaar, F. D.; Belser, P.; De Cola, L.; Williams, R. M. Tripodal Osmium Polypyridyl Complexes for Self-Assembly on Platinum Nanoparticles. *J. Phys. Chem. Lett.* **2011**, *2*, 1460−1463.
(25) Bertoncello, P.; Kefalas, E.; Pikramenou, Z.; Unwin, P.; Forster, R. Adsorption Dynamics and Electrochemical and Photophysical Properties of Thiolated Ruthenium 2,2′-Bipyridine Monolayers. *J. Phys. Chem. B* **2006**, *110*, 10063−10069.
(26) Lo, K. K.-W.; Choi, A. W.-T.; Law, W. H.-T. Applications of Luminescent Inorganic and Organometallic Transition Metal Complexes as Biomolecular and Cellular Probes. *Dalton Trans.* **2012**, *41*, 6021−6047.
(27) Filby, M. H.; Muldoon, J.; Dabb, S.; Fletcher, N. C.; Ashcroft, A. E.; Wilson, A. J. Protein Surface Recognition Using Geometrically Pure Ru(II) Tris(bipyridine) Derivatives. *Chem. Commun.* **2011**, *47*, 559−561.
(28) Anfossi, L.; Baggiani, C.; Giovannoli, C.; Giraudi, G. Homogeneous Immunoassay Based on Gold Nanoparticles and Visible Absorption Detection. *Anal. Bioanal. Chem.* **2009**, *394*, 507−512.
(29) Mendes, P. M. Stimuli-Responsive Surfaces for Bio-Applications. *Chem. Soc. Rev.* **2008**, *37*, 2512−2529.
(30) Jetty, R.; Bandera, Y. P.; Daniele, M. A.; Hanor, D.; Hung, H.-I.; Ramshesh, V.; Duperreault, M. F.; Nieminen, A.-L.; Lemasters, J. J.; Foulger, S. H. Protein Triggered Fluorescence Switching of near-Infrared Emitting Nanoparticles for Contrast-Enhanced Imaging. *J. Mater. Chem. B* **2013**, *1*, 4542−4554.
(31) Wang, C.; Ouyang, J.; Ye, D.-K.; Xu, J.-J.; Chen, H.-Y.; Xia, X.-H. Rapid Protein Concentration, Efficient Fluorescence Labeling and Purification on a Micro/Nanofluidics Chip. *Lab Chip* **2012**, *12*, 2664−2671.
(32) Chung, C. Y.-S.; Yam, V. W.-W. Induced Self-Assembly and Forster Resonance Energy Transfer Studies of Alkynylplatinum(II) Terpyridine Complex through Interaction with Water-Soluble Poly(Phenylene Ethynylene Sulfonate) and the Proof-of-Principle Demonstration of This Two-Component Ensemble for Selective Label-Free Detection of Human Serum Albumin. *J. Am. Chem. Soc.* **2011**, *133*, 18775−18784.
(33) Shi, H. Q.; Tsai, W. B.; Garrison, M. D.; Ferrari, S.; Ratner, B. D. Template-Imprinted Nanostructured Surfaces for Protein Recognition. *Nature* **1999**, *398*, 593−597.
(34) Kober, E. M.; Caspar, J. V.; Sullivan, P. B.; Meyer, T. J. Synthetic Routes to New Polypridyl Complexes of Osmium(II). *Inorg. Chem.* **1988**, *27*, 4587−4598.
(35) Sprouse, S.; King, K. A.; Spellane, P. J.; Watts, R. J. Photophysical Effects of Metal-Carbon $\sigma$ Bonds in Ortho-Metalated Complexes of Ir(III) and Rh(III). *J. Am. Chem. Soc.* **1984**, *106*, 6647−6653.
(36) Hong, Y.-R.; Gorman, C. B. Synthetic Approaches to an Isostructural Series of Redox-Active, Metal Tris(bipyridine) Core Dendrimers. *J. Org. Chem.* **2003**, *68*, 9019−9025.
(37) Sullivan, B. P.; Salmon, D. J.; Meyer, T. J. Mixed Phosphine 2,2′-Bipyridine Complexes of Ruthenium. *Inorg. Chem.* **1978**, *17*, 3334−3341.
(38) Gaudiello, J. G.; Bradley, P. G.; Norton, K. A.; Woodruff, W. H.; Bard, A. J. Electrochemistry in Liquid Sulfur Dioxide. 5. Oxidation of Bipyridine and Phenanthroline Complexes of Osmium, Ruthenium and Iron. *Inorg. Chem.* **1984**, *23*, 3−10.
(39) Slinker, J. D.; Gorodetsky, A. A.; Lowry, M. S.; Wang, J.; Parker, S.; Rohl, R.; Bernhard, S.; Malliaras, G. G. Efficient Yellow Electrochemiluminescence from a Single Layer of a Cyclometalated Iridium Complex. *J. Am. Chem. Soc.* **2004**, *126*, 2763−2767.
(40) Kumar, A.; Biebuyck, H. A.; Whitesides, G. M. Patterning Self-Assembled Monolayers: Applications in Materials Science. *Langmuir* **1994**, *10*, 1498−1511.
(41) Nazeeruddin, M. K.; Zakeeruddin, S. M.; Kalyanasundaram, K. Enhanced Intensities of the Ligand-to-Metal Charge-Transfer Transitions in Ru(III) and Os(III) Complexes of Substituted Bipyridines. *J. Phys. Chem.* **1993**, *97*, 9607−9612.
(42) Creutz, C.; Chou, M.; Netzel, T. L.; Okumura, M.; Sutin, N. Lifetimes, Specta, and Quenching of the Excited-States of Polypyridine Complexes of Iron(II), Ruthenium(II), and Osmium (II). *J. Am. Chem. Soc.* **1980**, *102*, 1309−1319.
(43) Kober, E. M.; Sullivan, B. P.; Dressick, W. J.; Caspar, J. V.; Meyer, T. J. Highly Luminescent Polypyridyl Complexes of Osmium(II). *J. Am. Chem. Soc.* **1980**, *102*, 7385−7387.
(44) Hou, Y.; Xie, P.; Wu, K.; Wang, J.; Zhang, B.; Cao, Y. Synthetic Control of the Photophysical and Photoelectrochemical Properties of Ruthenium(II) Polypyridyl Complexes. *Sol. Energy Mater. Sol. Cells* **2001**, *70*, 131−139.
(45) Juris, A.; Balzani, V.; Barigelletti, F.; Campagna, S.; Belser, P.; von Zelewsky, A. Ru(II) Polypyridine Complexes - Photophysics, Photochemistry, Electrochemistry, and Chemi-Luminescence. *Coord. Chem. Rev.* **1988**, *84*, 85−277.
(46) Neve, F.; Crispini, A.; Campagna, S.; Serroni, S. Synthesis, Structure, Photphysical Properties, and Redox Behavior of Cyclometalated Complexes of Iridium(III) with Functionalized 2,2′-Bipyridines. *Inorg. Chem.* **1999**, *38*, 2250−2258.
(47) Lowry, M. S.; Goldsmith, J. I.; Slinker, J. D.; Rohl, R.; Pascal, R. A.; Malliaras, G. G.; Bernhard, S. Single-Layer Electrochemiluminescent Devices and Photoinduced Hydrogen Production from an Ionic Iridium(III) Complex. *Chem. Mater.* **2005**, *17*, 5712−5719.
(48) King, K. A.; Watts, R. J. Dual Emission from an Ortho-Metalated Ir(III) Complex. *J. Am. Chem. Soc.* **1987**, *109*, 1589−1590.
(49) Colombo, M. G.; Güdel, H. U. Synthesis and High-Resolution Optical Spectroscopy of Bis(2-(2-Thienyl)Pyridinato-$C^8$,$N'$)(2,2′-Bipyridine)Iridium(III). *Inorg. Chem.* **1993**, *32*, 3081−3087.
(50) Kober, E. M.; Caspar, J. V.; Lumpkin, R. S.; Meyer, T. J. Application of the Energy Gap Law to Excited-State Decay of Osmium(II)-Polypyridine Complexes: Calculation of Relative Nonradiative Decay Rates from Emission Spectral Profiles. *J. Phys. Chem.* **1986**, *90*, 3722−3734.
(51) Lumpkin, R. S.; Kober, E. M.; Worl, L. A.; Murtaza, Z.; Meyer, T. J. Metal-to-Ligand Charge-Transfer (MLCT) Photochemistry - Experimental-Evidence for the Participation of a Higher Lying Mlct State in Polypyridyl Complexes of Ruthenium(II) and Osmium(II). *J. Phys. Chem.* **1990**, *94*, 239−243.
(52) Faiz, J. A.; Williams, R. M.; Silva, M. J. J. P.; De Cola, L.; Pikramenou, Z. A Unidirectional Energy Transfer Cascade Process in a Ruthenium Junction Self-Assembled by $\alpha$- and $\beta$-Cyclodextrins. *J. Am. Chem. Soc.* **2006**, *128*, 4520−4521.
(53) Haider, J. M.; Williams, R. M.; De Cola, L.; Pikramenou, Z. Vectorial Control of Energy-Transfer Processes in Metallocyclodextrin Heterometallic Assemblies. *Angew. Chem., Int. Ed.* **2003**, *42*, 1830−1833.
(54) Nakamaru, K. Synthesis, Luminescence Quantum Yields, and Lifetimes of Trischelated Ruthenium(Ii) Mixed-Ligand Complexes

Including 3,3′-Dimethyl-2,2′-Bipyridyl. *Bull. Chem. Soc. Jpn.* **1982**, *55*, 2697−2705.
(55) Willey, T. M.; Vance, A. L.; Bostedt, C.; van Buuren, T.; Meulenburg, R. W.; Terminello, L. J.; Fadley, C. S. Surface Structure and Chemical Switching of Thioctic Acid Adsorbed on Au(111) as Observed Using near-Edge X-Ray Absorption Fine Structure. *Langmuir* **2004**, *20*, 4939−4944.
(56) Altman, M.; Zenkina, O. V.; Ichiki, T.; Iron, M. A.; Evmenenko, G.; Dutta, P.; van der Boom, M. E. Positive Constructs: Charges Localized on Surface-Confined Organometallic Oligomers. *Chem. Mater.* **2009**, *21*, 4676−4684.
(57) Yeung, C. L.; Iqbal, P.; Allan, M.; Lashkor, M.; Preece, J. A.; Mendes, P. M. Tuning Specific Biomolecular Interactions Using Electro-Switchable Oligopeptide Surfaces. *Adv. Funct. Mater.* **2010**, *20*, 2657−2663.
(58) Stenberg, E.; Persson, B.; Roos, H.; Urbaniczky, C. Quantitative Determination of Surface Concentration of Protein with Surface Plasmon Resonance Using Radiolabeled Proteins. *J. Colloid Interface Sci.* **1990**, *143*, 513−526.
(59) Lahiri, J.; Isaacs, L.; Tien, J.; Whitesides, G. M. A Strategy for the Generation of Surfaces Presenting Ligands for Studies of Binding Based on an Active Ester as a Common Reactive Intermediate: A Surface Plasmon Resonance Study. *Anal. Chem.* **1999**, *71*, 777−790.
(60) Davis, T. M.; Wilson, W. D. Determination of the Refractive Index Increments of Small Molecules for Correction of Surface Plasmon Resonance Data. *Anal. Biochem.* **2000**, *284*, 348−353.
(61) Peterlinz, K. A.; Georgiadis, R. In Situ Kinetics of Self-Assembly by Surface Plasmon Resonance Spectroscopy. *Langmuir* **1996**, *12*, 4731−4740.
(62) Dong, Y.; Abaci, S.; Shannon, C.; Bozack, M. J. Self-Assembly and Electrochemical Desorption of Thioctic Acid Monolayers on Gold Surfaces. *Langmuir* **2003**, *19*, 8922−8926.
(63) Alcock, N. W.; Barker, P. R.; Haider, J. M.; Hannon, M. J.; Painting, C. L.; Pikramenou, Z.; Plummer, E. A.; Rissanen, K.; Saarenketo, P. Red and Blue Luminescent Metallo-Supramolecular Coordination Polymers Assembled through $\pi-\pi$ Interactions. *Dalton Trans.* **2000**, 1447−1461.
(64) D'Aléo, A.; Williams, R. M.; Chriqui, Y.; Iyer, V. M.; Belser, P.; Vergeer, F.; Ruiz, V.; Unwin, P. R.; De Cola, L. Electrochemical and Photophysical Properties of Ruthenium(II) Bipyridyl Complexes with Pendant Alkanethiol Chains in Solution and Anchored to Metal Surfaces. *Open Inorg. Chem. J.* **2007**, *1*, 26−36.
(65) De Wolf, F. A.; Brett, G. M. Ligand-Binding Proteins: Their Potential for Application in Systems for Controlled Delivery and Uptake of Ligands. *Pharmacol. Rev.* **2000**, *52*, 207−236.
(66) Spector, A. A. Fatty-Acid Binding to Plasma Albumin. *J. Lipid Res.* **1975**, *16*, 165−179.
(67) Lo, K. K.-W.; Lee, T. K.-M.; Lau, J. S.-Y.; Poon, W.-L.; Cheng, S.-H. Luminescent Biological Probes Derived from Ruthenium(II) Estradiol Polypyridine Complexes. *Inorg. Chem.* **2008**, *47*, 200−208.
(68) Rogozea, A.; Matei, I.; Turcu, I. M.; Ionita, G.; Sahini, V. E.; Salifoglou, A. EPR and Circular Dichroism Solution Studies on the Interactions of Bovine Serum Albumin with Ionic Surfactants and Beta-Cyclodextrin. *J. Phys. Chem. B* **2012**, *116*, 14245−14253.

## 2.4 Conclusions

In this chapter, the synthesis of surface-active transition metal complexes is described and fully characterised. The photophysical properties of the complexes are examined and show comparable properties to similar compounds. Monolayers of the complexes are shown to form on gold substrates through ellipsometric, SPR and luminescence studies. The luminescence data reveals that not only is quenching eliminated for monolayers of **RubpySS** and **IrbpySS**, but the luminescence lifetimes are in fact extended when attached to gold surfaces. Through the use of μCP we have shown that monolayers of both **RubpySS** and **IrbpySS** can be deposited in a controlled manner. We have also shown that **RubpySS** and **IrbpySS** will interact with BSA in both solution and on gold substrates, changing the environment in which the complexes sit, resulting in red shifts in luminescence and extended lifetimes, attributed to the increase in hydrophobicity around the metal centres. We envisage that these types of metal complexes can be used in device formation as recognition platforms, particularly if the ancillary ligands of the complexes can be functionalised to incorporate more selective binding motifs. Indeed, in chapter 4, this concept is elaborated.

# 2.5 Experimental

**$Os(bpy)_2Cl_2$**

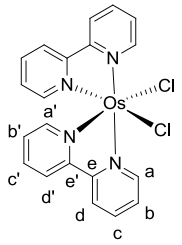


$Os(bpy)_2Cl_2$ was prepared following a synthetic route outlined by Kober *et al.*[64]. Briefly, ammonium hexachloroosmate(IV) (1.00 g, 2.3 mmol) and 2,2′-bipyridyl (0.72 g, 4.6 mmol) were suspended in ethylene glycol and heated to 200 °C for 1.5 hours. The resultant black mixture was cooled naturally to room temperature, to which saturated aqueous sodium dithionite (50 mL) was added. The precipitate was filtered under vacuum and washed with copious amounts of water and diethyl ether before air drying to give the black microcrystalline title compound in a 53% yield (0.69 g, 1.2 mmol); $\lambda_{max}$ (MeCN) / nm ($\varepsilon$ / $M^{-1}$ $cm^{-1}$) 239 (27500), 297 (43800), 382 (9900), 459 (9100), 551 (10600); $\delta_H$(300 MHz, $d_6$-DMSO) 6.80 (2H, dd, *J* = 6.0, 1.4, H-b/b′), 7.26-7.35 (4H, m, H-c/c′), 7.52-7.65 (4H, m, b/b′, a′), 8.38 (2H, dd, *J* = 8.5, 1.1, H-d/d′), 8.60 (2H, dd, *J* = 7.2, 1.8, H-d/d′) 9.68 (2H, dd, *J* = 5.0, 1.8, H-a); MS (ESI+) m/z: 574 $(M+H)^+$.

**OsbpyBoc**

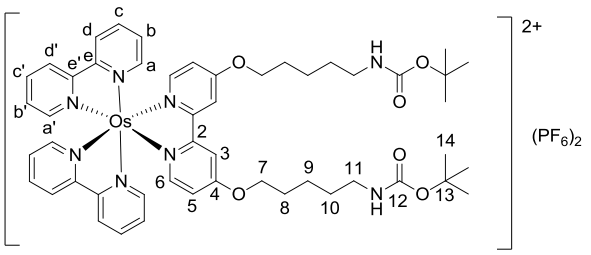


$Os(bpy)_2Cl_2$ (0.17 g, 0.3 mmol) and **bpyBoc** (0.16 g, 0.3 mmol) were suspended in ethanol (100 mL) and heated to reflux for 17 hours. The black mixture was then allowed to cool to room temperature, and the solvent was concentrated *in vacuo* to *ca.* 20 mL. Water (50 mL) was added, followed by a saturated methanolic solution of ammonium hexafluorophosphate (2 mL). The resulting black precipitate was filtered under vacuum and washed with copious amounts of water and ether. The compound was dried under vacuum for 8 hours to give the **OsbpyBoc** in a 69% yield and used in the next stage without further purification (0.27 g, 0.2 mmol); $\delta_H$(300 MHz, $CD_3CN$) 1.23 (18H, s, H-14), 1.26-1.38 (8H, m, H-8,9), 1.66 (4H, qu, *J* = 6.8, H-10), 2.82-2.94 (4H, m, H-11), 4.05 (4H, t, *J* = 6.6, H-7), 5.13 (2H, s, N*H*), 6.71 (2H, dd, *J* = 6.7, 2.7, H-5), 7.08 (2H, dd, *J* = 5.8, 1.3, H-b/b′), 7.15 (2H, d, *J* = 6.7, H-6), 7.16 (2H, dd, *J* = 5.8, 1.3, H-b/b′), 7.46 (2H, d, *J* = 5.8, H-a/a′), 7.58 (2H, d, *J* = 5.8, H-a/a′), 7.65 (4H, td, *J* = 7.8, 1.3, H-c,c′), 7.80 (2H, d, *J* = 2.7, H-3), 8.29 (4H, dd, *J* = 7.8, 7.8, H-d,d′); $\delta_C$(100 MHz, $CD_3CN$) 22.6 (C-9), 27.6 (C-14), 28.0 (C-8) 29.4 (C-10), 39.8 (C-11), 69.7 (C-7), 114.5 (C-5), 124.3 (C-d,d′), 127.9 (C-b,b′), 136.5 (C-3), 150.5 (C-c,c′), 151.0 (6/a,a′), 151.3 (6/a,a′), 159.4 (C-2,e,e′), 166.0 (C-12).

**RubpyBoc**

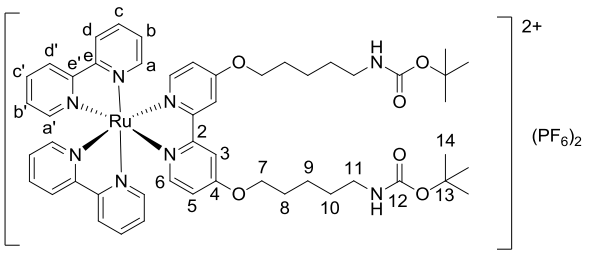

Ru(bpy)$_2$Cl$_2$ (0.14 g, 0.3 mmol), **bpyBoc** (0.16 g, 0.3 mmol) and ethanol (100 mL) were reacted as above to give **RubpyBoc** as a red solid in a 63% yield (0.23 g, 0.2 mmol) and used in the next step without further purification; $\delta_H$(300 MHz, $CD_3CN$) 1.40 (18H, s, H-14), 1.44-1.56 (8H, m, H-8,9), 1.84 (4H, qu, *J* = 6.9, H-10), 3.00-3.10 (4H, m, H-11), 4.20 (4H, t, *J* = 6.5, H-7), 5.30 (2H, s, N*H*), 6.92 (2H, dd, *J* = 6.6, 2.6, H-5), 7.37 (2H, dd, *J* = 5.6, 1.3, H-b/b′), 7.43 (2H, d, *J* = 6.6, H-6), 7.44 (2H, dd, *J* = 5.6, 1.3, H-b/b′), 7.73 (2H, d, *J* = 5.6, H-a/a′), 7.83 (2H, d, *J* = 5.6, H-a/a′), 7.98-8.10 (6H, m, H-3,c,c′), 8.49 (4H, dd, *J* = 8.1, 3.3, H-d,d′); $\delta_C$(100 MHz, $CD_3CN$) 22.6 (C-9), 27.6 (C-14), 28.0 (C-8), 29.4 (C-10), 39.8 (C-11), 69.6 (C-7), 111.3 (C-3), 114.1 (C-5), 124.3 (C-4,d,d′), 127.1 (C-b,b′), 151.6 (C-a,a′), 152.0 (C-6), 157.1 (C-2,e,e′).

**OsbpyNH$_2$**

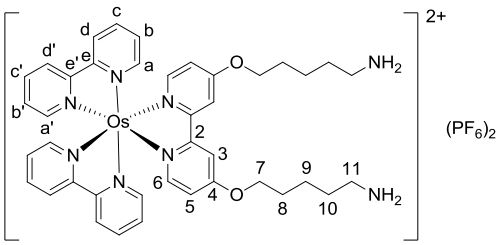

**OsbpyBoc** (0.26 g, 0.2 mmol) in trifluoroacetic acid (15 mL) was stirred at room temperature for 1 hour. After this time, the solvent was removed *in vacuo* to yield a brown oil, which was purified by flash column chromatography (eluting with 70:29:1 MeCN:$H_2O$:sat. aq. $KNO_3$) collecting the black/green band. The fractions were concentrated *in vacuo* to remove the

acetonitrile and a saturated methanolic solution of ammonium hexafluorophosphate (3 mL) was added. The product was extracted with dichloromethane (3 × 50 mL) and the combined organic extracts were washed with water (50 mL), with the solvent removed *in vacuo* to leave a glassy black solid **OsbpyNH$_2$** in a 45% yield (0.10 g, 0.09 mmol); $\lambda_{max}$ (MeCN) / nm ($\varepsilon$ / M$^{-1}$ cm$^{-1}$) 291 (42000), 378 (6400), 455 (6700), 489 (6500); $\delta_H$(300 MHz, $CD_3CN$) 1.36-1.51 (4H, m, H-8/9), 1.55-1.80 (8H, m, H-8/9,10), 2.89 (2H, t, *J* = 7.5, H-11), 3.54 (2H, t, *J* = 7.5, H-11′), 4.07-4.19 (4H, m, H-7), 6.02 (s, N*H*$_2$), 6.79 (2H, dd, *J* = 6.6, 2.5, H-5), 7.16 (2H, dd, *J* = 6.0, 0.9, H-b/b′), 7.20-7.28 (4H, m, H-b/b′,6), 7.55 (2H, d, *J* = 5.5, H-a/a′), 7.66 (2H, d, *J* = 5.5, H-a/a′), 7.73 (4H, dd, *J* = 7.8, 1.1, H-c,c′), 7.87 (2H, d, *J* = 2.5, H-3), 8.38 (4H, t, *J* = 7.8, H-d,d′); $\delta_C$(100 MHz, $CD_3CN$) 22.1 (C-9), 26.2 (C-8), 27.4 (C-10), 39.8 (C-11), 69.0 (C-7), 111.1 (C-3), 114.2 (C-5), 124.0 (C-d,d′), 127.6 (C-b,b′), 136.2 (C-c,c′), 150.2 (C-a/a′/6), 150.6 (C-a/a′/6), 151.0 (C-a/a′/6), 159.3 (C-2,e,e′).

**RubpyNH$_2$**

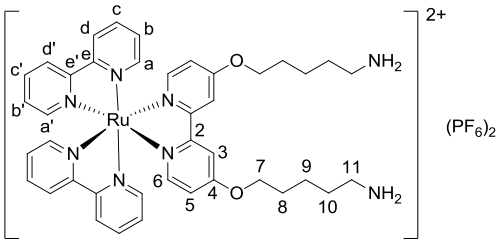


**RubpyBoc** (0.23 g, 0.2 mmol) and trifluoroacetic acid (15 mL) were treated as above to yield RubpyNH$_2$ as a sticky red solid in a 36% yield (0.07 g, 0.07 mmol); $\lambda_{max}$ (MeCN) / nm ($\varepsilon$ / M$^{-1}$ cm$^{-1}$) 289 (34000), 461 (6600); $\delta_H$(300 MHz, $CD_3CN$) 1.46-1.62 (4H, m, H-8/9), 1.64-1.92 (8H, m, H-8/9,10), 2.99 (2H, t, *J* = 7.4, H-11), 3.64 (2H, t, *J* = 7.4, H-11′), 4.16-4.27 (4H, m, H-7), 6.93 (2H, dd, *J* = 6.4, 2.7, H-5), 7.34-7.50 (4H, m, H-b,b′), 6.48 (2H, d, *J* = 6.4, H-6), 7.74 (2H, d, *J* = 5.3, H-a/a′), 7.84 (2H, d, *J* = 5.3, H-a/a′), 7.99-8.11 (6H, m, H-c,c′,3), 8.50 (4H, dd, *J* = 8.0, 3.0, H-d,d′); $\delta_C$(100 MHz, $CD_3CN$) 21.9 (C-8,9), 27.1 (C-10), 38.9 (C-11), 69.0 (C-7),

111.0 (C-3), 114.0 (C-5), 123.8 (C-d,d′), 127.1 (C-b,b′), 137.0 (C-3,c,c′), 151.2 (C-a/a′/6), 151.4 (C-a/a′/6), 151.5 (C-a/a′/6), 156.8 (C-e/e′/2), 157.0 (C-e/e′/2), 157.8 (C-e/e′/2); MS (ESI+) m/z: 1102 $(M+K)^+$ 1063 $(M+H)^+$, 917 $(M-PF_6)^+$.

# 2.6 References


1. S. J. Adams, D. J. Lewis, J. A. Preece and Z. Pikramenou, *ACS Appl. Mater. Interfaces*, 2014, **6**, 11598-11608.
2. H. Häkkinen, *Nat. Chem.*, 2012, **4**, 443-455.
3. J. C. Love, L. E. Estroff, J. K. Kriebel, R. G. Nuzzo and G. M. Whitesides, *Chem. Rev.*, 2005, **105**, 1103-1169.
4. J. L. Brennan, T. E. Keyes and R. J. Forster, *Langmuir*, 2006, **22**, 10754-10761.
5. P. Bertoncello, E. T. Kefalas, Z. Pikramenou, P. R. Unwin and R. J. Forster, *J. Phys. Chem. B*, 2006, **110**, 10063-10069.
6. R. J. Forster, Y. Pellegrin, D. Leane, J. L. Brennan and T. E. Keyes, *J. Phys. Chem. C*, 2007, **111**, 2063-2068.
7. E. Figgemeier, L. Merz, B. A. Hermann, Y. C. Zimmerman, C. E. Housecroft, H.-J. Güntherhodt and E. C. Constable, *J. Phys. Chem. B*, 2003, **107**, 1157-1162.
8. E. Figgemeier, E. C. Constable, C. E. Housecroft and Y. C. Zimmerman, *Langmuir*, 2004, **20**, 9242-9248.
9. D. M. Collard and M. A. Fox, *Langmuir*, 1991, **7**, 1192-1197.
10. M. D. Porter, T. B. Bright, D. L. Allara and C. E. D. Chidsey, *J. Am. Chem. Soc.*, 1987, **109**, 3559-3568.
11. C. E. D. Chidsey, C. R. Bertozzi, T. M. Putvinski and A. M. Mujsce, *J. Am. Chem. Soc.*, 1990, **112**, 4301-4306.
12. M. T. Rojas, R. Koeniger, J. F. Stoddart and A. E. Kaifer, *J. Am. Chem. Soc.*, 1995, **117**, 336-343.
13. D. T. Gryko, C. Clausen and J. S. Lindsey, *J. Org. Chem.*, 1999, **64**, 8635-8647.
14. F. A. Murphy, S. Suárez, E. Figgemeier, E. R. Schofield and S. M. Draper, *Chem. Eur. J.*, 2009, **15**, 5740-5748.
15. T. M. Willey, A. L. Vance, C. Bostedt, T. van Buuren, R. W. Meulenburg, L. J. Terminello and C. S. Fadley, *Langmuir*, 2004, **20**, 4939-4944.
16. E. Coronado, A. Forment-Aliaga, P. Gavina and F. M. Romero, *Inorg. Chem.*, 2003, **42**, 6959-6961.
17. P. D. Beer, J. J. Davis, D. A. Drillsma-Milgrom and F. Szemes, *Chem. Commun.*, 2002, 1716-1717.
18. S. Zanarini, E. Rampazzo, D. Bich, R. Canteri, L. Della Ciana, M. Marcaccio, E. Marzocchi, M. Montalti, C. Panciatichi, C. Pederzolli, F. Paolucci, L. Prodi and L. Vanzetti, *J. Phys. Chem. C*, 2008, **112**, 2949-2957.
19. S. Yasutomi, T. Morita, Y. Imanishi and S. Kimura, *Science*, 2004, **304**, 1944-1947.
20. Y. Xia, J. A. Rogers, K. E. Paul and G. M. Whitesides, *Chem. Rev.*, 1999, **99**, 1823-1848.
21. Y. Xia, X.-M. Zhao and G. M. Whitesides, *Microelectron. Eng.*, 1996, **32**, 255-268.
22. Y. Taur, D. A. Buchanan, W. Chen, D. J. Frank, K. E. Ismail, S.-H. Lo, G. A. Sai-Halasz, R. G. Viswanathan, H.-J. C. Wann, S. J. Wind and H.-S. Wong, *P. IEEE*, 1997, **85**, 486-504.
23. A. Kumar, H. A. Biebuyck and G. M. Whitesides, *Langmuir*, 1994, **10**, 1498-1511.
24. M. W. J. Beulen, J. Bügler, M. R. de Jong, B. Lammerink, J. Huskens, H. Schönherr, G. J. Vancso, B. A. Boukamp, H. Wieder, A. Offenhäuser, W. Knoll, F. C. J. M. van Veggel and D. N. Reinhoudt, *Chem. Eur. J.*, 2000, **6**, 1176-1183.
25. A. Perl, D. N. Reinhoudt and J. Huskens, *Adv. Mater.*, 2009, **21**, 2257-2268.

26. Y. Xia, N. Venkateswaran, D. Qin, J. Tien and G. M. Whitesides, *Langmuir*, 1998, **14**, 363-371.
27. J. Lahiri, E. Ostuni and G. M. Whitesides, *Langmuir*, 1999, **15**, 2055-2060.
28. H. Kind, M. Geissler, H. Schmid, B. Michel, K. Kern and E. Delamarche, *Langmuir*, 2000, **16**, 6367-6373.
29. S. Rapino, G. Valenti, R. Marcu, M. Giorgio, M. Marcaccio and F. Paolucci, *J. Mater. Chem.*, 2010, **20**, 7272-7275.
30. K. H. Drexhage, *J. Lumin.*, 1970, **1,2**, 693-701.
31. H. Kuhn, *J. Chem. Phys.*, 1970, **53**, 101-108.
32. C. J. Breshike, R. A. Riskowski and G. F. Strouse, *J. Phys. Chem. C*, 2013, **117**, 23942-23949.
33. S. Ramachandra, K. C. Schuermann, F. Edafe, P. Belser, C. A. Nijhuis, W. F. Reus, G. M. Whitesides and L. De Cola, *Inorg. Chem.*, 2011, **50**, 1581-1591.
34. A. D'Aléo, R. M. Williams, Y. Chriqui, V. M. Iyer, P. Belser, F. Vergeer, V. Ruiz, P. R. Unwin and L. De Cola, *Open Inorg. Chem. J.*, 2007, **1**, 26-36.
35. H. C. Zhao, J. P. Harney, Y.-T. Huang, J.-H. Yum, M. K. Nazeeruddin, M. Grätzel, M.-K. Tsai and J. Rochford, *Inorg. Chem.*, 2012, **51**, 1-3.
36. N. Vlachopoulos, P. Liska, J. Augustynski and M. Grätzel, *J. Am. Chem. Soc.*, 1988, **110**, 1216-1220.
37. M. K. Nazeeruddin, A. Kay, I. Rodicio, R. Humphry-Baker, E. Müller, P. Liska, N. Vlachopoulos and M. Grätzel, *J. Am. Chem. Soc.*, 1993, **115**, 6382-6390.
38. P. Wang, C. Klein, R. Humphry-Baker, S. M. Zakeeruddin and M. Grätzel, *J. Am. Chem. Soc.*, 2005, **127**, 808-809.
39. J. Faiz, A. I. Philippopoulos, A. G. Kontos, P. Falaras and Z. Pikramenou, *Adv. Funct. Mater.*, 2007, **17**, 54-58.
40. R. Argazzi, C. A. Bignozzi, T. A. Heimer, F. N. Castellano and G. J. Meyer, *J. Phys. Chem. B*, 1997, **101**, 2591-2597.
41. R. Argazzi, C. A. Bignozzi, T. A. Heimer, F. N. Castellano and G. J. Meyer, *Inorg. Chem.*, 1994, **33**, 5741-5749.
42. K.-L. Wu, S.-T. Ho, C.-C. Chou, Y.-C. Chang, H.-A. Pan, Y. Chi and P.-T. Chou, *Angew. Chem. Int. Ed.*, 2012, **51**, 5642-5646.
43. W. B. Heuer, H.-L. Xia, W. Ward, Z. Zhou, W. H. Pearson, M. A. Siegler, A. A. Narducci Sarjeant, M. Abrahamsson and G. J. Meyer, *Inorg. Chem.*, 2012, **51**, 3981-3988.
44. P. Pramod, P. K. Sudeep, K. G. Thomas and P. V. Kamat, *J. Phys. Chem. B*, 2006, **110**, 20737-20741.
45. M. Jebb, P. K. Sudeep, P. Pramod, K. G. Thomas and P. V. Kamat, *J. Phys. Chem. B*, 2007, **111**, 6839-6844.
46. T. J. Meyer, G. J. Meyer, B. W. Pfennig, J. R. Schoonover, C. J. Timpson, J. F. Wall, C. Kobusch, X. Chen, B. M. Peek, C. G. Wall, W. Ou, B. W. Erickson and C. A. Bignozzi, *Inorg. Chem.*, 1994, **33**, 3952-3964.
47. Q. Zhao, F. Li and C. Huang, *Chem. Soc. Rev.*, 2010, **39**, 3007-3030.
48. V. Fernández-Moreira, F. L. Thorp-Greenwood and M. P. Coogan, *Chem. Commun.*, 2010, **46**, 186-202.
49. P. Yager, T. Edwards, E. Fu, K. Helton, K. Nelson, M. R. Tam and B. H. Weigl, *Nature*, 2006, **442**, 412-418.
50. J. Homola, *Chem. Rev.*, 2008, **108**, 462-493.

51. J. G. Collins, A. D. Sleeman, J. R. Aldrich-Wright, I. Greguric and T. W. Hambley, *Inorg. Chem.*, 1998, **37**, 3133-3141.
52. A. M. Pyle, J. P. Rehmann, R. Meshoyrer, C. V. Kumar, N. J. Turro and J. K. Barton, *J. Am. Chem. Soc.*, 1989, **111**, 3051-3058.
53. R. M. Hartshorn and J. K. Barton, *J. Am. Chem. Soc.*, 1992, **114**, 5919-5925.
54. C. V. Kumar, J. K. Barton and N. J. Turro, *J. Am. Chem. Soc.*, 1985, **107**, 5518-5523.
55. J. M. Kelly, A. B. Tossi, D. J. McConnell and C. OhUigin, *Nucleic Acids Res.*, 1985, **13**, 6017-6034.
56. J. S.-Y. Lau, P.-K. Lee, K. H.-K. Tsang, C. H.-C. Ng, Y.-W. Lam, S.-H. Cheng and K. K.-W. Lo, *Inorg. Chem.*, 2009, **48**, 708-718.
57. J. Muldoon, A. E. Ashcroft and A. J. Wilson, *Chem. Eur. J.*, 2010, **16**, 100-103.
58. C. Y.-S. Chung and V. W.-W. Yam, *J. Am. Chem. Soc.*, 2011, **133**, 18775-18784.
59. A. Vaish, W.-S. Liao, M. J. Shuster, J. M. Hinds, P. S. Weiss and A. M. Andrews, *Anal. Chem.*, 2011, **83**, 7451-7456.
60. R. Blankespoor, B. Limoges, B. Schöllhorn, J.-L. Syssa-Magalé and D. Yazidi, *Langmuir*, 2005, **21**, 3362-3375.
61. S. Farabi, *PhD. Thesis - University of Birmingham*, 2012.
62. N. J. Rogers, S. Claire, R. M. Harris, S. Farabi, G. Zikeli, I. B. Styles, N. J. Hodges and Z. Pikramenou, *Chem. Commun.*, 2014, **50**, 617-619.
63. L. E. P. Kyllonen, *PhD. Thesis - University of Birmingham*, 2009.
64. E. M. Kober, J. V. Caspar, P. B. Sullivan and T. J. Meyer, *Inorg. Chem.*, 1988, **27**, 4587-4598.
65. J. N. Demas and G. A. Crosby, *J. Phys. Chem.*, 1971, **75**, 991-1024.
66. K. Nakamaru, *Bull. Chem. Soc. Jpn.*, 1982, **55**, 2697-2705.
67. A. Juris, V. Balzani, F. Barigelletti, S. Campagna, P. Belser and A. von Zelewsky, *Coord. Chem. Rev.*, 1988, **84**, 85-277.
68. C. J. Timpson, C. C. Carter and J. Olmsted, *J. Phys. Chem.*, 1989, **93**, 4116-4120.
69. J. G. Gaudiello, P. G. Bradley, K. A. Norton, W. H. Woodruff and A. J. Bard, *Inorg. Chem.*, 1984, **23**, 3-10.
70. S. Welter, N. Salluce, A. Benetti, N. Rot, P. Belser, P. Sonar, A. C. Grimsdale, K. Mullen, M. Lutz, A. L. Spek and L. De Cola, *Inorg. Chem.*, 2005, **44**, 4706-4718.
71. J. D. Slinker, A. A. Gorodetsky, M. S. Lowry, J. Wang, S. Parker, R. Rohl, S. Bernhard and G. G. Malliaras, *J. Am. Chem. Soc.*, 2004, **126**, 2763-2767.

# 2.7 Appendix

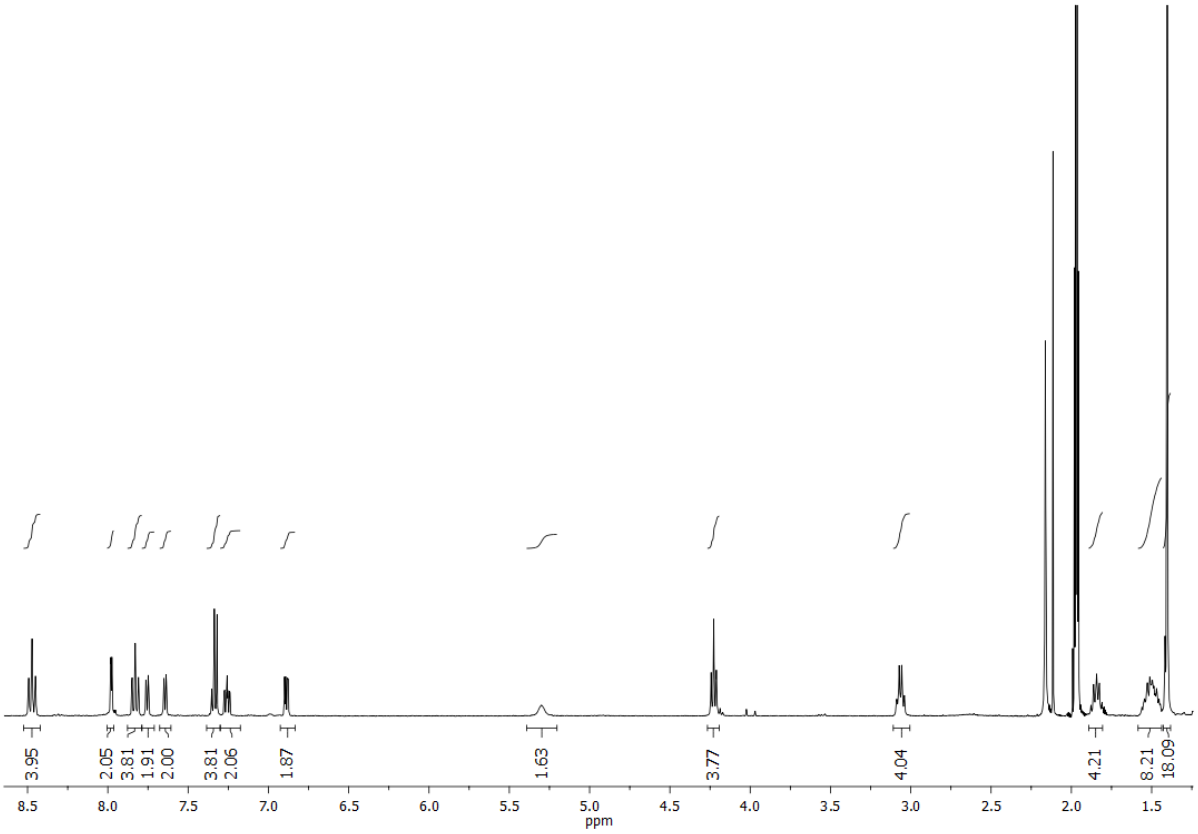


**Figure 2.A1.** $^{1}$H NMR spectrum of **OsbpyBoc** in $CD_3CN$.

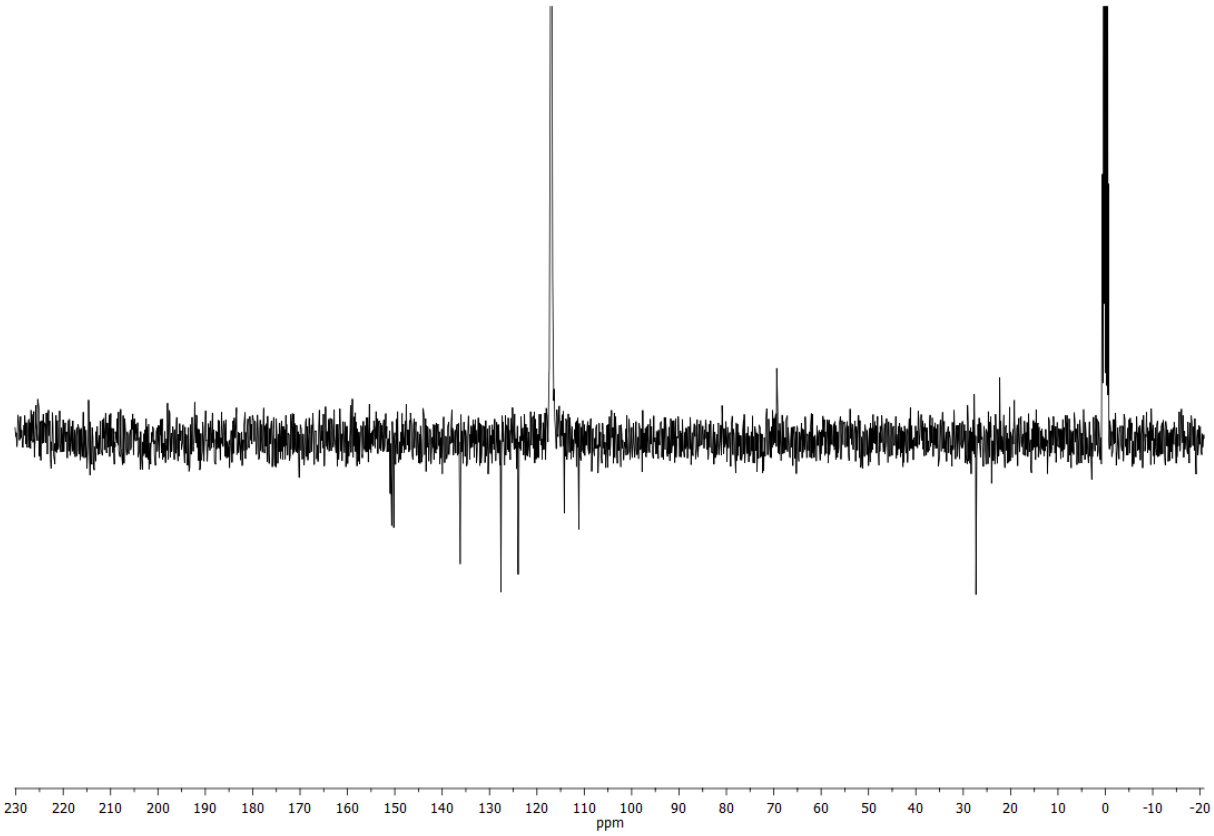


**Figure 2.A2.** $^{13}C$ NMR spectrum of **OsbpyBoc** in $CD_3CN$.

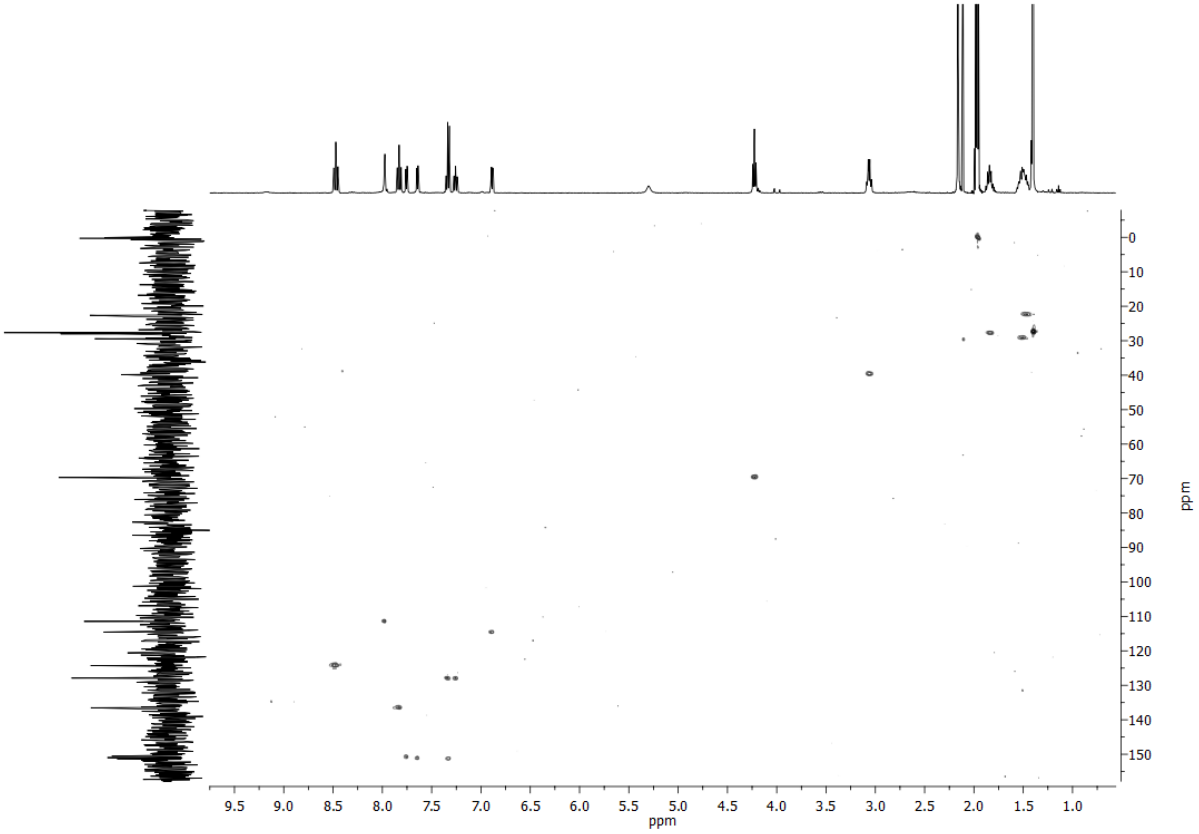


**Figure 2.A3.** HSQC spectrum of **OsbpyBoc** in $CD_3CN$.

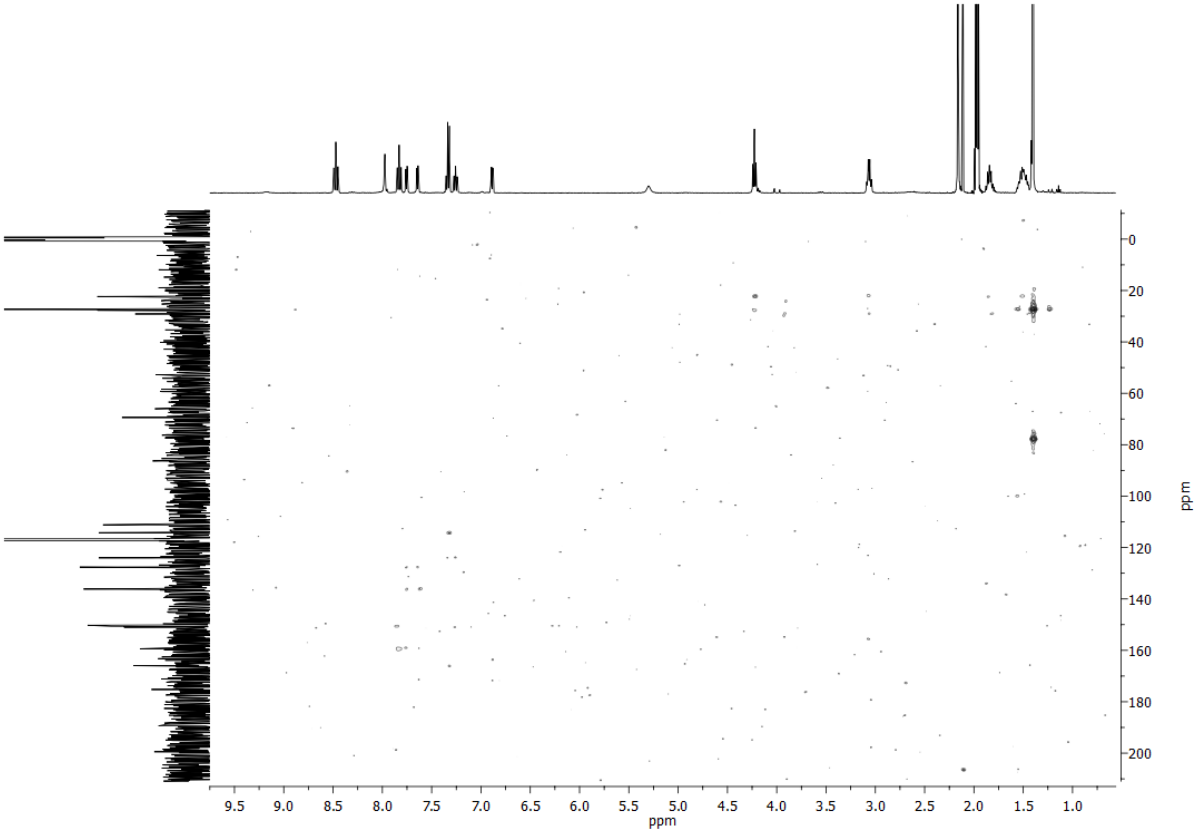


**Figure 2.A4.** HMBC spectrum of **OsbpyBoc** in $CD_3CN$.

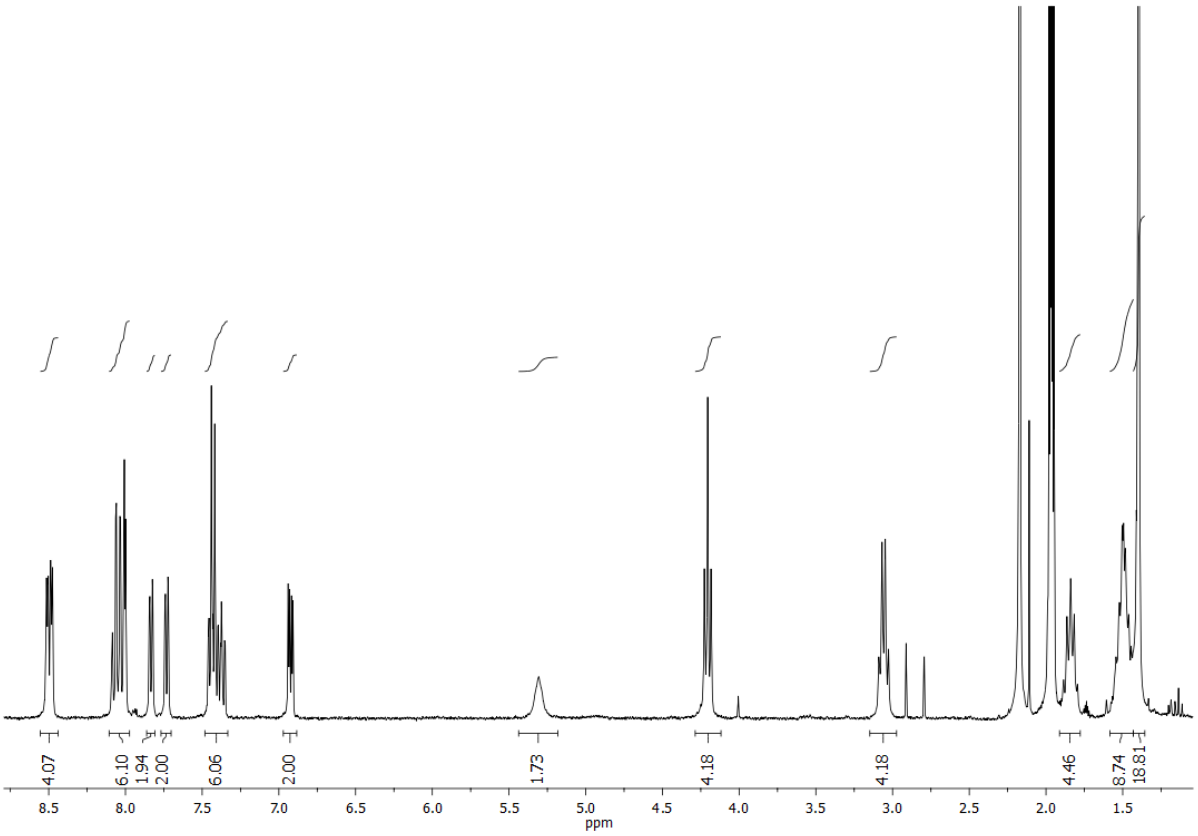


**Figure 2.A5.** $^{1}$H NMR spectrum of **RubpyBoc** in $CD_3CN$.

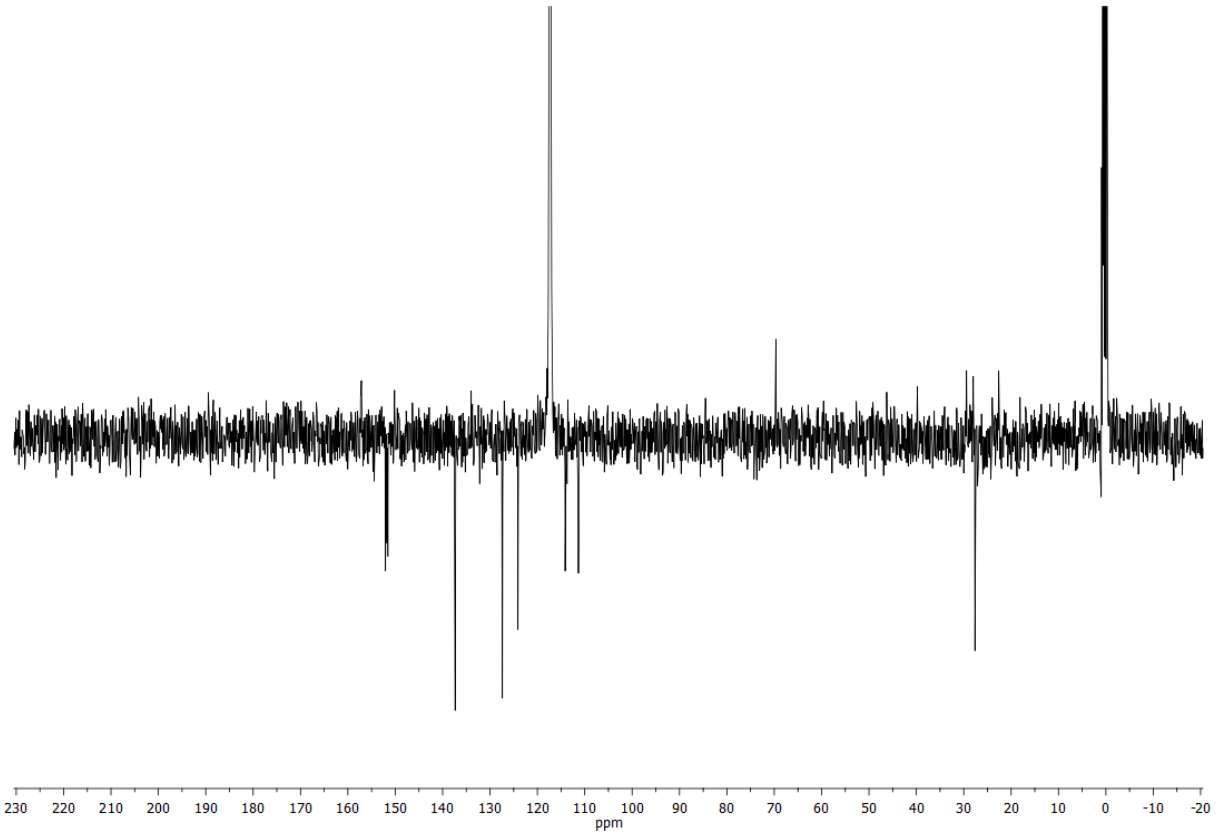


**Figure 2.A6.** $^{13}C$ NMR spectrum of **RubpyBoc** in $CD_3CN$.

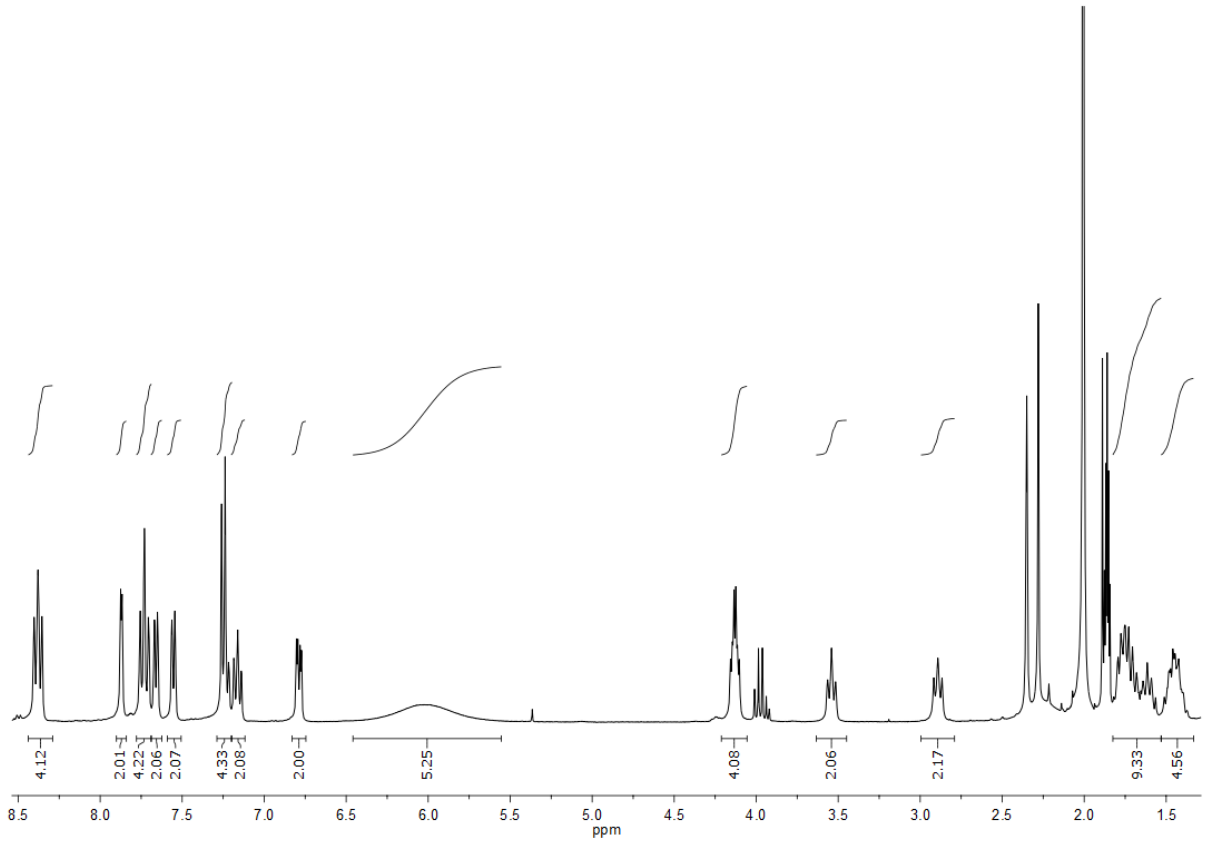


**Figure 2.A7.** $^{1}$H NMR spectrum of **Osbpy$NH_2$** in $CD_3CN$.

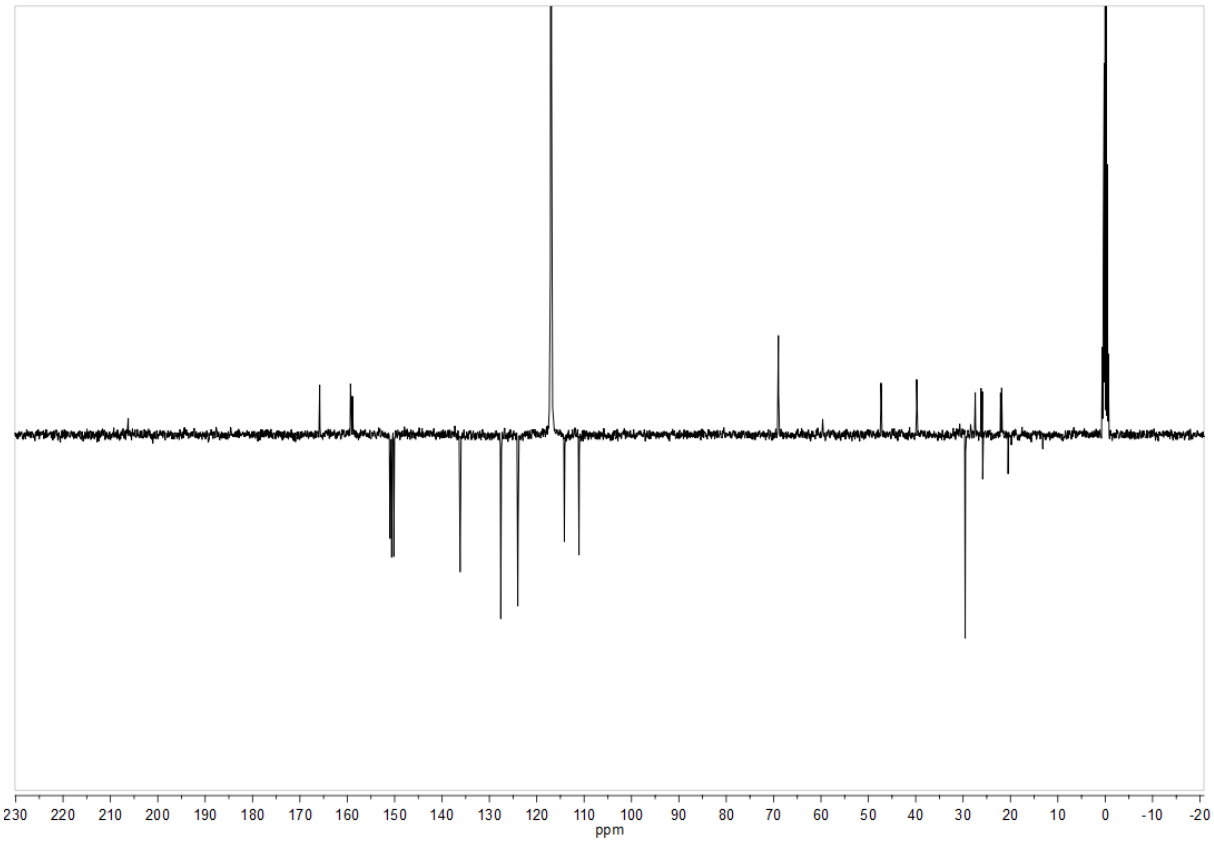


**Figure 2.A8.** $^{13}C$ NMR spectrum of **$OsbpyNH_2$** in $CD_3CN$.

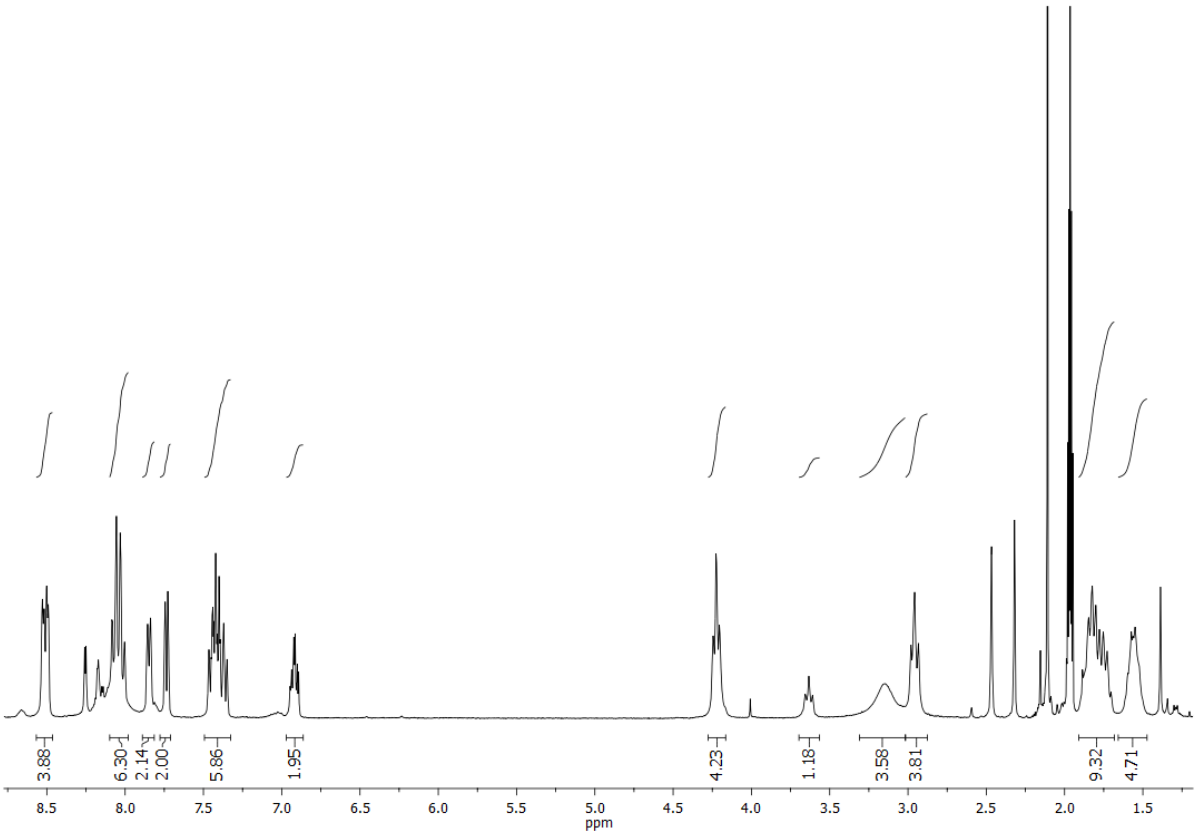


**Figure 2.A9.** $^{1}$H NMR spectrum of **RubpyNH$_2$** in $CD_3CN$.

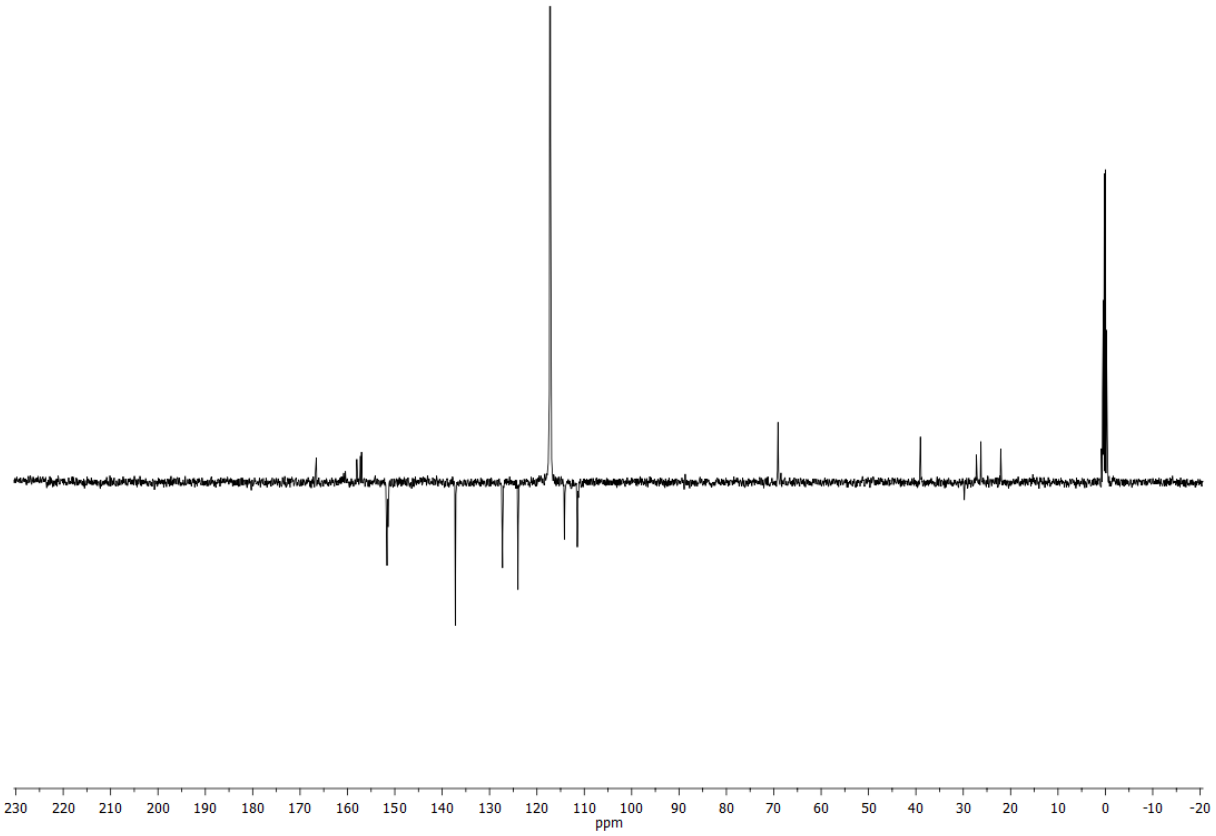


**Figure 2.A10.** $^{13}C$ NMR spectrum of **RubpyNH$_2$** in $CD_3CN$.

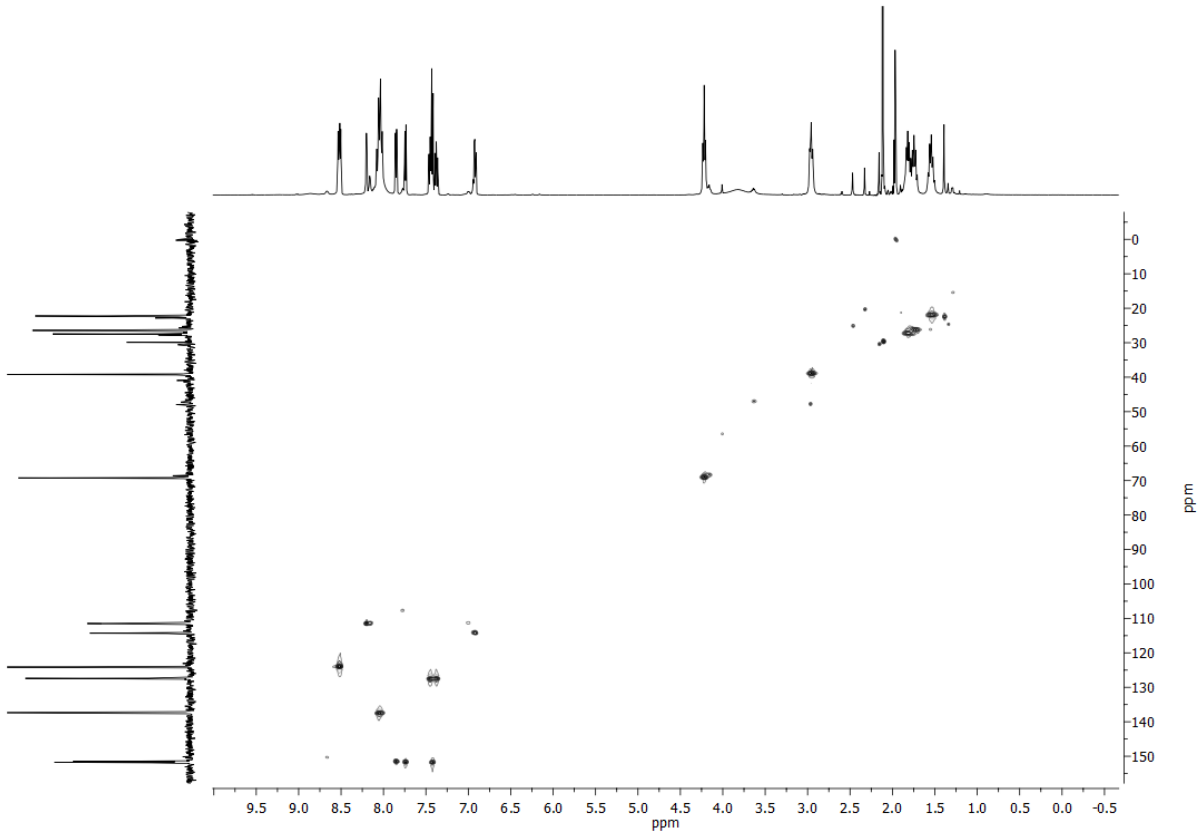


**Figure 2.A11.** HSQC spectrum of **RubpyNH$_2$** in $CD_3CN$.

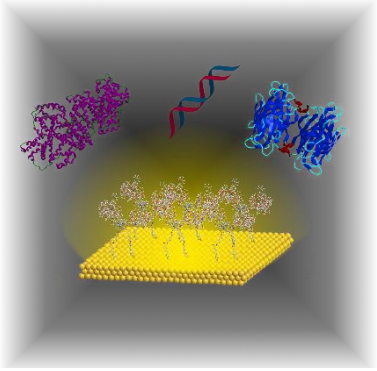

# Chapter Three

# Transition Metal Complexes for Patterning and Recognition at the Interface

# 3.1 Surface Properties and Recognition of Proteins on Gold Surfaces Functionalized with Transition Metal Complexes and Surfactants

## 3.1.1 Introduction

As discussed in chapter two, the area of self-assembly to surfaces is very diverse and complex, with a wide range of chemistries available to exploit to create nanofabricated devices. However, the composition and density of adhered layers at the surface can also have significant effects upon the properties of the surface, for example with interactions with the surface,[1-4] or orientation of bound species.[5, 6] In particular, interactions with the surface may not always be favourable, such as in biological systems where biomolecular interactions may interfere. One example of this is in the use of nanoparticles for cellular uptake.

The Pikramenou group has been interested in the formation of nanoparticles bearing tethered metal complexes for nearly a decade.[7] The attractive properties and ease of synthesis[8] of nanoparticle systems makes them attractive in cell[9, 10] and flow imaging.[11, 12] However, until recently, the use of charged metal complexes such as those of ruthenium(II) and iridium(III) in these systems was unfavourable due to the inherent instability of the modified particles due to a drastic reduction in overall negative charge instigated by the addition of the positively charged complexes. The use of commercially available surfactants in these systems as co-adsorbents has allowed the synthesis of these systems without the instability caused in their formation.[13]

With the proliferation of nanoparticle research in biological systems, many studies have been carried out into the role of serum or media proteins in nanoparticle interactions. It is generally accepted that materials will be coated in proteins upon their introduction to a biological

environment,[14] and therefore it is of no surprise that there is a growing body of evidence that supports the formation of a protein 'corona' (Figure 3.1) around polystyrene,[15, 16] silver[17] and gold[18, 19] nanoparticles when they are subjected to cell media.[14, 20]

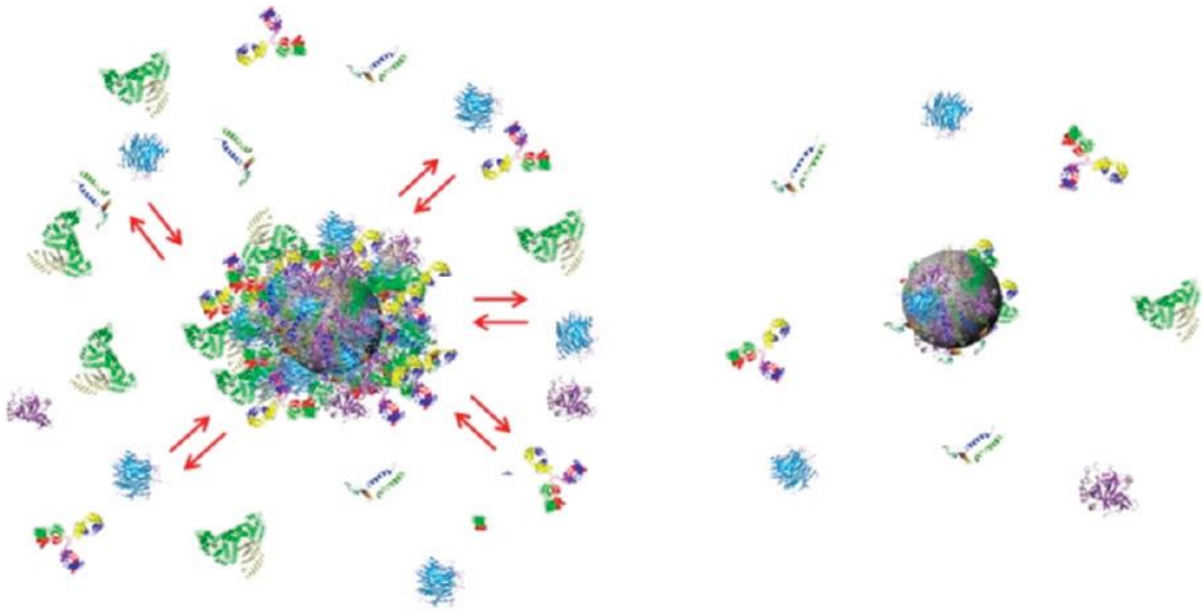

**Figure 3.1.** Schematic of protein corona formation through fast (left) or slow (right) exchange processes. Adapted with permission from reference (15). Copyright 2010 American Chemical Society.

Surface Plasmon Resonance (SPR) spectroscopy is a valuable tool for detecting biomolecular interactions on surfaces. In essence, the technique monitors refractive index changes (Figure 3.2) at a plasmonic interface (commonly gold or silver). Monochromatic incident light is directed at the surface and excites the plasmon at the interface. At a certain angle known as the resonance angle (Θ), the light is fully absorbed, and this is measured by the detector. The change in resonance angle directly relates to the amount of adsorbate within the area of the evanescent wave (*ca.* 300 nm depth from the surface), and so can be used to estimate surface coverage. Multiple reviews on the topic have also been published.[21-23]

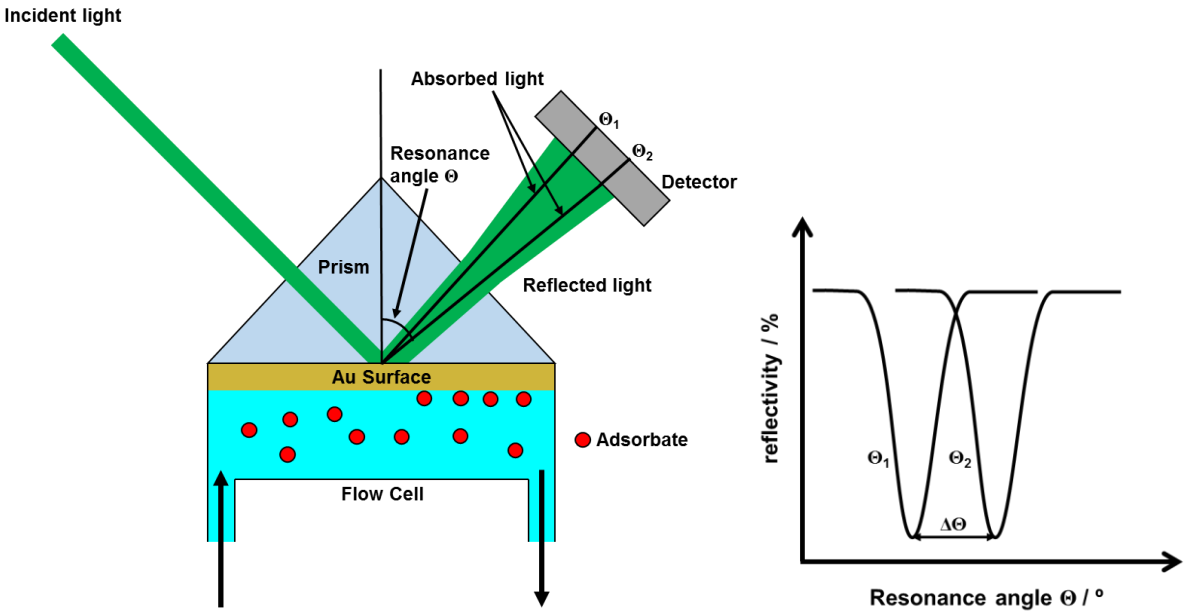


**Figure 3.2.** Schematic of typical SPR system.

### 3.1.2 Section Outline

In this section we seek to examine through luminescence and SPR spectroscopy, the changes in properties of the previously examined (Chapter two) complexes **RubpySS** and **IrbpySS** on gold surfaces co-coated with four commercially available surfactants (Figure 3.3). We examine the subsequent adsorption of the protein BSA and the more biologically relevant Fetal Bovine Serum (FBS). Utilising these techniques, we seek to establish whether gold nanoparticles functionalised with these complexes would be more or less susceptible to protein corona formation when co-coated with surfactants.

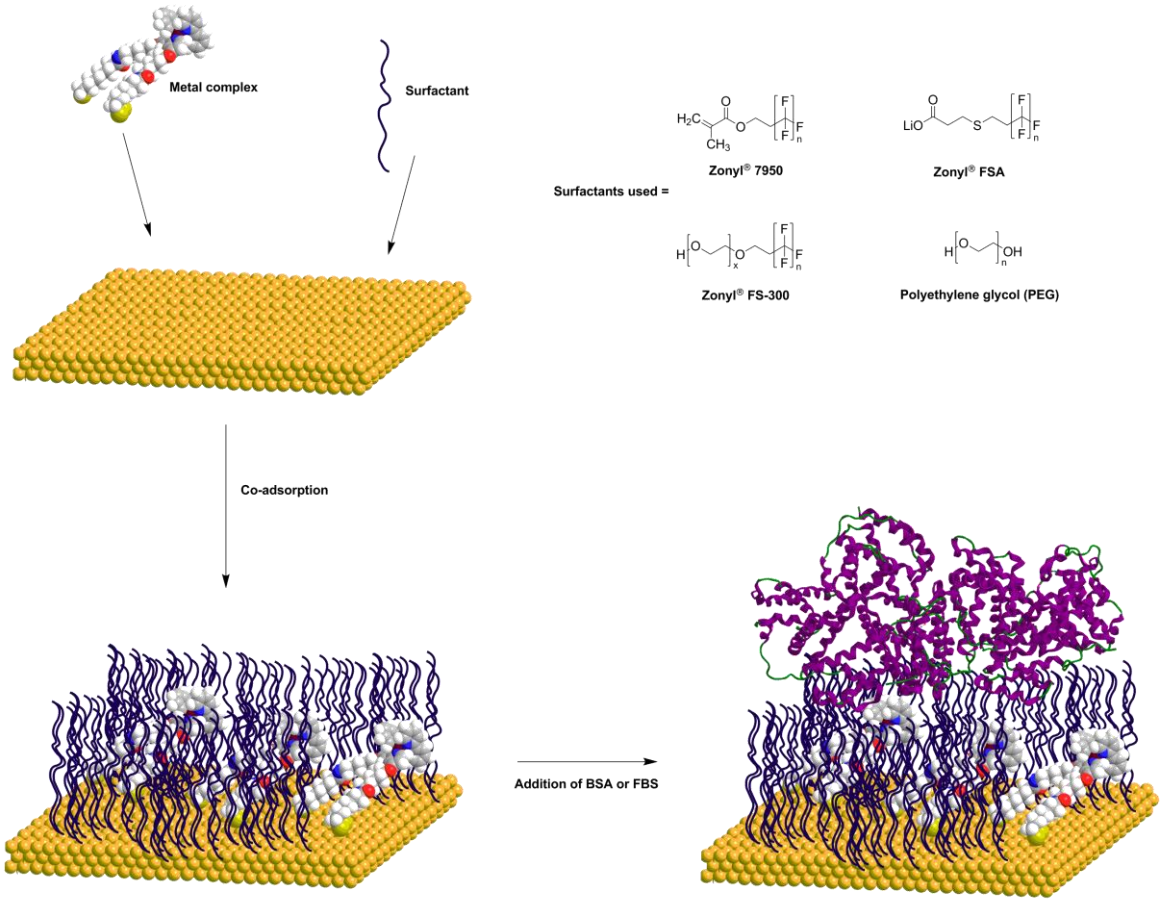


**Figure 3.3.** Schematic diagram of co-adsorption of complexes and surfactant and subsequent addition of BSA or FBS.

### 3.1.3 Photophysical Properties of Transition Metal Complex and Surfactant Mixed Monolayers

In order to examine the photophysical properties of the mixed monolayer systems on gold, a cleaned gold substrate was immersed in a 1 mM solution of **RubpySS** or **IrbpySS** containing *ca.* 50 µL of surfactant for 24 hours. Following this, the substrates were washed in acetonitrile and examined by steady state and time-resolved luminescence spectroscopy. Substrates were then further examined for changes upon the immersion of the substrates in a 16.5 µM solution of BSA in water for 30 minutes, followed by washing with water.

The data collected is summarised in Table 3.1 for **RubpySS** surfaces and Table 3.2 for **IrbpySS** surfaces. In general, it is observed that the addition of surfactant to **RubpySS** surfaces (Table 3.1) causes little or no shift in emission maximum. The changes in emission maxima for **IrbpySS** surfaces are more stark, in particular for **IrbpySS:PEG·Au**, where a 30 nm red shift is observed. It is also observed for surfaces of **IrbpySS** co-coated with **Zonyl® 7950** and **Zonyl® FSA** (Figure 3.A1) that artefacts also form in the spectra, as a result of possible Raman scattering caused by the presence of the surfactant.

A large red shift of the emission maxima for both complexes immersed with **Zonyl® 7950** upon the addition of BSA are observed, particularly a shift of 40 nm for **RubpySS** (Figure 3.4). Upon the addition of BSA to the other co-coated surfaces (Figure 3.4 and Figure 3.5), it is observed that the emission spectra exhibit small blue shifts, or do not shift at all, as is the case with **RubpySS:PEG·Au** and **IrbpySS:FS-300·Au**.

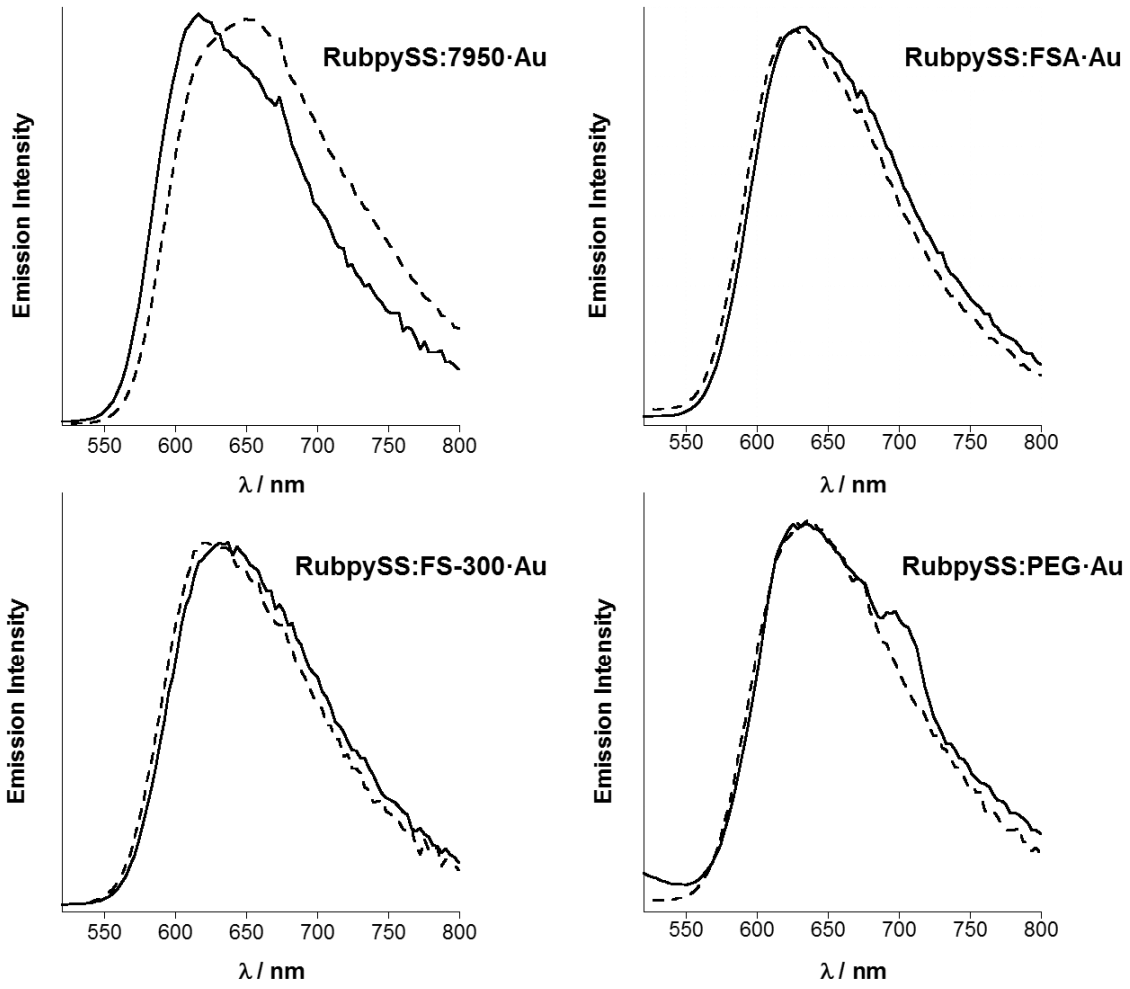


**Figure 3.4.** Steady state emission spectra of **RubpySS** co-coated with ethylene glycol containing surfactants before (solid) and after (dash) addition of BSA. $\lambda_{exc}$ = 465 nm, spectra corrected for instrument response. Spectral intensities are not to scale.

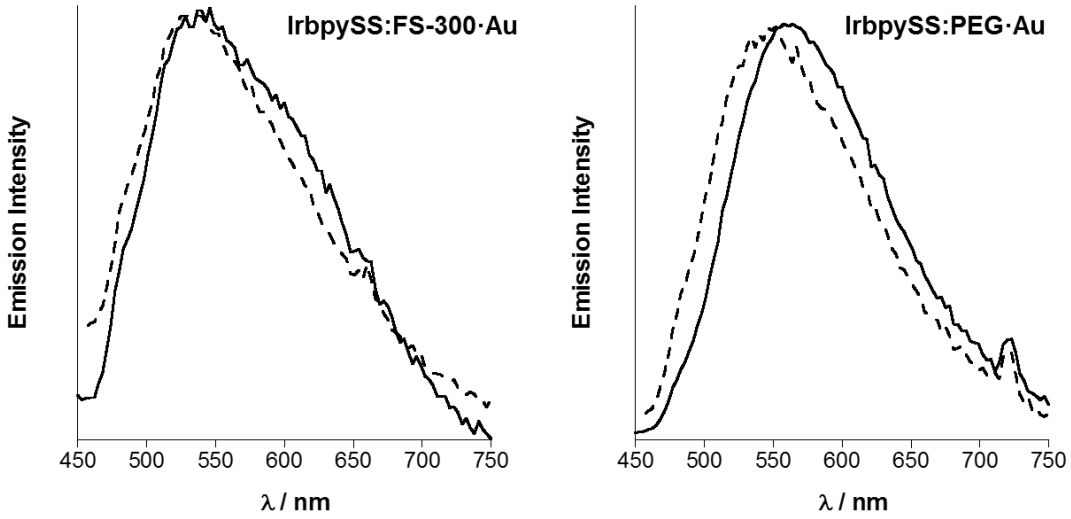


**Figure 3.5.** Steady state emission spectra of **IrbpySS** co-coated with ethylene glycol containing surfactants before (solid) and after (dash) addition of BSA. $\lambda_{exc}$ = 360 nm, spectra corrected for instrument response. Spectral intensities are not to scale.

**Table 3.1.** Photophysical properties of **RubpySS** co-coated with surfactant on gold. $\lambda_{exc}$ = 445 or 465 nm. $\lambda_{em}$ ($\tau$) = 620 nm.

| | $\lambda_{em}$ / nm | | $\tau$ / ns | |
|---|---|---|---|---|
| Surfactant used | without BSA | with BSA | without BSA | with BSA |
| **None (RubpySS·Au)** | 630 | 640 | 210 | 283 |
| **Zonyl® 7950** | 610 | 650 | 115 (10%)<br>475 (90%) | 214 (28%)<br>581 (72%) |
| **Zonyl® FSA** | 635 | 630 | 165 (14%)<br>765 (86%) | 31 (10%)<br>444 (90%) |
| **Zonyl® FS-300** | 640 | 620 | 51 (7%)<br>440 (93%) | 267 |
| **PEG** | 630 | 630 | 59 (5%)<br>546 (95%) | 24 (6%)<br>475 (94%) |

**Table 3.2.** Photophysical properties of **IrbpySS** co-coated with surfactant on gold. $\lambda_{exc}$ = 330, 360 or 376 nm. $\lambda_{em}$ ($\tau$) = 480 or 520 nm.

| | $\lambda_{em}$ / nm | | $\tau$ / ns | |
|---|---|---|---|---|
| Surfactant used | without BSA | with BSA | without BSA | with BSA |
| **None (IrbpySS·Au)** | 532 | 550 | 12 (17%)<br>130 (83%) | 15 (30%)<br>170 (70%) |
| **Zonyl® 7950** | 480 | 520 | 7 (52%)<br>64 (48%) | 133 (18%)<br>541 (82%) |
| **Zonyl® FSA** | 530 | 530 | 31 (14%)<br>245 (86%) | 67 (21%)<br>381 (79%) |
| **Zonyl® FS-300** | 540 | 540 | 106 (23%)<br>462 (78%) | 41 (13%)<br>310 (87%) |
| **PEG** | 560 | 550 | 80 (11%)<br>428 (89%) | 30 (16%)<br>351 (84%) |

The time-resolved data (Figure 3.6 and Figure 3.7) however does appear to show larger differences with respect to each surfactant. In particular, large increases in lifetimes for both complexes upon the addition of BSA for **Zonyl® 7950** (Figure 3.A2 and Figure 3.A3) containing surfaces is observed, as well as an increase in lifetime for **IrbpySS:FSA·Au** surfaces, of which both contain perfluorinated methylene groups. However, a significant decrease in luminescence lifetime is observed for **RubpySS:FSA·Au** (Figure 3.6), with the major component of the lifetime falling from 765 (86%) ns to 444 (90%) ns upon the addition of BSA. When ethylene glycol ether groups are present in the surfactant, we observe a decrease in the luminescence lifetime of the complexes upon the addition of BSA (Figure 3.6 and Figure 3.7), as evidenced by both the **Zonyl® FS-300** and **PEG** mixed monolayer systems. In particular, **Zonyl® FS-300** contains both perfluorinated methyl groups and ethylene glycol ether groups in its structure (Figure 3.3) suggesting that these ethylene glycol groups may affect the luminescence lifetimes of the complexes more than the fluorinated groups in the studied

systems. It is also observed that the lifetimes of all of the complex:surfactant systems on gold substrates are longer than when no surfactant is present with the exception of **IrbpySS:7950·Au**, which has a lifetime of 7 (52%), 64 (48%) ns compared with 12 (17%), 130 (83%) ns without a surfactant present.

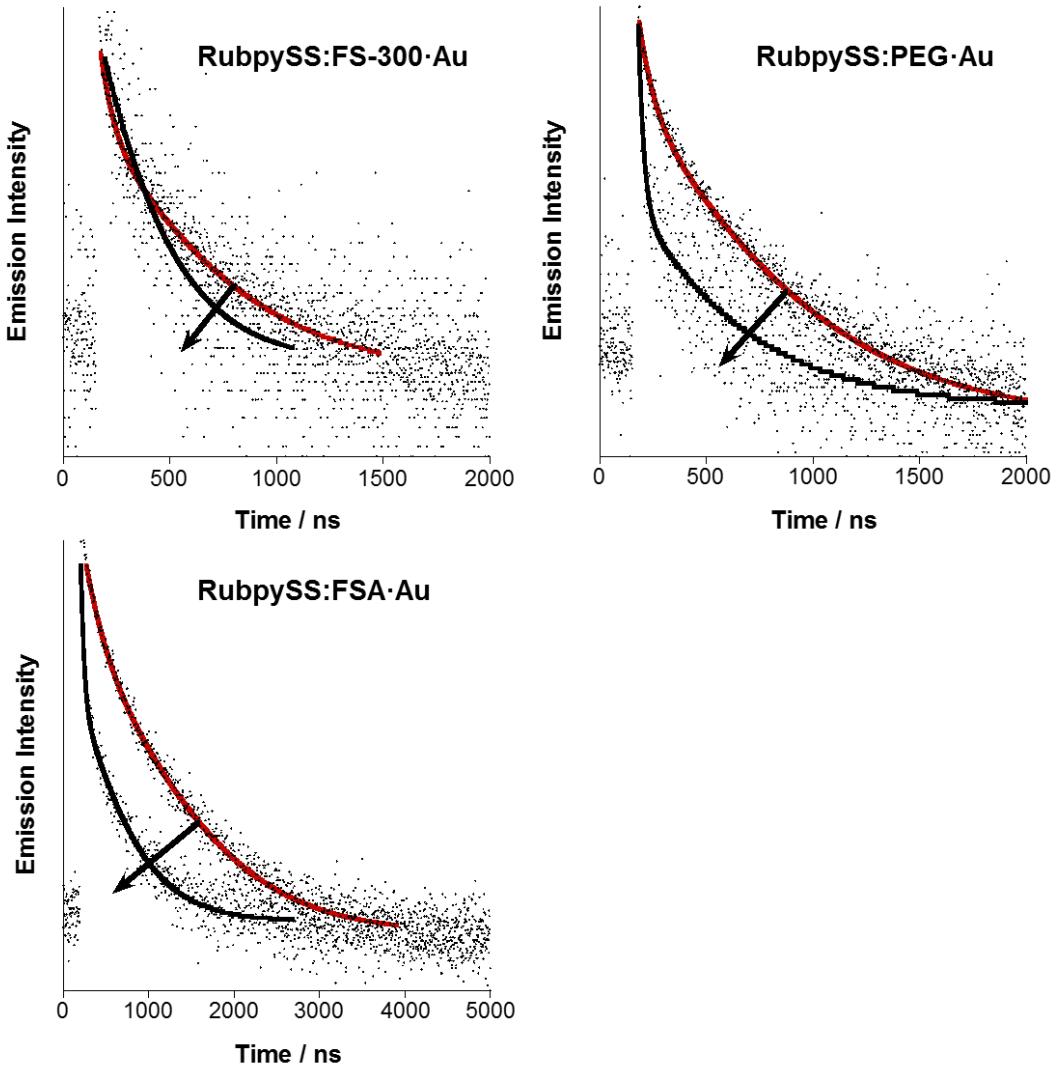


**Figure 3.6.** Fitted luminescence decays (dots with fitting lines) of **RubpySS** surfaces co-coated with surfactants, before (red) and after (black) BSA addition. $\lambda_{exc}$ = 445 nm, $\lambda_{em}$ = 620 nm. Luminescence intensities are not to scale.

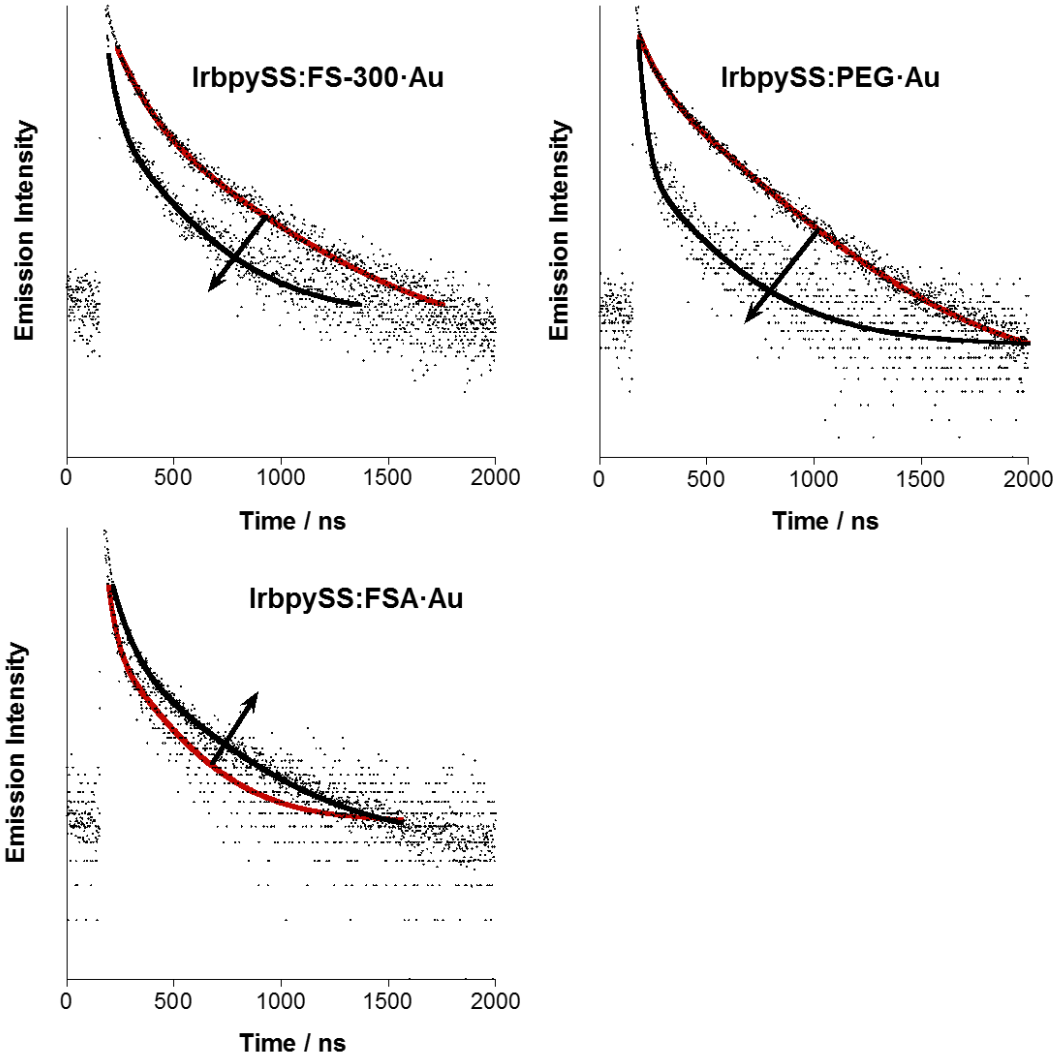


**Figure 3.7.** Fitted luminescence decays (dots with fitting lines) of **IrbpySS** surfaces co-coated with surfactants, before (red) and after (black) BSA addition. $\lambda_{exc}$ = 376 nm, $\lambda_{em}$ = 520 nm. Luminescence intensities are not to scale.

Given the increases in lifetimes observed when a surfactant is present for **RubpySS** and **IrbpySS**, we sought to determine whether this approach could be used to observe osmium(II) luminescence on a gold substrate. Previously, **OsbpySS**, an osmium(II) centred analogue of **RubpySS** was synthesised, however on gold surfaces we could not observe luminescence,[24]

and so therefore, we created a mixed monolayer system with **Zonyl® 7950** as the surfactant as described above. Figure 3.8 shows the steady state emission spectrum obtained, demonstrating that with complex:surfactant mixed monolayers we can observe the characteristic $^3$MLCT **OsbpySS** luminescence at the surface, centred at *ca*. 740 nm. The lifetime of the emission is determined to be 38 ns, which is longer than the lifetime of **OsbpySS** in aerated solution (20 ns).[24]

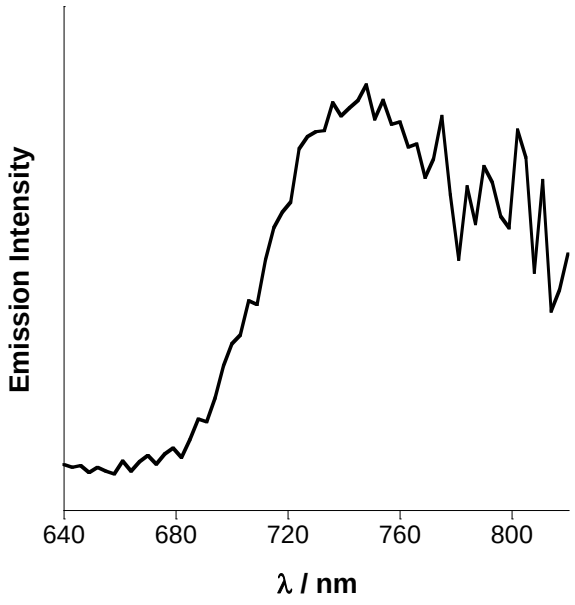


**Figure 3.8.** Steady state emission spectrum of **OsbpySS:Zonyl® 7950·Au**. $\lambda_{exc}$ = 480 nm. Spectrum corrected for instrument response.

## 3.1.4 Surface Plasmon Resonance Recognition Studies of Transition Metal Complex and Surfactant Mixed Monolayers

In order to examine the interaction between the mixed monolayer systems and biological media, we employed SPR spectroscopy to measure the recognition of the substrates by both BSA, and

fetal bovine serum (FBS), a proteinous mixture extracted from bovine blood. FBS was chosen because of its common use in *in vitro* cell studies as a cell medium.[19, 25] Substrates were formed as above, before equilibrating the substrates by flowing water over them at 50 µL $min^{-1}$, followed by injecting the protein across the surface at 1500 µL $min^{-1}$ for 10 seconds. The flow rate was then reduced to 10 µL $min^{-1}$ to allow recognition to occur, before 2 minutes of washing at 1500 µL $min^{-1}$ and a further 10 minutes at 50 µL $min^{-1}$. The results are shown in Figure 3.9 for **RubpySS** systems and Figure 3.10 for **IrbpySS** systems.

The results show that for all mixed monolayer systems, injection of either BSA or FBS results in a large increase in response (ΔΘ) from the surfaces, indicating that both BSA and FBS do indeed bind to the mixed monolayer surfaces. In particular, it is observed for all surfaces with the exception of **RubpySS:Zonyl® FS-300·Au** (Figure 3.9 c), that after washing of the surfaces, the response for BSA is decreased when compared with the same system without co-coating with surfactant. (Figure 3.9 and Figure 3.10). In the case of **RubpySS:Zonyl® FS-300·Au** (Figure 3.9, c) we observe that the response is the same (0.42º), subsequent to the washing step. Interestingly, the response of FBS when injected across the mixed monolayer systems was lower than that of BSA, with the exception of substrates where **Zonyl® 7950** was used as the surfactant. We postulate that the increased hydrophobicity of the surfactant compared with the other surfactants may induce binding with a more hydrophobic component of FBS, causing the increase in response compared with that of BSA.

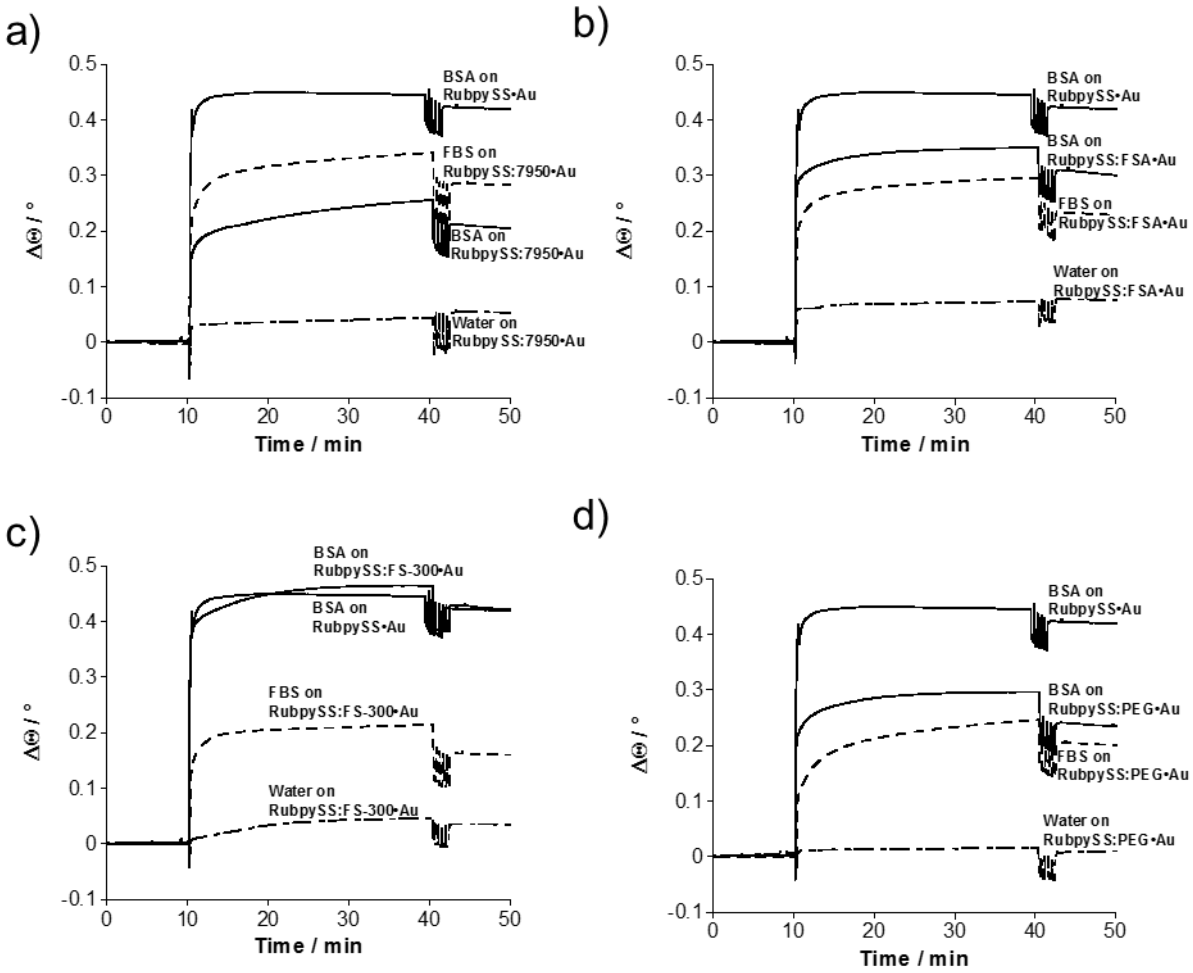


**Figure 3.9.** SPR sensorgrams of **RubpySS** and surfactant mixed monolayers. Surfactants used in each graph are **Zonyl® 7950** (a), **Zonyl® FSA** (b), **Zonyl® FS-300** (c) and **PEG** (d).

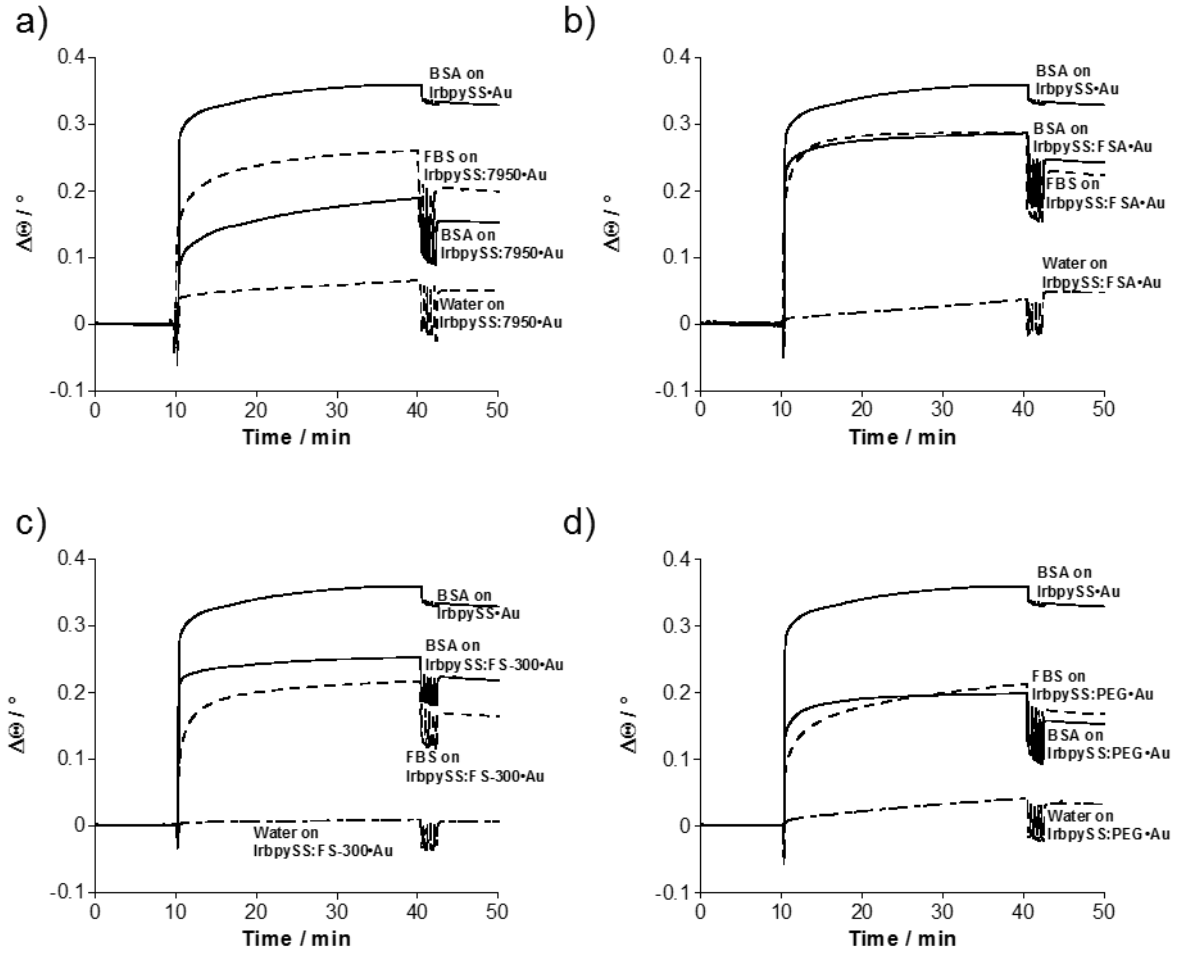


**Figure 3.10.** SPR sensorgrams of **IrbpySS** and surfactant mixed monolayers. Surfactants used in each graph are **Zonyl® 7950** (a), **Zonyl® FSA** (b), **Zonyl® FS-300** (c) and **PEG** (d).

## 3.1.5 Conclusions

In this section we have shown that transition metal complexes **RubpySS** and **IrbpySS** can be co-coated with various commercially available surfactants, whilst still allowing observable luminescence. Strikingly, **OsbpySS** luminescence could also be observed by co-coating in this way. Interestingly, but unsurprisingly, the luminescence lifetimes of **RubpySS** and **IrbpySS** are altered upon co-coating with surfactants, most likely due to the effects of being presented with more hydrophilic or hydrophobic environments. In general, it was observed that the

luminescence lifetime of the complexes in the presence of BSA was enhanced when co-coated with hydrophobic surfactants, and quenched in the presence of more hydrophilic surfactants. Through SPR spectroscopy we show that in general, BSA adsorption is decreased when the surfaces are co-coated, again with the exception of **RubpySS:Zonyl® FS-300**. The results with FBS treated surfaces proved more complex, however the results indicate that surfaces co-coated with **Zonyl® 7950** are most susceptible to biomolecular recognition in FBS, while less so in BSA. The results illustrate the complexity of interactions between protein mixtures and functionalised surfaces, but continued research in this field will invariably lead to targeted design of bionanosystems, and indeed solution and nanoparticle studies with these complexes are ongoing.

# 3.2 Preparation and Properties of β-cyclodextrin containing transition metal complexes

## 3.2.1 Introduction

Microcontact printing (μCP) provides a facile and inexpensive alternative to 'bottom-up' approaches of nanofabrication.[26] Despite its commercial failings in the semiconductor industry, the technique, first outlined by Whitesides,[27] has allowed researchers to utilise and expand the technique to improve its usefulness in other fields.[28] In its infancy, μCP was used as a method for directing assembly of thin films onto surfaces in order to create a chemical resist in order to allow the etching of the surface to create patterned substrates for microelectronics. Further studies of the technique however also allowed chemistry to be performed. An early example by Yan *et al*.[29] (Figure 3.11) illustrates this through a patterned amide coupling reaction. Here, a gold surface functionalised with a carboxylic acid terminated alkanethiol was deposited on the surface through self-assembly and reacted to form an acid anhydride terminated surface. Through μCP, poly(ethylene)imine was brought into close contact with the surface allowing a reaction to take place, leading to the patterned surface. Atomic force microscopy experiments indicated that indeed, patterns could be formed on surfaces through the microcontact chemistry method. As such, many other studies have emulated this, employing other chemistries such as 'click' chemistry,[30, 31] photochemistry[32] and even metal complexation,[33] as well as other amide coupling conditions such as through acid fluoride terminated surfaces[34] and aminolysis.[35, 36]

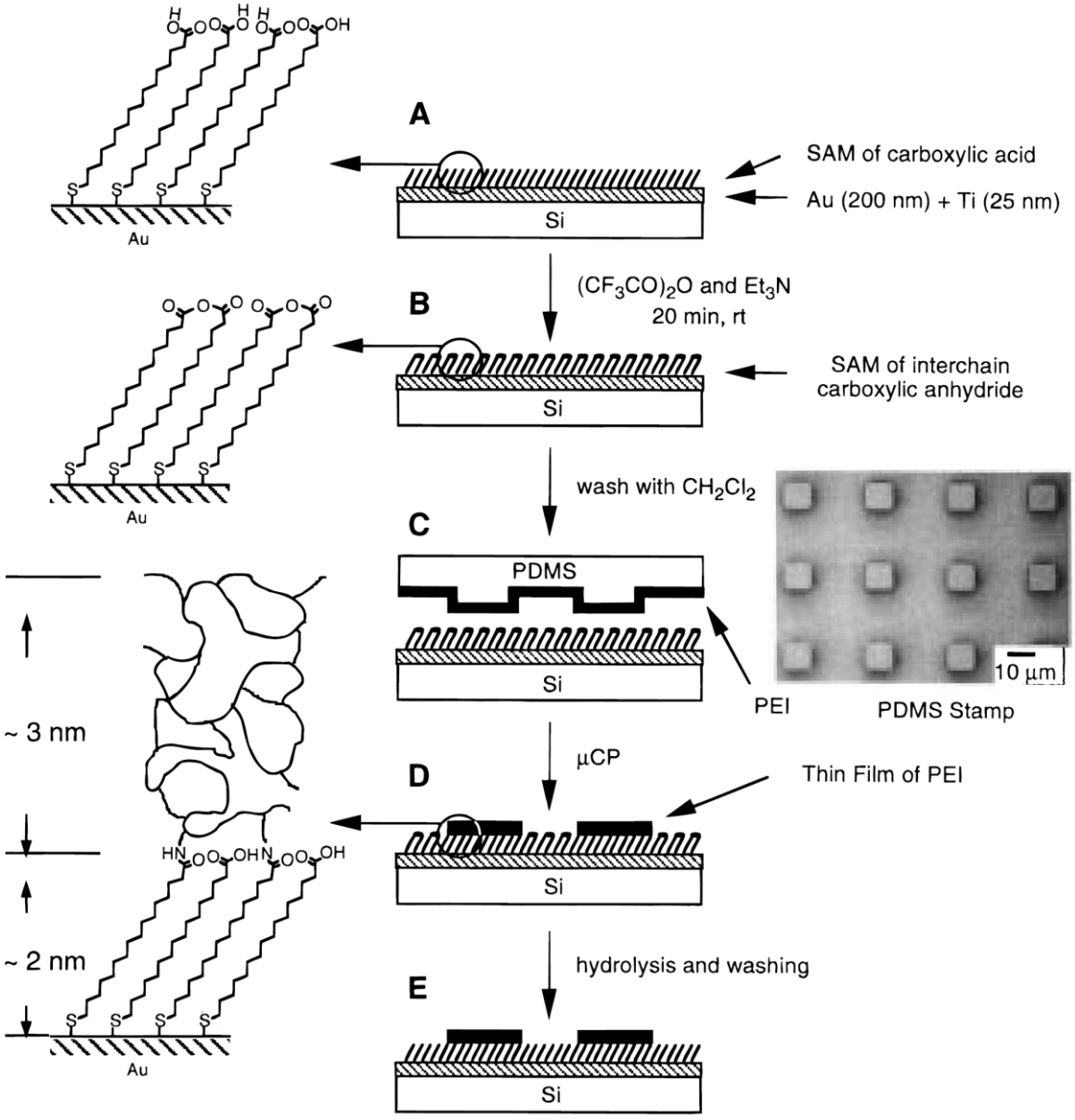


**Figure 3.11.** Schematic of patterned amide coupling of poly(ethylene)imine on carboxylic acid terminated surfaces. Reprinted with permission from reference (29). Copyright 1999 American Chemical Society.

The technique however is not only limited to chemical processes, but can also be utilised using supramolecular interactions. The development of cyclodextrin functionalised surfaces as 'molecular printboards' has allowed the formation of nanostructures in a facile manner, due to

the removal of the need for bond formation. The design of these systems is simple (Figure 3.12), cyclodextrin terminated monolayers are brought into contact with the molecule of interest, which generally bears adamantyl groups, and a host-guest complex of the cyclodextrin and adamantyl group is formed, leading to the creation of nanostructures through supramolecular interactions. Using this technique, many different nanostructures can be formed, and indeed many examples exist in the literature of complex patterned nanostructures created using this technique.[37-43]

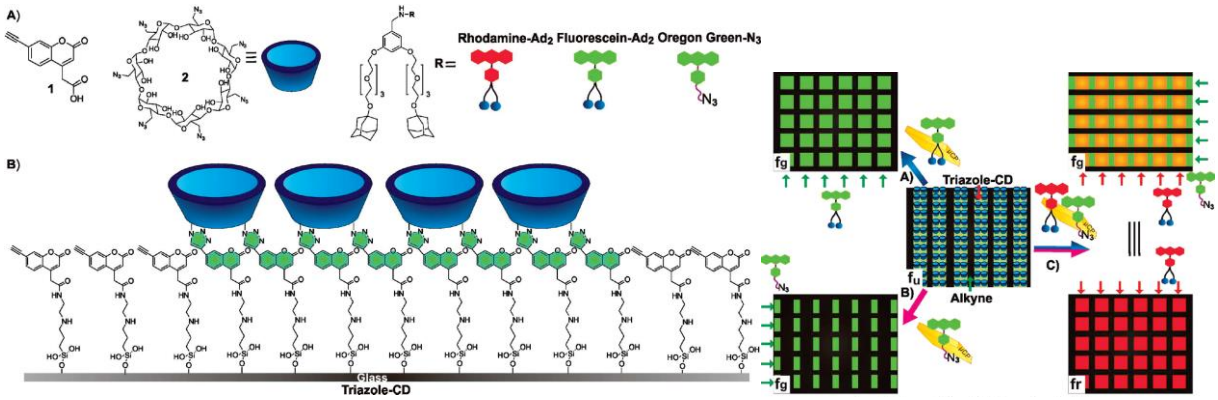


**Figure 3.12.** Example of mixture of microcontact chemistry and supramolecular µCP. Reprinted with permission from reference (43). Copyright 2010 American Chemical Society.

## 3.2.2 Section Outline

In this section we seek to expand the µCP protocol used in chapter two to allow more facility in the directed assembly of luminescent metal complexes at interfaces. We report the synthesis and characterisation of cyclodextrin containing complexes with ruthenium(II) or iridium(III) centres for the purposes of supramolecular µCP. Utilising adamantyl functionalised gold surfaces, it is shown that layers of the complexes can be formed through supramolecular interactions, and that µCP can be carried out under much shorter timescales than the chemically bound systems of **RubpySS** and **IrbpySS**. We also show that utilising this technique, we can

direct assembly of both the ruthenium(II) and iridium(III) complex onto the surface to create multicomponent patterned surfaces.

### 3.2.3 Synthesis of β-cyclodextrin containing transition metal complexes

The synthetic route to the functionalization of 2,2′-bipyridine with β-cyclodextrin is elaborated and discussed in chapter 4. Scheme 3.1 shows the synthetic route used to obtain **Rubpy-CD (2)** and **Irbpy-CD (3)** in acceptable yields. Briefly, the complexes were synthesised by modified routes originally outlined by Sullivan *et al.*[44] and Slinker *et al.*[45] where $Ru(bpy)_2Cl_2$ or $[Ir(ppy)_2Cl]_2$ are heated in solution with **bpy-CD (1)**, followed by purification of the complexes by size exclusion chromatography.

The multiplet peak at 5.04-5.28 ppm corresponds to the anomeric centre H-g-1. The aromatic region displays 4 prominent environments – H-5 at 7.32-7.46 ppm, H-6 at 7.67-7.79 ppm, H-4 at 8.01-8.12 ppm and H-3 at 8.49-8.55 ppm. Interestingly, the environments in each of the bipyridyl ligands are not split by the asymmetric nature of **bpy-CD (1)**, however the peaks are observed to be broader than expected, most likely due to that reason. The $^{13}C$ NMR spectrum agrees well with similar cyclodextrin containing complexes produced in the group.[48, 49] The ESI(+) mass spectrum shows one ion envelope at 998 Da corresponding to $(M\text{-}2[PF_6])^{2+}$ confirming the formation of the product. The yield of the synthesis is low (8%), which is attributed to the difficulty of separation. In particular, it was found that precipitation of the hexafluorophosphate salt was very wasteful, due to the solubility of the cyclodextrin moiety in a wide range of organic solvents. For this reason, subsequent syntheses were performed without salt exchange.

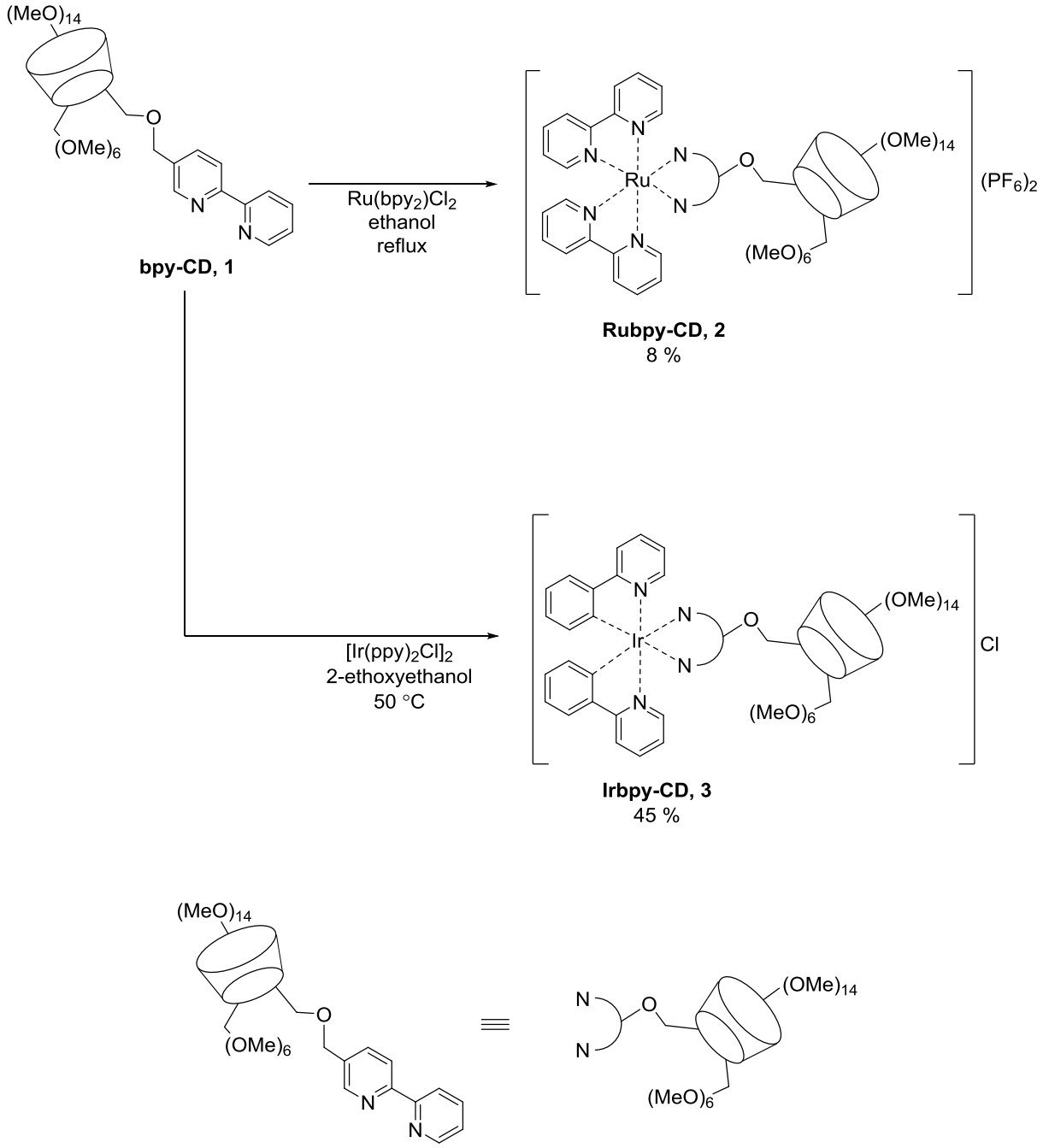


**Scheme 3.1.** Synthetic route to the formation of cyclodextrin containing complexes.

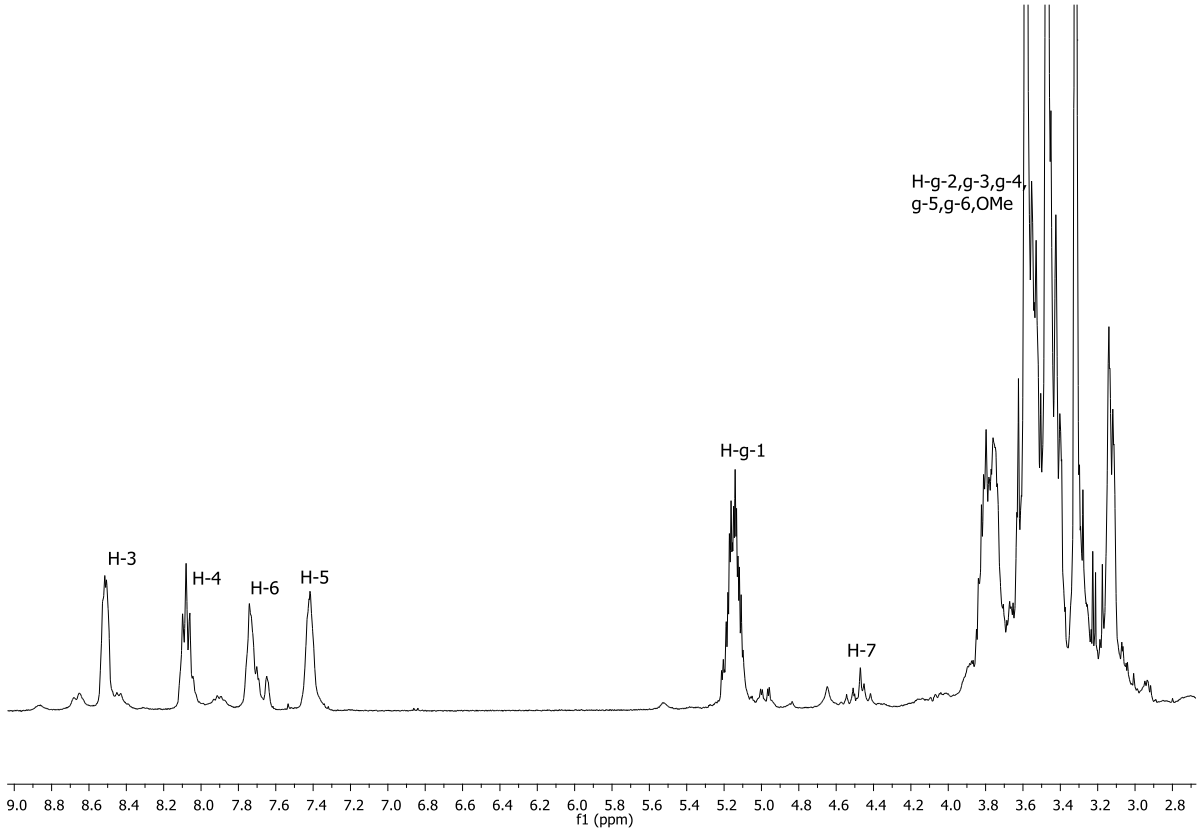


**Figure 3.13.** $^{1}$H NMR spectrum of **Rubpy-CD (2)** in $CD_3CN$.

**Irbpy-CD (3)** was characterised by $^{1}$H, $^{13}$C and 2D NMR spectroscopy, and ESI(+) mass spectrometry. The $^{1}$H NMR spectrum (Figure 3.14) reveals a similar pattern of peaks, with the region at 2.96-4.27 ppm agreeing well with the spectrum of **Rubpy-CD (2)**. In this spectrum we can see the peak at 3.98-4.20 ppm, corresponding to H-g-6, and again we see peaks at 4.29-4.87 ppm corresponding to H-7. A broad multiplet at 5.08-5.23 ppm is observed corresponding to H-g-1. The aromatic protons appear between 6.20-8.93 ppm and integrate fairly well with H-g-1, however exact assignments could not be made. The pattern of peaks is expectedly different to that of **Rubpy-CD (2)** due to the inherent asymmetric nature of the ancillary ligand 2-phenylpyridine compared with 2,2′-bipyridine. This, coupled with the formation of many possible stereoisomers around the iridium(III) centre leads to the arisal of many peaks. Once again the $^{13}$C NMR spectrum agrees fairly well with similar cyclodextrin containing

complexes.[48, 49] The ESI(+) mass spectrum reveals one ion envelope at 1051 corresponding to $(M\text{-}Cl+NH_4)^+$ confirming the formation of the product.

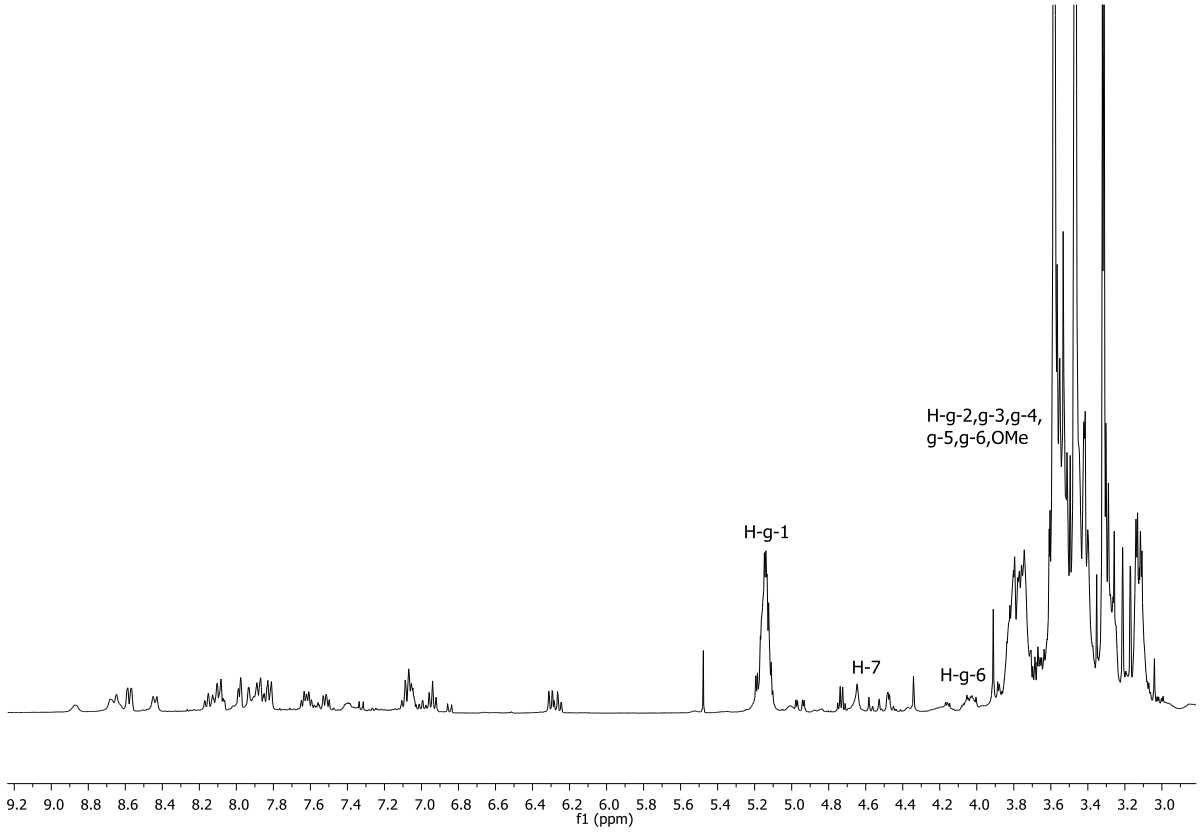


**Figure 3.14.** $^1$H NMR spectrum of **Irbpy-CD (3)** in $CD_3CN$

## 3.2.4 Photophysical Properties of β-cyclodextrin Containing Transition Metal Complexes

To elucidate the photophysical properties of the complexes, each were studied by UV-vis absorption spectroscopy and steady state and time-resolved luminescence spectroscopy in acetonitrile solutions. The results are summarised in Table 3.3. The UV-vis absorption spectrum of **Rubpy-CD (2)** (Figure 3.15) reveals two large absorption bands at 288 and 451 nm corresponding to the $^1\pi$-$\pi^*$ and $^1$MLCT transitions respectively.[47] The UV-vis spectrum is very comparable to that of $[Ru(bpy)_3]^{2+}$, with a very small hypsochromic shift of 1 nm in the $^1$MLCT

transition for **Rubpy-CD (2)**. It is also observed that the molar absorptivity of the $^1$MLCT band for **Rubpy-CD (2)** is approximately half that of $[Ru(bpy)_3]^{2+}$, which is attributed to the large, non-chromophoric cyclodextrin moiety. A similar picture emerges for **Irbpy-CD (3)** (Figure 3.16), with a large single peak at 249 nm, agreeing fairly well with $[Ir(ppy)_2bpy]^+$.[50] The luminescence properties of both **Rubpy-CD (2)** (Figure 3.15) and **Irbpy-CD (3)** (Figure 3.16) also agree well with their less functionalized counterparts, with emission maxima of 620 and 605 nm respectively, compared with 615 nm for $[Ru(bpy)_3]^{2+}$ and 610 nm for $[Ir(ppy)_2bpy]^+$. The luminescence lifetimes of **Rubpy-CD (2)** in both aerated and deaerated acetonitrile solution are comparable to those of $[Ru(bpy)_3]^{2+}$, and luminescence quantum yield data is also very similar, with identical (10%) deaerated quantum yields, and relatively similar aerated quantum yields of 2% and 1% for **Rubpy-CD (2)** and $[Ru(bpy)_3]^{2+}$ respectively. The luminescence lifetimes of **Irbpy-CD (3)** were found to be biexponential, with values of 37 (9%) ns and 84 (91%) ns reported in aerated solution, and 306 (87%) ns and 714 (13%) ns in dearated acetonitrile solution. The major component of the deaerated lifetime is comparable to that of $[Ir(ppy)_2bpy]^+$.

**Table 3.3.** Summarised photophysical properties of **Rubpy-CD (2)**, **Irbpy-CD (3)** and comparable complexes in acetonitrile solution.

| Complex | $\lambda_{max}$ / nm ($\varepsilon$ / $10^4$ $M^{-1}$ $cm^{-1}$) | $\lambda_{em}$ / nm | $\tau$ / ns | | $\Phi$ / % | |
|---|---|---|---|---|---|---|
| | | | aerated | deaerated | aerated | deaerated |
| **Rubpy-CD (2)** | 288 (3.6) 451 (0.5) | 620 | 189 | 934 | 2 | 10 |
| **Irbpy-CD (3)** | 249 (2.4) 266 (2.3) sh 314 (1.0) sh 380 (0.3) sh | 605 | 37 (9%) 84 (91%) | 306 (87%) 714 (13%) | 1 | 6 |
| $[Ru(bpy)_3]^{2+}$ | 452 (1.3)[51] | 615[51] | 172 | 840 | 1 | 10 |
| $[Ir(ppy)_2bpy]^+$ | 230 (7.0) 250 (6.5) sh 310 (3.0) sh 380 (0.45) sh[50] | 610[50] | | 350[50] | | |

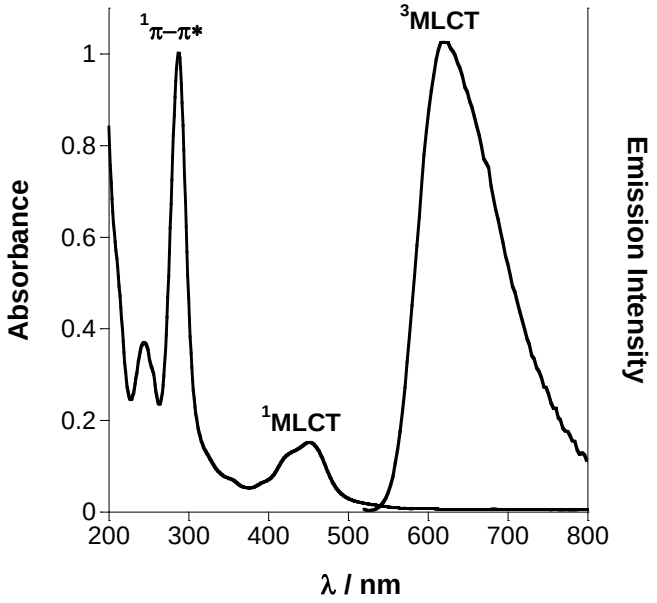


**Figure 3.15.** UV-vis absorption spectrum (left) and steady state emission spectrum (right) of **Rubpy-CD (2)** in acetonitrile solution (28 µM). $\lambda_{exc}$ = 460 nm. Emission spectrum corrected for instrument response.

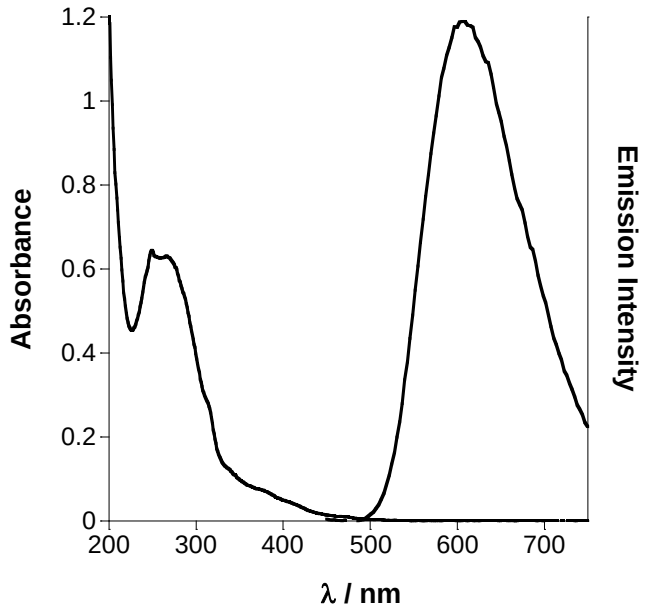


**Figure 3.16.** UV-vis absorption spectrum (left) and steady state emission spectrum (right) of **Irbpy-CD (3)** in acetonitrile solution (27.4 μM). $\lambda_{exc}$ = 350 nm. Emission spectrum corrected for instrument response.

## 3.2.5 Preparation of Adamantyl Containing Surface-Active Linker for Recognition of Cyclodextrin Groups on the Surface

In order to study the photophysical properties of **Rubpy-CD (2)** and **Irbpy-CD (3)** on the surface, a necessary scaffold needed to be created in order for the complexes to bind. To this end, a simple surface-active linker bearing an adamantyl group (Scheme 3.2) was synthesised to facilitate surface binding of the cyclodextrin (**AdSS**, **4**). Such a molecule had been synthesised previously in the group, for studying a similar homoleptic *tris*-bipyridyl ruthenium(II) complex bearing three cyclodextrin moieties.[52] In this study, 1-adamantylamine and α-lipoic acid were subjected to amide coupling conditions to yield **AdSS (4)** in a low but acceptable yield.

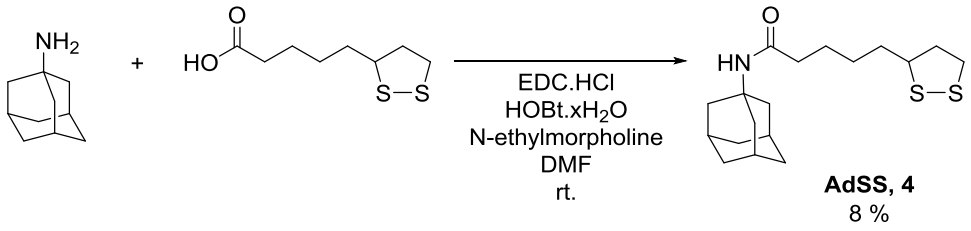


**Scheme 3.2.** Route to adamantyl functionalized surface-active linker **AdSS (4)**.

**AdSS (4)** was characterised by $^{1}H$, $^{13}C$ and 2D NMR spectroscopy, and ESI(+) mass spectrometry. NMR assignments were confirmed by COSY, HSQC and HMBC and assignments agree with previously published results.[53] Figure 3.A12 shows the $^{1}H$ NMR spectrum of the product, revealing the expected number of environments, while the integrals of protons associated with each of the moieties agree well with each other, particularly H-6 (1H) against H-b (3H, partially masked by H-2) and H-c (6H, partially masked by H-7′). The ESI(+) mass spectrum reveals 3 ion envelopes at 340 $(M+H)^{+}$, 362 $(M+Na)^{+}$ and 701 Da $(2M+Na)^{+}$, confirming the formation of the product.

## 3.2.6 Surface Studies of β-Cyclodextrin Containing Transition Metal Complexes

In order to study the properties of **Rubpy-CD (2)** and **Irbpy-CD (3)** on gold surfaces and to test the efficacy of functionalising surfaces with these complexes *via* a μCP method, a scaffold was first formed by immersing plain gold substrates in a 1 mM solution of **AdSS (4)** in ethanol. The substrates were then washed in acetonitrile and methanol, allowing the functionalization of the surfaces with the complexes, as shown in Scheme 3.3.

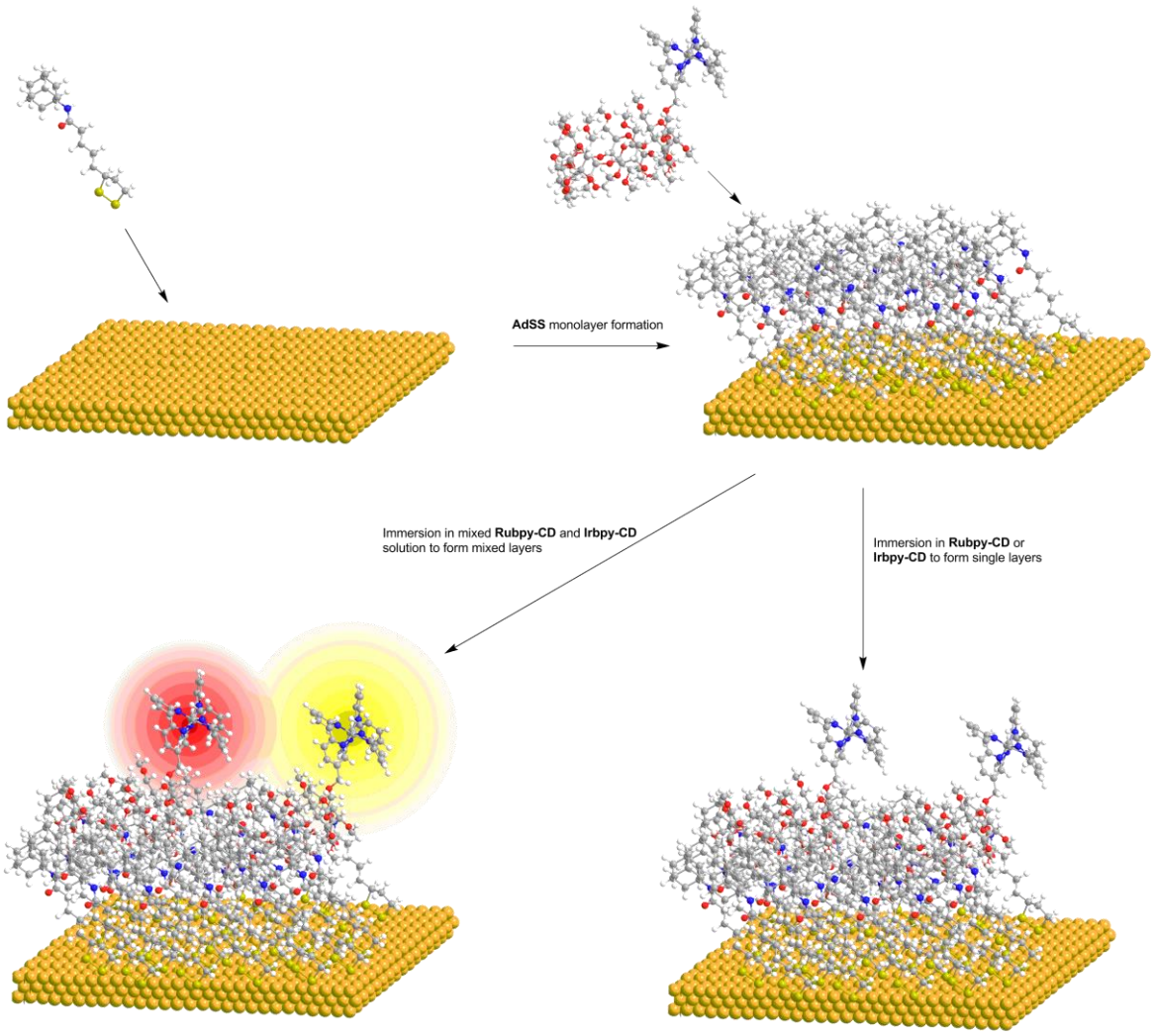


**Scheme 3.3.** Schematic diagram illustrating the route to formation of **AdSS (4)** monolayers and subsequent functionalisation with **Mbpy-CD** complexes.

To elucidate whether the complexes would indeed bind to the **AdSS (4)** functionalised substrates (**AdSS·Au**), ellipsometric, steady state and time-resolved luminescence studies were carried out. **AdSS·Au** substrates were immersed in 1 mM solutions in acetonitrile of each complex, washed (acetonitrile) and tested. The results (Figure 3.17) reveal the layer thickness of **AdSS·Au** to be 1.5±0.2 nm. This result is slightly higher than the expected thickness (*ca.* 1 nm) suggesting a well packed monolayer is formed. The results for the compexes show increases in layer thickness, particularly for **Rubpy-CD:AdSS·Au**, which has increased to

2.9±0.5 nm, agreeing fairly well with the expected height, and indicating that the host-guest complex between **Rubpy-CD (2)** and **AdSS (4)** forms at the interface. A similar result is reported for **Irbpy-CD:AdSS·Au**, with a layer thickness of 2.2±0.6 nm.

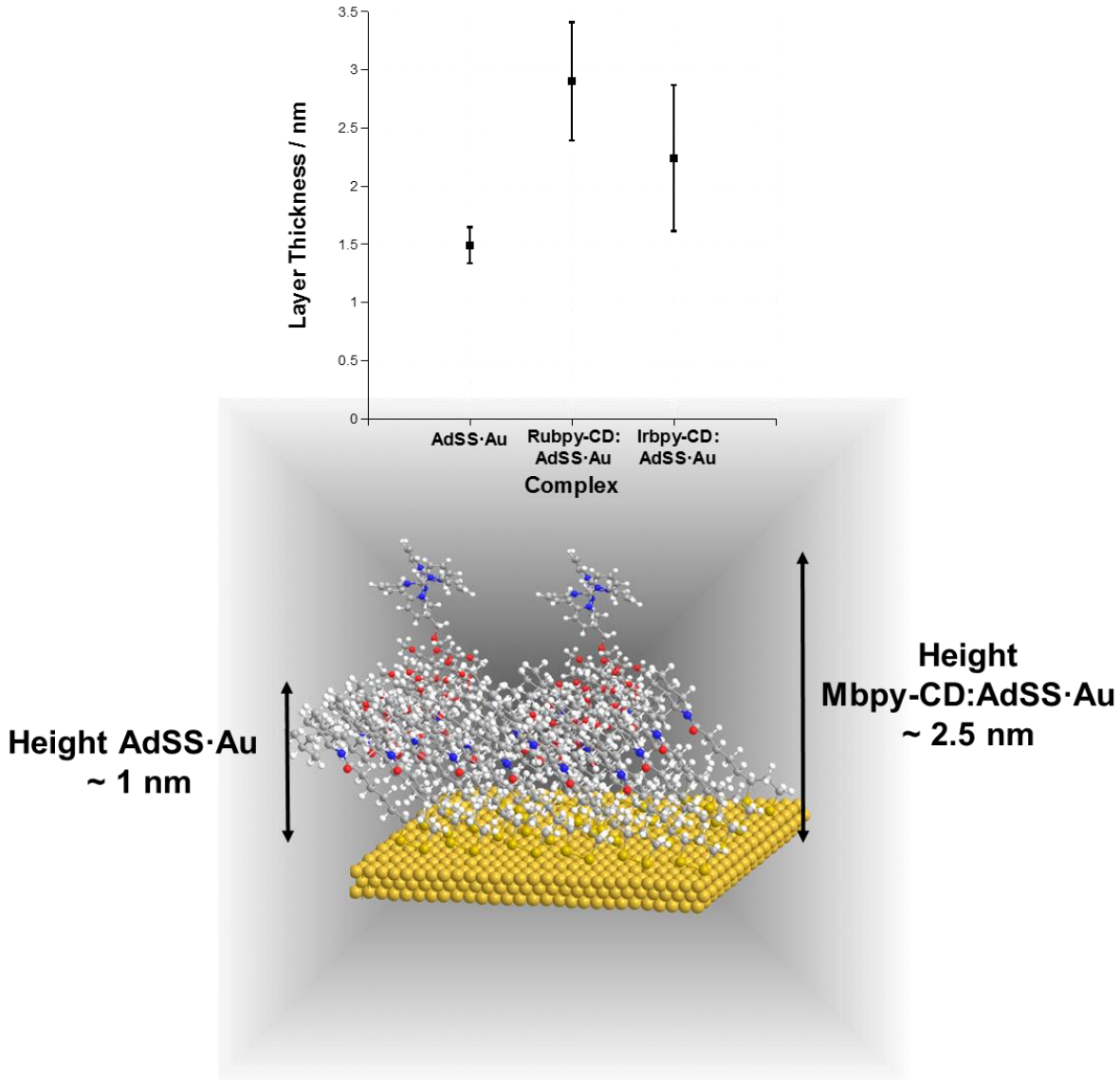


**Figure 3.17.** Top – Ellipsometric data for **AdSS·Au** and host-guest complexes at surface. Bottom – Schematic of **AdSS·Au** monolayer and host-guest complexes at surface.

The luminescence data is summarised in Table 3.4. The luminescence emission spectra (Figure 3.18) reveal broad emission bands centred at 590 and 525 nm for **Rubpy-CD:AdSS·Au** and **Irbpy-CD:AdSS·Au** respectively. These bands have large blue shifts compared with those in acetonitrile solution, with shifts of 30 nm for **Rubpy-CD (2)** and 80 nm for **Irbpy-CD (3)**. Such blue shifts have been observed previously for transition metal complexes on gold surfaces.[24] An instrumental artefact is also observed on the spectrum for **Irbpy-CD:AdSS·Au** centred at *ca.* 720 nm, and is due to second order scattering arising from the excitation source (360 nm). Luminescence experiments were also carried out on plain gold substrates immersed in each complex and washed as above. Neither **Rubpy-CD** nor **Irbpy-CD** substrates produced any detectable luminescence, indicating that the method of binding to the surface for both of these complexes is through the terminal adamantyl groups of **AdSS**.

**Table 3.4.** Summarised luminescence data of **Rubpy-CD** and **Irbpy-CD** complexes on the surface and in solution. [a]In aerated acetonitrile solution.

| Complex | $\lambda_{em}$ / nm | $\tau$ / ns |
|---|---|---|
| **Rubpy-CD:AdSS·Au** | 590 | 209 (15%)<br>1042 (85%) |
| **Rubpy-CD (2)**[a] | 620 | 189 |
| **Irbpy-CD:AdSS·Au** | 525 | 116 (13%)<br>987 (87%) |
| **Irbpy-CD (3)**[a] | 605 | 37 (9%)<br>84 (91%) |

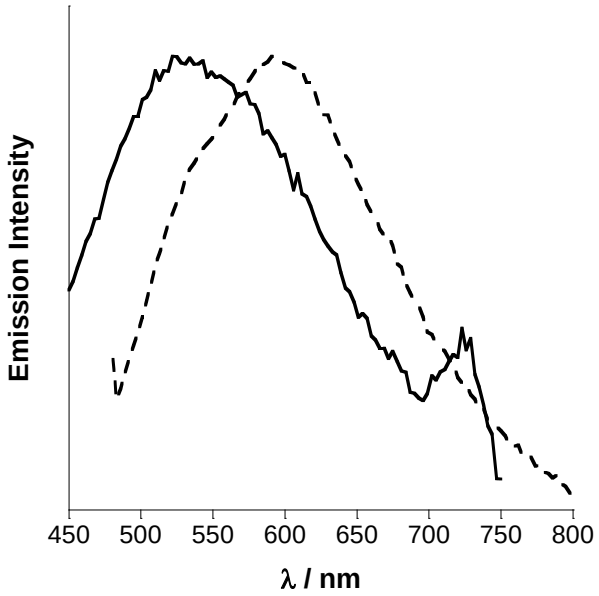


**Figure 3.18.** Steady state emission spectra of **Irbpy-CD:AdSS·Au** (solid, $\lambda_{exc}$ = 360 nm) and **Rubpy-CD:AdSS·Au** (dash, $\lambda_{exc}$ = 460 nm). Spectral intensities not to scale, spectra corrected for instrument response.

To examine whether the spectrum of luminescence in such systems could be increased, a mixed monolayer of **Irbpy-CD** and **Rubpy-CD** on **AdSS·Au** was formed and examined by steady state and time-resolved luminescence spectroscopy. **AdSS·Au** substrates were formed as above, before immersing them in a 1:1 mixture (1 mM in acetonitrile) of the two complexes, before washing (acetonitrile) and drying. The luminescence spectra (Figure 3.19) illustrate two similar emission bands when subjected to different excitation wavelengths. All of the bands are centred at *ca.* 610 nm, however when using an excitation wavelength of 320 nm, where the molar absorptivity of **Irbpy-CD (3)** is relatively high, and **Rubpy-CD (2)** is relatively low, we observe the FWHM of the emission band increase from 130 nm ($\lambda_{exc}$ = 290, 460 nm) to 140 nm ($\lambda_{exc}$ = 320 nm), indicating the presence of both complexes on the surface of the substrate.

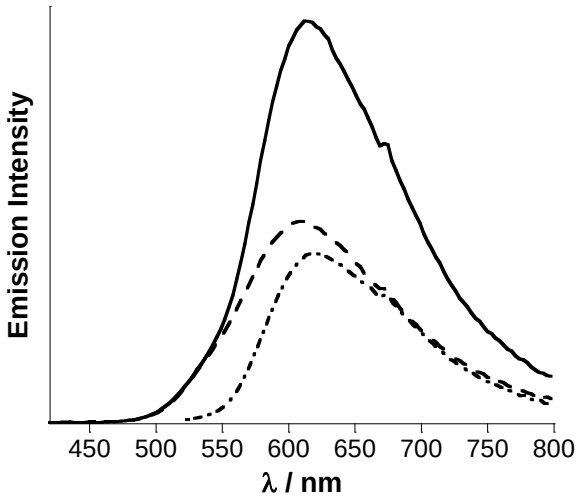


**Figure 3.19.** Steady state emission spectra of mixed monolayer **Rubpy-CD/Irbpy-CD:AdSS·Au**. $\lambda_{exc}$ = 290 nm (solid), 320 nm (dash), 460 nm (dot dash). Spectra corrected for instrument response.

To examine whether a μCP protocol could be used to stamp **Rubpy-CD (2)** or **Irbpy-CD (3)** on **AdSS·Au** substrates, luminescence microscopy studies were carried out. Scheme 3.4, step i) illustrates the protocol carried out. **AdSS·Au** substrates were produced as above, before immersing PDMS stamps (10 μm long square features) with a 1 mM solution of **Rubpy-CD (2)** or **Irbpy-CD (3)** in methanol for 20 minutes and subsequently drying. The complexes were then stamped on the **AdSS·Au** substrates for 2 minutes and washed with 10% methanol in water.

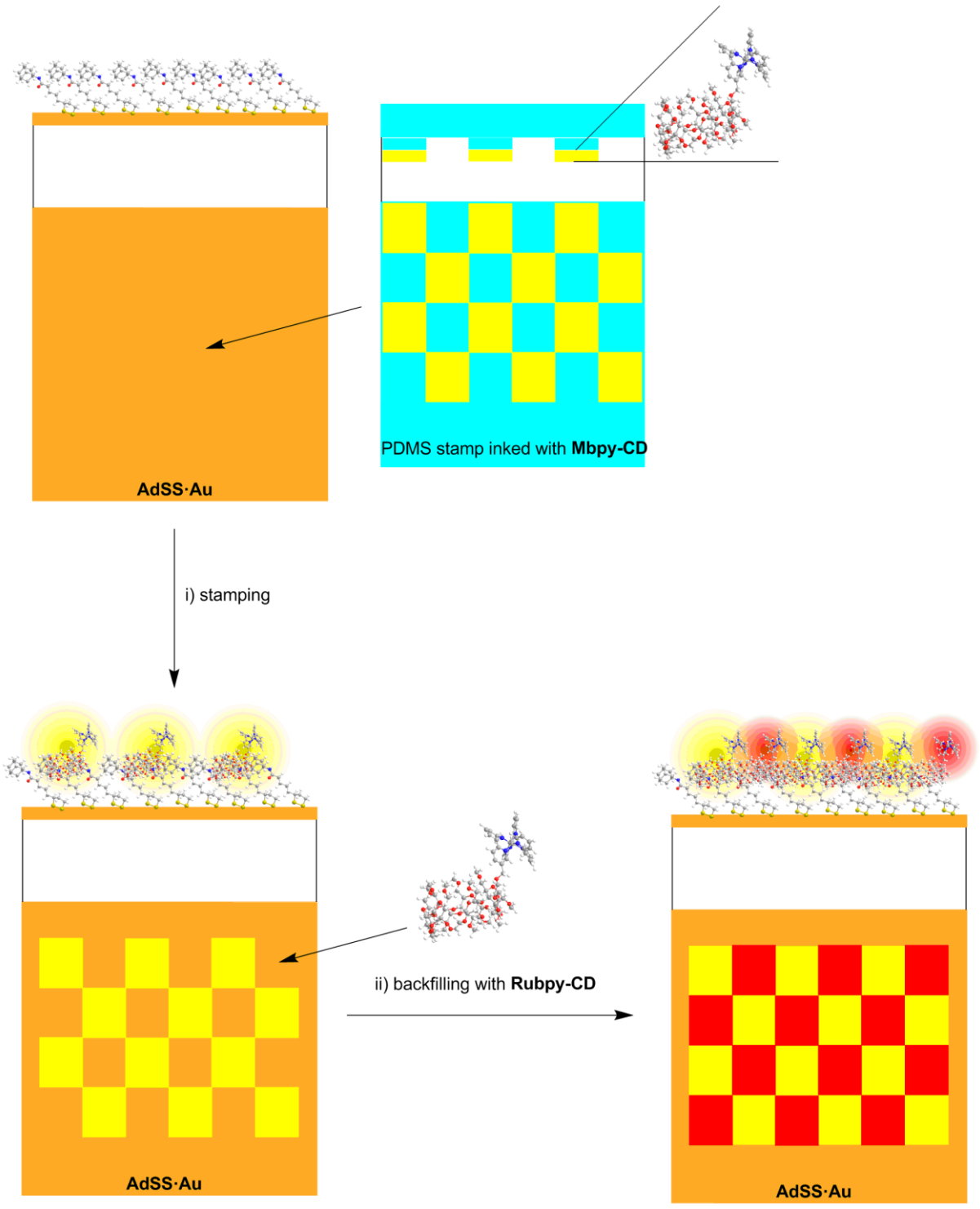


**Scheme 3.4.** Schematic diagram of stamping of **Mbpy-CD** onto **AdSS (4)** functionalised gold substrates.

The luminescence microscope images (Figure 3.20) reveal luminescence from each of the complexes, demonstrating that the printing method was indeed successful. For **Rubpy-CD:AdSS·Au** and **Irbpy-CD:AdSS·Au** we observe the features of the stamp (Figure 3.20). One notable difference between the two images is the presence of more defects and less coverage for that of **Rubpy-CD:AdSS·Au**, which we attribute to the stamping method. For **Rubpy-CD:AdSS·Au**, no pressure was applied to the stamp during the stamping process, whereas for **Irbpy-CD:AdSS·Au**, the stamp was kept firmly in place with tweezers during the stamping process. The pressure leads to more of the stamp coming into contact with the gold surface, and ultimately a more uniform pattern.

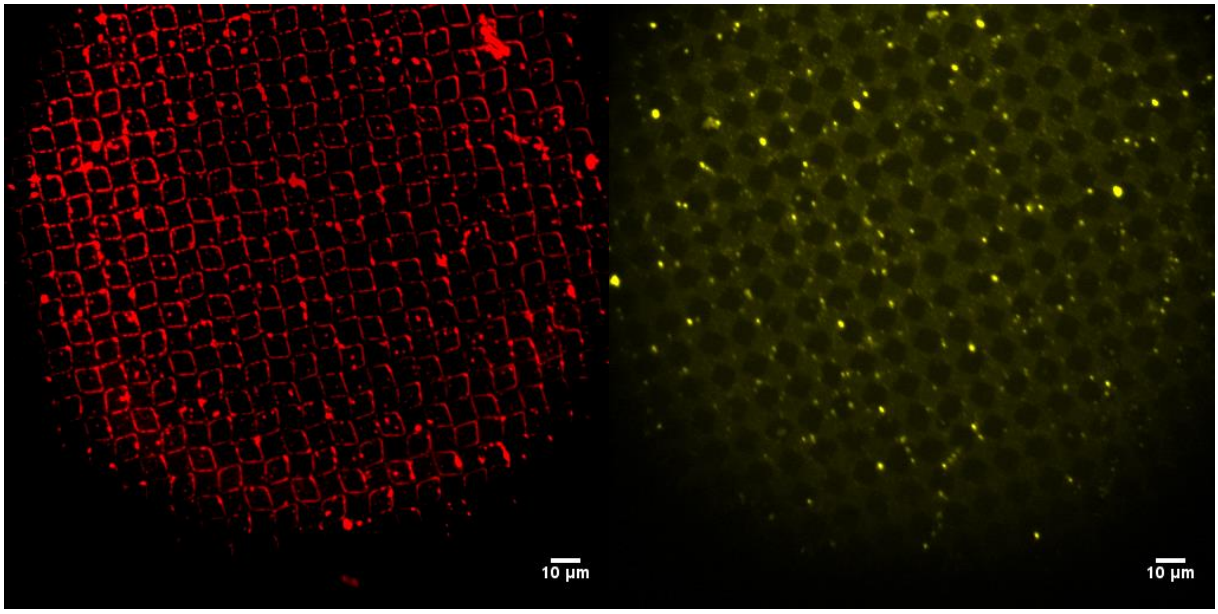


**Figure 3.20.** Luminescence microscope images of stamped **Rubpy-CD:AdSS·Au** (left) and **IrbpyCD-AdSS·Au** (right). $\lambda_{exc}$ = 460 nm (**Ru**), 360 nm (**Ir**). Both images acquired with 510 nm dichroic mirror.

The method was further extended to incorporate both complexes patterned on one substrate as illustrated in Scheme 3.4, by first stamping an **AdSS·Au** substrate with **Irbpy-CD (3)**, before immersing the stamped substrate in a 0.1 mM solution of **Rubpy-CD (2)** in 10% methanol in

water for 30 minutes, followed by washing (methanol) and drying. The luminescence microscope images (Figure 3.21, left) indicate that the patterning of the substrate with **Irbpy-CD (3)** is again successful, with 10 µm square features visible. We can also observe from the luminescence data and images (Figure 3.A17 and Figure 3.21) that both species appear to be present on the surface. It can be seen from the luminescence microscope images (Figure 3.21) that **Rubpy-CD (2)** has occupied free adamantyl sites on the surface, as illustrated by the example blue squares on the images, where lighter areas illuminated by 460 nm (high **Rubpy-CD** absorption, no **Irbpy-CD** absorption) light appear as darker areas when illuminated with 360 nm (high **Irbpy-CD** absorption, low **Rubpy-CD** absorption) light. However we do see that the contrast of the pattern when illuminated with 460 nm light is relatively low, indicating that some displacement of the bound **Irbpy-CD** with **Rubpy-CD** may have occurred.

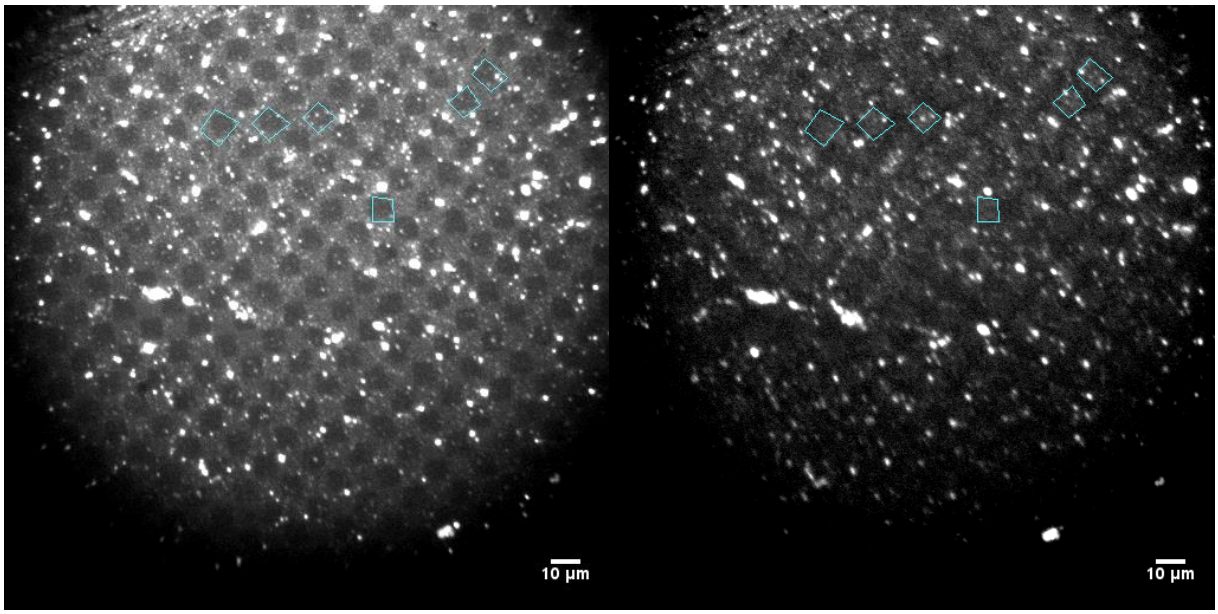


**Figure 3.21.** Luminescence microscope images of mixed layers of stamped **Irbpy-CD:AdSS·Au** followed by subsequent immersion in **Rubpy-CD (2)**. Left – $\lambda_{exc}$ = 360 nm, right - $\lambda_{exc}$ = 460 nm, taken with 530 nm long pass filter. Both images taken with 510 nm dichroic mirror.

### 3.2.7 Conclusions

Two cyclodextrin containing transition metal complexes (**Rubpy-CD**, **2**, **Irbpy-CD**, **3**) were synthesised and characterised. It has been shown that the complexes will bind to adamantyl terminated gold surfaces and an enhancement of the luminescence lifetimes compared with aerated acetonitrile solution is reported. Through the use of supramolecular microcontact printing, the complexes can be attached to the surface *via* controlled deposition with greater ease than chemically bound systems such as **RubpySS** and **IrbpySS**.[24] By extending the methodology to incorporate a second complex on the surface through immersion, greater control over deposition of both components can be achieved as evidenced by luminescence microscopy. The use of the microcontact printing in this manner allows scope for metal complexes such as these to be deposited in arrays on the surface, and could find use in optoelectronic devices such as OLEDs, utilising red, green and blue emissive compounds in a multiplex array. Another area of future research could be into multiplex sensing motifs; whereby patterned metal complexes could act as reporter groups for proximal receptors, or where the receptor group is attached the complex itself. Through this, multicolour arrays capable of sensing two or more analytes at once could be constructed.

# 3.3 Experimental

## 3.3.1 General Experimental

The synthesis of **bpy-CD (1)** is elaborated in chapter four.

## 3.3.2 Synthetic Procedures

**Rubpy-CD (2)**

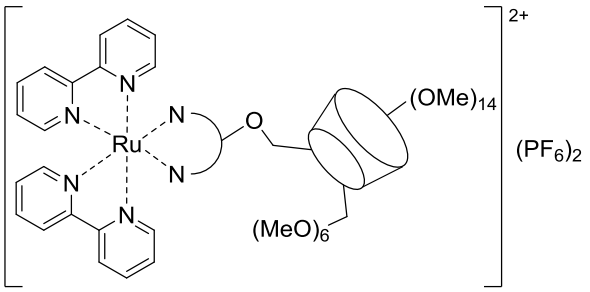


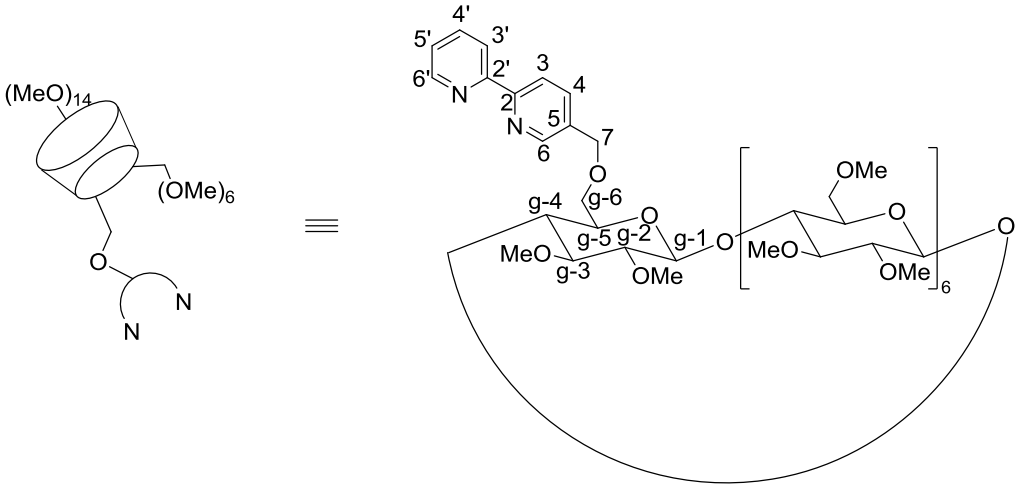


$Ru(bpy)_2Cl_2$ (50 mg, 0.11 mmol) and **bpy-CD (1)** (200 mg, 0.13 mmol) were dissolved in ethanol (10 mL) and heated to reflux for 24 hours, upon which time the reaction mixture was cooled and the solvent concentrated *in vacuo* to *ca.* 2 mL. Water (20 mL) and saturated aqueous $NH_4PF_6$ (6 mL) were added, and the product was extracted with DCM (2 × 50 mL) with the solvent from the combined extracts removed *in vacuo*. The red residue was purified by size exclusion chromatography (Sephadex® LH20) in chloroform, collecting the red band, followed

by trituration in hexane to yield the title compound **Rubpy-CD (2)** (20 mg, $8.5 \times 10^{-6}$ mol, 8%); $\lambda_{max}$ (MeCN) / nm ($\varepsilon$ / $M^{-1}$ $cm^{-1}$) 288 (36000) 451 (5000); $\delta_H$ (300 MHz, $CD_3CN$) 2.84-4.24 (m, H-g-2, H-g-3, H-g-4, H-g-4, H-g-5, H-g-6, OMe), 4.35-4.58 (m, H-7,g-6), 5.04-5.28 (m, H-g-1), 7.32-7.46 (m, H-5,5′), 7.67-7.79 (m, H-6,6′), 8.01-8.12 (m, H-4,4′), 8.49-8.55 (H-3,3′); $\delta_C$ (100 MHz, $CD_3CN$) 57.6-57.9, 58.1, 70.8, 71.4, 817, 82.1-82.2, 97.9, 124.3, 127.6, 137.8, 151.6; m/z $(ESI)^+$ 998 $(M\text{-}2(PF_6))^{2+}$.

**Irbpy-CD (3)**

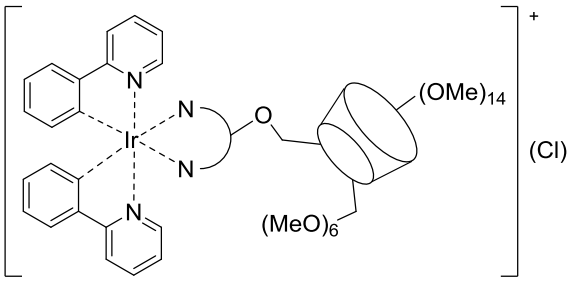


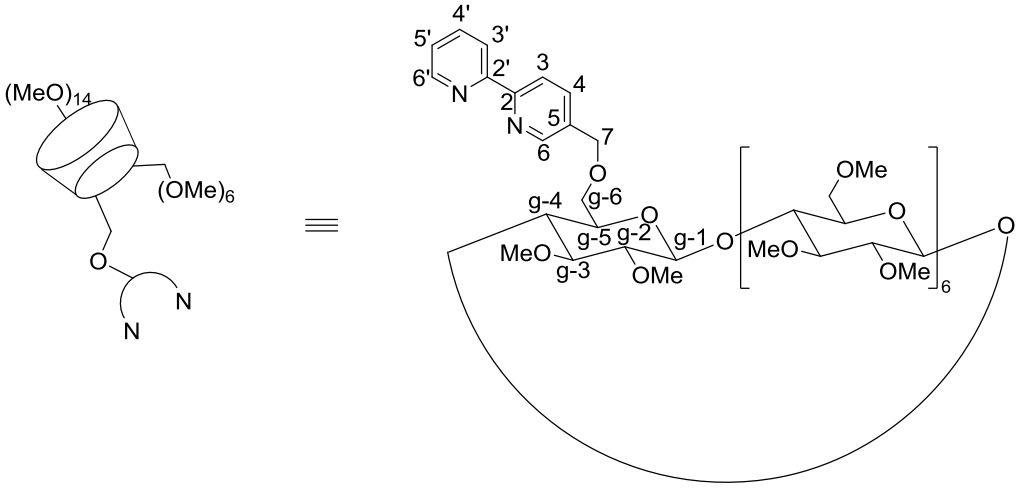


Tetrakis-2-phenylpyridine-(μ-dichloro)diiridium(III) (35 mg, $3.3 \times 10^{-5}$ mol) and **bpy-CD (1)** (100 mg, $6.3 \times 10^{-5}$ mol) were dissolved in 2-ethoxyethanol (30 mL) and heated to 50 °C for 24 hours, upon which time the reaction mixture was cooled to room temperature and the solvent was removed *in vacuo*. The resulting yellow residue was repeatedly purified by size exclusion chromatography (Sephadex® LH20), eluting the yellow band to yield the title compound

**Irbpy-CD (3)** (31.2 mg, 1.5 × $10^{-5}$ mol, 45%); $\lambda_{max}$ (MeCN) / nm ($\varepsilon$ / $M^{-1}$ $cm^{-1}$) 249 (24000) 266 (23000) sh 314 (10000) sh 380 (3000) sh; $\delta_H$ (300 MHz, $CD_3CN$) 2.96-4.27 (m, H-g-2, H-g-3, H-g-4, H-g-4, H-g-5, H-g-6, OMe), 3.98-4.20 (m, H-g-6), 4.29-4.87 (m, H-7), 5.08-5.23 (7H, m, H-g-1), 6.20-8.93 (23H, m, H-ar); $\delta_C$ (100 MHz, $CD_3CN$) 58.3, 58.5, 58.7, 61.1, 65.1, 66.4, 69.7, 70.2, 70.8, 71.4, 71.9, 79.4, 79.7, 79.9, 80.1, 82.0, 82.2, 82.7, 98.5, 120.5, 120.8, 121.1, 122.0, 123.1, 123.3, 124.0, 124.5, 125.0, 125.2, 125.5, 128.8, 130.9, 131.9, 137.6, 138.5, 139.1, 139.9, 149.0, 149.4, 149.7, 150.8, 151.1; m/z $(ESI)^+$ 1051 $(M\text{-}Cl+NH_4)^{2+}$.

**AdSS (4)**

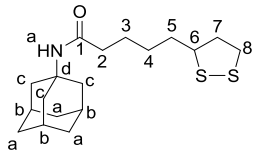


α-Lipoic acid (1.00 g, 4.9 mmol) and 1-hydroxybenzotriazole hydrate (0.72 g, 5.3 mmol) were dissolved in dry DMF (20 mL) and cooled to 0-5 °C, upon which EDC.HCl was added (5.4 mmol) and the mixture stirred until all of the EDC.HCl was dissolved. The mixture was then allowed to warm to room temperature under continued stirring (1 hour) before 1-adamantylamine (0.81 g, 5.4 mmol) and N-ethylmorpholine (1.23 g, 10.7 mmol) in dry DMF (20 mL) were added to the solution. The mixture was then stirred overnight at room temperature, after which time water (50 mL) was added, and the mixture extracted with DCM (3 × 50mL). The combined organic extracts were dried ($MgSO_4$), filtered and the solvent removed *in vacuo*. The pale residue was purified by silica column chromatography eluting with 5% MeOH in DCM to yield the title compound **AdSS (4)** as an off-white solid (0.12 g, 0.4 mmol, 8%). $\delta_H$ (300 MHz, $CDCl_3$) 1.33-1.50 (2H, m, H-3/4/5), 1.51-1.74 (10H, m, H-3/4/5,a), 1.88 (1H, dddd, J= 5.9, 6.7, 6.9, 7.1, H-7′), 1.96 (6H, d, J= 3.0, H-c), 2.00-2.10 (5H, m, H-2,b), 2.43 (1H, dddd, J= 5.6, 5.9, 6.7, 6.9, H-7), 3.04-3.19 (2H, m, H-8), 3.50-3.58 (1H, m, H-6),

5.27 (1H, br s, N*H*); $\delta_C$ (100 MHz, $CDCl_3$) 25.5 (C-3), 28.8 (C-4), 29.4 (C-b), 34.6 (C-5), 36.4 (C-a), 37.3 (C-2), 38.5 (C-8), 40.2 (C-7), 41.6 (C-c), 51.7 (C-d), 56.5 (C-6), 171.9 (C-1); m/z (ESI)$^+$ 340 $(M+H)^+$, 362 $(M+Na)^{2+}$, 701 $(2M+Na)^+$. Data agrees with previously published results.[53]

# 3.4 References


1. L. Li, S. Chen, J. Zheng, B. D. Ratner and S. Jiang, *J. Phys. Chem. B*, 2005, **109**, 2934-2941.
2. E. Ostuni, L. Yan and G. M. Whitesides, *Colloid. Surface. B*, 1999, **15**, 3-30.
3. F. Ricci, R. Y. Lai, A. J. Heeger, K. W. Plaxco and J. J. Sumner, *Langmuir*, 2007, **23**, 6827-6834.
4. F. Frederix, K. Bonroy, W. Laureyn, G. Reekmans, A. Campitelli, W. Dehaen and G. Maes, *Langmuir*, 2003, **19**, 4351-4357.
5. H. Tokuhisa, M. Zhao, L. A. Baker, V. T. Phan, D. L. Dermody, M. E. Garcia, R. F. Peez, R. M. Crooks and T. M. Mayer, *J. Am. Chem. Soc.*, 1998, **120**, 4492-4501.
6. S. V. Atre, B. Liedberg and D. L. Allara, *Langmuir*, 1995, **11**, 3882-3893.
7. D. J. Lewis, T. M. Day, J. V. MacPherson and Z. Pikramenou, *Chem. Commun.*, 2006, 1433-1435.
8. M. Brust, M. Walker, D. Bethell, D. J. Schiffrin and R. Whyman, *J. Chem. Soc. Chem. Commun.*, 1994, 801-802.
9. N. J. Rogers, S. Claire, R. M. Harris, S. Farabi, G. Zikeli, I. B. Styles, N. J. Hodges and Z. Pikramenou, *Chem. Commun.*, 2014, **50**, 617-619.
10. A. Davies, D. J. Lewis, S. P. Watson, S. G. Thomas and Z. Pikramenou, *Proc. Natl. Acad. Sci.*, 2012, **109**, 1862-1867.
11. D. J. Lewis, V. Dore, M. J. Goodwin, A. C. Savage, G. B. Nash, P. Angeli and Z. Pikramenou, *Meas. Sci. Technol.*, 2012, **23**, 084004.
12. D. J. Lewis, V. Dore, N. J. Rogers, T. K. Mole, G. B. Nash, P. Angeli and Z. Pikramenou, *Langmuir*, 2013, **29**, 14701-14708.
13. Z. Pikramenou and N. J. Rogers, WO2013004989 A1, 2013.
14. I. Lynch and K. A. Dawson, *Nano Today*, 2008, **3**, 40-47.
15. D. Walczyk, F. B. Bombelli, M. P. Monopoli, I. Lynch and K. A. Dawson, *J. Am. Chem. Soc.*, 2010, **132**, 5761-5768.
16. M. Lundqvist, J. Stigler, G. Elia, I. Lynch, T. Cedervall and K. A. Dawson, *Proc. Natl. Acad. Sci.*, 2008, **105**, 14265-14270.
17. R. Podila, R. Chen, P. C. Ke, J. M. Brown and A. M. Rao, *Appl. Phys. Lett.*, 2012, **101**, 263701.
18. T. Cedervall, I. Lynch, S. Lindman, T. Berggård, E. Thulin, H. Nilsson, K. A. Dawson and S. Linse, *Proc. Natl. Acad. Sci.*, 2007, **104**, 2050-2055.
19. G. Maiorano, S. Sabella, B. Sorce, V. Brunetti, M. A. Malvindi, R. Cingolani and P. P. Pompa, *ACS Nano*, 2010, **4**, 7481-7491.
20. A. E. Nel, L. Mädler, D. Velegol, T. Xia, E. M. V. Hoek, P. Somasundaran, F. Klaessig, V. Castranova and M. Thompson, *Nat. Mater.*, 2009, **8**, 543-557.
21. J. Homola, S. S. Yee and G. Gauglitz, *Sensor. Actuat. B-Chem.*, 1999, **54**, 3-15.
22. J. Homola, *Chem. Rev.*, 2008, **108**, 462-493.
23. B. Liedberg, I. Lundström and E. Stenberg, *Sensor. Actuat. B-Chem.*, 1993, **11**, 63-72.
24. S. J. Adams, D. J. Lewis, J. A. Preece and Z. Pikramenou, *ACS Appl. Mater. Interfaces*, 2014, **6**, 11598-11608.
25. A. C. Sabuncu, J. Grubbs, S. Qian, T. M. Abdel-Fattah, M. W. Stacey and A. Beskok, *Colloid. Surface. B*, 2012, **95**, 96-102.
26. Y. Xia and G. M. Whitesides, *Annu. Rev. Mater. Sci.*, 1998, **28**, 153-184.
27. A. Kumar, H. A. Biebuyck and G. M. Whitesides, *Langmuir*, 1994, **10**, 1498-1511.

28. A. Perl, D. N. Reinhoudt and J. Huskens, *Adv. Mater.*, 2009, **21**, 2257-2268.
29. L. Yan, W. T. S. Huck, X.-M. Zhao and G. M. Whitesides, *Langmuir*, 1999, **15**, 1208-1214.
30. D. A. Rozkiewicz, D. Jańczewski, W. Verboom, B. J. Ravoo and D. N. Reinhoudt, *Angew. Chem. Int. Ed.*, 2006, **45**, 5292-5296.
31. J. M. Spruell, B. A. Sheriff, D. A. Rozkiewicz, W. R. Ditchel, R. D. Rohde, D. N. Reinhoudt, J. F. Stoddart and J. R. Heath, *Angew. Chem. Int. Ed.*, 2008, **47**, 9927-9932.
32. C. Wendeln, S. Rinnen, C. Schulz, H. F. Arlinghaus and B. J. Ravoo, *Langmuir*, 2010, **26**, 15966-15971.
33. C.-C. Wu, D. N. Reinhoudt, C. Otto, A. H. Velders and V. Subramaniam, *ACS Nano*, 2010, **4**, 1083-1091.
34. L. Scheres, J. ter Maat, M. Giesbers and H. Zuilhof, *Small*, 2010, **6**, 642-650.
35. C. Wendeln, O. Roling, C. Schulz, C. Hentschel and B. J. Ravoo, *Langmuir*, 2013, **29**, 2692-2699.
36. C. Wendeln and B. J. Ravoo, *Langmuir*, 2012, **28**, 5527-5538.
37. A. Mulder, S. Onclin, M. Péter, J. P. Hoogenboom, H. Beijleveld, J. ter Maat, M. F. García-Parajó, B. J. Ravoo, J. Huskens, N. F. van Hulst and D. N. Reinhoudt, *Small*, 2005, **1**, 242-253.
38. S. Onclin, J. Huskens, B. J. Ravoo and D. N. Reinhoudt, *Small*, 2005, **1**, 852-857.
39. O. Crespo-Biel, B. Dordi, P. Maury, M. Péter, D. N. Reinhoudt and J. Huskens, *Chem. Mater.*, 2006, **18**, 2545-2551.
40. M. J. W. Ludden, A. Mulder, K. Schulze, V. Subramaniam, R. Tampé and J. Huskens, *Chem. Eur. J.*, 2008, **14**, 2044-2051.
41. V. B. Sadhu, A. Perl, M. Péter, D. I. Rozkiewicz, G. Engbers, B. J. Ravoo, D. N. Reinhoudt and J. Huskens, *Langmuir*, 2007, **23**, 6850-6855.
42. C. M. Bruinink, C. A. Nijhuis, M. Péter, B. Dordi, O. Crespo-Biel, T. Auletta, A. Mulder, H. Schönherr, G. J. Vancso, J. Huskens and D. N. Reinhoudt, *Chem. Eur. J.*, 2005, **11**, 3988-3996.
43. A. Gonzalez-Campo, S.-H. Hsu, L. Puig, J. Huskens, D. N. Reinhoudt and A. H. Velders, *J. Am. Chem. Soc.*, 2010, **132**, 11434-11436.
44. B. P. Sullivan, D. J. Salmon and T. J. Meyer, *Inorg. Chem.*, 1978, **17**, 3334-3341.
45. J. D. Slinker, A. A. Gorodetsky, M. S. Lowry, J. Wang, S. Parker, R. Rohl, S. Bernhard and G. G. Malliaras, *J. Am. Chem. Soc.*, 2004, **126**, 2763-2767.
46. Z. Chen, J. S. Bradshaw and M. L. Lee, *Tetrahedron Lett.*, 1996, **37**, 6831-6834.
47. A. Juris, V. Balzani, F. Barigelletti, S. Campagna, P. Belser and A. von Zelewsky, *Coord. Chem. Rev.*, 1988, **84**, 85-277.
48. J. A. Faiz, *PhD. Thesis - University of Birmingham*, 2005.
49. E. T. Kefalas, *PhD. Thesis - University of Birmingham*, 2004.
50. K. A. King and R. J. Watts, *J. Am. Chem. Soc.*, 1987, **109**, 1589-1590.
51. K. Nakamaru, *Bull. Chem. Soc. Jpn.*, 1982, **55**, 2697-2705.
52. L. E. P. Kyllonen, *PhD. Thesis - University of Birmingham*, 2009.
53. M. Wilhelm, R. Koch and H. Strasdeit, *New J. Chem.*, 2002, **26**, 560-566.

# 3.5 Appendix

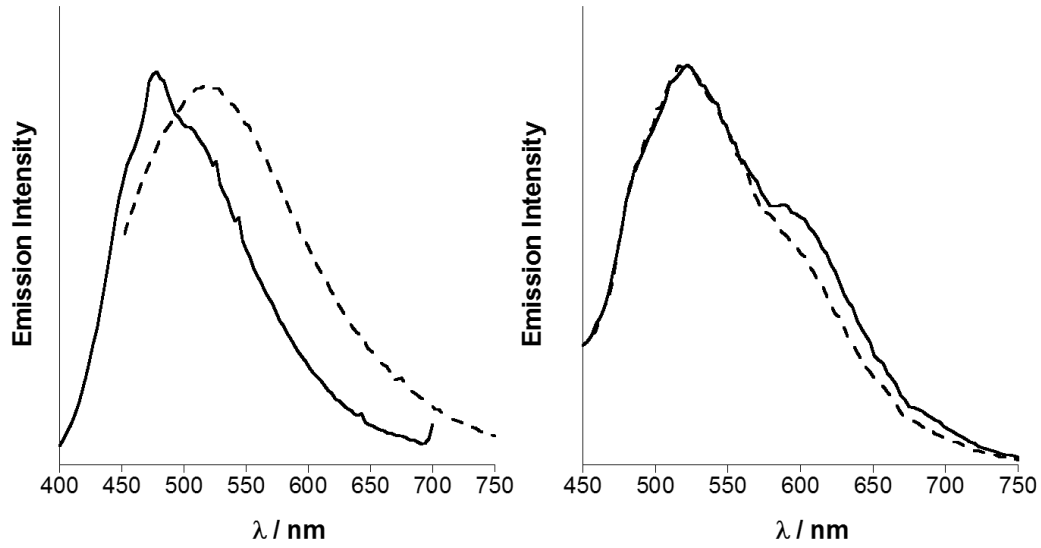


**Figure 3.A1.** Emission spectra of **IrbpySS** surfaces co-coated with **Zonyl® 7950** (left) and **Zonyl® FSA** (right) before (solid) and after (dash) BSA addition. $\lambda_{exc}$ = 360 nm, left spectrum corrected for instrument response. Spectral intensities are not to scale.

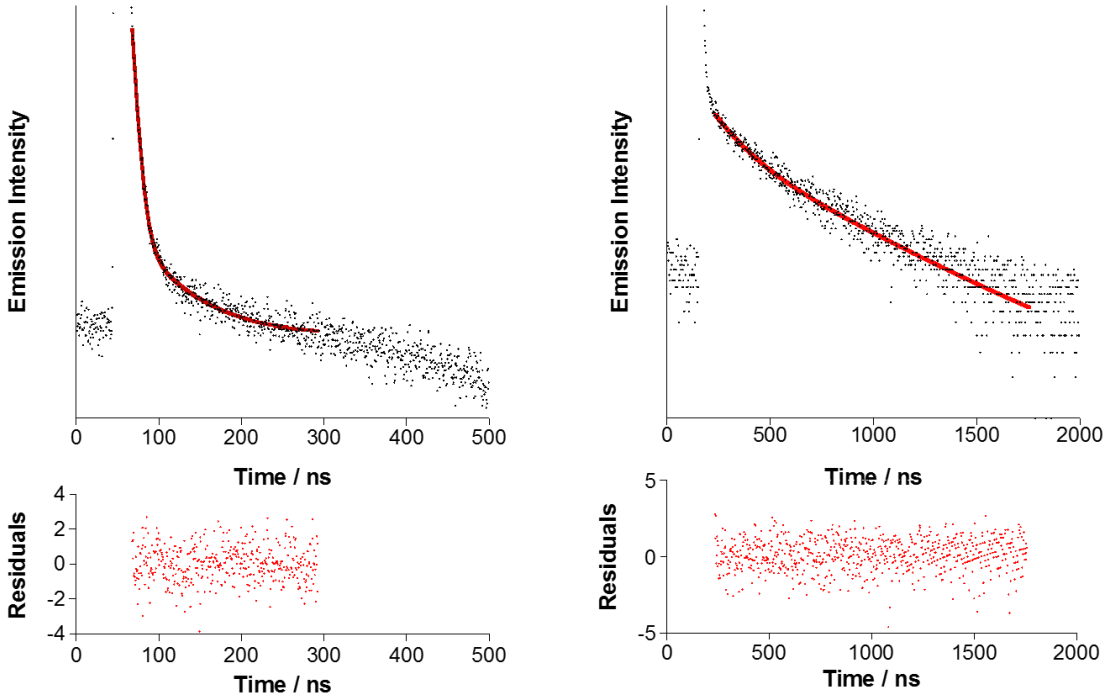


**Figure 3.A2.** Luminescence decay plots of **IrbpySS** surfaces co-coated with **Zonyl® 7950** before (left) and after (right) BSA addition. $\lambda_{exc}$ = 376 nm, $\lambda_{em}$ = 480 nm (before BSA), 520 nm (after BSA).

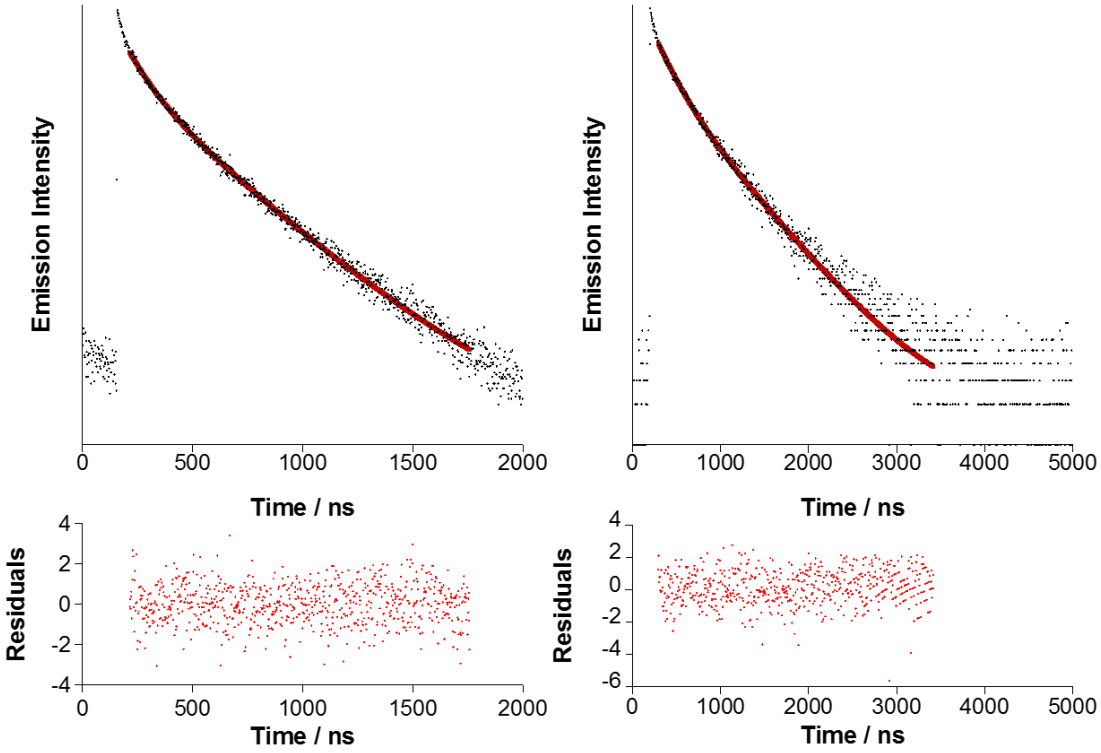


**Figure 3.A3.** Luminescence decay plots of **RubpySS** surfaces co-coated with **Zonyl® 7950** before (left) and after (right) BSA addition. $\lambda_{exc}$ = 445 nm, $\lambda_{em}$ = 620 nm.

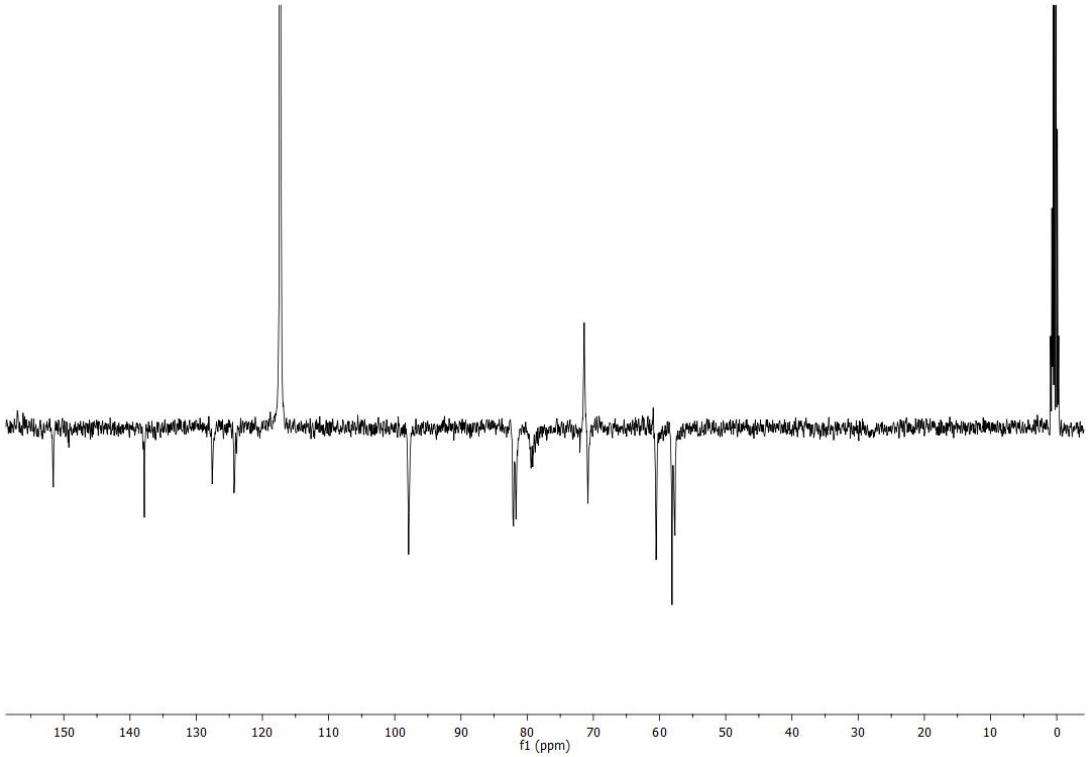


**Figure 3.A4.** $^{13}C$ NMR spectrum of **Rubpy-CD (2)** in $CD_3CN$.

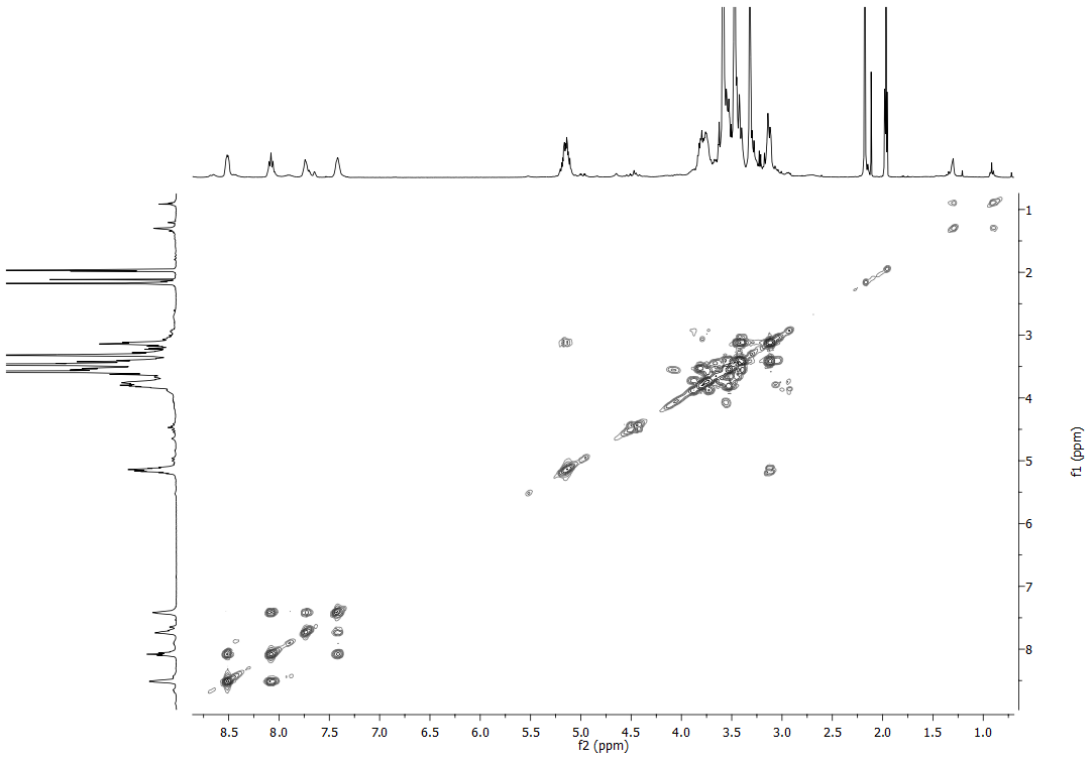


**Figure 3.A5.** COSY spectrum of **Rubpy-CD (2)** in $CD_3CN$.

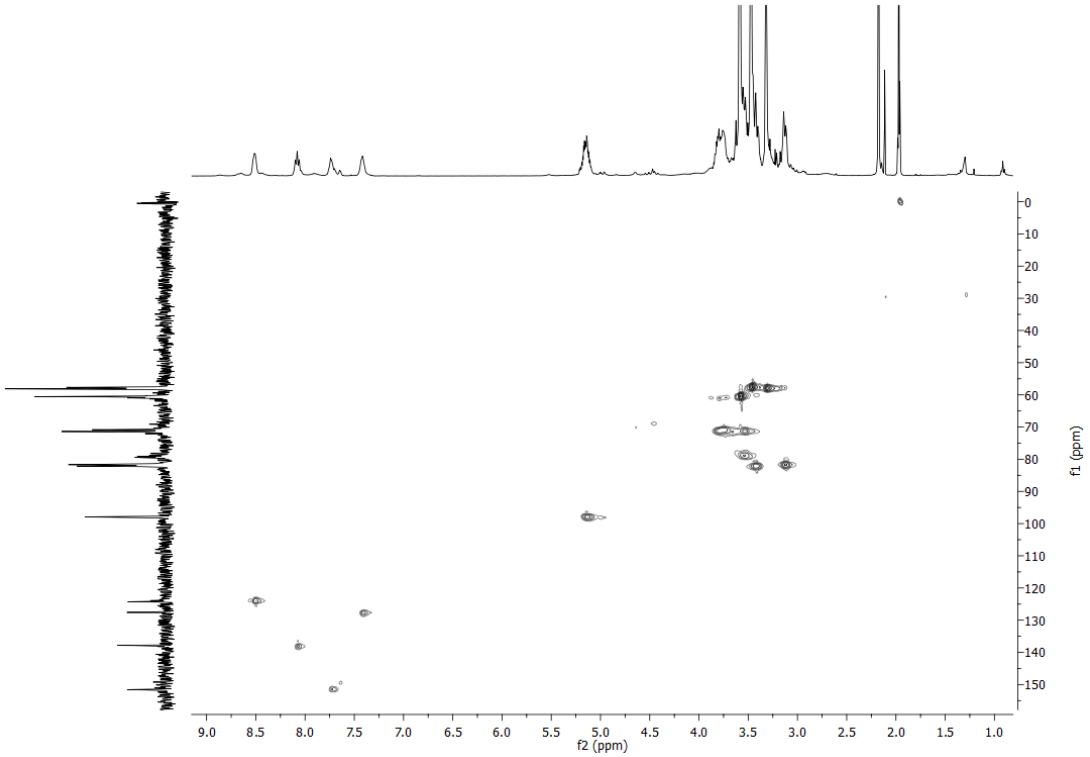


**Figure 3.A6.** HSQC spectrum of **Rubpy-CD (2)** in $CD_3CN$.

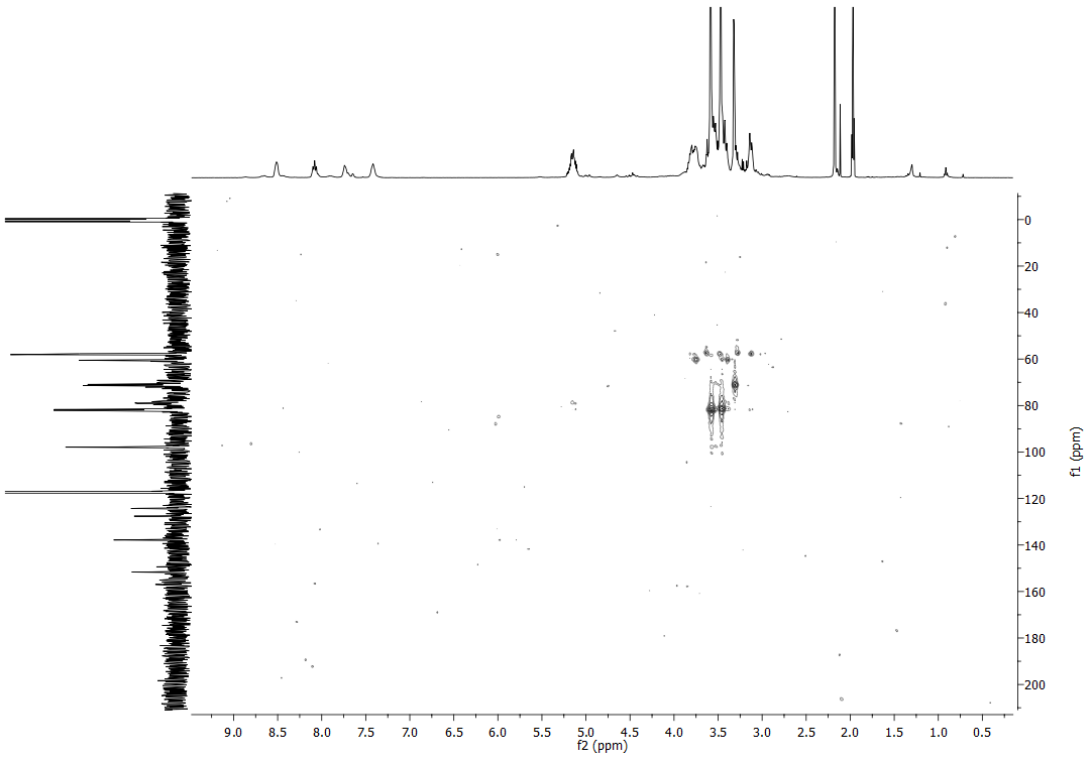


**Figure 3.A7.** HMBC spectrum of **Rubpy-CD (2)** in $CD_3CN$.

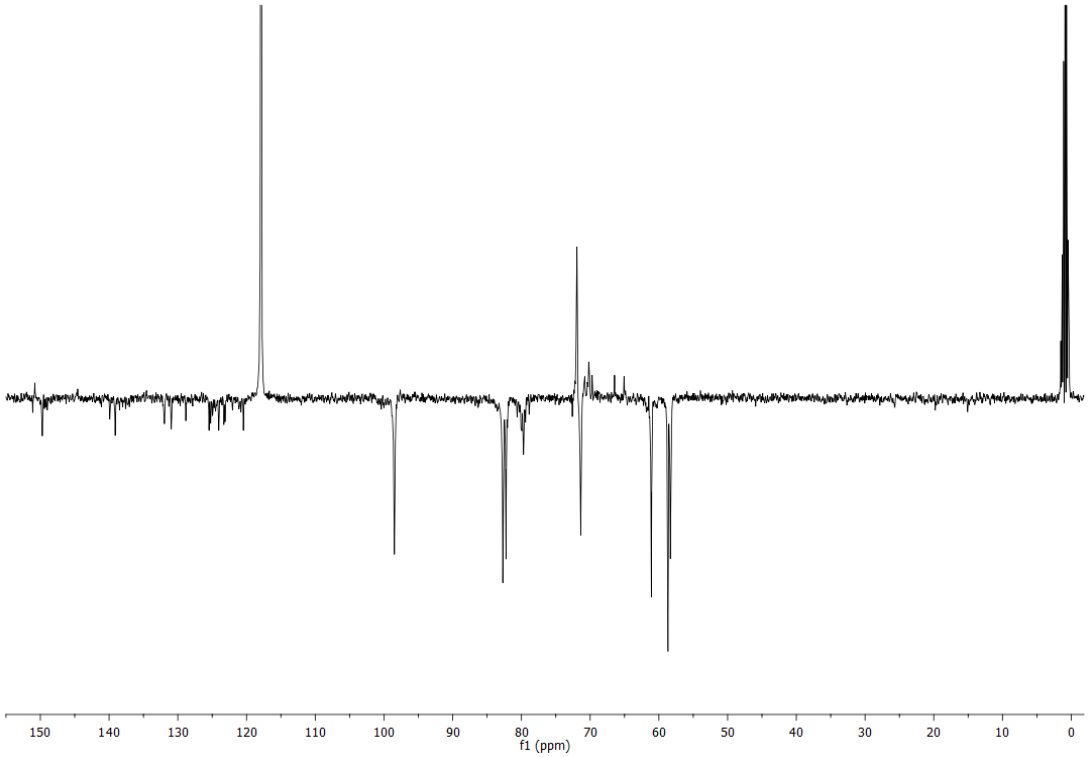


**Figure 3.A8.** $^{13}C$ NMR spectrum of **Irbpy-CD (3)** in $CD_3CN$.

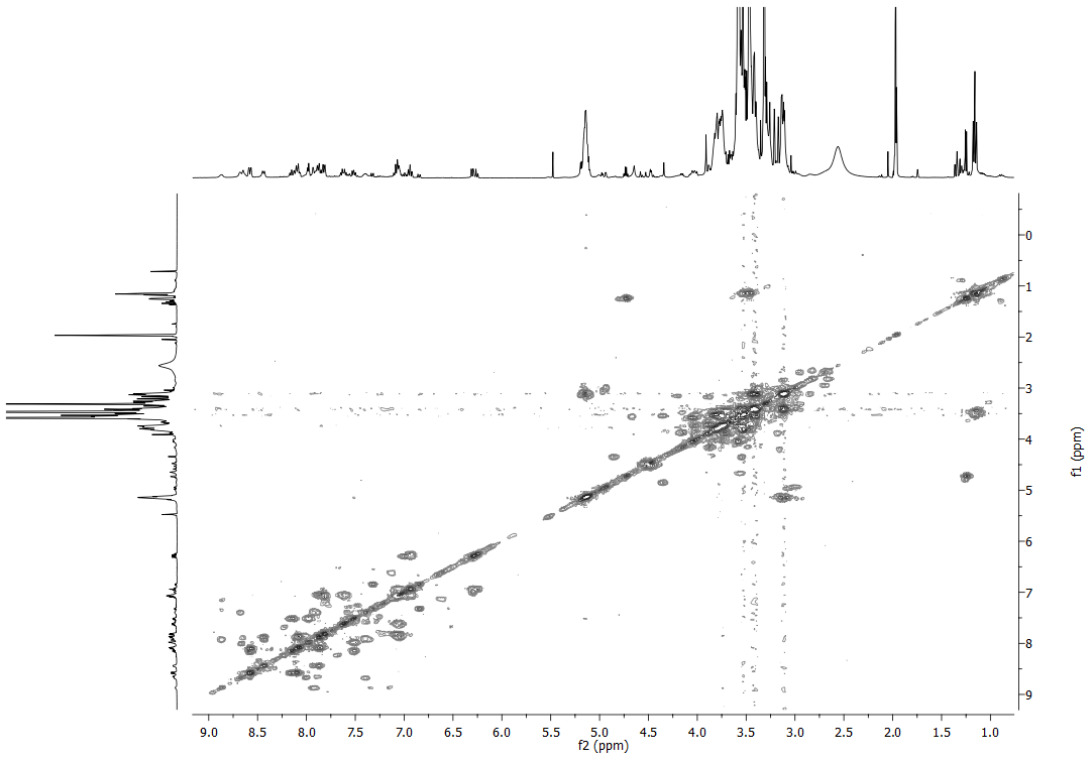


**Figure 3.A9.** COSY spectrum of **Irbpy-CD (3)** in $CD_3CN$.

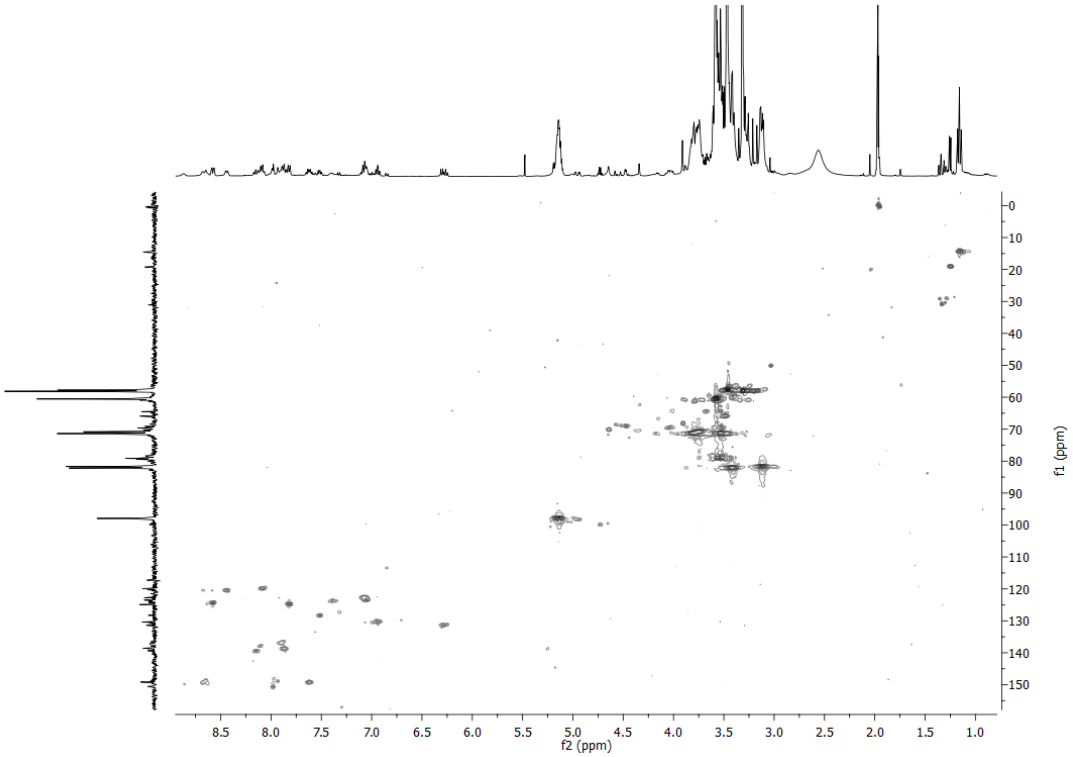


**Figure 3.A10.** HSQC spectrum of **Irbpy-CD (3)** in $CD_3CN$.

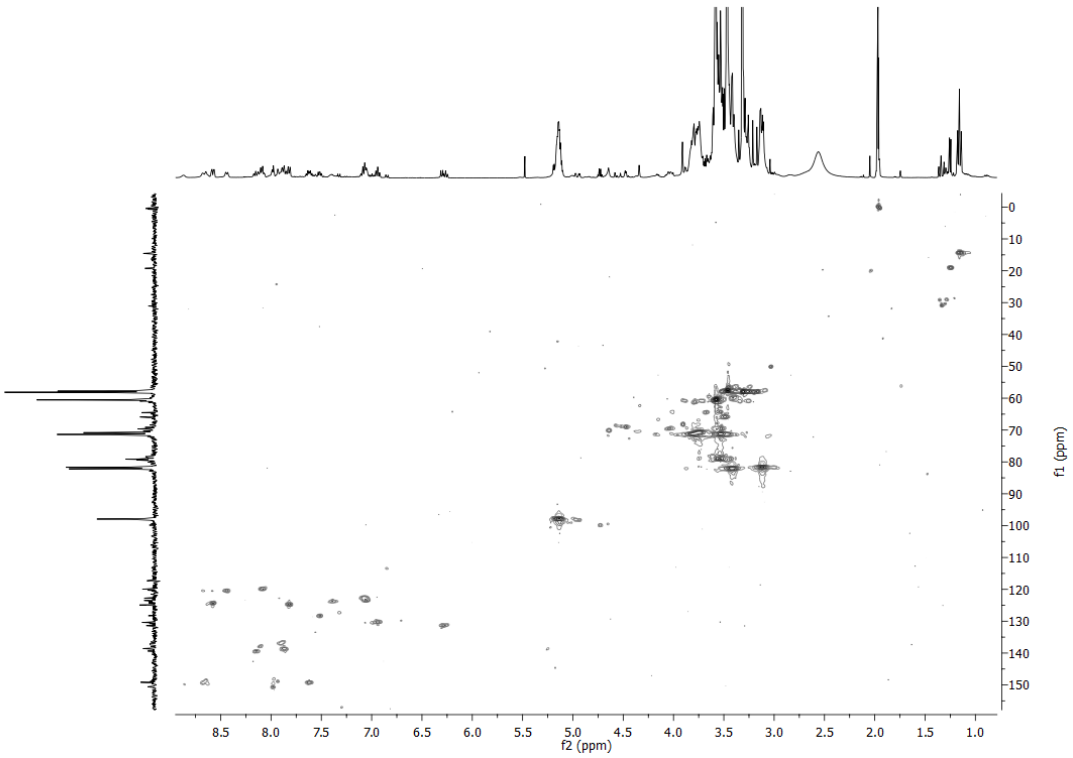


**Figure 3.A11.** HMBC spectrum of **Irbpy-CD (3)** in $CD_3CN$.

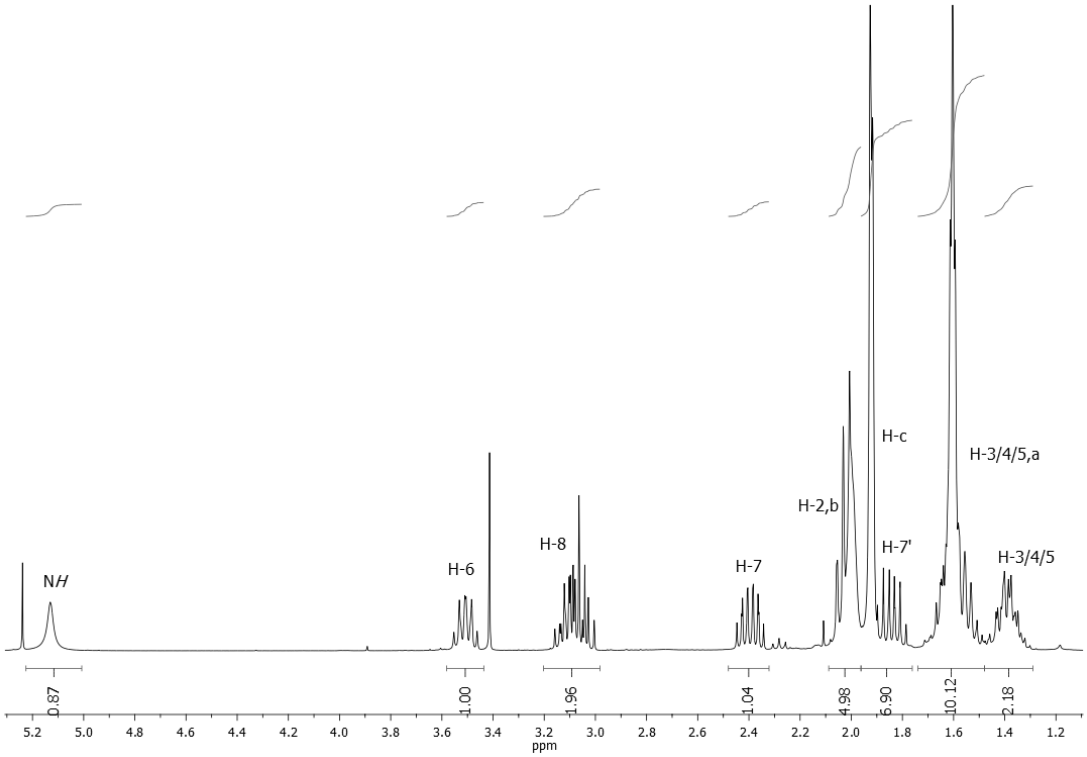


**Figure 3.A12.** $^{1}$H NMR spectrum of **AdSS (4)** in $CDCl_3$.

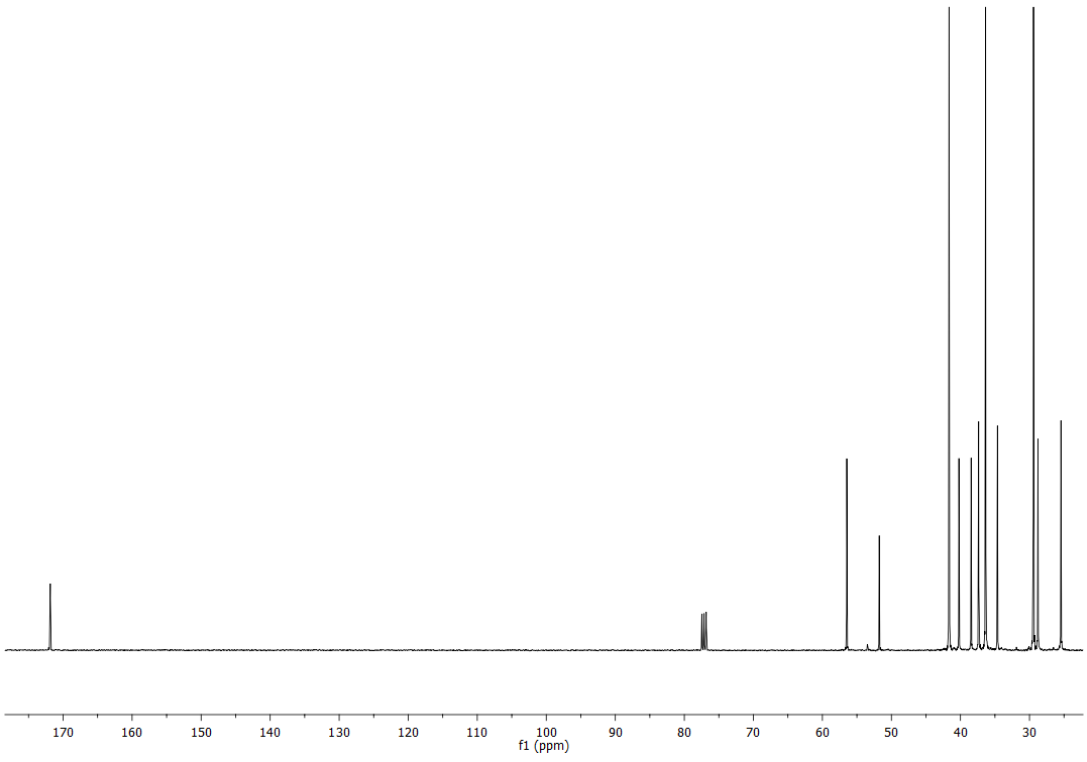


**Figure 3.A13.** $^{13}$C NMR spectrum of **AdSS (4)** in $CDCl_3$.

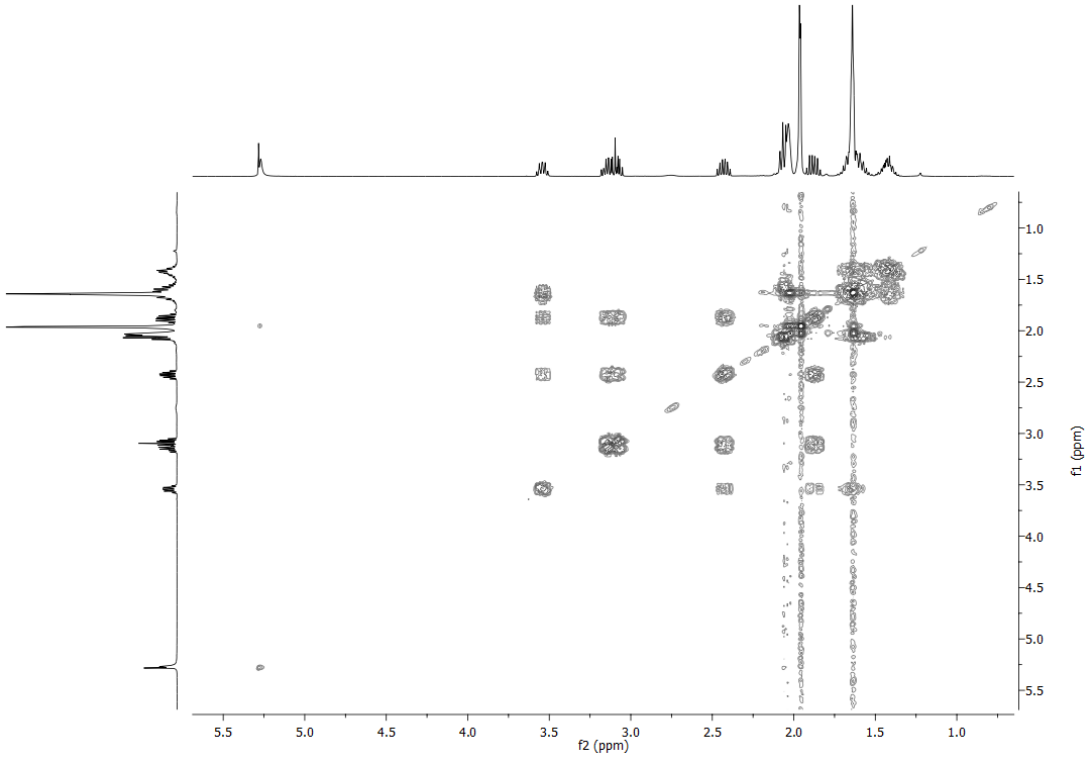


**Figure 3.A14.** COSY spectrum of **AdSS (4)** in $CDCl_3$.

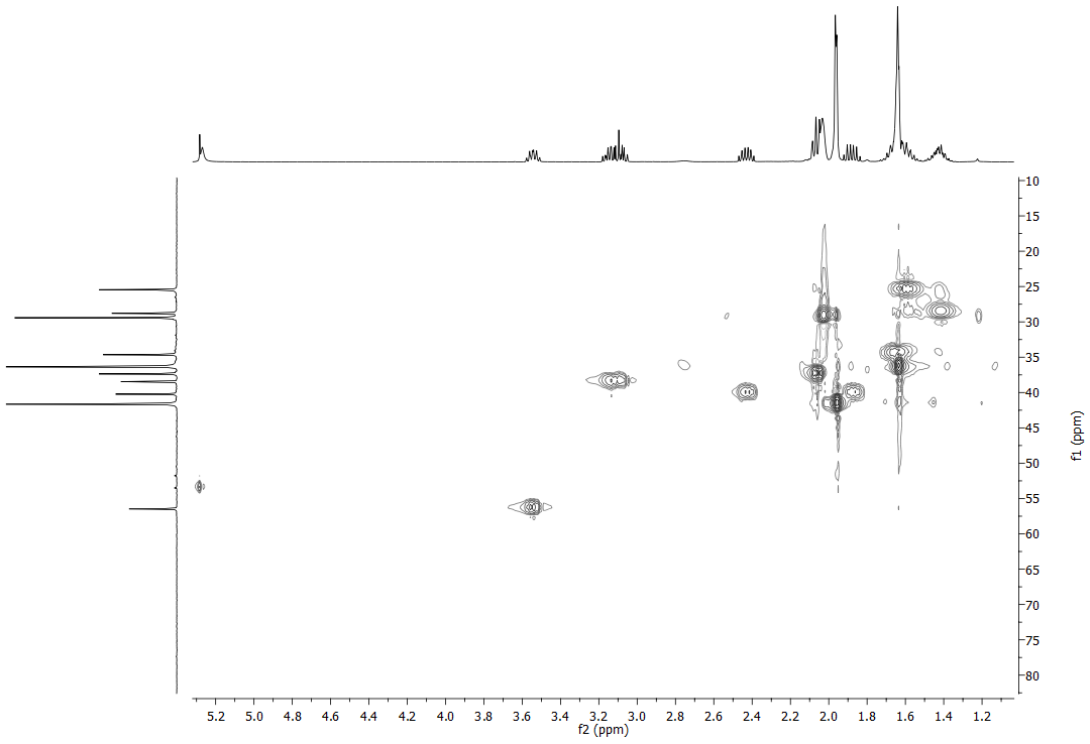


**Figure 3.A15.** HSQC spectrum of **AdSS (4)** in $CDCl_3$.

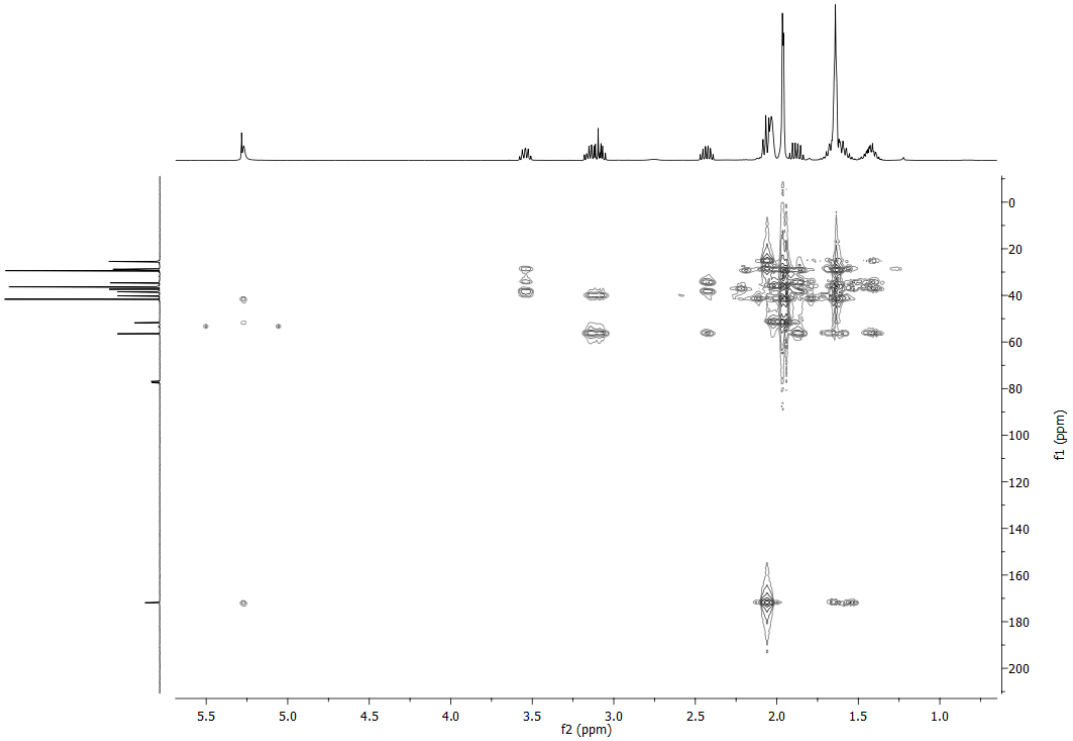


**Figure 3.A16.** HMBC spectrum of **AdSS (4)** in $CDCl_3$.

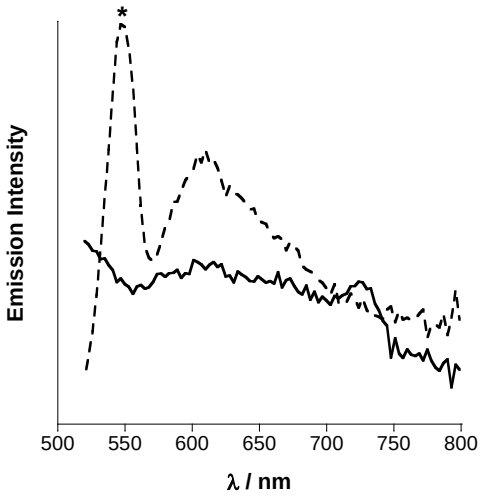


**Figure 3.A17.** Steady state emission spectra taken from substrate in Figure 3.21. Solid – $\lambda_{exc}$ = 360 nm, dash – $\lambda_{exc}$ = 460 nm. Spectra corrected from instrument response. * - Raman scattering peak.

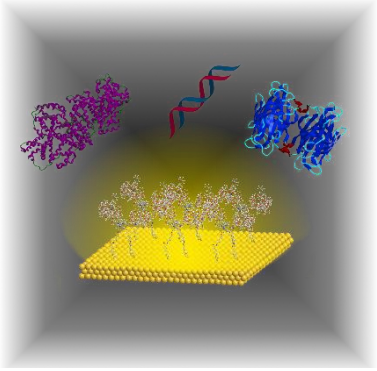

# Chapter Four

# Cyclodextrin Containing Transition Metal Complexes for Surface Attachment and Sensing

# 4.1 Introduction

Biomolecular interactions are wide ranging and diverse.[1, 2] In particular, small functional groups can display highly selective and strong binding affinities with proteins in biological systems. This 'lock and key' mechanism of biomolecular interaction is paramount in biological processes as a whole,[2] and thus represents a valuable tool that can be exploited in medical diagnostics and theranostics,[3-5] as well as fields such as environmental monitoring.[6] In particular, many commercial biomolecular recognition motifs in medical diagnostics are based on the production and immobilisation of antibodies that can recognise a biomolecule with high specificity.[5, 7] However, assay systems such as these are also reliant on the use of further functionalised antibodies in order to create a signal that can be detected, generally by fluorescence or absorbance.[8] As discussed earlier in this thesis, transition metal complexes can be used to exhibit biomolecular recognition, as well as provide a signal which can be analysed. The use of supramolecular chemistry in such systems allows the scope and design of such systems to be greatly increased, and indeed many solution based examples of supramolecular chemistry can be found in the literature.[9-15]

## 4.1.1 Cyclodextrin Based Supramolecular Motifs for Stepwise Assembly and Molecular Recognition

Supramolecular chemistry can also be very useful at the interface through the formation of complex nanostructures through stepwise assembly.[16] Many supramolecular motifs have been exploited in this way, including calixarenes,[17, 18] cucurbiturils,[19, 20] rotaxanes[21, 22] and cyclodextrins. The immobilisation of cyclodextrin functionalised compounds to surfaces is well studied, particularly on gold,[23-27] glass[28] or titania.[29, 30] This is due to their relative ease of synthesis[31, 32] and good commercial availability.

One particularly novel use for cyclodextrins on surfaces is that of fragrance release, as demonstrated by Schofield and Badyal.[33] In this study, silicon surfaces were functionalised by 4-vinylbenzyl chloride and subsequently reacted with β-cyclodextrin under Williamson ether conditions. The surfaces were then loaded with vanillin by exposure to vapour and monitored by quartz crystal microbalance studies. The results the group obtained indicated that vanillin did indeed reversibly bind into the cavity, and could be regenerated and reloaded by vacuum or vapour treatment. Using this method of β-cyclodextrin functionalization, the group also modified polypropylene cloth vanillin, resulting in a much slower rate of release of the molecule from the cloth compared with samples that were not modified with β-cyclodextrin.

A study by Yu *et al*.[34] (Figure 4.1) demonstrates a method for attaching a ruthenium(II) complex to single-walled carbon nanotubes *via* supramolecular interactions. In this example, the complex is functionalised with a β-cyclodextrin moiety, and a separate linker bearing pyrene and adamantyl groups is also synthesised. In the proposed system, the pyrene groups interact with the nanotubes through π -π stacking interactions, with subsequent assembly of the complex through host-guest chemistry facilitated by the interaction between the adamantyl and cyclodextrin groups. Through, UV-vis absorption, luminescence and XPS spectroscopy, the group were able to show the assembly of the system, in particular showing quenching of the ruthenium(II) excited state by photoinduced charge transfer processes originating from the pyrene moiety in the assembled system.

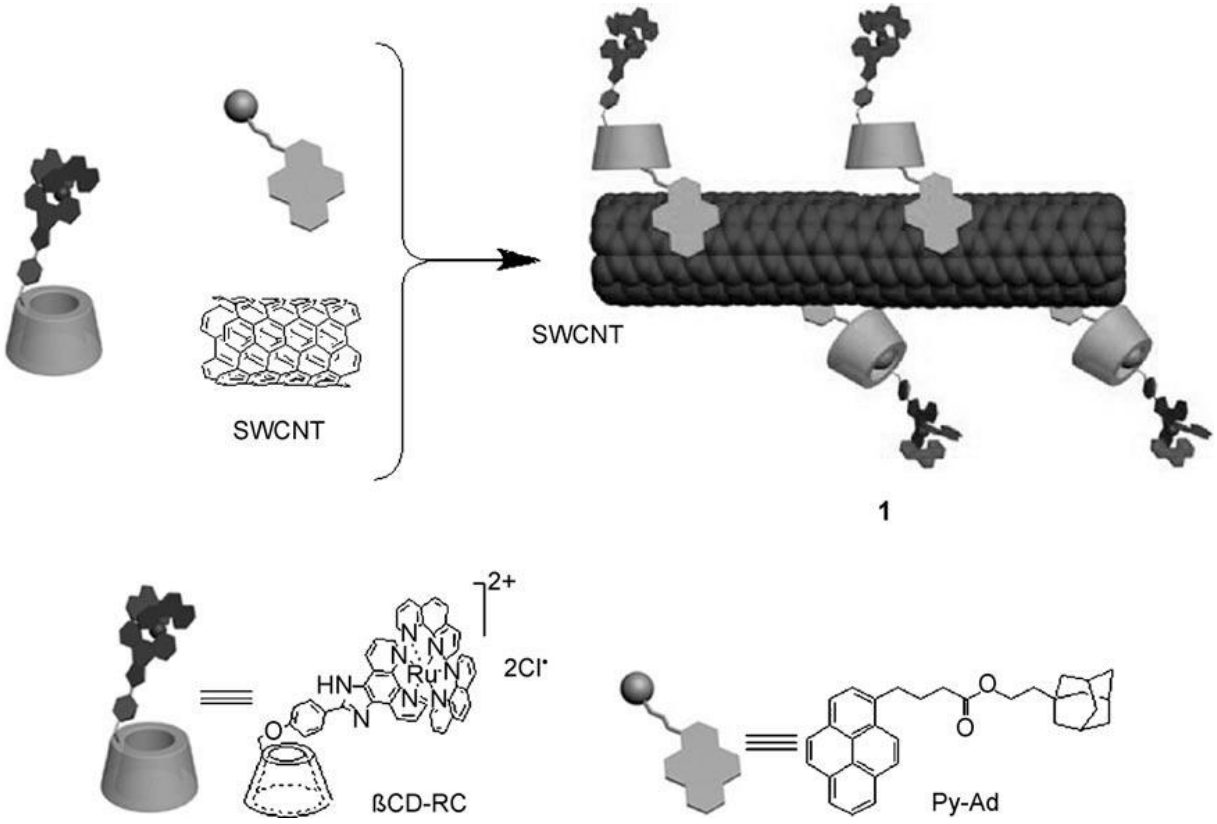


**Figure 4.1.** Schematic of attachment of ruthenium(II) complex to single-walled carbon nanotubes through host-guest chemistry. Image reproduced with permission from reference (34). Copyright 2009 John Wiley and Sons.

Work by Crespo-Biel *et al.*[35] (Figure 4.2) illustrates a method for immobilising gold nanoparticles on a gold or glass surface through the use of molecular printboards. In this example, the surfaces were immersed in alternating solutions of adamantyl terminated dendrimers and β-cyclodextrin terminated gold nanoparticles. SPR spectroscopy, ellipsometry and UV-vis absorption spectroscopy revealed that successive bilayers of dendrimers and nanoparticles could indeed be formed with precise control over the thickness of the structures formed. Surface regeneration experiments were also attempted but yielded only partially successful results. Reversibility in supramolecular systems is an attractive property in surface regeneration, and through similar redox chemistry described earlier, Ling *et al.*[36] (Figure 4.2)

demonstrated the reversible immobilisation of gold nanoparticles to a molecular printboard through ferrocenyl terminated dendrimers. Through electrochemical oxidation and reduction, the group were able to reversibly adhere gold nanoparticles to the surface through the binding of ferrocene into the β-cyclodextrin cavities, yielding a method to reversibly build more complex nanostructures.

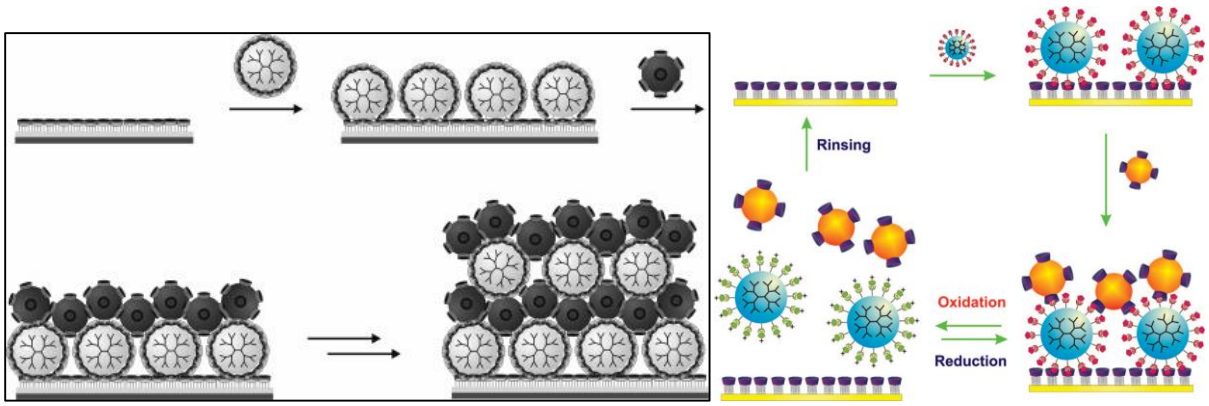


**Figure 4.2.** Schematic of non-reversible (left) and reversible (right) binding of β-cyclodextrin terminated gold nanoparticles to molecular printboards. Adapted with permission from references (35, 36). Copyright 2005 and 2008 American Chemical Society.

Another study by Crespo-Biel *et al.*[37] (Figure 4.3) demonstrates a method for the formation of a transition metal complex at the surface mediated by supramolecular interactions. In this example, a molecular printboard was immersed into a complex solution containing free β-cyclodextrin, copper(II) or nickel(II) ions and a monovalent linker bearing adamantyl and ethylenediamine groups to complex to β-cyclodextrin and the metal ion respectively. Through SPR spectroscopy and isothermal calorimetry experiments, as well as modelling of the complex system as a function of pH, it was found that formation of the divalent copper(II) complex was enhanced by 100 fold relative to the solution, showing that systems such as these can be useful in directing complex formation due to the localisation of ligands at very short distances from each other (*ca.* 2 nm) at the interface.[37] The idea of complexation on molecular printboards was

further extended by Ludden *et al*.[38] (Figure 4.4). In this example, nitrilotriacetate (NTA) functionalised linkers bearing adamantyl groups were adhered to molecular printboards in competition with a non-functionalised linker. Nickel(II) ions and histidine tagged proteins were also passed over the surface in order to induce binding to the surface and immobilise the proteins. SPR spectroscopy revealed that the binding could be partially reversed and cycled through alternating complexation and wash steps, using EDTA and β-cyclodextrin.

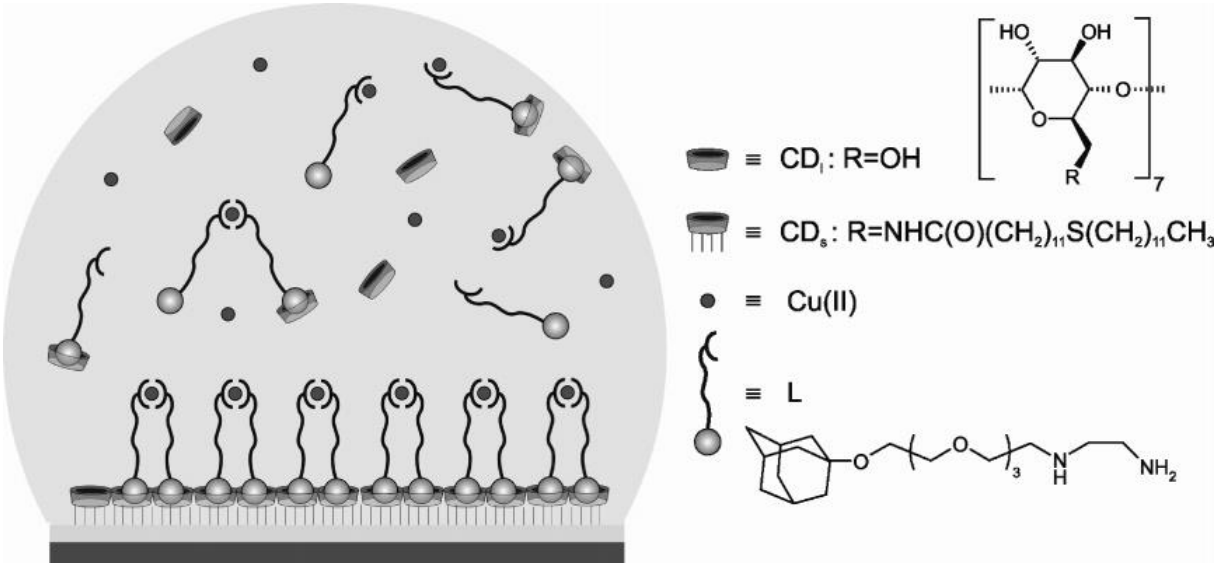


**Figure 4.3.** Schematic of copper(II) complex formation on molecular printboard. Reprinted with permission from reference (37). Copyright 2006 American Chemical Society.

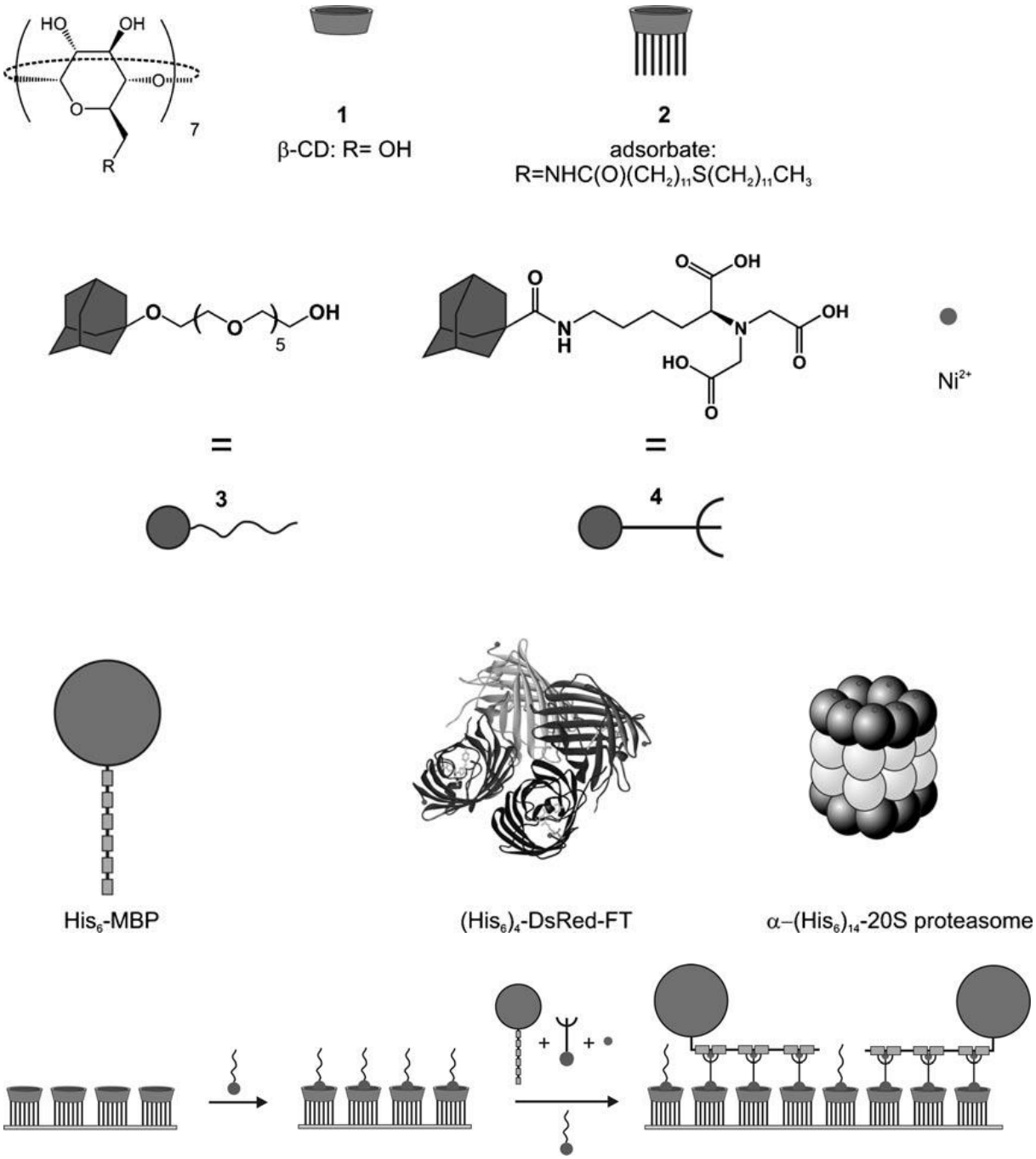


**Figure 4.4.** Structures of components used in nickel(II) complex system (top) and schematic of nanostructure formation (bottom). Image reproduced with permission from reference (38). Copyright 2008 John Wiley and Sons.

### 4.1.2 Interfacial Biomolecular Interactions Involving Cyclodextrins

Cyclodextrins have also been used in an array of biomolecular recognition motifs, due to their versatility in host-guest chemistry. Recently, work by Chen *et al.*[39] described a detection motif for recognising thrombin, a component of the blood clotting process. Figure 4.5 illustrates the motif, in which a DNA aptamer known to recognise thrombin was attached to a glassy carbon electrode. A $[Ru(bpy)_3]^{2+}$ functionalised β-cyclodextrin was then introduced and bound to the aptamer. The ECL signal from the electrode was then treated as a reference signal, before the thrombin was introduced to a second aptamer functionalised electrode. The second electrode was washed with Tris(bpyRu)-β-CD (Figure 4.5) and the reduction in signal compared with the reference used to indicate the detection of thrombin. By repeating the experiment with different concentrations of thrombin, a calibration curve could be obtained, demonstrating the usefulness of the system as a thrombin sensor.

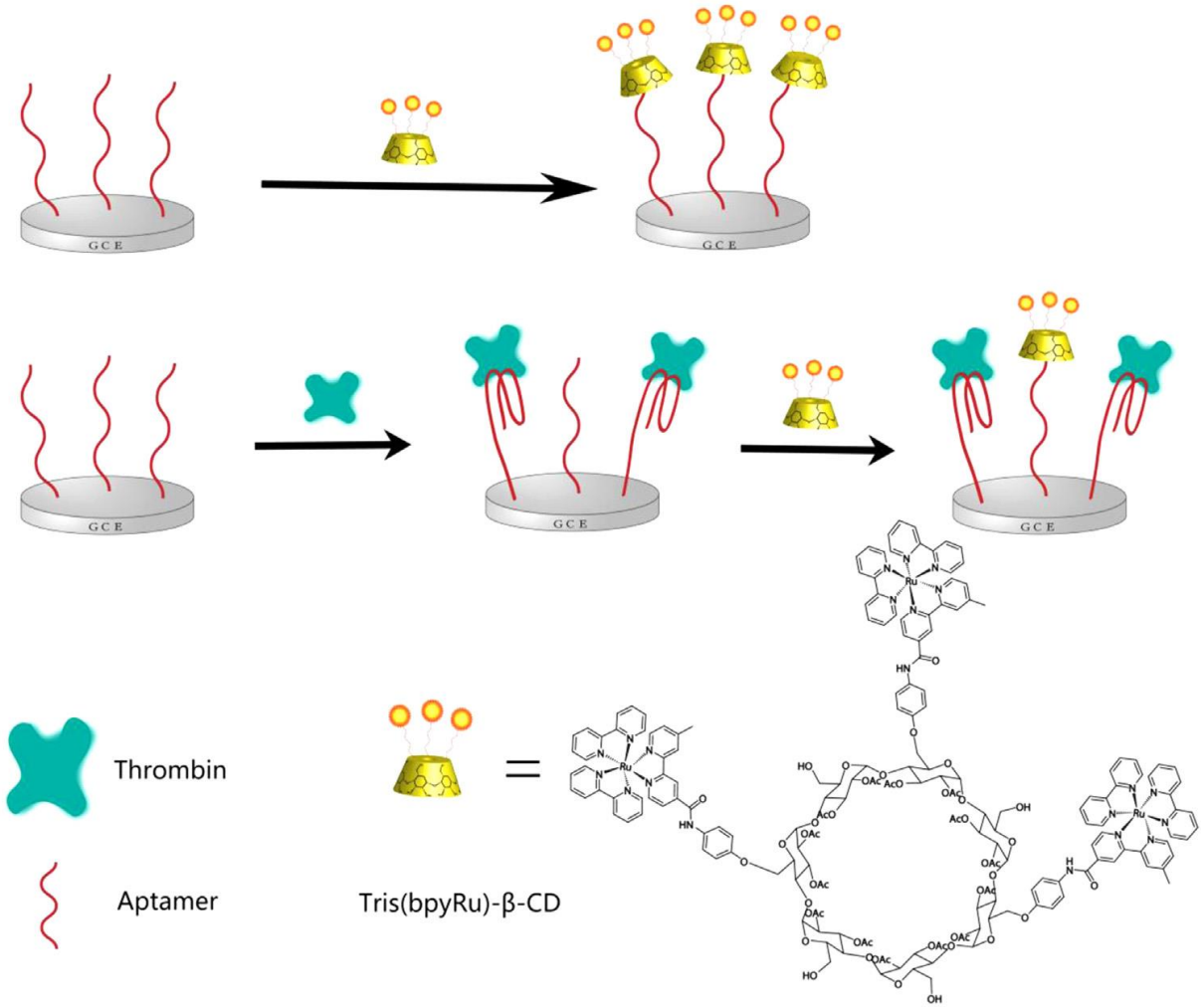


**Figure 4.5.** Schematic of aptasensor for recognising thrombin utilising a ruthenium(II) complex functionalised cyclodextrin as a luminescent reporter moiety. Reprinted from reference (39), copyright 2014, with permission from Elsevier.

A study published by Frasconi and Mazzei[40] showed by electrochemical methods that glucocorticoids could be detected *via* supramolecular interactions. Figure 4.6 shows part of the binding scheme, in which ferrocene carboxylic acid (FCA) is electrochemically incorporated into the cavities of a thiolated-β-cyclodextrin monolayer on gold. A glucocorticoid was then introduced to the surface and the reduction in peak current from the ferrocenyl moiety was monitored. The results obtained showed that as the concentration of glucocorticoid was

increased, the reduction in peak current increased, indicating greater binding of the glucocorticoid into the cyclodextrin cavities. The results shown illustrate once more the use of multicomponent sensing architectures that do not require specific binding between the analyte and the reporting group. Indeed, electrochemical markers that can permeate cyclodextrin monolayers but are blocked when a guest is present have also been used with similar results.[41]

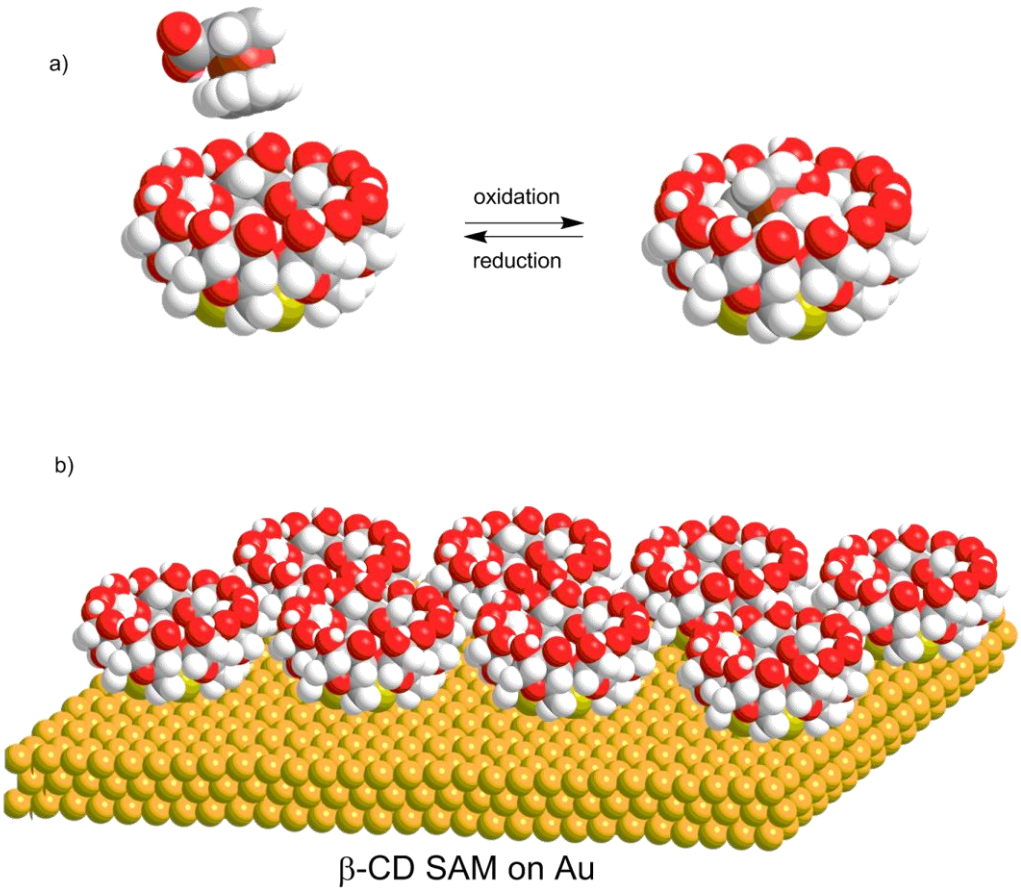


**Figure 4.6.** Schematic representation of a) electrochemically induced host-guest chemistry between FCA and thiolated β-cyclodextrin and b) thiolated β-cyclodextrin monolayer for electrochemically induced adsorption of FCA for detection of glucocorticoids.[40]

Banerjee *et al.*[42] reported the reversible immobilisation of azobenzene functionalised peptide nanotubes using α-cyclodextrin monolayers on gold. In this study (Figure 4.7), the phenyl groups of the *trans*-azobenzene moieties could bind into the cavities of the immobilised

cyclodextrin under dark conditions, but when irradiated with UV light would afford the *cis*-configuration and be expelled from the cavities. SEM images of the nanotubes obtained indicated that reversible binding was indeed happening in this way, with nanotubes observed on the gold substrates under dark conditions, and the removal of nanotubes upon irradiation. The concept was also further extended, with nanotubes functionalised with ferrocene moieties that would be recognised by β-cyclodextrin monolayers. These nanotubes could then be removed through electrochemical stimulus, in analogous fashion to previously shown examples of ferrocene-cyclodextrin binding.[43]

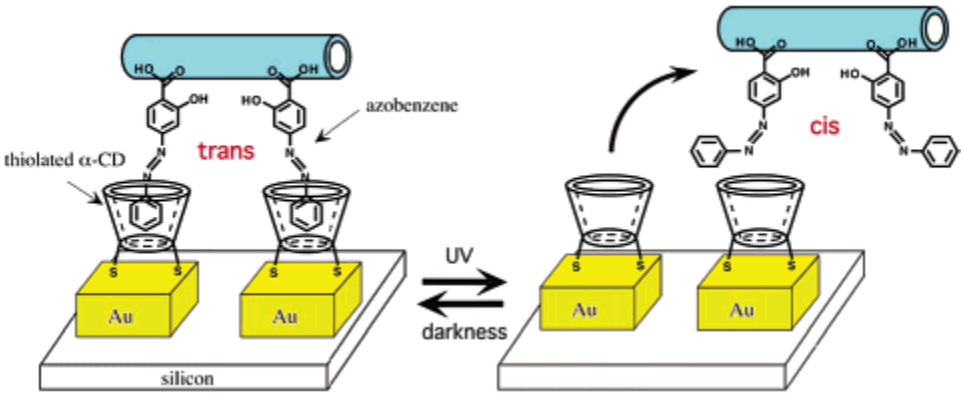


**Figure 4.7.** Schematic of reversible peptide nanotube binding to cyclodextrins. Reprinted with permission from reference (42). Copyright 2003 American Chemical Society.

One example from Ludden *et al.*[44] describes the assembly of streptavidin (Figure 4.8, **6**) onto 'molecular printboards' on gold. The streptavidin was attached to the surface in multiple ways, with monovalent (Figure 4.8, **3**) or divalent (Figure 4.8, **4**) linker molecules bearing one biotinyl and 1-2 adamantyl groups. The first route was to assemble the components in solution before immersing the molecular printboard into the complex solution. The second route involved the use of stepwise assembly to build the complex architecture through successive build and wash steps. SPR results revealed that the components could be assembled successfully in either fashion, and subsequently reversed by the introduction of a β-cyclodextrin solution to break the

supramolecular linkage between the adamantyl groups and surface bound β-cyclodextrin. The use of streptavidin and divalent linkers in building nanostructures was further investigated (Figure 4.9),[45] whereby biotinylated and non-biotinylated antibodies were adhered to the streptavidin terminated nanostructures either through binding of the biotin moiety or direct binding of the antibody itself, for the purposes of cell counting. SPR spectroscopy confirmed that the nanostructures were formed as expected, allowing fluorescence microscopy imaging of cell adhesion to be carried out. The results showed that specific binding could be achieved, as with other studied systems,[46] allowing complex nanostructures to be formed at the surface of the gold, lending itself to diagnostic applications. The use of adamantyl groups in binding of surface bound β-cyclodextrins has also been examined for other protein systems, including adamantyl functionalised cytochrome c,[47] choline,[48] and immunoglobins.[49] However, through the versatility of the cyclodextrin moiety, many other hydrophobic groups can also be used as guests for cyclodextrin binding.[50, 51]

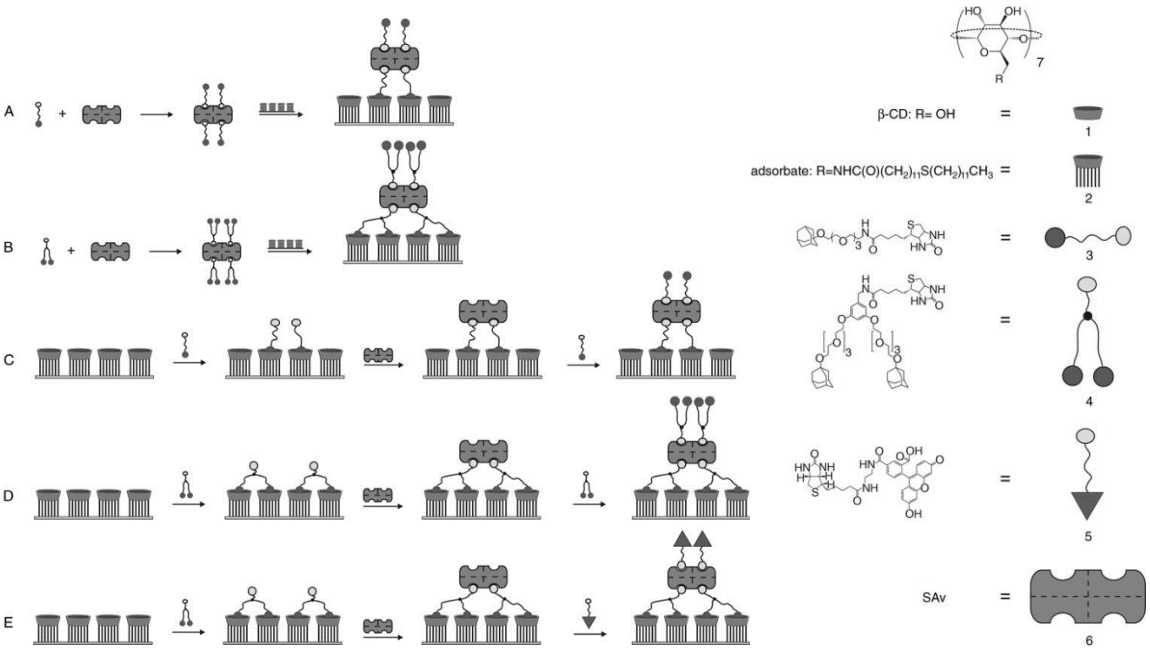


**Figure 4.8.** Schematic of adsorption schemes (left) and structures of components (right). Image reproduced with permission from reference (44). Copyright 2006 John Wiley and Sons.

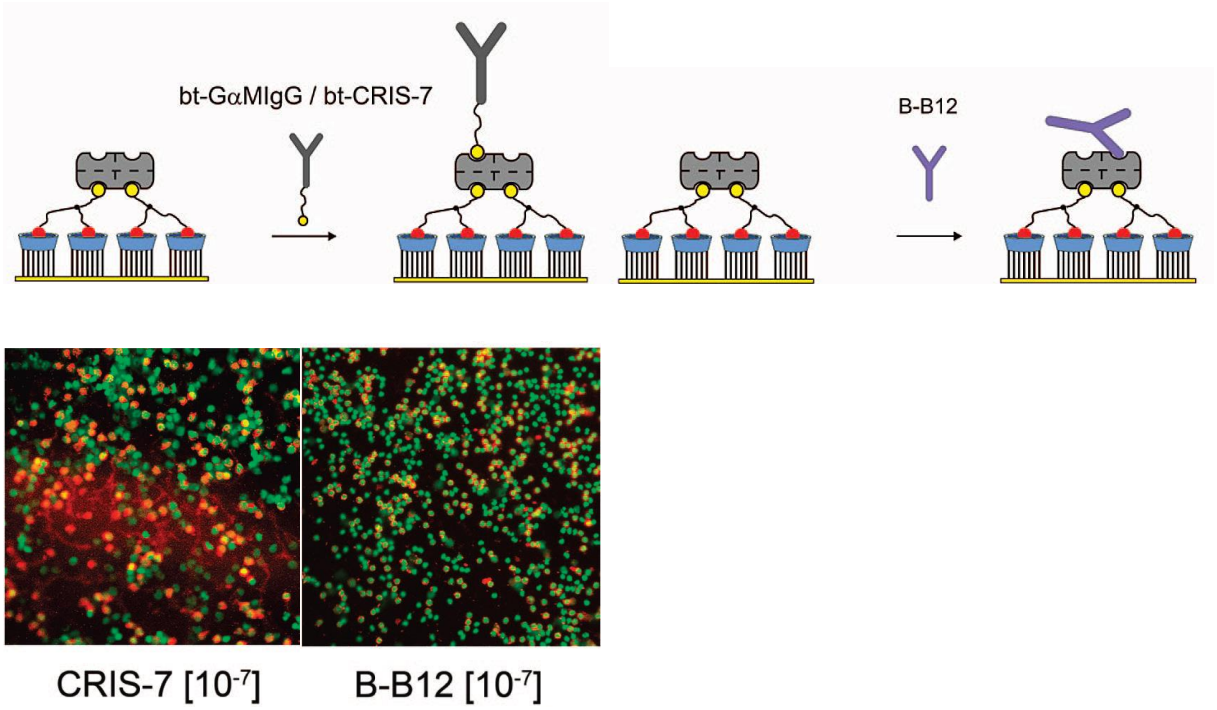


**Figure 4.9.** Schematic of attachment of antibodies to streptavidin monolayers (top) and overlayed fluorescence microscopy images of cell counting experiments of each system (bottom). Adapted with permission from reference (45). Copyright 2008 American Chemical Society.

A recent study by Holzinger *et al.*[52] demonstrates that biotinyl moieties can also be used as guests for β-cyclodextrins. In this example, the binding constant of biotin and β-cyclodextrin was determined by NMR to be $3 \times 10^2$ $M^{-1}$, and subsequently the binding pair was tested in a variety of conditions, including the immobilisation of biotinylated proteins glucose oxidase and polyphenyl oxidase. Through the study of the enzymatic processes of these proteins on β-cyclodextrin functionalised glassy carbon electrodes, the group found that binding of the proteins through biotin-cyclodextrin interactions had occurred, and thus showed that such a couple could be used as an alternative guest in the immobilisation of biomolecules at the interface.

### 4.1.3 Biomolecule-Ligand Interactions in Biomolecular Binding on Surfaces

As discussed earlier, biomolecular interactions are also a useful tool in recognition at the surface, due to the selectivity and diversity of interactions. A particularly useful motif for biomolecular recognition is that of protein-ligand interactions. A study by Hyun *et al.*[53] illustrates a method for the patterned stepwise assembly of biomolecules through protein-ligand interactions on gold surfaces. Figure 4.10 shows the formation of these structures, first by creating a monolayer of mercaptohexadecanoic acid *via* dip-pen nanolithography (DPN) and subsequently backfilling the gold surface with a triethylene glycol derivative. Amide coupling the terminal carboxylic acids with an amine functionalised biotinyl derivative afforded a surface that could recognise streptavidin. Once the streptavidin was bound, biotin functionalised BSA was able to bind into free recognition sites on the surface of the streptavidin to create the assembled nanostructure. Through this method, the group were able to demonstrate patterned nanostructures with features as small as 200 nm in diameter. AFM measurements revealed that BSA recognition would only occur when the BSA itself was biotinylated, and that if the free binding sites on the surface of the streptavidin were blocked, binding would also be prevented. These results showed that specific binding sites can mediate recognition through biomolecular interactions, with the goal of binding a biomolecule of interest from a complex mixture. This approach therefore lends itself quite well to both sensing and purification applications.

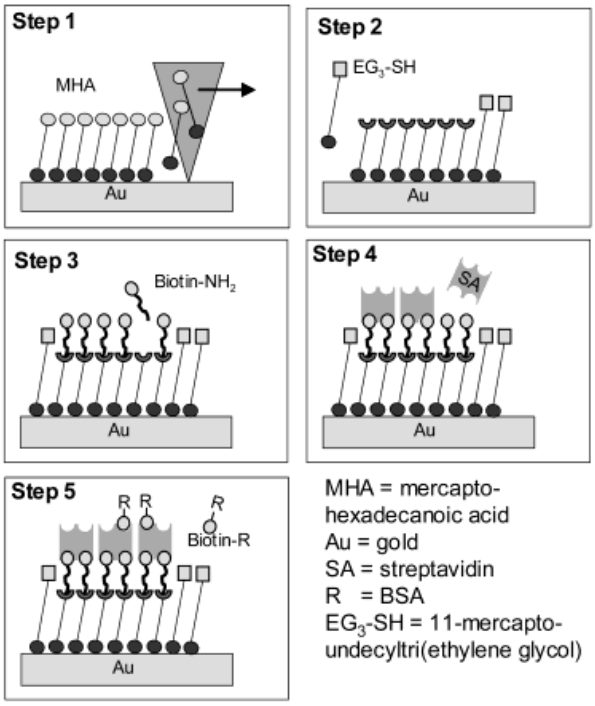


**Figure 4.10.** Schematic representation of method for creating surface bound biomolecular nanostructures through stepwise assembly. Reprinted with permission from reference (53). Copyright 2002 American Chemical Society.

Work by Hoshi *et al*.[54] demonstrates a method for the attachment of the enzyme glucose oxidase to platinum electrodes for the purposes of glucose sensing. In this example (Figure 4.11), the protein avidin was adsorbed to the surface of the platinum electrode, before subsequent alternate immersions of the electrode in solutions of biotinylated glucose oxidase (B-GOx) and avidin, resulting in multilayers of the enzyme. With this system, the group were able to sense the presence and concentration of glucose in a given solution, through the formation and subsequent electrochemical oxidation of hydrogen peroxide, a by-product in the enzymatic breakdown of glucose. The use of this particular method in fabricating these sensors allowed the group to precisely control the number of multilayers formed in a relatively facile way, and also greatly increase the output current in order to sense one order of magnitude lower concentrations of glucose.

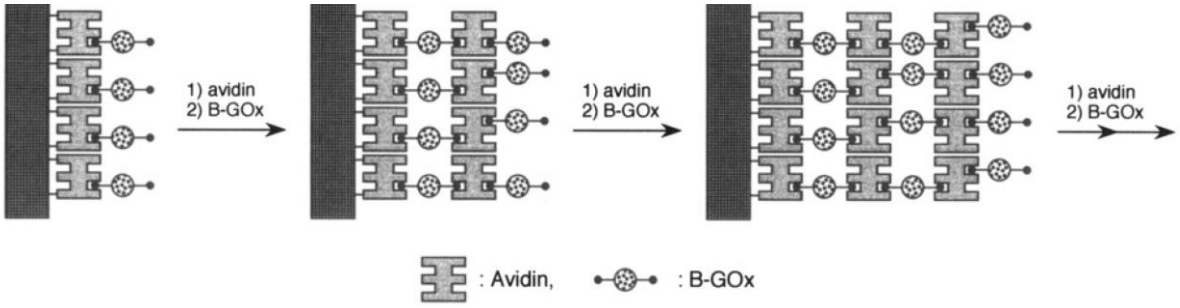


**Figure 4.11.** Schematic representation of multilayer formation of avidin and biotinylated glucose oxidase (B-GOx) on a platinum electrode. Reprinted with permission from reference (54). Copyright 1995 American Chemical Society.

A study by Yoon *et al.*[55] demonstrates a surface-bound avidin recognition system (Figure 4.12) based on fourth generation poly(amidoamine) dendrimers attached to an 11-mercaptoundecanoic acid monolayer on gold *via* amide coupling. The group then functionalised the dendritic nanostructure with a biotin-like molecule (desthiobiotin) that would still bind avidin. Once the avidin was bound the surface, it was found by the group that the avidin could then be removed by washing the surface with biotin, which has a stronger affinity with the avidin, thus displacing the desthiobiotin. In order to monitor this, the group employed electrochemical methods, loading the surface with biotinylated glucose oxidase (B-GOx) and monitoring its activity. The group found that even with multiple avidin adsorption/desorption cycles that the surface could be reliably regenerated, indicating its value as a method of regenerating sensor surfaces through displacement.

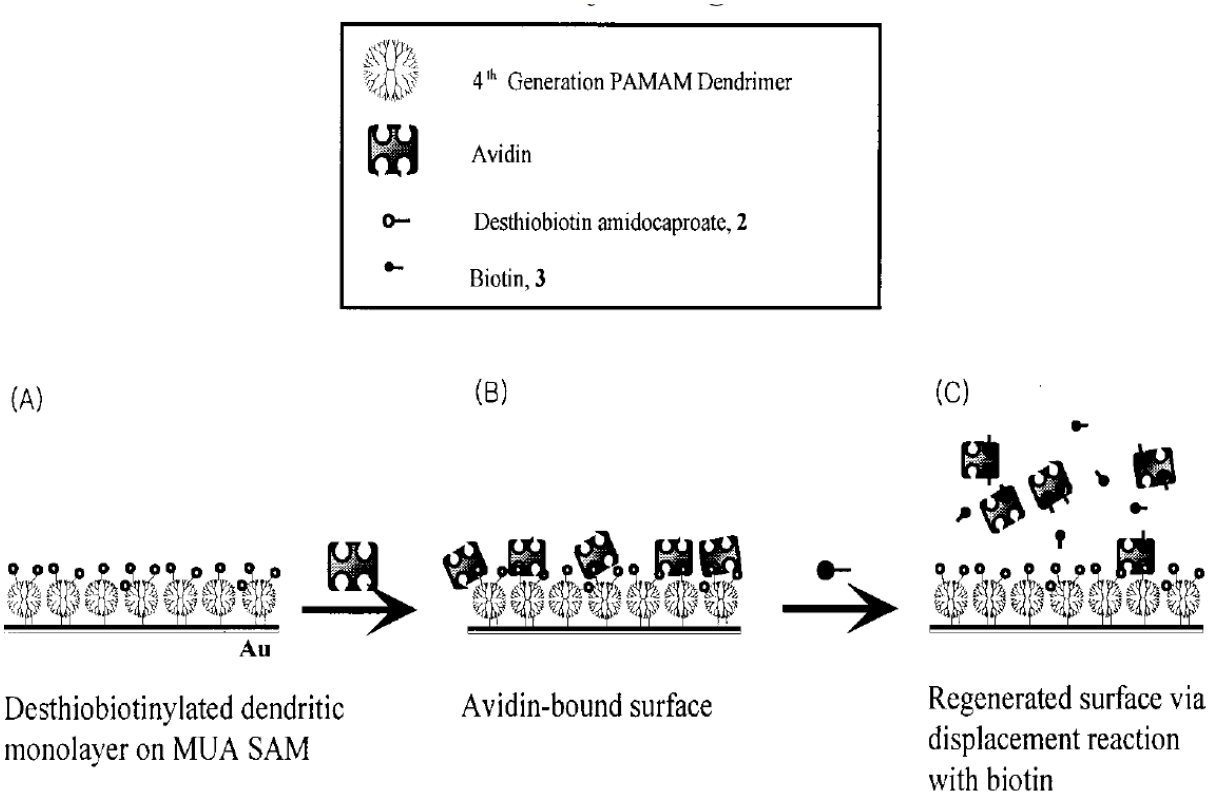


**Figure 4.12.** Schematic of regenerable surface-bound avidin recognition motif. Reprinted with permission from reference (55). Copyright 2001 American Chemical Society.

Metal ions can also be employed as biomolecular ligands as demonstrated by Turygin *et al.*[56] In this example (Figure 4.13), SAMs of octanethiol were formed on gold surfaces, before Langmuir-Blodgett deposition of dicetylcyclen. $Zn^{2+}$ ions were then deposited on the surface through complexation with the cyclen moieties. Through SPR and electrochemical methods, the group found that biomolecular recognition of nucleobases was possible, through the adsorption of adeninetriphosphate or uridinetriphosphate. The group then showed (Figure 4.13) that complementary base pairing could be used to further functionalise the surfaces, in order to create biomolecular terminated surfaces through layer-by-layer assembly involving not only chemical adsorption, but also physisorption and biomolecular interactions.

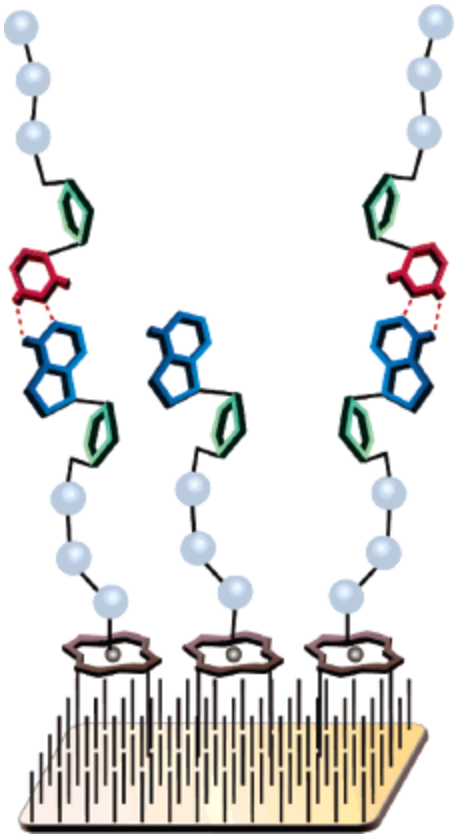

**Figure 4.13.** Schematic of nucleotide bilayer attached to $Zn^{2+}$-dicetylcyclen terminated surfaces formed through stepwise assembly. Reprinted with permission from reference (56). Copyright 2007 American Chemical Society.

### 4.1.4 Previous Work

The group of Pikramenou has been interested in utilising the host-guest chemistry that cyclodextrins afford for many years.[57, 58] In particular, solution based architectures have been shown to allow funnelling of energy between photoactive units through energy transfer processes.[10, 59, 60] Examples such as the one shown in Figure 4.14 illustrate the potential of cyclodextrin containing complexes as supramolecular building blocks in larger architectures. One area of particular interest is extending the idea of supramolecular architectures toward device fabrication, with advantages such as allowing stepwise assembly and wash steps, as well as a greater facility in fabrication due to the removal of chemical processes such as bond

formation. Immobilisation also affords reusability of the architecture, as well as an opportunity to easily separate components in the architecture after they have been used through the use of solvents.

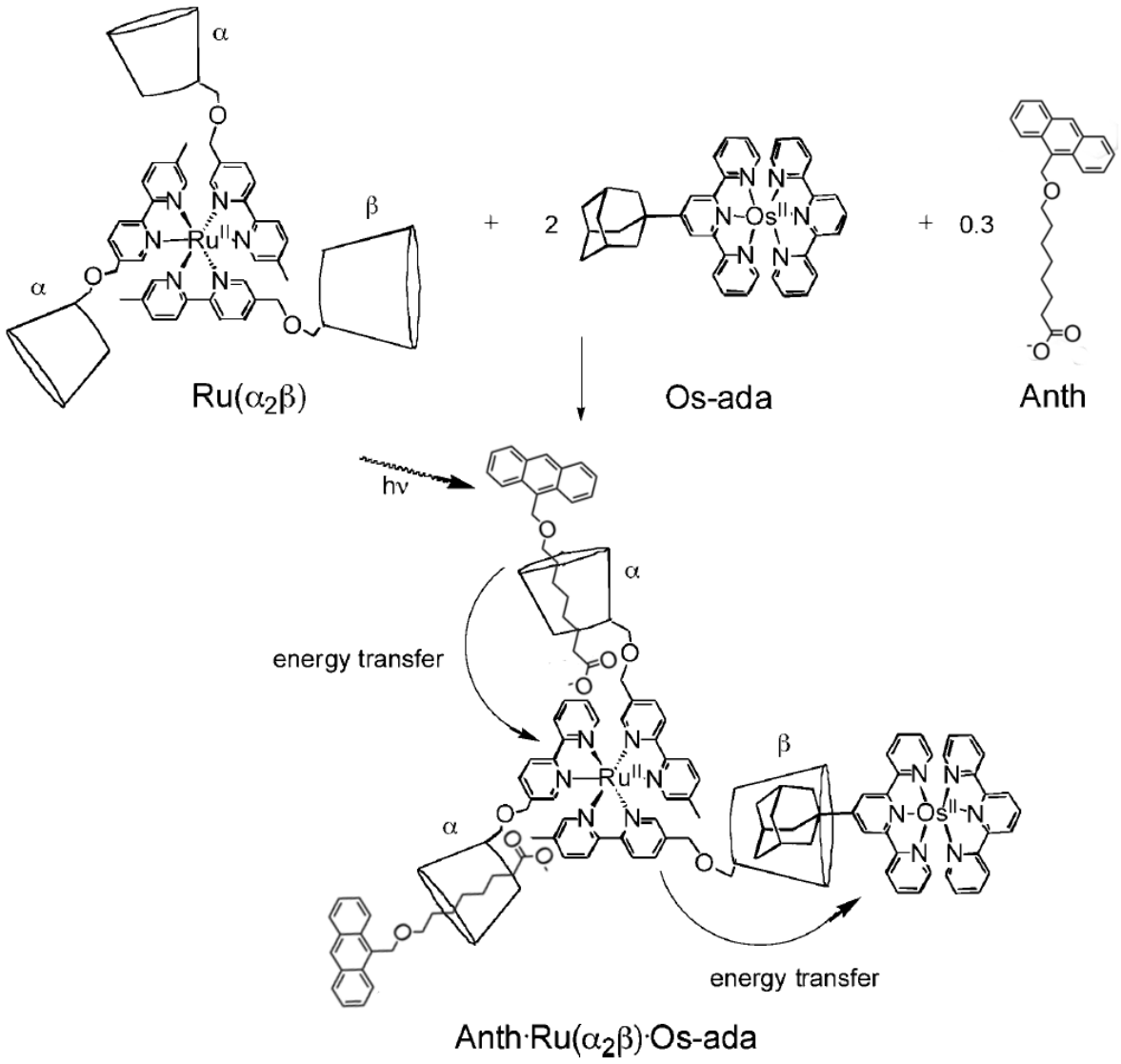


**Figure 4.14.** Example of a three component vectorial energy transfer system. Adapted with permission from reference (60). Copyright 2006 American Chemical Society.

One example of the use of cyclodextrins on surfaces by the group is that shown in Figure 4.15.[61] In this example, a monolayer of γ-cyclodextrin is achieved on platinum by terminating the primary alcohol positions with pyridyl groups, which bind to the platinum through the nitrogen donor. It was found through electrochemical studies that monolayer formation occurred through the decrease in capacitance between the electrode and a redox-active component in the electrolyte, indicating that the component was blocked from interacting with the surface. This decrease was more substantial when the monolayers were backfilled with 1-nonanethiol, showing that the backfilled SAMs had a larger coverage. To determine whether the cyclodextrins could be used to recognise species from the electrolyte, a redox-active terpyridyl based cobalt(II) complex bearing a biphenyl moiety was introduced. Interestingly, it was found that without backfilling, the expected response from the cobalt centre was surpressed (Figure 4.15), indicating that the cyclodextrin cavities were arranging in such a way as to block host-guest chemistry with the biphenyl moiety. However, when the layer was back-filled with 1-nonanethiol, a response from the cobalt complex could be observed, indicating that the tori of the cyclodextrins rearrange in order to allow binding. This particular result illustrated surface orientation is an important factor to consider when designing supramolecular devices, a point that is also echoed in other studies.[62]

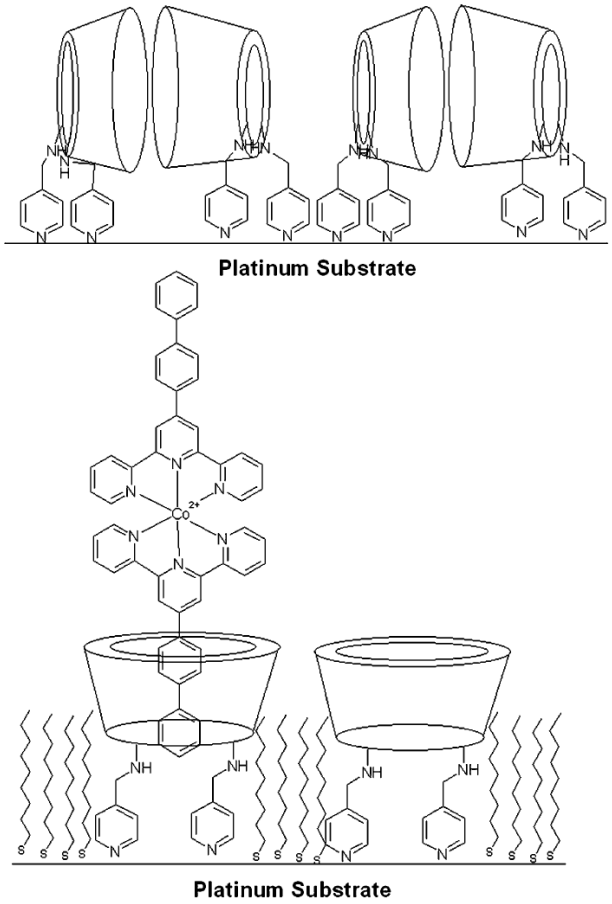


**Figure 4.15.** Top – Schematic of proposed possible orientation of γ-CD molecules on a platinum surface. Bottom – Schematic of probable reorientation of cyclodextrin molecules at platinum surface upon backfilling with 1-nonanethiol, and inclusion complex formation. Reprinted with permission from reference (61). Copyright 2007 American Chemical Society.

A more recent study utilising cyclodextrin monolayers is illustrated in figure 4.16.[63] In this example, a lipoic acid functionalised β-cyclodextrin monolayer is deposited on a gold surface, and subsequently functionalised with a terpyridyl based iridium(III) complex bearing biphenyl moieties through host-guest chemistry. STM studies revealed successful formation of the monolayer and the inclusion complex formed with the iridium guest. Using I-V spectroscopy, the group established that the electron tunnelling characteristics between the gold surface and the STM tip was aided in the presence of the iridium(III) complex, increasing the conductance

of the device and demonstrating the usefulness of supramolecular chemistry in the formation of electrical contacts at the nanoscale.

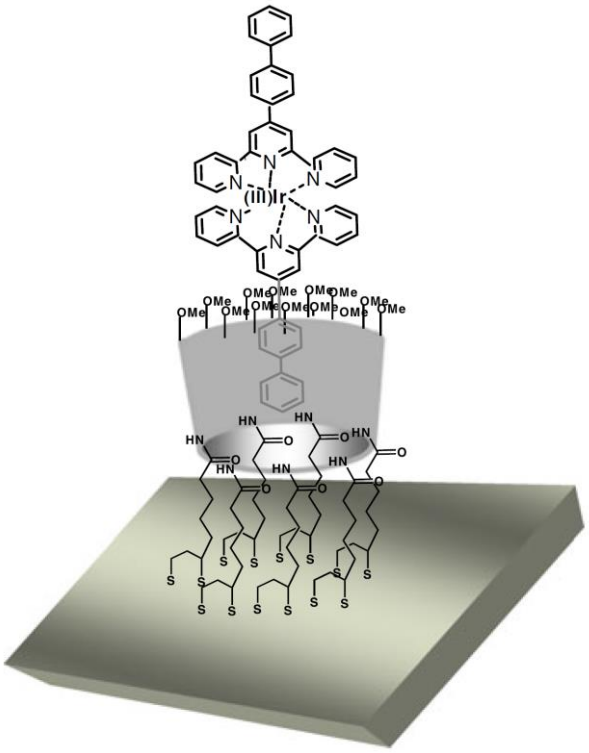

**Figure 4.16.** Schematic of terpyridyl iridium(III) complex binding to gold surface bound β-cyclodextrin functionalised monolayer. Image reproduced with permission from reference (63). Copyright 2011 John Wiley and Sons.

One example of the use of transition metal complexes bearing a cyclodextrin functionalised ligand in devices is shown in Figure 4.17.[64] Here, a terpyridyl based ruthenium(II) complex with a β-cyclodextrin moiety at one end of the complex and a thiol moiety at the other was attached to two closely spaced gold nanoelectrodes through adsorption. Gold nanoparticles with terminal adamantyl groups could then bind into the surface bound cyclodextrin moieties in order to bridge the gap between the two electrodes in order to create molecular diodes. Current-voltage studies of the electrodes revealed that the nanoparticles did indeed bridge the electrodes

and thus illustrates the usefulness of cyclodextrins as building blocks, in this particular example to create supramolecular wires.

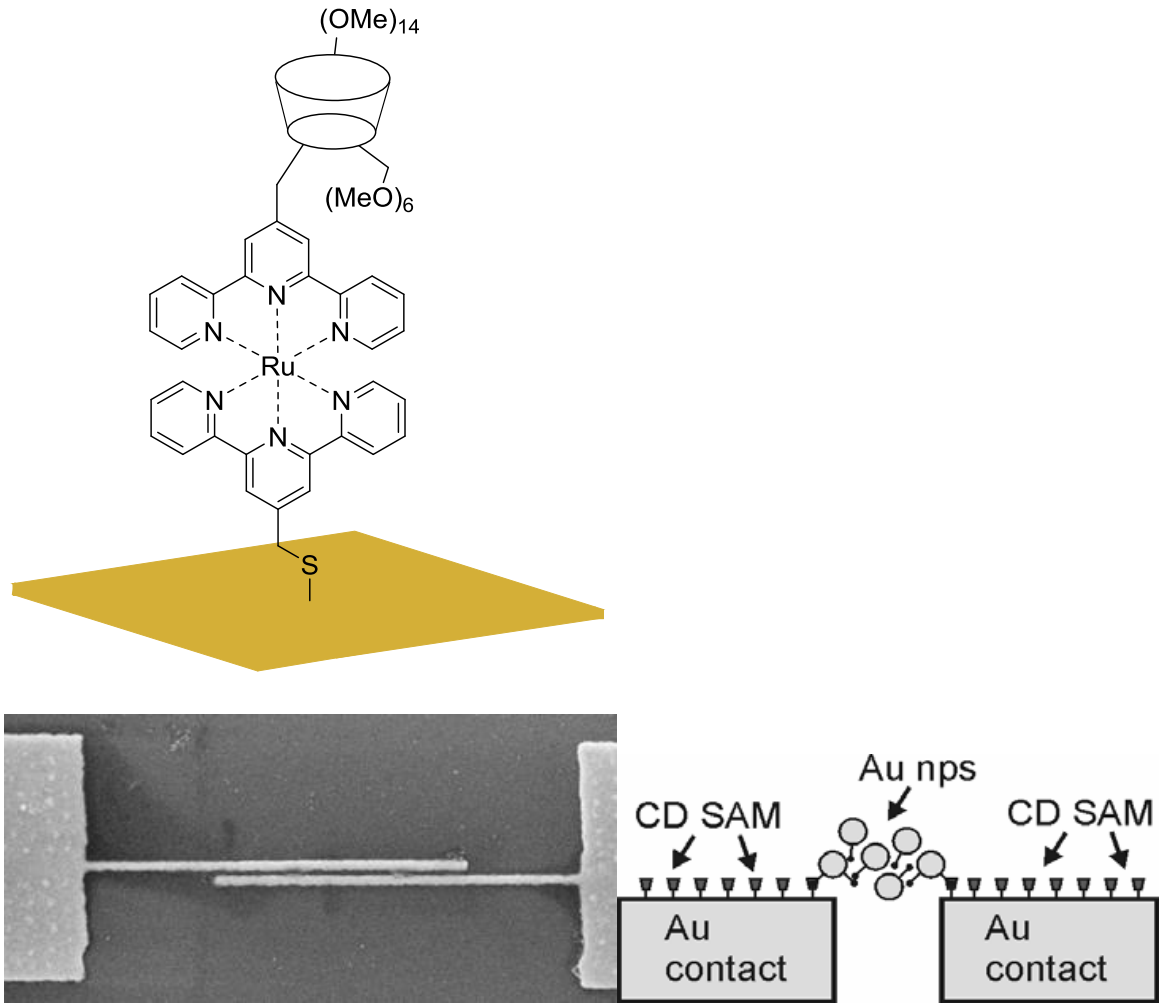


**Figure 4.17.** Top – Structure of terpyridyl ruthenium(II) complex bearing cyclodextrin and thiol functionality. Bottom left – SEM micrograph of nanoelectrodes used. Bottom right – Schematic of electrode bridging by adamantyl functionalised gold nanoparticles. Image reproduced in part with permission from reference (64). Copyright 2008 John Wiley and Sons.

### 4.1.5 Chapter Outline

Given the usefulness of cyclodextrin containing compounds for their facile host-guest chemistry; which allows the construction of large supramolecular architectures; we sought to continue the design and investigation of such compounds attached to luminescent scaffolds.

The design of surface-active complexes based on those utilising the **bpySS** architecture, but incorporating the supramolecular chemistry of cyclodextrin moieties allowed us to access facile host-guest chemistry at the surface and also utilise the luminescent properties of the complexes as part of sensing or communicative motifs. We therefore in this chapter investigate the synthesis and solution and surface properties of bis-heteroleptic complexes of ruthenium(II) and iridium(III) containing both the **bpySS** ligand and ancillary ligands that display a β-cyclodextrin moiety. We also investigate an energy transfer system based on these complexes utilising a biphenyl containing osmium(II) *bis*-terpyridine complex (**Osbiptpy**) provided by Dr. Jonathan Faiz and also a sensing platform based on using supramolecular building blocks. In the present study, the building block is a compound (**Ad-biotin**) containing an adamantyl group for binding into the cyclodextrin, and a biotinyl moiety for recognising the protein streptavidin. This particular system was chosen for its ease of preparation (one synthetic step) and the respective binding strengths of each of the moieties, with binding constants of $10^3$ $M^{-1}$ for adamantyl-cyclodextrin systems and $10^{15}$ $M^{-1}$ for biotin-streptavidin systems.[65,66] Through SPR spectroscopy we seek to show that specific binding of proteins can be achieved through the use of supramolecular chemistry and stepwise assembly.

# 4.2 Preparation of Complexes Bearing Cyclodextrin Functionalised Ancillary Ligands

## 4.2.1 Synthesis of Cyclodextrin Functionalised Bidentate Ligands

The cyclodextrin containing ligands used in this work are pyridyl based and contain an ether linkage to attach a cyclodextrin to the ligand. Two synthetic methods were followed so that a bromide group could be attached to the ligand, and subsequently reacted with a hydroxyl group present on the cyclodextrin.

The first synthetic route (Scheme 4.1) is designed to allow functionalization of **1** with another aromatic ring *via* a two-step process to form either a phenylpyridine or bipyridyl based ligand, which then allowed functionalization of the cyclodextrin moiety *via* another cross coupling reaction. The method was first tested with a second dibromopyridyl group to form **3** *via* a Stille cross coupling reaction described by Schwab *et al.*[67] The cyclodextrin moiety could then be attached *via* a Buchwald-Hartwig cross coupling step as outlined by Gowrisankar *et al.*[68] to afford **4**.

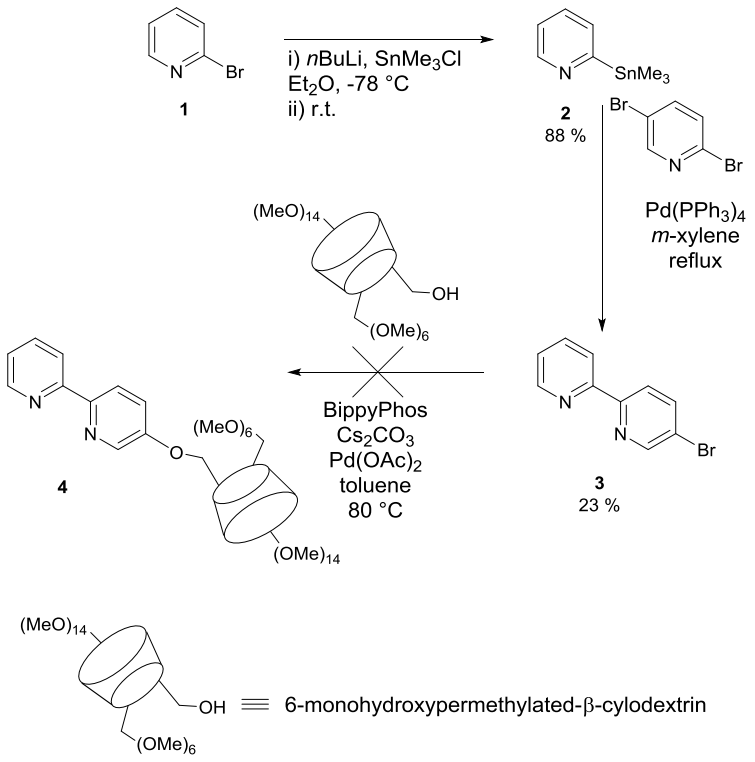


**Scheme 4.1.** Proposed synthetic route to cyclodextrin functionalised ligands with aryl ether bonds.

The preparation of **2** was confirmed by $^{1}$H NMR spectroscopy, which displayed 5 environments corresponding to the expected proton environments.[67] The environment at 0.31 ppm, a singlet with an integral of 9 protons and characteristic satellite peaks from coupling to tin confirms the presence of the trimethyltin group.

**3** was characterised by $^{1}$H, $^{13}$C and 2D NMR spectroscopy, and ESI(+) mass spectrometry. The $^{1}$H NMR spectrum reveals 7 aromatic environments corresponding to each of the protons in the molecule as would be expected due to its asymmetric nature. Assignments for the proton environments agree with the published results. $^{13}$C NMR data reveals 10 aromatic peaks corresponding to each of the carbon environments in the compound, agreeing well with published data.[67] Further analysis of the compound by HSQC yielded assignments for all carbon environments. The ESI(+) mass spectrum reveals one adduct at 237 corresponding to $(M+H)^{+}$.

The mass spectrum also shows the characteristic isotope pattern of bromine, indicating that it is also present in the product.

The next stage of the synthesis involved cross coupling **3** with 6-monohydroxy-permethylated-β-cyclodextrin. Multiple attempts to synthesise the final product **4** bearing the cyclodextrin moiety utilising the catalyst system BippyPhos and $Pd(OAc)_2$ were unsuccessful. TLC analysis of reaction mixtures indicated that the reaction had not proceeded, which we postulate is due to competition between the bipyridine derivative and BippyPhos for coordination to the palladium centre *via* nitrogen and phosphorus donors respectively. We also postulate that there could be competition between the 6-monohydroxy-β-cyclodextrin and BippyPhos, due to *tert*-butyl groups on the BippyPhos which could enter the cavity of the cyclodextrin and disrupt the catalytic cycle. Similar attempts with the catalytic system CuI/bipyridine were also unsuccessful and thus the route was abandoned.

The second synthetic route (Scheme 4.2) involving free radical bromination with asymmetric pyridyl derivatives was proposed, based on work previously carried out within the group.[9, 10] In brief, **5** was lithiated and stannylated (**6**), before Stille cross coupling to yield bidentate methyl containing ligands (**7** and **8**).[67, 69] These were subjected to free radical bromination (**9** and **10**) and subsequent Williamson ether synthesis with a mono-unprotected β-cyclodextrin derivative to yield cyclodextrin containing ligands **12** and **13** in acceptable yields.

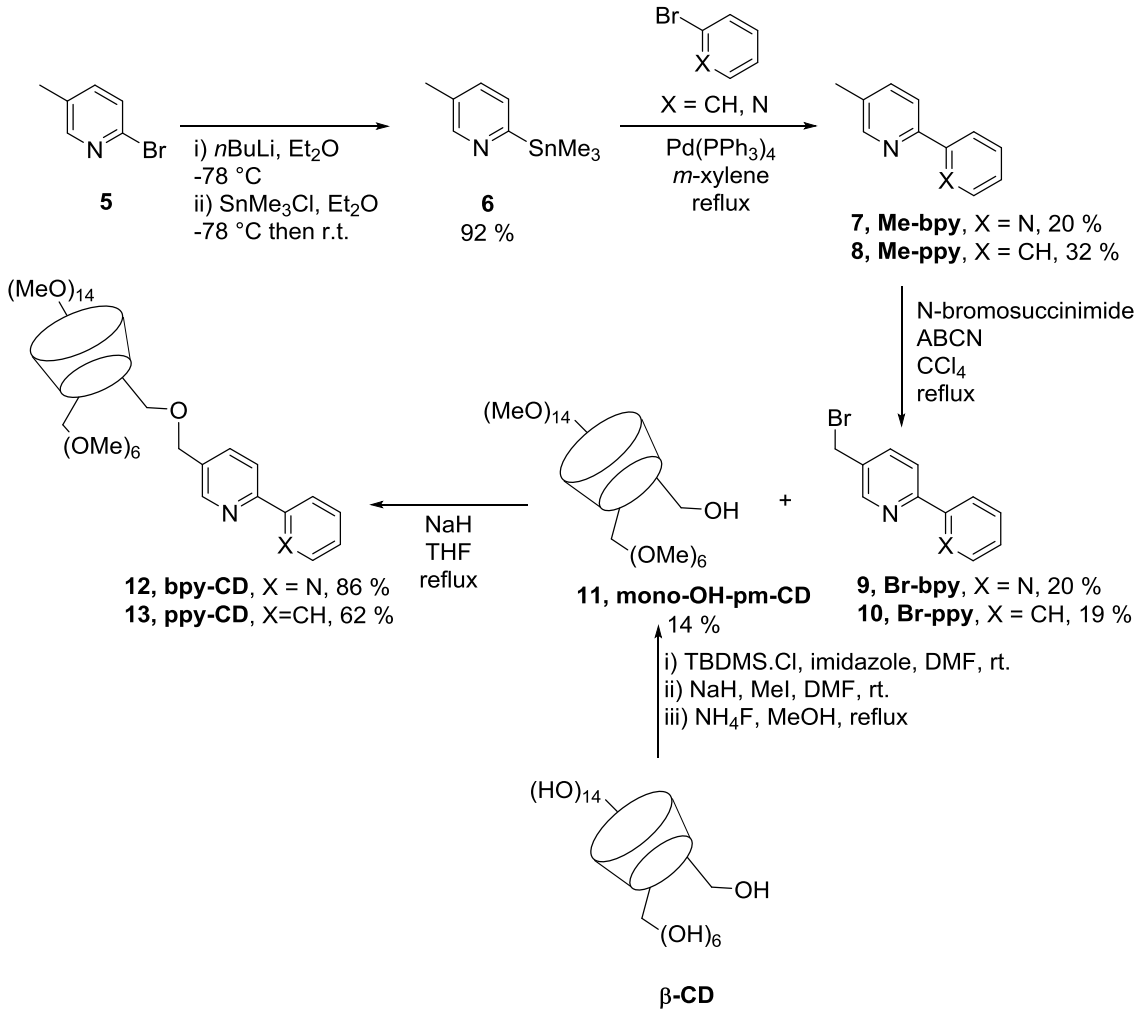


**Scheme 4.2.** Synthetic route to cyclodextrin functionalised ligands *via* free radical bromination.

**2-trimethylstannyl-5-methylpyridine (6)** was characterised by $^{1}H$, $^{13}C$ and 2D NMR spectroscopy. NMR assignments were confirmed by COSY, HSQC and HMBC experiments and previous studies.[69] Figure 4.A1 shows the $^{1}H$ NMR spectrum of the product, which contains four environments. The characteristic singlet trimethyltin peak at 0.29 ppm with satellites integrates well with the other peaks in the spectrum, along with another singlet peak at 2.25 ppm, corresponding to H-7. Interestingly, H-3 and H-4 are assigned to a single doublet peak with satellites at 7.30 ppm which integrates for 2 protons. H-6 is assigned to a multiplet peak at *ca.* 8.56 ppm. The $^{13}C$ spectrum contains 6 environments corresponding to the 5 aromatic

environments and C-7. The trimethyltin peak was not observed within the range of the HSQC experiment and thus not assigned, however a candidate for this environment is present at -9.5 ppm by PENDANT $^{13}C$ NMR. Some impurities are present in both spectra, however due to the expected instability of the trimethyltin derivative and confirmation of the desired product within the mixture, the compound was carried forward to the next step without further purification.

**Me-bpy (7)** was characterised by $^{1}H$, $^{13}C$ and 2D NMR spectroscopy, and ESI(+) mass spectrometry. NMR assignments were confirmed by COSY, HSQC and HMBC experiments and previous studies.[69] Figure 4.A2 shows the $^{1}H$ NMR spectrum, revealing 8 peaks corresponding to each of the protons in the compound, with negligible impurity. The singlet peak for H-7 at 2.36 ppm is shifted downfield by 0.11 ppm relative to **2-trimethylstannyl-5-methylpyridine (6)** by the introduction of another pyridyl ring in place of the trimethyltin group. The aromatic resonances of H-3,4,6 have also shifted downfield with the introduction of the pyridyl ring, along with the splitting of peaks H-3 and H-4 due to the increased asymmetry of electronegativity across the product. 4 new environments are also observed for the second pyridyl ring, as expected, and the proton integrals match very well to each other. The loss of the trimethyltin peak also confirms that the product is formed. The $^{13}C$ NMR spectrum reveals 11 peaks corresponding to each of the carbon environments. The peak at 18.4 ppm for C-7 is not appreciably shifted from the spectrum of **2-trimethylstannyl-5-methylpyridine (6)**, however it is noted that the aromatic resonances C-2,3,5,6 are shifted upfield. The exception to this is C-4, which is shifted downfield. The spectrum also reveals 5 new environments corresponding to the second ring and the disappearance of the peak at -9.5 ppm which indicates formation of the product. The ESI(+) mass spectrum of the product reveals an adduct at 171 corresponding to $(M+H)^{+}$, confirming the success of the reaction. Similar results were also

observed for **Me-ppy (8)** with the expected NMR results (appendix) and an adduct at 170 $(M+H)^+$ in the ESI(+) mass spectrum.

The free radical bromination reactions performed in the group were historically performed using carbon tetrachloride and either benzoyl peroxide or AIBN as radical initiators.[70, 71] However, as we were interested in using more environmentally friendly solvents and safer reagents, the combination of 1,2-dichloroethane as solvent and ABCN as radical initiator was tested to determine its efficacy. Multiple attempts at the synthesis with this method were performed using N-bromosuccinimide as a source of bromine, however all attempts resulted in the failure of the desired reaction and the formation of an orange solution. It was also noted that N-bromosuccinimide was particularly soluble in 1,2-dichloroethane compared with carbon tetrachloride, which may have contributed to the failure of the reaction. For this reason, the synthesis was again attempted with carbon tetrachloride as the solvent and ABCN as the radical initiator, yielding the desired products in acceptable yields.

**Br-bpy (9)** was characterised by $^1$H, $^{13}$C and 2D NMR spectroscopy, and ESI(+) mass spectrometry. NMR assignments were confirmed by COSY, HSQC and HMBC experiments, as well as previous studies.[70, 72] Figure 4.A4 shows the $^1$H NMR spectrum of the product. It is immediately noticeable that each set of aromatic environments H-3,3′, H-4,4′ and H-6,6′ have coalesced upon introduction of the bromide moiety with H-3, H-4 and H-6 shifted downfield by *ca.* 0.1, 0.2 and 0.15 ppm respectively. The peak assigned to H-7 has also shifted downfield by 2.11 ppm and has an integral of 2, indicating the loss of a proton and the introduction of the bromide moiety. The $^{13}$C spectrum of the product is much the same as that of **Me-bpy (7)**, with minimal shifts in the aromatic region. However, the peak for C-7 is shifted downfield considerably from 18.4 ppm to 29.6 ppm, with the addition of the peak also being distinguished as coupled to an even number of protons in the PENDANT NMR, indicating that there is a loss

of a proton and the introduction of the bromide group. ESI(+) mass spectrometry reveals a single adduct at 251 corresponding to $(M+H)^+$. The peak also displays the characteristic isotope pattern of bromine, confirming the successful formation of the product. Similar results were also observed for **Br-ppy (10)** with the expected NMR results (appendix) and an adduct at 250 $(M+H)^+$ in the ESI(+) mass spectrum.

**mono-OH-pm-CD (11)** is characterised by $^1$H and $^{13}$C NMR spectroscopy, and MALDI mass spectrometry. Figure 4.18 shows the $^1$H NMR spectrum. The spectrum has two distinctive regions, the first between *ca.* 3.1 and 4.1 ppm corresponding to protons on each of the glucose units at H-g-2 through g-6, and also the methoxy protons. The second and more interesting region is that of *ca.* 5.0-5.3 ppm, ascribed to the anomeric centre H-g-1.[32] Due to the asymmetric nature of the monohydroxy-β-cyclodextrin, this assignment appears very characteristically as separate environments, and is in good agreement with previously published results.[32] A small amount of residual ethyl acetate is also present from the purification of the compound at 4.15 ppm, as well as at 2.15 and 1.27 ppm (not shown). The $^{13}$C NMR spectrum is also in good agreement. The MALDI mass spectrum was obtained using gentisic acid as a matrix and displays two ion envelopes at 1438 and 1454 Da corresponding to $(M+Na)^+$ and $(M+K)^+$ respectively, in good agreement with previous results,[9, 10] confirming formation of the product.

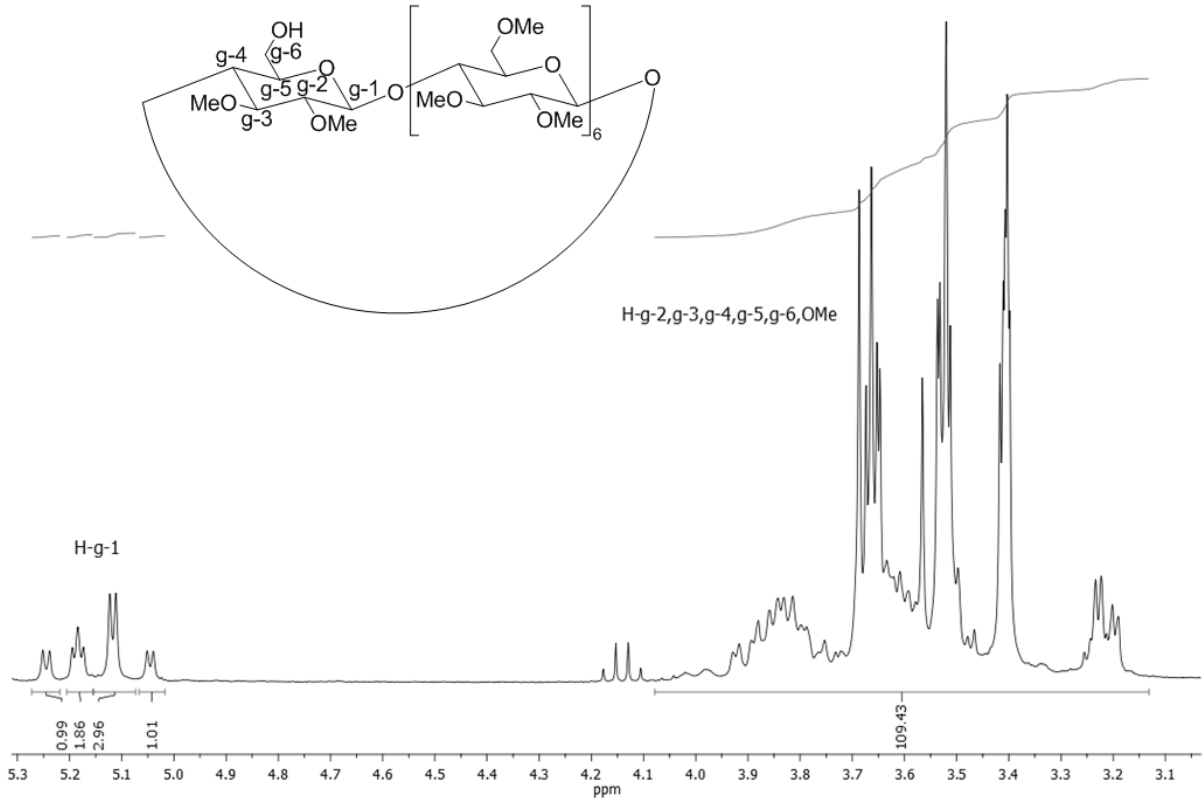


**Figure 4.18.** $^{1}$H NMR spectrum of **mono-OH-pm-CD (11)** in $CDCl_3$.

**bpy-CD (12)** was characterised by $^{1}$H, $^{13}$C and 2D NMR spectroscopy, and MALDI mass spectrometry. $^{1}$H NMR assignments were confirmed by COSY experiments. Figure 4.19 shows the $^{1}$H NMR spectrum of the product. It can be seen that there is an addition of 5 peaks compared with the spectrum of **mono-OH-pm-CD (11)**, corresponding to each of the proton environments of the bipyridine. These integrate well with H-g-1 (4.91-5.18 ppm), indicating the success of the reaction. The proton environment H-7 at *ca.* 4.6 ppm is also shifted downfield in its main singlet peak by *ca.* 0.2 ppm with respect to **Br-bpy (9)**, and we can see the peak is also broader and has a shoulder, caused by the chiral nature of the cyclodextrin ring. Because the ring can be either left or right handed in nature, the proton environment at H-7 becomes diastereotopic in nature, giving rise to the different peak pattern in agreement with previous results for similar compounds.[70] The peak at 4.91-5.18 ppm corresponding to H-g-1 is also

different to that of **mono-OH-pm-CD (11)** due to the attachment of the methylene group of bipyridyl moiety, which causes the characteristic peaks to merge into a broad unresolved peak. This is due to the methylene group being more similar to the methyl groups in the methoxy moieties and thus a loss of asymmetry compared with the monohydroxy moiety. This observation is also in concordance with previous results.[70] Some solvent impurities are present, notably traces of dichloromethane and ethyl acetate. However, these impurities would not interfere with the next stage in the synthesis and so the product was carried forward. $^{13}$C NMR spectroscopy reveals peaks that are in good agreement with similar previously studied compounds.[70] The MALDI mass spectrum was obtained using 2,3-dihydroxybenzoic acid as a matrix, and reveals three ion envelopes at 1583, 1605 and 1621 Da corresponding to $(M+H)^+$, $(M+Na)^+$ and $(M+K)^+$ respectively, confirming formation of the product. Similar results were also observed for **ppy-CD (13)** with the expected NMR results (appendix) and ion envelopes at 1604 Da $(M+Na)^+$, 1620 Da $(M+K)^+$ in the MALDI(+) mass spectrum.

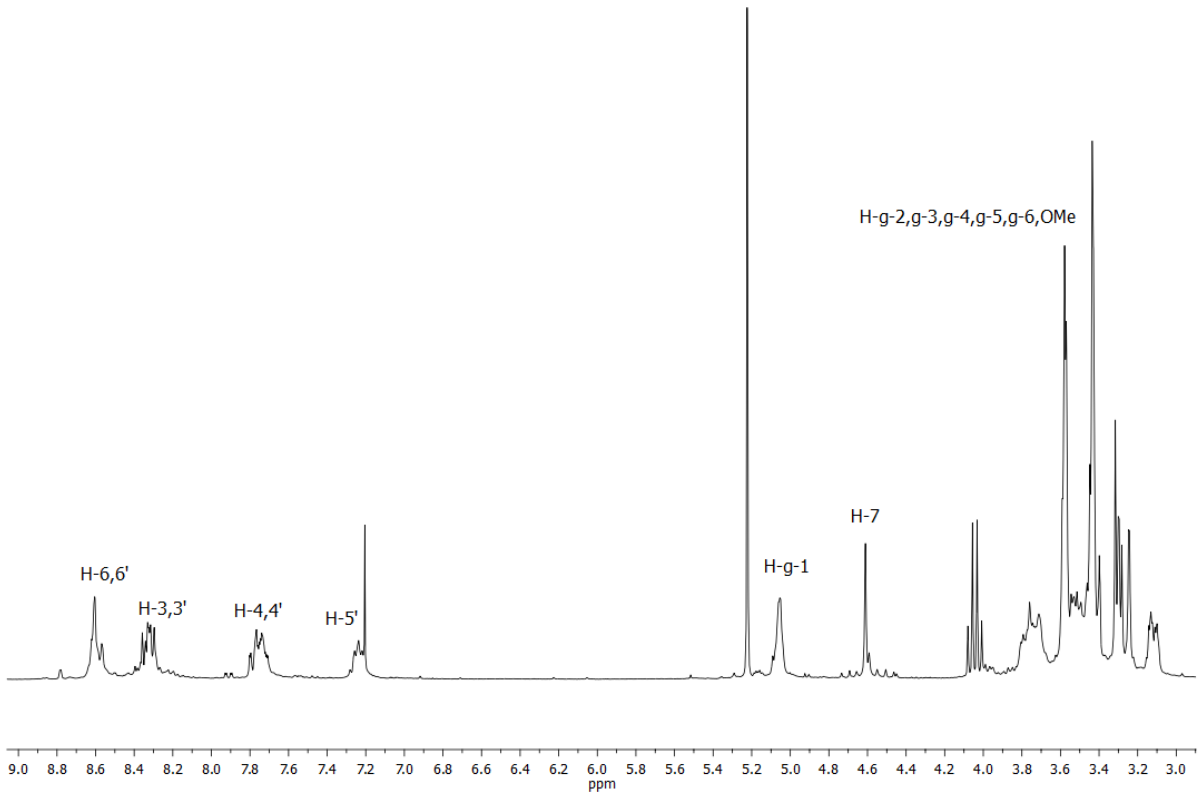


**Figure 4.19.** $^{1}$H NMR spectrum of **bpy-CD (12)** in $CDCl_3$.

## 4.2.2 Synthesis of Transition Metal Complexes Bearing Cyclodextrin Functionalised Ligands

Scheme 4.3 illustrates the synthetic route to bis-heteroleptic metal complexes bearing ancillary cyclodextrin functionalised ligands and a surface-active ligand. In brief, the ruthenium(II) complex is synthesised by reacting **bpy-CD (12)** with dichloro(cylooctadienyl)ruthenium(II) polymer $[Ru(COD)Cl_2]_n$ in the presence of chloride ions to form **$Ru(bpy\text{-}CD)_2Cl_2$ (14)**, followed by a further complexation reaction with **bpySS** to displace the chloride ligands and form **$Ru(bpy\text{-}CD)_2(bpySS)$ (16)**. Due to the asymmetry of the **bpy-CD (12)** ligand, the synthetic route to **14** causes multiple isomers to be formed. Figure 4.20 shows the possible configurations of the cyclodextrin ligands around the ruthenium centre, and to reflect the

ambiguity in the way these ligands are coordinated, a schematic representation of the final complex **Ru(bpy-CD)$_2$(bpySS) (16)**. **Ir(ppy-CD)$_2$(bpySS) (17)** is synthesised in a similar fashion to **16**, first reacting **ppy-CD (13)** with $IrCl_3$ to form the **[Ir(ppy-CD)$_2$Cl]$_2$ (15)** dimer, with subsequent complexation with **bpySS** to break the dimer and form **Ir(ppy-CD)$_2$(bpySS) (17)**. However, due to *trans* directing effects of the chloride ligands in the formation of the carbon σ-bonds in **15** (Scheme 4.3),[73] we expect only to observe one isomer to be formed. Both complexes were successfully formed in acceptable yields.

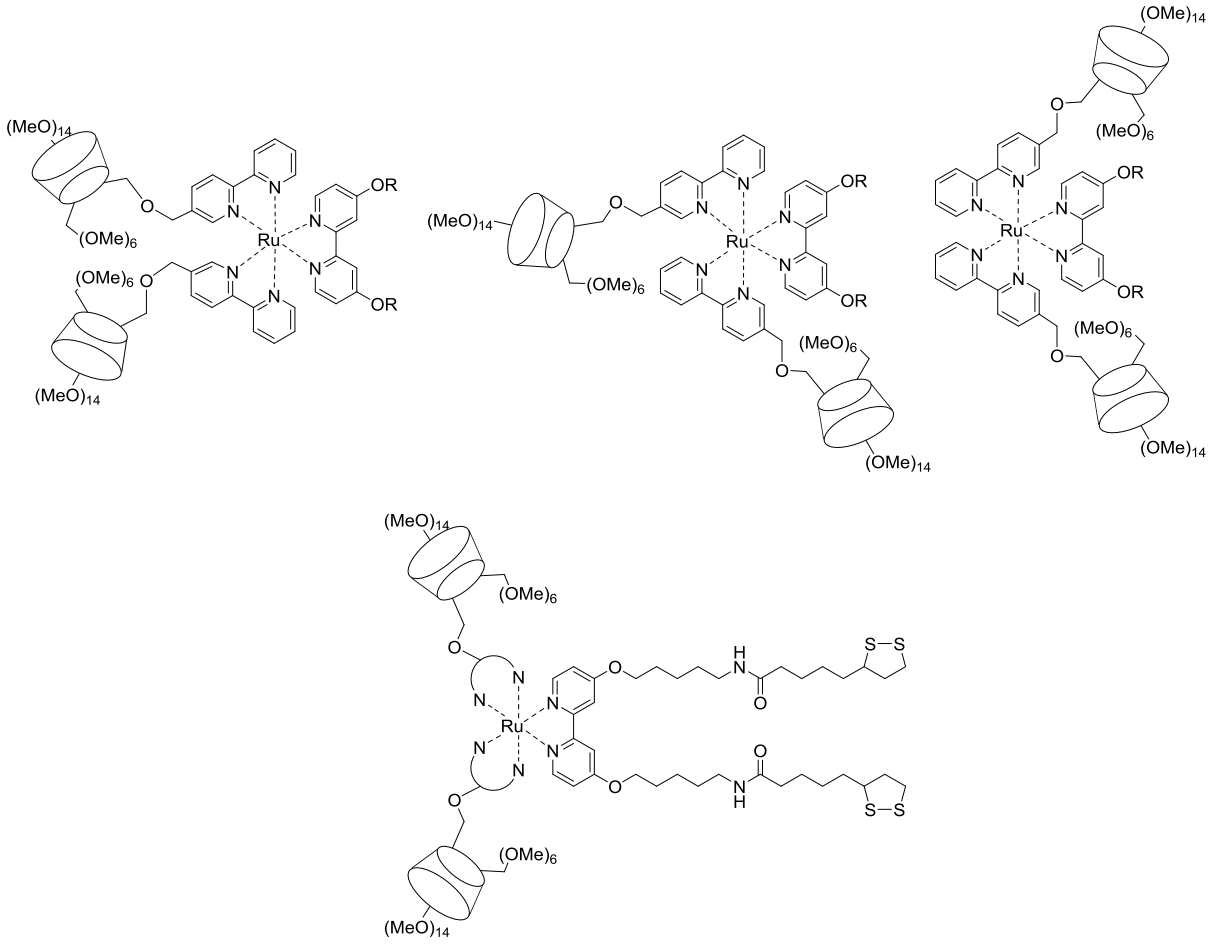


**Figure 4.20.** Schematic illustrating possible isomers of ruthenium(II) complex (top) and schematic representation of **Ru(bpy-CD)$_2$(bpySS) (16)**.

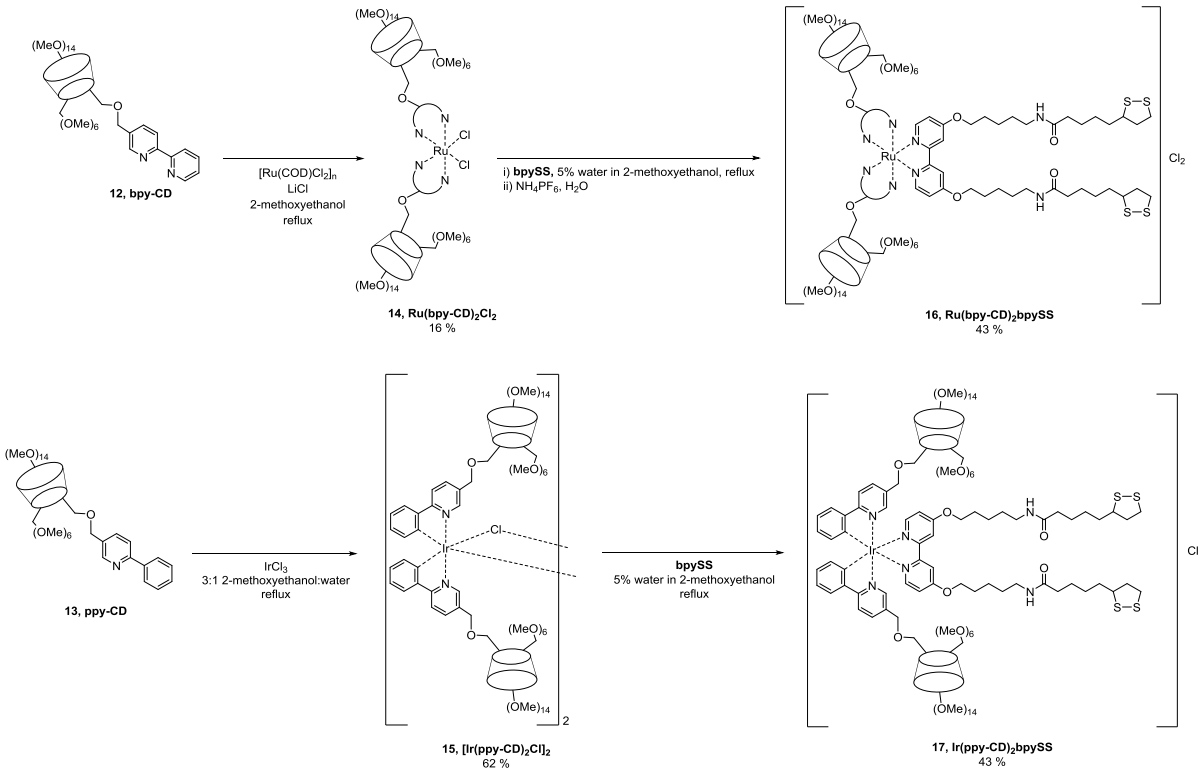


**Scheme 4.3.** Synthetic route to cyclodextrin functionalised transition metal complexes.

**Ru(bpy-CD)$_2$Cl$_2$ (14)** was characterised by MALDI mass spectrometry. A $^1$H NMR spectrum of the product was recorded, however due to the weakness of the spectrum interpretation of the spectrum is very limited. We do however observe peaks (Figure 4.A15) in the aliphatic region where we expect to see peaks arising from the cyclodextrin moiety, particularly for H-g-1 at *ca.* 5 ppm, and aromatic peaks as high as *ca.* 10 ppm which are not observed for **bpy-CD (12)**. The MALDI mass spectrum was obtained using norharmane as a matrix and reveals a single adduct at 3421 corresponding to $(M+2\cdot MeCN+H)^+$, confirming the formation of the product.

**Ru(bpy-CD)$_2$(bpySS) (16)** was characterised by $^1$H NMR spectroscopy and ESI(+) mass spectrometry. Figure 4.21 shows the $^1$H NMR spectrum of the complex, revealing the addition of the proton environments associated with **bpySS** in the regions 0.75-2.55, 2.91-4.02 and 4.10-4.52 ppm, as well as peaks for the amide protons at 5.47-5.73 ppm. The aromatic region of the spectrum reveals many new peaks consistent with the formation of multiple isomers, and we

observe an increase in the overall integration of the aromatic region (20H). Indeed this integration agrees well with the amide N*H* (2H) and H-g-1 at 4.97-5.27 (14H), confirming formation of the desired product. The ESI(+) mass spectrum reveals one adduct at 2002 corresponding to $(M\text{-}2Cl)^+$ confirming the desired product is formed. The isotope pattern is also in good agreement with the expected result.

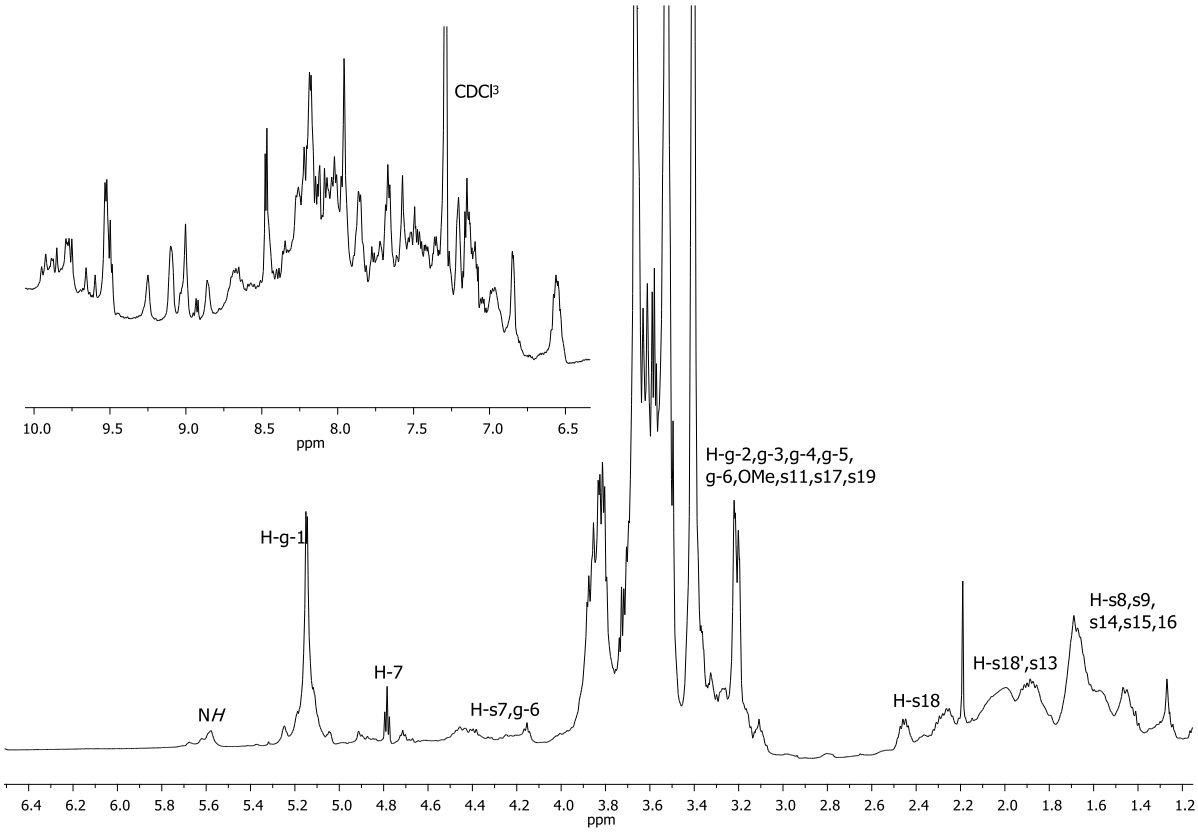


**Figure 4.21.** 500 MHz $^1$H NMR spectrum of **Ru(bpy-CD)$_2$(bpySS) (16)** in $CDCl_3$. Inset – aromatic region.

**[Ir(ppy-CD)$_2$Cl]$_2$ (15)** was characterised by $^1$H NMR spectroscopy and MALDI mass spectrometry. Figure 4.22 shows the $^1$H NMR spectrum, revealing the peak at 4.98-5.12 corresponding to H-g-1. We also observe changes in the aromatic region, with small downfield shifts of *ca*. 0.7, 0.5 and 0.1 ppm for H-6, H-9 and H-3,4 respectively, indicating coordination to the iridium (III) centre. The environment at 4.55-4.71 ppm corresponding to H-7 is also

changed, with the peak having lost its multiple singlet features and is now a broad unresolved singlet, also indicating a change in structure. The MALDI mass spectrum was obtained using norharmane as a matrix and reveals a single peak at 3355 corresponding to $(Ir(ppy\text{-}CD)_2)^+$, indicating formation of the complex. The reason we observe only half of the dimer in mass spectra with this complex and also the previously studied complex $[Ir(ppy)_2Cl]_2$ is likely due to the lability of the chloride groups in ligating solutions which allow the complex to exist in a fluxional solution structure.[74] Indeed, under the conditions of the mass spectrometer we therefore believe that these bonds would easily break.

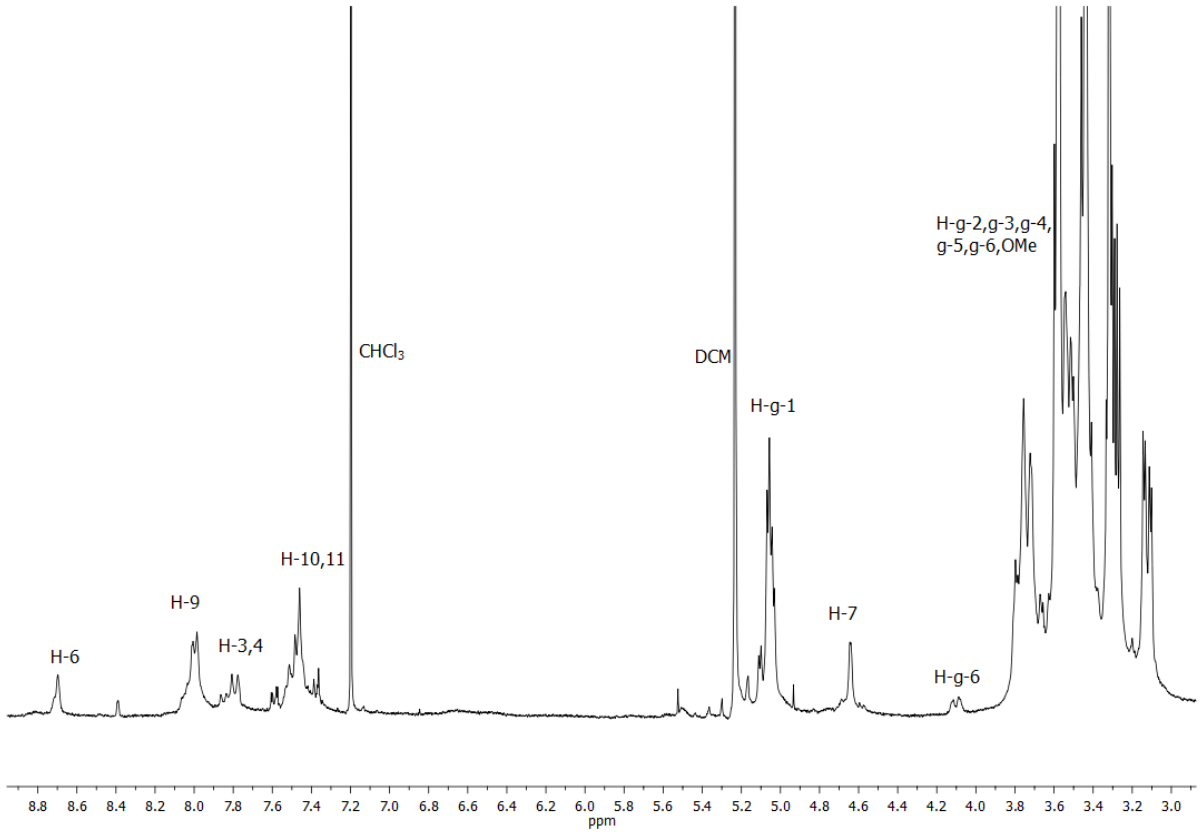


**Figure 4.22.** $^1H$ NMR spectrum of **$[Ir(ppy\text{-}CD)_2Cl]_2$ (15)** in $CDCl_3$.

**$Ir(ppy\text{-}CD)_2(bpySS)$ (17)** was characterised by $^1H$, $^{13}C$ and 2D NMR spectroscopy, and MALDI mass spectrometry. Figure 4.23 shows the $^1H$ NMR spectrum of the complex, revealing

the addition of the proton environments associated with **bpySS** in the regions 0.70-2.48 and 2.90-3.89 ppm, as well as the amide N*H* protons assigned at 6.89-6.99 ppm, concordant with the similar complex **IrbpySS**.[75] The integration of the peak at 4.90-5.13 ppm corresponding to H-g-1 (14H) correlates well with the integrals of the peaks for the amide region at 6.89-6.99 (2H), H-s6 at 7.78-7.84 ppm (2H), indicating successful formation of the complex. The presence of only one set of aromatic environments for the complex confirms that excluding optical isomers, one structure is formed during the synthesis of the dimer (Scheme 4.3). The peaks in the $^{13}$C NMR spectrum are reported and although they are unassigned, they agree fairly well with both $^{13}$C data for **bpySS** and **ppy-CD (13)**. The MALDI mass spectrum was obtained using norharmane as the matrix and reveals a single adduct at 4124 corresponding to $(M+H)^+$, confirming formation of the desired product.

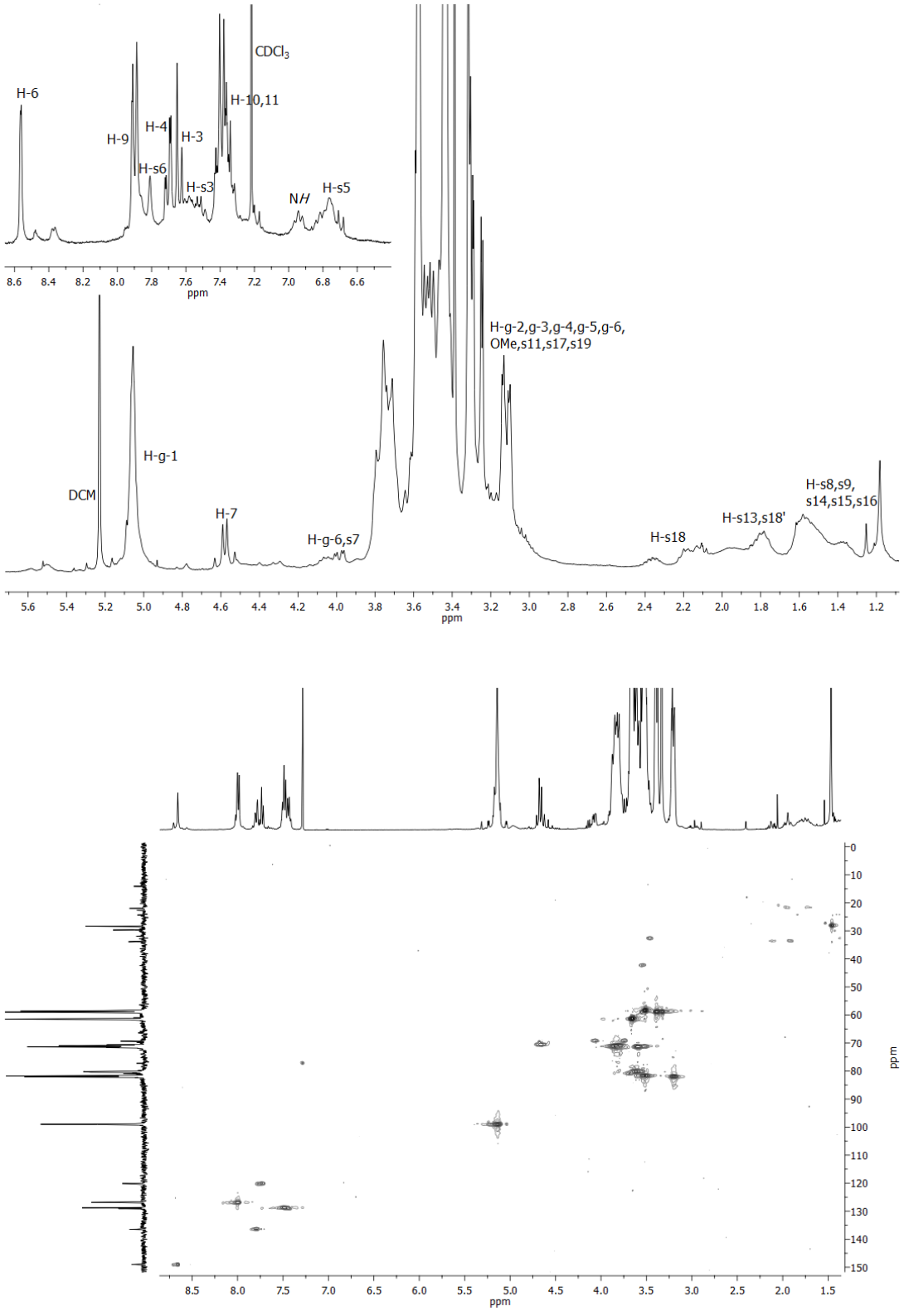


**Figure 4.23.** 300 MHz $^{1}$H (top) and 400 MHz HSQC (bottom) NMR spectra of **Ir(ppy-CD)$_2$(bpySS) (17)** in $CDCl_3$.

# 4.3 Physical Properties of Surface-Active Transition Metal Complexes Bearing Cyclodextrin Functionalised Ancillary Ligands

## 4.3.1 Photophysical Properties of Ru(bpy-CD)$_2$(bpySS) and Ir(ppy-CD)$_2$(bpySS) in Solution

The photophysical properties of the complexes are summarised in Table 4.1. The UV-vis absorption spectrum of **Ru(bpy-CD)$_2$(bpySS) (16)** in methanolic solution (Figure 4.24) reveals two main absorption bands, the first at 293 nm displaying a sharp transition, corresponding to the $^1\pi$-$\pi^*$ band. The second is a broad absorption band centred at 467 nm, corresponding to the $^1$MLCT transition.[76] The $^1$MLCT band displays a bathochromic shift compared with simpler ruthenium(II) complexes such as $[Ru(bpy)_3]^{2+}$ (14 nm), however the results are comparable to those of **RubpySS** in acetonitrile solutions, with bathochromic shifts of 4 and 6 nm for $^1\pi$-$\pi^*$ and $^1$MLCT transitions respectively.[75] The emission spectrum (Figure 4.24) displays a broad $^3$MLCT based emission band centred at 660 nm. This band again displays a large 49 nm red shift compared with $Ru(bpy)_3^{2+}$, and a smaller 15 nm red shift compared to **RubpySS**.[75] The bathochromic shift compared with **RubpySS** can be rationalised by the increased polarity of the solvent, stabilising the excited state of the complex. However, the quantum yield of **Ru(bpy-CD)$_2$(bpySS) (16)**; 0.3% and 0.8% in aerated and deaerated solutions respectively; is significantly lower than $[Ru(bpy)_3]$ type complexes and **RubpySS**.[75, 76] This decrease in luminescence quantum yield is postulated to be caused by the introduction of large and bulky cyclodextrin moieties which prevent optimal coordination to the ruthenium centre, an effect that has been observed previously with ruthenium(II) complexes bearing short chain

cyclodextrin functionalised bipyridine ligands.[77] The luminescence lifetimes of the complex in methanol were found to be monoexponential (Table 4.1), with an aerated lifetime of 180 ns and a deaerated lifetime of 548 ns.

**Table 4.1.** Summarised photophysical properties of **Ru(bpy-CD)$_2$(bpySS) (16)**, **Ir(ppy-CD)$_2$(bpySS) (17)** and comparable complexes in methanolic solutions.

| | | | τ / ns | | Φ / % | |
|---|---|---|---|---|---|---|
| Complex | $\lambda_{max}$ / nm (ε / $10^4$ $M^{-1}$ $cm^{-1}$) | $\lambda_{em}$ / nm | aerated | deaerated | aerated | deaerated |
| **Ru(bpy-CD)$_2$(bpySS) (16)** | 293 (5.3), 467 (0.8) | 660 | 180 | 548 | 0.3 | 0.8 |
| **Ir(ppy-CD)$_2$(bpySS) (17)** | 252 (37.7), 273 (31.8) sh, 412 (1.7) sh | 590 | 36 (47%)<br>142 (53%) | 242 (15%)<br>715 (85%) | 0.5 | 1 |
| **RubpySS** | 289 (7.8), 323 (1.3), 461 (1.5) | 645 | 130 | 707 | 1 | 4 |
| **IrbpySS** | 255 (5.0), 298 (1.8) sh, 337 (0.8) sh | 580 | 25 (68%)<br>80 (32%) | 35 (34%)<br>246 (66%) | 0.5 | 3 |
| $[Ru(bpy)_3]^{2+}$ | 453 (1.5)[78] | 609[78] | | 720[78] | | 4.5[78] |
| $[Ir(ppy)_2bpy]^{+}$ | 230 (7.0), 250 (6.5), sh, 310 (3.0) sh, 380 (0.45) sh[79] | 610[79] | | 350[79] | | |

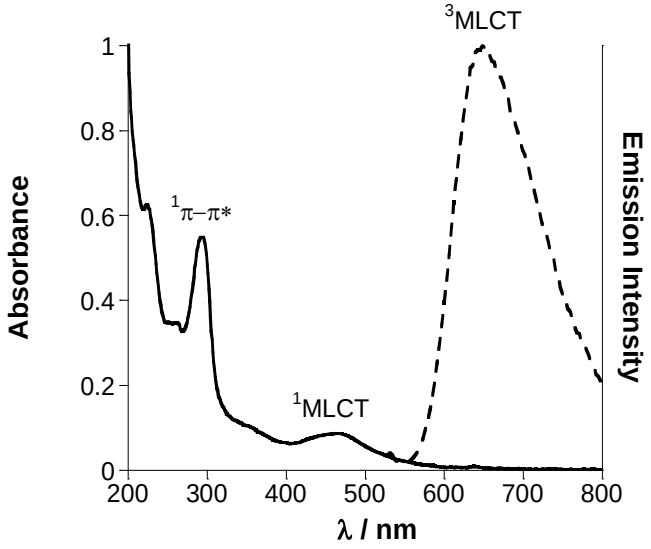


**Figure 4.24.** UV-vis absorption (solid) and steady state emission (dotted) spectra of **Ru(bpy-CD)$_2$(bpySS) (16)** (10 μM in MeOH). $\lambda_{exc}$ = 460 nm, emission spectrum corrected for spectral response.

The photophysical properties of **Ir(ppy-CD)$_2$(bpySS) (17)** in methanolic solutions are summarised in Table 4.1. The absorption spectrum (Figure 4.25) displays the characteristic mixed $^1\pi$-$\pi^*$ and $^1$MLCT states as described by Güdel *et al*. and evidenced previously by similar iridium(III) compounds.[75, 79-81] The complex displays broad emission centred at 590 nm, a red shift of 10 nm compared to **IrbpySS** in acetonitrile. Again, this shift could be rationalised by the increased polarity of the solvent, stabilising the excited state. The luminescence quantum yield of **Ir(ppy-CD)$_2$(bpySS) (17)** is comparable to that of **IrbpySS** in aerated solvent, however where we see a six-fold increase in quantum yield in **IrbpySS** (0.5% to 3%), in **Ir(ppy-CD)$_2$(bpySS)** this increase is much smaller (0.5% to 1%). This is rationalised by the sterically large cyclodextrin groups that partially prevent $^3O_2$ diffusing to the metal centre and quenching the excited state.[77, 82] The lifetimes of **Ir(ppy-CD)$_2$(bpySS)** (Table 4.1) are found to be relatively long compared to similar iridium(III) complexes.

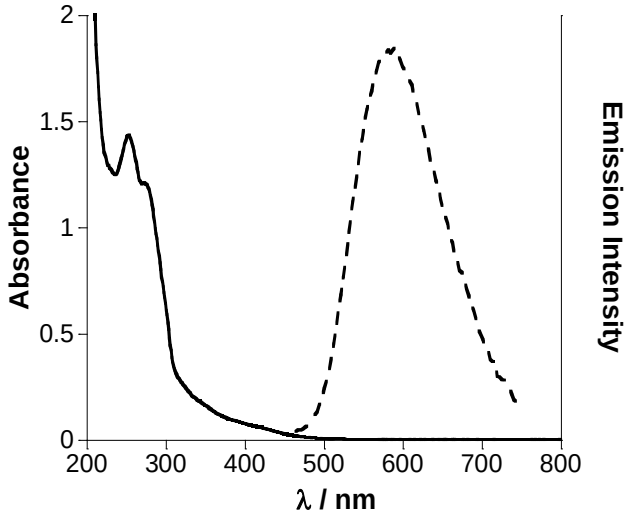


**Figure 4.25.** UV-vis absorption (solid) and steady state emission (dotted) spectra of **Ir(ppy-CD)$_2$(bpySS) (17)** (3.8 μM in MeOH). $\lambda_{exc}$ = 360 nm, emission spectrum corrected for spectral response.

### 4.3.2 Properties of Surface Bound Complexes Ru(bpy-CD)$_2$(bpySS) and Ir(ppy-CD)$_2$(bpySS)

In order to examine the properties of monolayers of **Ru(bpy-CD)$_2$(bpySS) (16)** and **Ir(ppy-CD)$_2$(bpySS) (17)**, surfaces were immersed in solutions of the two complexes. The surfaces were then characterised by ellipsometry, SPR spectroscopy, steady state and time resolved luminescence spectroscopy. The kinetic ellipsometric data (Figure 4.26) allows insight into the formation of monolayers of the complexes on gold, and reveals a large increase in layer thicknesses of both complexes over the first 20 minutes until plateau, with full coverage achieved within 30 minutes. The layer thicknesses calculated for both complexes at 30 minutes, 3.5±0.4 and 3.2±0.2 nm for **Ru(bpy-CD)$_2$(bpySS)·Au** and **Ir(ppy-CD)$_2$(bpySS)·Au** respectively, corresponds well with the modelled thickness of the monolayer (Chem3D), which

we expect to be *ca.* 3 nm. The small discrepancies between calculated and observed values is most likely due to the large cyclodextrin moieties which could have significant freedom of movement in order to find the most energetically stable orientation on the gold surface, influencing the layer thickness quite greatly. The layer thicknesses for the complexes on gold are significantly higher than similar monolayers such as **RubpySS·Au** (1.8 nm) and **IrbpySS·Au** (1.7 nm), which is expected due to the addition of ligands containing large cyclodextrin moieties.

To further examine whether monolayers are formed by the complexes, SPR spectroscopy experiments were also carried out. Plain gold chips were equilibrated in acetonitrile in the instrument before injection with a 0.1 mM solution of each complex in acetonitrile over a period of 30 minutes. The chips were then washed at a higher flow rate (1.5 mL $min^{-1}$) before stabilising the final readings at 50 µL $min^{-1}$. The results show the change in resonance angle of the instrument, which is related to the change in refractive index of the system. This change in refractive index is related to refractive index increment (dn/dc), which in turn is determined by the amount of material adsorbed. The sensorgram (Figure 4.27) reveals a large increase in response upon injection of the two complexes, rising up to *ca.* 0.1 º for **Ru(bpy-CD)$_2$(bpySS)·Au** and *ca.* 0.25 º for **Ir(ppy-CD)$_2$(bpySS)·Au** over a period of a few minutes after injection, before stabilising and increasing mildly until washing, when non-specifically bound complex is washed away. Subsequent to washing we observe readings of 0.12 º and 0.27 º for **Ru(bpy-CD)$_2$(bpySS)·Au** and **Ir(ppy-CD)$_2$(bpySS)·Au** respectively, compared with 0.03 º for a blank run with acetonitrile. As the refractive index increments for the complexes were not measured in this study, we are unable to make estimates of the surface concentrations for each complex. Comparisons between the measured resonance angles of the above complexes and also similar monolayer systems such as **RubpySS·Au** and **IrbpySS·Au** also

cannot be made as the complexes may have different refractive index increments. However, we can conclude from these results that material is bound to the surfaces of each system after washing with acetonitrile, indicating monolayer formation.

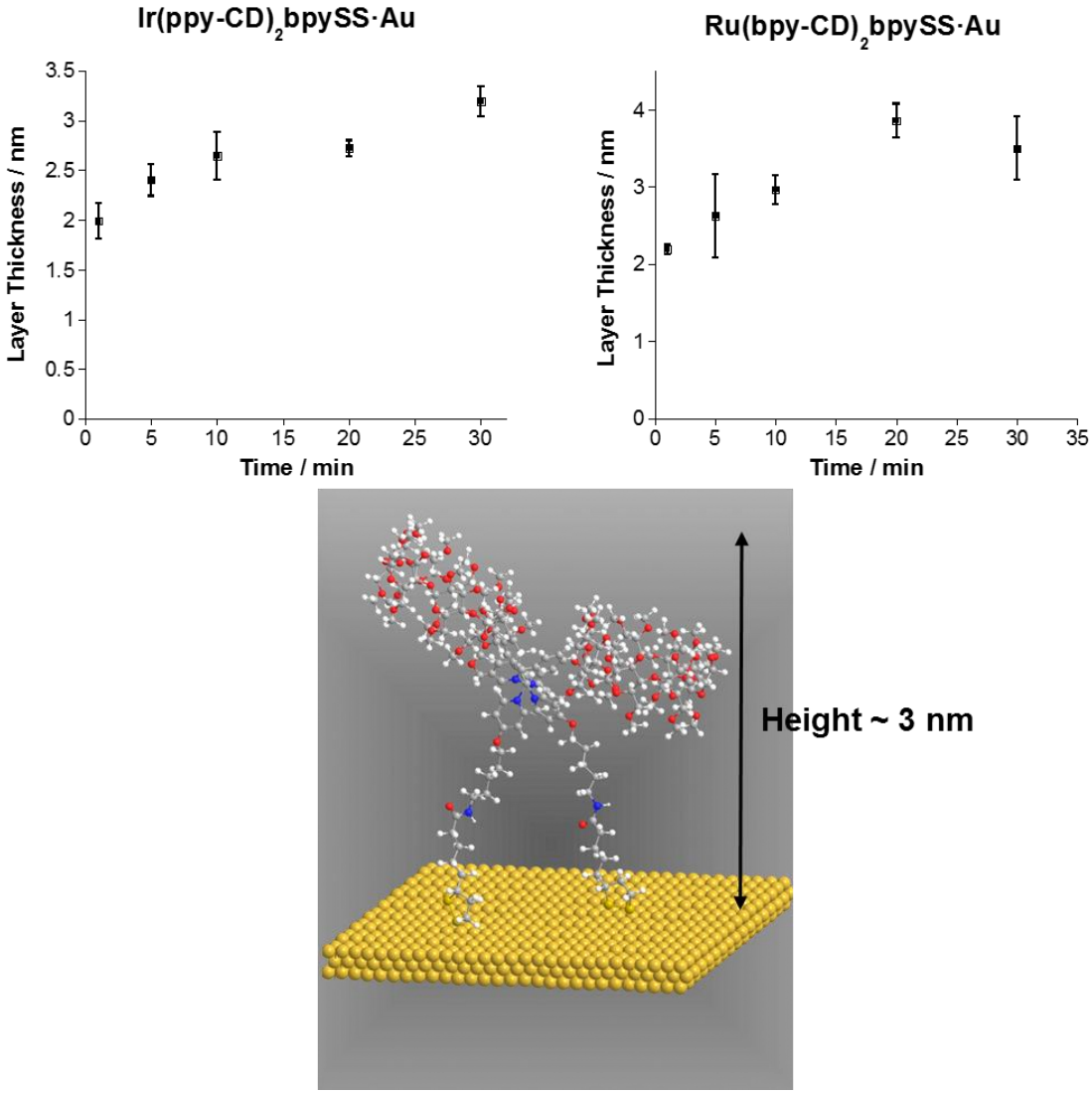


**Figure 4.26.** Kinetic ellipsometric data for complexes (top) and schematic model of cyclodextrin functionalised complexes attached to a gold surface (bottom).

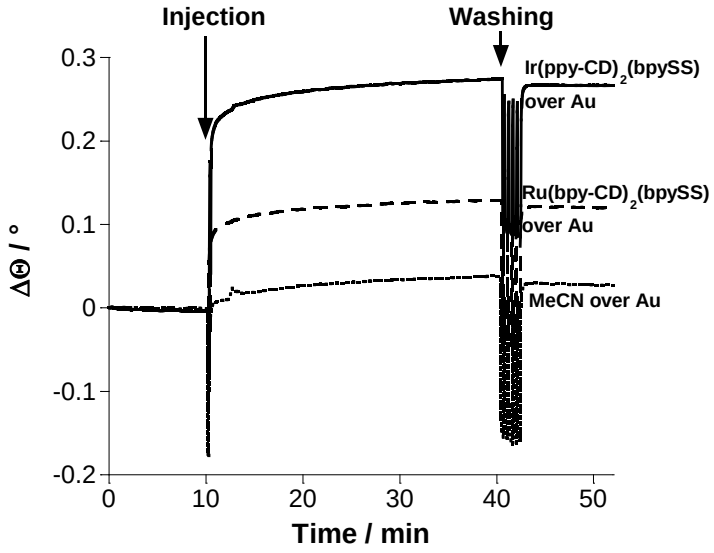


**Figure 4.27.** SPR sensorgram of adsorption of **Ir(ppy-CD)$_2$(bpySS)·Au** (solid), **Ru(bpy-CD)$_2$(bpySS)·Au** (dash) and MeCN (dotted) over gold.

The luminescence results, summarised in table 4.2, depict contrasting results for the two complexes. For **Ru(bpy-CD)$_2$(bpySS)·Au**, surface immobilisation results in a bathochromic shift of 10 nm compared to that of a methanolic solution, and a large decrease in luminescence intensity. Indeed, the luminescence from the complex on the surface was so weak that a lifetime was not obtained for this system. **Ir(ppy-CD)$_2$(bpySS)·Au** exhibits markedly different properties, with a hypsochromic shift of 20 nm compared to methanolic solutions of the complex, and increases in the luminescence lifetime. The increase in luminescence lifetimes is particularly large, increasing from 36 (47%), 142 (53%) ns to 203 (15%), 1321 (85%) ns. This large increase in luminescence lifetime is concordant with similar observations for **IrbpySS**, which also exhibited an enhancement of the luminescence lifetime when adsorbed to gold surfaces.[75]

**Table 4.2.** Summary of luminescence spectroscopy of **Ru(bpy-CD)$_2$(bpySS)** and **Ir(ppy-CD)$_2$(bpySS)** on gold and in aerated methanolic solution.

| Complex | $\lambda_{em}$ / nm | $\tau$ / ns |
|---|---|---|
| **Ru(bpy-CD)$_2$(bpySS)·Au** | 670 | |
| **Ru(bpy-CD)$_2$(bpySS) (16)** | 660 | 180 |
| **Ir(ppy-CD)$_2$(bpySS)·Au** | 570 | 203 (15%)<br>1321 (85%) |
| **Ir(ppy-CD)$_2$(bpySS) (17)** | 590 | 36 (47%)<br>142 (53%) |

# 4.4 Host-Guest Binding Studies of Surface-Active Cyclodextrin Containing Transition Metal Complexes

To test the potential of these monolayer systems as surface bound recognition units, **Ir(ppy-CD)$_2$(bpySS) (17)** monolayers were formed and immersed in solutions of two molecular building blocks, as outlined in Scheme 4.4. In pathway a), **Osbiptpy** is passed over the monolayers to create a surface that is both emissive in the yellow and far red regions of the visible spectrum. In pathway b), stepwise assembly is utilised to incorporate a recognition motif (**Ad-Biotin**) for streptavidin, a well characterised protein.

## 4.4.1 Recognition Studies of Ir(ppy-CD)$_2$(bpySS) (17) and Osbiptpy

To determine whether the complexes could be used for supramolecular chemistry at the interface, an osmium(II) complex **Osbiptpy** (Figure 4.28) (provided by Dr Jonathan Faiz) containing a biphenyl moiety was tested for host-guest interaction with **Ir(ppy-CD)$_2$(bpySS) (17)**. The biphenyl group has a well-known affinity for cyclodextrins,[63, 83] while the osmium(II) centre has a distinct emission band in the far red region of the visible spectrum, making it ideal as a test compound.

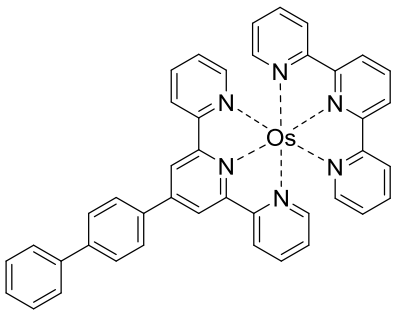


**Figure 4.28.** Structure of **Osbiptpy**.

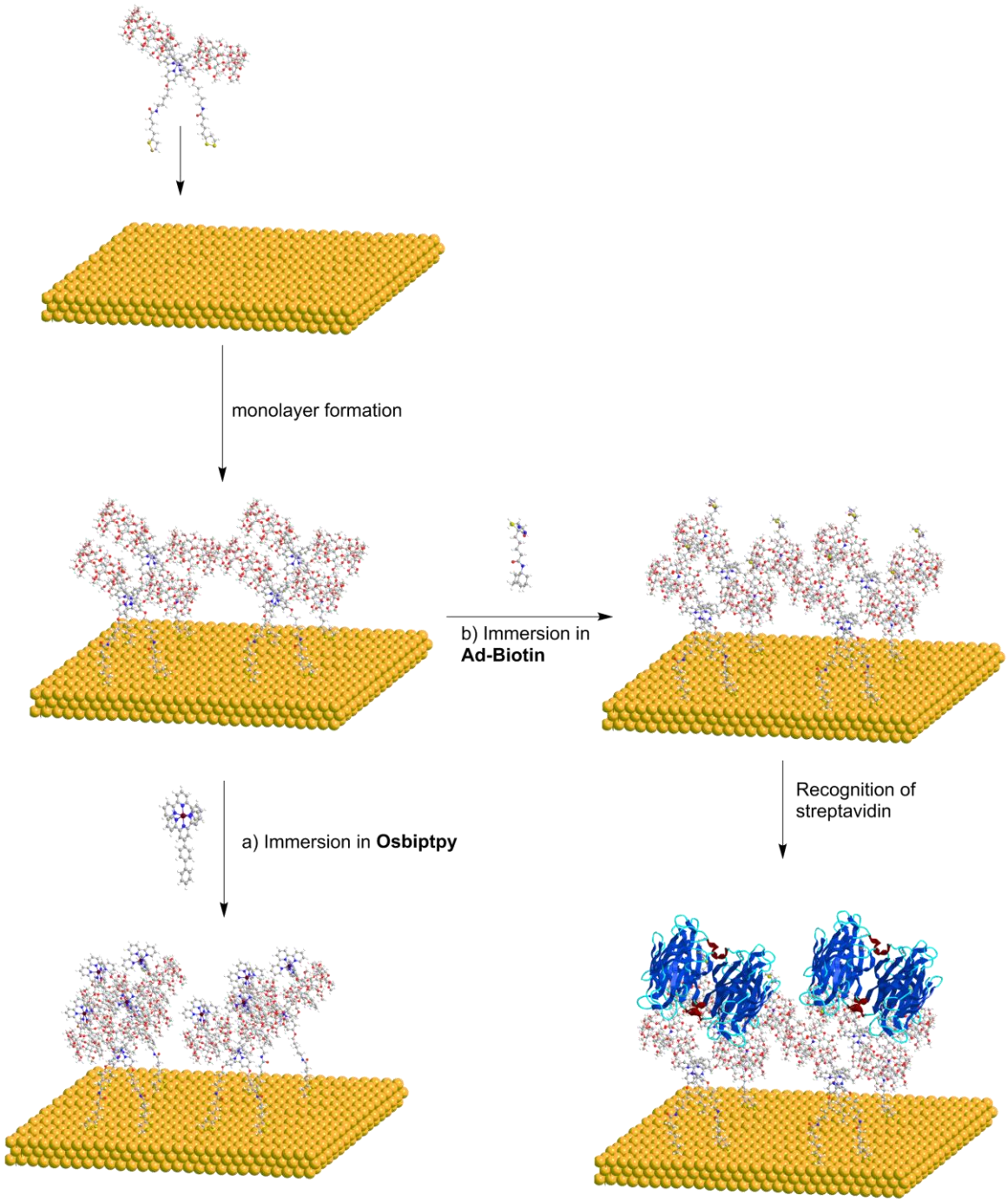


**Scheme 4.4.** Schematic diagram of stepwise assembly of components onto an **Ir(ppy-CD)$_2$(bpySS) (17)** SAM through supramolecular interactions and protein-ligand interactions.

The recognition of **Ir(ppy-CD)$_2$(bpySS) (17)** with **Osbiptpy** was studied in solution by steady state and time resolved luminescence spectroscopy, as well as on the surface by ellipsometry and steady state and time resolved luminescence spectroscopy, with the results summarised in table 4.3. The solution luminescence spectra (Figure 4.29) reveal two distinct bands centred at 575 and 750 nm, corresponding to **Ir(ppy-CD)$_2$(bpySS) (17)** and **Osbiptpy** respectively. Upon addition of a 4 fold excess of **Osbiptpy** to **Ir(ppy-CD)$_2$(bpySS) (17)**, it is shown that some communication between the two metal centres does occur, with the integration of the iridium peak falling by 10% and a shortening of the long component of the luminescence lifetime from 381 to 325 ns, a 15% decrease. However it is noted that there was no significant increase in either the integral of the osmium region of the spectrum, or the luminescence lifetime, which remains at *ca.* 110 ns. This result, albeit much weaker than previously observed results,[9, 84] indicates that binding does occur in the *bis*-β-cyclodextrin system.

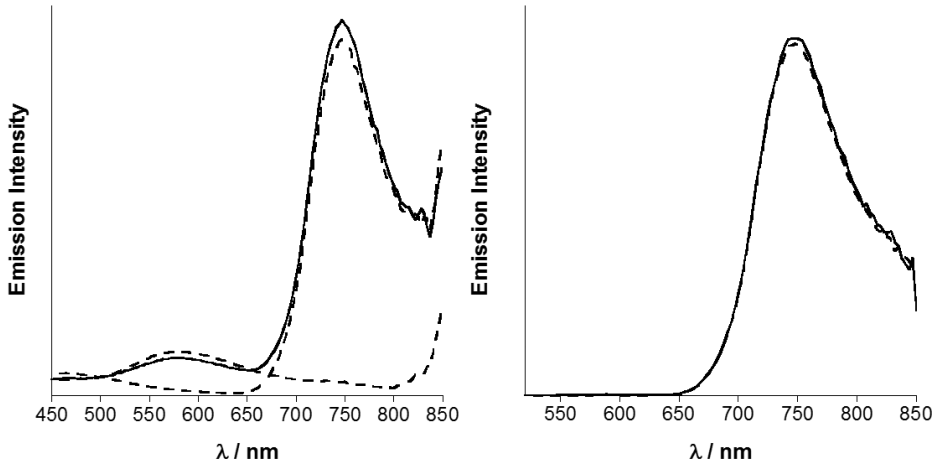


**Figure 4.29.** Top left - Steady state luminescence spectra of **Ir(ppy-CD)$_2$(bpySS) (17)** (3 μM, dotted), **Osbiptpy** (12 μM, dotted) and 4:1 (**Osbiptpy**:**Ir(ppy-CD)$_2$(bpySS)**, solid) mixed solution in 9% acetonitrile in water, $\lambda_{exc}$ = 360 nm. Top right – Steady state luminescence spectra of **Osbiptpy** (12 μM, solid) and 4:1 (**Osbiptpy**:**Ir(ppy-CD)$_2$(bpySS)**, dotted) mixed solution in 9% acetonitrile in water, $\lambda_{exc}$ = 490 nm. Spectra corrected for instrument response.

**Table 4.3.** Luminescence properties of **Ir(ppy-CD)$_2$(bpySS) (17)** and **Osbiptpy** in solution (9% acetonitrile in water) and on gold substrates. Iridium region – 450-660 nm, $\lambda_{em}$ = 580 nm; osmium region – 660-850 nm, $\lambda_{em}$ = (a) 750, (b) 700 nm. $\tau$ $\lambda_{exc}$ = 376 nm.

| Complex | Emission Integral | | τ / ns | |
|---|---|---|---|---|
| | Ir region | Os region | Ir region | Os region |
| **Ir(ppy-CD)$_2$(bpySS)** | 1 | | 81 (49%)<br>381 (51%) | |
| **Osbiptpy** | | 1 | | 114[a] |
| **Ir(ppy-CD)$_2$(bpySS):Osbiptpy** | 0.9 | 1.05 | 74 (51%)<br>325 (49%) | 113[a] |
| **Ir(ppy-CD)$_2$(bpySS)·Au** | | | 203 (15%)<br>1321 (85%) | |
| **Ir(ppy-CD)$_2$(bpySS):Osbiptpy·Au** | | | 249 (16%)<br>1381 (84%) | 267 (15%)<br>1382 (85%)[b] |

In order to confirm that **Osbiptpy** did indeed bind into the cavities of **Ir(ppy-CD)$_2$(bpySS)** on gold as outlined in Scheme 4.4a, ellipsometric and luminescence experiments were carried out. Substrates of **Ir(ppy-CD)$_2$(bpySS)·Au** were immersed in solutions of **Osbiptpy** in acetonitrile for 30 minutes, before washing with acetonitrile. The ellipsometric data (Figure 4.30) appears to show an increase in layer thickness from 2.7±0.6 nm to 3.1±0.6 nm, however as the results are within error we cannot conclude that binding has occurred. Binding is however indicated in the luminescence results, as an emission peak (Figure 4.31) at 750 nm is observed upon washing the substrates with acetonitrile, revealing that **Osbiptpy** is still present. Given the coverage of the gold surface with **Ir(ppy-CD)$_2$(bpySS)**, and the lack of an available surface binding moiety on **Osbiptpy**, this result suggests that **Osbiptpy** has bound within the cyclodextrin. The

luminescence lifetimes are also of particular interest, with results of 267 (15%) and 1382 (85%) ns, much longer than the solution lifetime of **Osbiptpy**, and also of other similar compounds in solution.[85]

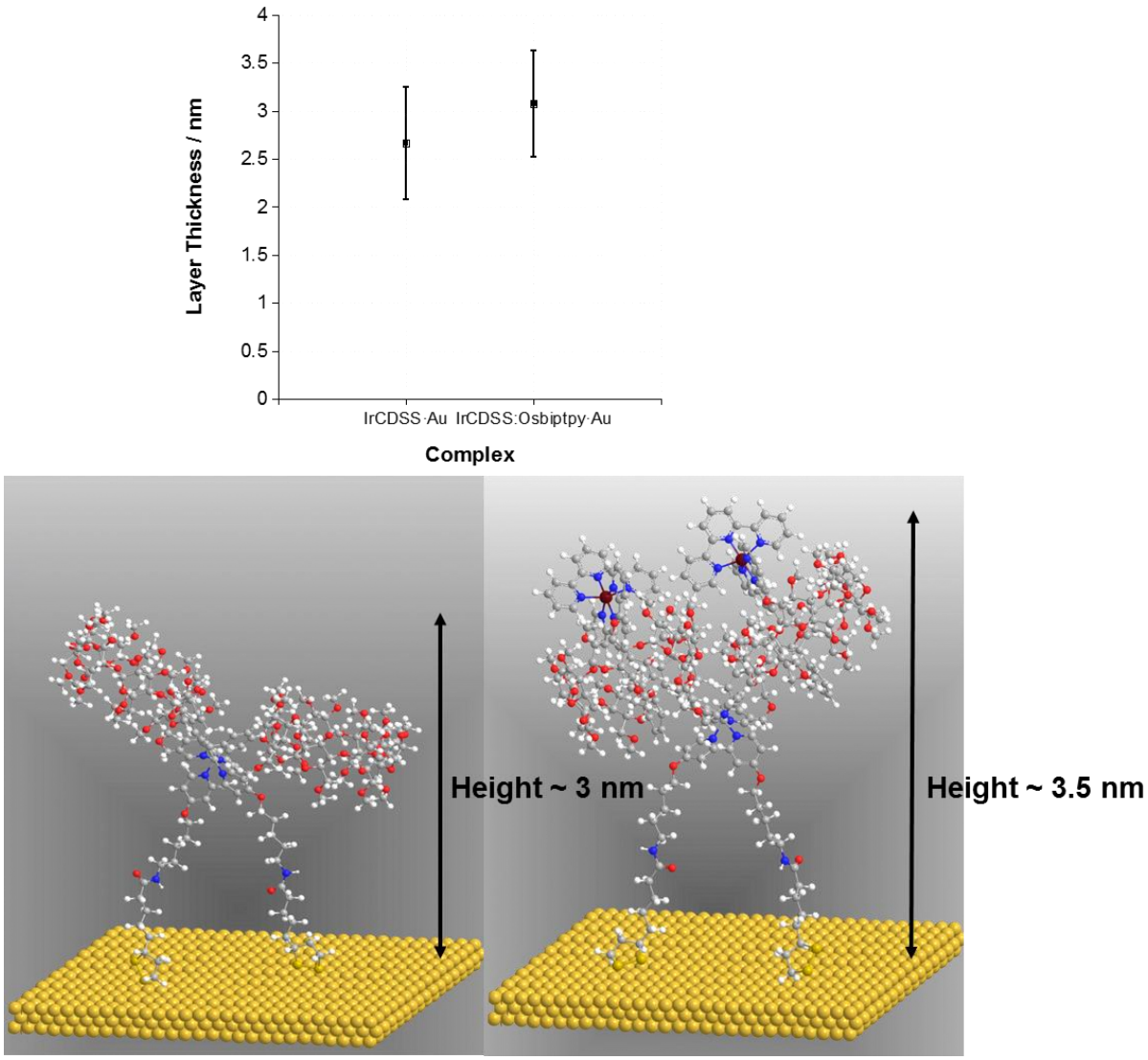


**Figure 4.30.** Plot of ellipsometric data from binding studies (top) and schematic models of **Ir(ppy-CD)$_2$(bpySS)** (bottom left) and **Ir(ppy-CD)$_2$(bpySS):Osbiptpy** (bottom right). **Ir(ppy-CD)$_2$(bpySS)** is abbreviated to **IrCDSS** on the plot for clarity.

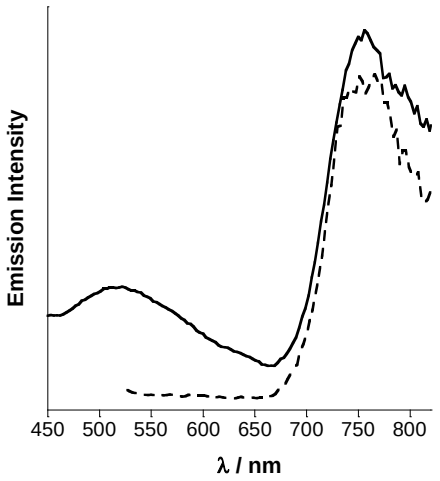


**Figure 4.31.** Emission Spectra of **Ir(ppy-CD)$_2$(bpySS):Osbiptpy·Au**. Solid - $\lambda_{exc}$ = 320 nm, dash - $\lambda_{exc}$ = 490 nm. Spectrum corrected for instrument response.

## 4.4.2 Preparation of Ad-Biotin for Recognition Studies with Ir(ppy-CD)$_2$(bpySS) (17) and Streptavidin

Utilising the cyclodextrin moieties in **Ir(ppy-CD)$_2$(bpySS) (17)**, we wished to design a sensing platform using a scaffold with multiple building blocks. Initially, **Ir(ppy-CD)$_2$(bpySS) (17)** would be immobilised on gold substrates, followed by attaching a sensing moiety through host-guest chemistry, and finally using this scaffold as a sensing motif. To this end, we designed a simple system for sensing streptavidin with a sensing moiety than contained an adamantyl group for binding in the cyclodextrin cavity, and a biotinyl group for sensing the streptavidin.

Scheme 4.5 illustrates the facile route to the preparation of **Ad-Biotin (18)**. Briefly, an amide coupling between biotin and 1-adamantylamine yielded **Ad-Biotin (18)** in a *ca.* 40% yield. **Ad-Biotin (18)** was characterised by $^{1}$H, $^{13}$C and 2D NMR spectroscopy, and ESI(+) mass spectrometry. NMR assignments were confirmed by COSY, HSQC and HMBC experiments.

The $^{1}$H NMR spectrum (Figure 4.32) indicates that the reaction is successful, with 13 resolvable peaks corresponding to the 14 environments around the compound. The spectrum agrees well with previously reported NMR data for biotin,[86] with the loss of the OH proton of biotin at *ca.* 12 ppm (appendix). A total integration of 3 amino protons is also observed, indicating the loss of one of the protons from 1-adamantylamine and product formation. The ESI(+) mass spectrum reveals two ion envelopes at 378 and 400 Da corresponding to $(M+H)^{+}$ and $(M+Na)^{+}$ respectively, confirming the formation of the product.

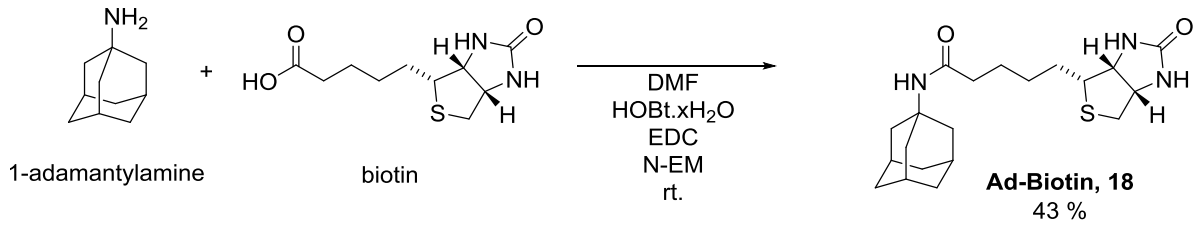


**Scheme 4.5.** Synthetic route to **Ad-Biotin (18).**

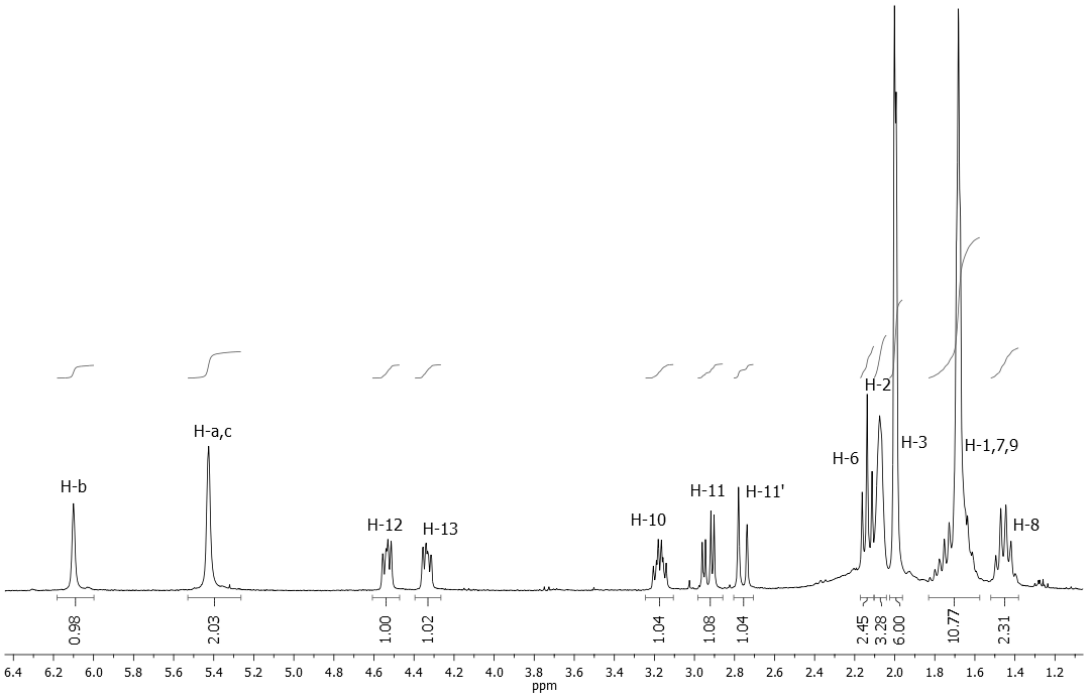


**Figure 4.32.** $^{1}$H NMR spectrum of **Ad-Biotin (18)** in $CDCl_3$.

### 4.4.3 Recognition Studies of Ir(ppy-CD)$_2$(bpySS) (17) with Ad-Biotin (18) and Streptavidin

To study the interaction between each of the components and the sensing system as a whole, we carried out experiments in solution, using steady state and time resolved luminescence spectroscopy, and on gold substrates by ellipsometry, SPR spectroscopy and steady state and time resolved luminescence spectroscopy. The luminescence data, summarised in table 4.4, shows that upon mixing **Ad-Biotin (18)** and **Ir(ppy-CD)$_2$(bpySS) (17)** in a 2:1 mixture in 3% acetonitrile in water, the solution luminescence spectra (Figure 4.33) reveal a 20% decrease in luminescence intensity. This decrease is coupled with an insignificant change in luminescence lifetime. Interestingly, the energy of the state remains unchanged, as both emission maxima are centred at *ca.* 585 nm. The emission maximum does however change upon binding to streptavidin, with a blue shift from 585 to 570 nm when a 2 nM concentration of streptavidin is introduced, coupled with a 13% increase in emission intensity from **Ir(ppy-CD)$_2$(bpySS):Ad-Biotin** to **Ir(ppy-CD)$_2$(bpySS):Ad-Biotin:streptavidin** and a significant increase in two of the components of the luminescence lifetime. Each of the longer components are increased from 180 (36%) to 274 (41%) ns and 693 (37%) to 919 (37%) ns respectively. These factors indicate that binding indeed occurs upon the formation of the sensing system. We postulate that the iridium complex is shielded from solvatochromic effects by the inclusion of streptavidin, due to the short linker between the adamantyl and biotinyl moieties in the sensing motif. This effect is also coupled with a shielding from $^3O_2$ in the solution which rationalises the observed increased in luminescence lifetime and emission increase.

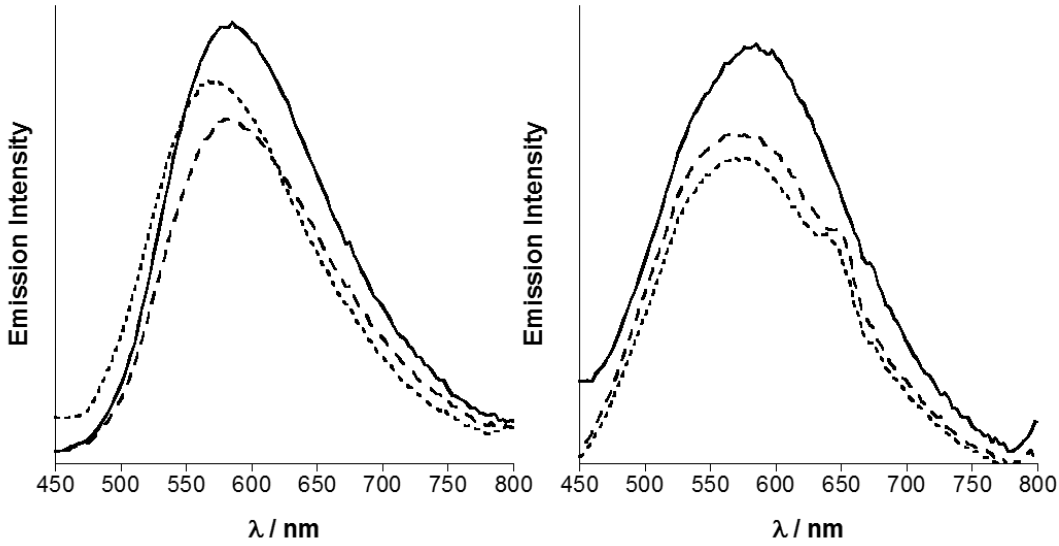


**Figure 4.33.** Left - Steady state luminescence spectra of **Ir(ppy-CD)$_2$(bpySS) (17)** (3 μM) (solid); **Ir(ppy-CD)$_2$(bpySS) (17)** (3μM) and **Ad-Biotin (18)** (6 μM) (dash); and **Ir(ppy-CD)$_2$(bpySS)** (3μM), **Ad-Biotin (18)** (6 μM) and streptavidin (2 nM) (dotted) in solutions of 3% acetonitrile in water. $\lambda_{exc}$ = 360 nm. Right – Steady state luminescence spectra of **Ir(ppy-CD)$_2$(bpySS)·Au** (solid); **Ir(ppy-CD)$_2$(bpySS):Ad-Biotin·Au** (dash); and **Ir(ppy-CD)$_2$(bpySS):Ad-Biotin:streptavidin** (dotted). $\lambda_{exc}$ = 320 nm. Spectra corrected for instrument response.

**Table 4.4.** Luminescence properties of **Ir(ppy-CD)$_2$(bpySS) (17)**, **Ad-Biotin (18)** and streptavidin in 3% acetonitrile in water solution and on gold substrates.

| Complex | $\lambda_{max}$ / nm | emission integral | τ / ns |
|---|---|---|---|
| **Ir(ppy-CD)$_2$(bpySS) (17)** | 585 | 1 | 58 (27%)<br>163 (36%)<br>687 (37%) |
| **Ir(ppy-CD)$_2$(bpySS):Ad-biotin** | 585 | 0.8 | 59 (27%)<br>180 (36%)<br>693 (37%) |
| **Ir(ppy-CD)$_2$(bpySS):Ad-biotin:streptavidin** | 570 | 0.9 | 69 (22%)<br>274 (41%)<br>919 (37%) |
| **Ir(ppy-CD)$_2$(bpySS)·Au** | 585 | | 203 (15%)<br>1321 (85%) |
| **Ir(ppy-CD)$_2$(bpySS):Ad-biotin·Au** | 575 | | 177 (12%)<br>1158 (88%) |
| **Ir(ppy-CD)$_2$(bpySS):Ad-biotin:streptavidin·Au** | 570 | | 349 (22%)<br>1974 (78%) |

To determine whether the same interaction of streptavidin by **Ir(ppy-CD)$_2$(bpySS)** is observed on the surface as outlined in Scheme 4.4b, preformed **Ir(ppy-CD)$_2$(bpySS)·Au** substrates were immersed in **Ad-Biotin** (1 mM in acetonitrile) and streptavidin (0.1 mg mL$^{-1}$ water) solutions. Luminescence spectroscopy studies of each of the systems studied reveal similar properties to those in solution. Upon immersion of **Ir(ppy-CD)$_2$(bpySS)·Au** in **Ad-Biotin** solution we observe a blue shift from 585 to 575 nm, which could be due to rearrangement of the complex on the surface to allow binding to occur, causing a destabilisation of the excited state. It is also observed that the luminescence lifetime of the iridium(III) centre remains unchanged upon binding **Ad-Biotin**, as observed with the solution data. Just as with the solution data, we see a blue shift (5 nm) upon the addition of streptavidin and a significant increase in luminescence

lifetime, from 177 (12%), 1158 (88%) ns to 349 (22%), 1974 (78%), agreeing with solution results and indicating that binding does indeed occur on gold substrates.

To further examine the properties of binding, ellipsometric data was gathered on the stepwise addition of components to the system, and the results are shown in Figure 4.34. The graph reveals that upon immersion of monolayer samples of **Ir(ppy-CD)$_2$(bpySS)·Au** in **Ad-Biotin (18)**, an increase in layer thickness is observed, with the layer thickness itself increasing from 2.7±0.6 to 3.2±0.1 nm. This increase agrees fairly well with the modelled inclusion complex (Figure 4.34) and further suggests that binding is successful. The addition of streptavidin however yields only a 0.4 nm increase in layer thickness, which is less than expected, with the diameter of streptavidin being *ca.* 4 nm.[87] This result could however be a consequence of the expected low coverage of the complex on the surface. This in turn would lead to a fairly low coverage of streptavidin on the surface and lead to a less than expected increase in layer thickness. Surface plasmon resonance experiments (Figure 4.35) give credence to this observation, as we observe an increase in resonance angle over a ten minute injection period to *ca.* 0.1º, and upon washing with water for 5 minutes we observe a resonance angle of 0.08º. As all proteins have similar refractive index increments, we can estimate the surface coverage of streptavidin to be ~ 1.5 pmol cm$^{-2}$ (appendix).[4, 88, 89] Indeed, comparisons with another recognition study utilising organic scaffolds to recognise streptavidin reveal that the present system yields a lower surface coverage.[90] The sensorgrams show an insignificant increase in response when 10% acetonitrile in water or a 0.1 mM solution of **Ad-Biotin (18)** in the same solvent is passed over the chips. The absence of a significant increase in response from **Ad-Biotin (18)** is likely due to its small size (377 Da), which results in an insignificant change in refractive index when it binds in the cyclodextrin cavity. We also observe a decrease in response

upon injection of the **Ad-Biotin (18)** solution due to small discrepancies in the measurement of the solvent mixtures, causing a change in refractive index when introduced into the instrument.

In order to determine the efficacy of recognition of the three component system and to examine whether the binding was specific, streptavidin and a control protein (bovine serum albumin, BSA) were passed over the **Ir(ppy-CD)$_2$(bpySS):Ad-Biotin·Au** substrates. Substrates were equilibrated at a constant flow rate of 50 µL min$^{-1}$, before injection of solutions at the same flow rate for 10 minutes. The substrates were then washed in solvent for 20 minutes at 50 µL min$^{-1}$. Figure 4.35 shows that after injection of streptavidin over the substrates, a significant increase in response is detected, which after 20 minutes of washing yields a response of 0.081º. When BSA is passed over **Ir(ppy-CD)$_2$(bpySS):Ad-Biotin·Au** a response of 0.036º is observed. Despite the smaller values of ΔΘ being observed for these systems compared with **IrbpySS·Au** or **RubpySS·Au**, we do observe a much greater degree of specificity, with over a 2 fold increase in binding with streptavidin compared with BSA on **Ir(ppy-CD)$_2$(bpySS):Ad-Biotin·Au**, as opposed to a 1.1 fold increase in binding with BSA compared with streptavidin on **IrbpySS·Au**. Binding of streptavidin is also observed when **Ad-Biotin** is not present on the surface, with a response of 0.055º after 20 minutes of washing. This result indicates that **Ad-Biotin** is important in allowing streptavidin to bind to the surface, with a *ca.* 50% enchancement in binding when **Ad-Biotin** is present. When a water control is passed over **Ir(ppy-CD)$_2$(bpySS):Ad-Biotin·Au** substrates, the response is negligible as expected.

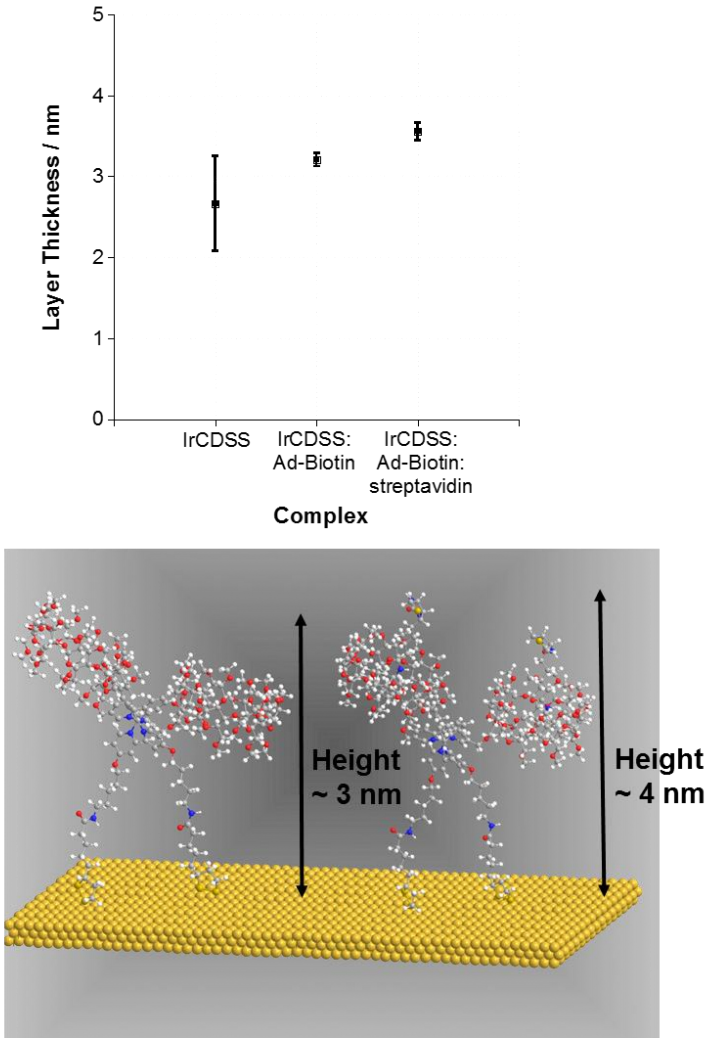


**Figure 4.34.** Top – Ellipsometric graph of stepwise addition **Ad-Biotin (18)** and streptavidin to **Ir(ppy-CD)$_2$(bpySS)·Au**. Bottom – Schematic models of **Ir(ppy-CD)$_2$(bpySS)·Au** (left) and **Ir(ppy-CD)$_2$(bpySS):Ad-Biotin·Au** (right). **Ir(ppy-CD)$_2$(bpySS)** is abbreviated to **IrCDSS** for clarity.

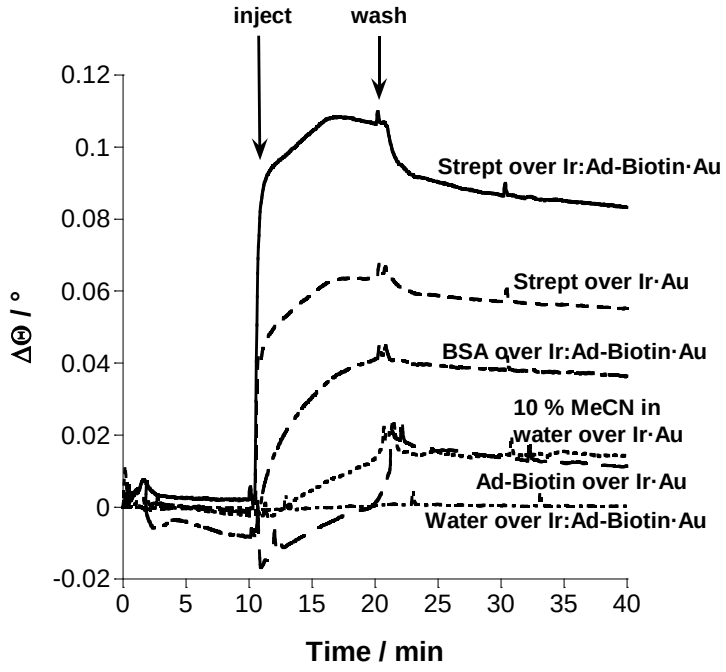


**Figure 4.35.** Left SPR sensorgram of recognition of molecules on **Ir(ppy-CD)$_2$(bpySS)·Au** substrates. **Ir(ppy-CD)$_2$(bpySS)** is abbreviated to **Ir** for clarity.

# 4.5 Conclusions

The synthesis of novel cyclodextrin bidentate ligands and *bis*-heteroleptic surface-active complexes is reported and the properties of the complexes in solution and on gold surfaces are elaborated. The complexes show acceptable luminescence properties in solution and **Ir(ppy-CD)$_2$(bpySS) (17)** displays good luminescence properties on planar substrates. Indeed, **Ir(ppy-CD)$_2$(bpySS) (17)** displays an enhancement of luminescence on gold substrates that has been observed previously for **IrbpySS**.[75] Surfaces of both **Ir(ppy-CD)$_2$(bpySS)·Au** and **Ru(bpy-CD)$_2$(bpySS)·Au** form monolayers within 30 minutes as shown by ellipsometric and surface plasmon resonance spectroscopy experiments. The design of the complexes allows host-guest chemistry to be performed at the surface, and this has been shown using a biphenyl functionalised complex **Osbiptpy**, allowing a more complex sensing architecture to be constructed. This was achieved by using facile chemistry to synthesise **Ad-Biotin (18)**, which contains both a moiety for host-guest chemistry with β-cyclodextrin, and a biotin label for the recognition of streptavidin. The sensing architecture was successfully assembled as evidenced by surface plasmon resonance spectroscopy and luminescence spectroscopy. The specificity for streptavidin against bovine serum albumin is also shown, with the sensing architecture giving a 2 fold higher response for streptavidin than BSA. These results indicate not only that multimodal detection of analytes is possible through the use of surface plasmon resonance spectroscopy and time resolved luminescence spectroscopy, but also that these types of systems show promise in the production of multiple sensing architectures based on modifying the sensing group toward the production of a ‘one size fits all’ lab-on-chip type detector. This coupled with the potential for breaking the supramolecular bond between the cyclodextrin and the adamantyl moiety allows scope for the investigation of reusable and interchangeable sensing architectures based on this design, whereby multiple adamantyl containing sensing components

can be reversibly bound in turn to the sensor surface to allow a fast, cheap and reliable method of multiple analyte detection.

# 4.6 Experimental

## 2-(trimethylstannyl)pyridine (2)

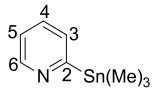


**2-(trimethylstannyl)pyridine (2)** was prepared in analogous fashion to Schwab *et al.*[67] 2-bromopyridine (**1**, 8.5 g, 53.8 mmol) was charged into a flask, before twice evacuating and refilling with dry nitrogen. Dry diethyl ether (100 mL) was added via syringe, and the solution was cooled to -78 °C. n-Butyllithium (2.0 M in cyclohexane, 29 mL, 58 mmol) was added dropwise by syringe over five minutes whilst maintaining the solution at -78 °C. The resulting dark red solution was stirred at -78 °C for 2 hours, at which point trimethyltin chloride (1.0 M in THF, 58 mL, 58 mmol) was added dropwise by syringe over five minutes whilst maintaining the solution at -78 °C. The resulting dark green mixture was stirred at -78 °C for 3 hours, before being allowed to warm to room temperature gradually under stirring overnight. The resulting orange solution was subsequently concentrated *in situ in vacuo* using short path distillation, and dry hexane (100 mL) was added by syringe. The resulting orange mixture was stirred under nitrogen for 10 minutes, before insoluble by-products were filtered off under nitrogen and the filtrate concentrated *in vacuo* to yield a red oil **2-(trimethylstannyl)pyridine** (11.45 g, 47.3 mmol, 88%) which was used in the next step without further purification. $\delta_H$ (300 MHz; $CDCl_3$) 0.31 (9H, s, Sn(*Me*)$_3$), 7.10 (1H, ddd, J= 1.8, 4.9, 7.5, H-5), 7.41 (1H, ddd, J= 1.0, 1.8, 7.5, H-3), 7.48 (1H, ddd, J= 1.8, 7.5, 7.5, H-4), 8.71 (1H, ddd, J= 1.0, 1.8, 4.9, H-6). Data agrees with published results.[67]

## 5-bromo-2,2′-bipyridine (3)

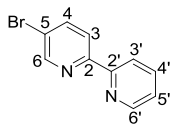


**5-bromo-2,2′-bipyridine (3)** was prepared by a modification to a method outlined by Schwab *et al.*[67] 2,5-bromopyridine (12.30 g, 51.9 mmol) was charged into a flask, before twice evacuating and refilling with dry nitrogen. 2-(trimethylstannyl)pyridine (**2**, 11.45 g, 47.3 mmol) in dry *m*-xylene (100 mL) was transferred by syringe into the reaction vessel under nitrogen, and the mixture was degassed under nitrogen whilst stirring for 1 hour. At this time, $Pd(PPh_3)_4$ (0.54 g, 0.5 mmol, 1 mol%) was added, and the mixture was heated to 120 °C overnight. The mixture was then cooled, poured into aqueous sodium hydroxide solution (2 M, 100 mL) and separated. The aqueous phase was extracted with toluene (2 × 25 mL), and the combined organic extracts were dried ($Na_2SO_4$), filtered and the solvent removed *in vacuo* to yield 12.78 g of crude material. The crude product was purified twice by column chromatography on alumina, eluting first with 5:1 hexane:ethyl acetate, and then with 1% ethyl acetate in hexane to yield **5-bromo-2,2′-bipyridine (3)** as a pale yellow solid (2.58 g, 11.0 mmol, 23%). $\delta_H$ (300 MHz, $CDCl_3$) 7.26 (1H, ddd, J= 1.0, 4.9, 7.5, H-5′), 7.75 (1H, ddd, J= 1.8, 7.5, 7.5, H-4′), 7.87 (1H, dd, J= 2.2, 8.5, H-4), 8.25 (1H, d, J= 8.5, H-3), 8.30 (1H, ddd, J= 1.0, 1.8, 7.5, H-3′), 8.60 (1H, d, J= 4.9, H-6′), 8.65 (1H, d, J=2.2, H-6); $\delta_C$ (100 MHz, $CDCl_3$) 121.0 (C-3′), 121.2 (C-5), 122.4 (C-3), 124.0 (C-5′), 137.1 (C-4′), 139.5 (C-4), 149.2 (C-6′), 150.2 (C-6), 154.6 (C-2′), 155.1 (C-2); MS ($ESI^+$) m/z: 237 $(M+H)^+$. Data agrees with published results.[67]

## 2-(trimethylstannyl)-5-methylpyridine (6)

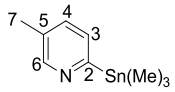


**2-(trimethylstannyl)-5-methylpyridine (6)** was synthesised by a modification to a method outlined by Schwab *et al.*[67] 2-bromo-5-methylpyridine (**5**, 6.60 g, 38.4 mmol) was charged into a flask, before twice evacuating and refilling with dry nitrogen. Dry diethyl ether (72 mL) was added by syringe, and the solution was cooled to -78 °C. n-Butyllithium (2.0 M in cyclohexane, 21 mL, 42.0 mmol) was added dropwise by syringe over five minutes whilst maintaining the temperature at -78 °C. The resulting burgundy solution was stirred at -78 °C for 2 hours, upon which trimethyltin chloride (1.0 M in THF, 42 mL, 42.0 mmol) was added dropwise by syringe over five minutes whilst maintaining the temperature at -78 °C. The resulting yellow-brown mixture was stirred at -78 °C for 3 hours, before being allowed to warm gradually to room temperature under stirring overnight. The solvent was removed *in situ in vacuo* by short path distillation, and dry hexane (70 mL) was added by syringe. The resulting orange mixture was stirred under nitrogen for 10 minutes, before insoluble by-products were filtered off under nitrogen and the filtrate concentrated *in vacuo* to yield a red oil **2-(trimethylstannyl)-5-methylpyridine** (**6**, 8.97 g, 35.0 mmol, 92%) which was used in the next step without further purification. $\delta_H$ (300 MHz, $CDCl_3$) 0.29 (9H, s, Sn(*Me*)$_3$), 2.25 (3H, s, H-7), 7.30 (2H, d, J= 1.8, H-3,4), 8.54-8.59 (1H, m, H-6); $\delta_C$ (100 MHz, $CDCl_3$) 18.5 (C-7), 131.1 (C-3/4), 131.6 (C-5), 134.2 (C-3/4), 151.3 (C-6), 169.2 (C-2). Data agrees with published results.[69]

## 5-methyl-2,2′-bipyridine (7)

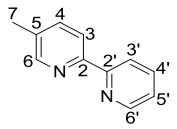


**5-methyl-2,2′-bipyridine (7)** was synthesised by a modification to a method outlined by Schwab *et al.*[67] 2-bromopyridine (6.00 g, 38.0 mmol) was charged into a flask, before twice evacuating and refilling with dry nitrogen. 2-(trimethylstannyl)-5-methylpyridine (**6**, 8.97 g, 35.0 mmol) in dry *m*-xylene (70 mL) was transferred by syringe into the reaction vessel under nitrogen, and the mixture was degassed under nitrogen whilst stirring for 1 hour. At this time, $Pd(PPh_3)_4$ (0.44 g, 0.4 mmol, 1 mol%) was added, and the mixture was heated to 120 °C overnight. The mixture was then cooled, poured into aqueous sodium hydroxide solution (2 M, 100 mL) and separated. The aqueous phase was extracted with toluene (2 × 25 mL), and the combined organic extracts were dried ($Na_2SO_4$), filtered and the solvent removed *in vacuo* to yield 6.10 g of crude material. The crude product was dried *in vacuo* at 50 °C for 2.5 hours before purification by column chromatography on alumina, eluting with 5:1 hexane:ethyl acetate to yield **5-methyl-2,2′-bipyridine (7)** as a brown oil (1.18 g, 6.9 mmol, 20%). $\delta_H$ (300 MHz, $CDCl_3$) 2.36 (3H, s, H-7), 7.25 (1H, dd, J= 4.5, 7.3, H-5′), 7.59 (1H, dd, J= 1.8, 8.0, H-4), 7.77 (1H, ddd, J= 1.7, 7.3, 7.9, H-4′), 8.25 (1H, d, J= 8.0, H-3), 8.32 (1H, d, J= 7.9, H-3′), 8.47 (1H, s, H-6), 8.63 (1H, d, J= 4.5, H-6′); $\delta_C$ (100 MHz, $CDCl_3$) 18.4 (C-7), 120.6 (C-3), 120.8 (C-3′), 123.4 (C-5′), 133.5 (C-5), 136.9 (C-4′), 137.5 (C-4), 149.1 (C-6′), 149.6 (C-6), 153.6 (C-2), 156.2 (C-2′); MS ($ESI^+$) m/z: 171 $(M+H)^+$. Data agrees with published results.[69]

## 2-phenyl-5-methylpyridine (8)

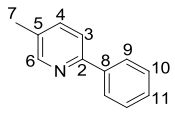


**2-phenyl-5-methylpyridine (8)** was synthesised by a modification to a method outlined by Schwab *et al.*[67] Bromobenzene (6.03 g, 38.4 mmol) was charged into a flask, before twice evacuating and refilling with dry nitrogen. 2-(trimethylstannyl)-5-methylpyridine (**6**, 7.49 g, 29.3 mmol) in dry *m*-xylene (70 mL) was transferred by syringe into the reaction vessel under nitrogen, and the mixture was degassed under nitrogen whilst stirring for 1 hour. At this time, $Pd(PPh_3)_4$ (0.46 g, 0.5 mmol, 1 mol%) was added, and the mixture was heated to 120 °C overnight. The mixture was then cooled, poured into aqueous sodium hydroxide solution (2 M, 100 mL) and separated. The aqueous phase was extracted with toluene (2 × 25 mL), and the combined organic extracts were dried ($Na_2SO_4$), filtered and the solvent removed *in vacuo* to yield 4.44 g of crude material. The crude product was dried *in vacuo* at 80 °C for 16 hours before purification by column chromatography on alumina, eluting with 5:1 hexane:ethyl acetate to yield **2-phenyl-5-methylpyridine (8)** as a brown oil (2.05 g, 12.1 mmol, 32%). $\delta_H$ (300 MHz, $CDCl_3$) 2.29 (3H, s, H-7), 7.26-7.42 (3H, m, H-10,11), 7.46 (1H, dd, J= 2.2, 8.1, H-4), 7.55 (1H, d, J= 8.1, H-3), 7.85-7.92 (2H, m, H-9), 8.42-8.46 (1H, m, H-6); $\delta_C$ (100 MHz, $CDCl_3$) 18.2 (C-7), 120.1 (C-3), 126.7 (C-9), 128.6 (C-11), 128.7 (C-10), 131.6 (C-5), 137.4 (C-4), 139.4 (C-2), 150.1 (C-6), 154.8 (C-8); MS $(ESI)^+$ m/z: 170 $(M+H)^+$. Data agrees with published results.[91]

## 5-bromomethyl-2,2′-bipyridine (9)

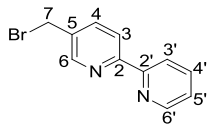


**5-bromomethyl-2,2′-bipyridine (9)** was synthesised by a modification to previously attempted methods.[92] N-bromosuccinimide (0.88 g, 4.9 mmol) and ABCN (cat., 100 mg) was added to a solution of 5-methyl-2,2′-bipyridine (**7**, 0.84 g, 4.9 mmol) in $CCl_4$ (20 mL) and heated to reflux under an atmosphere of nitrogen for 2 hours. The reaction mixture was hot filtered and the solvent removed *in vacuo*. The crude material was dissolved in DCM (20 mL), filtered and the solvent removed *in vacuo* before purification by column chromatography on alumina eluting with 2.5% ethyl acetate in hexane to yield **5-bromomethyl-2,2′-bipyridine (9)** as a pale yellow solid (0.24 g, 0.9 mmol, 20%). $\delta_H$ (300 MHz, $CDCl_3$) 4.47 (2H, s, H-7), 7.26 (1H, dd, J= 1.2, 4.8, H-5′), 7.72-7.82 (2H, m, H-4,4′), 8.31-8.36 (2H, m, H-3,3′), 8.59-8.64 (2H, m, H-6,6′); $\delta_C$ (100 MHz, $CDCl_3$) 29.6 (C-7), 121.1 (C-3/3′), 121.3 (C-3/3′), 124.0 (C-5′), 133.7 (C-5), 137.1 (C-4′), 137.6 (C-4), 149.2 (C-6), 149.3 (C-6′), 155.4 (C-2′), 155.9 (C-2); MS $(ESI)^+$ m/z: 251 $(M+H)^+$. Data agrees with published results.[72]

## 2-phenyl-5-bromomethylpyridine (10)

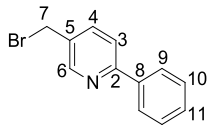


**2-phenyl-5-bromomethylpyridine (10)** was synthesised by a modification to previously attempted methods.[92] N-bromosuccinimide (0.84 g, 4.7 mmol) and ABCN (cat., 50 mg) was added to a solution of 2-phenyl-5-methylpyridine (**8**, 0.80 g, 4.7 mmol) in $CCl_4$ (30 mL) and heated to reflux under an atmosphere of nitrogen for 2 hours. The reaction mixture was hot

filtered and the solvent removed *in vacuo*. The crude material was dissolved in DCM (30 mL), filtered and the solvent removed *in vacuo* before purification by column chromatography on alumina eluting with 2.5% ethyl acetate in hexane to yield **2-phenyl-5-bromomethylpyridine (10)** as a pale yellow solid (0.22 g, 0.9 mmol, 19%). $\delta_H$ (300 MHz, $CDCl_3$) 4.46 (2H, s, H-7), 7.31-7.47 (3H, m, H-10,11), 7.66 (1H, dd, J= 0.7, 8.3, H-3), 7.73 (1H, dd, J= 2.4, 8.3, H-4), 7.89-7.95 (2H, m, H-9), 8.63 (1H, d, J= 2.4, H-6); $\delta_C$ (100 MHz, $CDCl_3$) 29.8 (C-7), 120.5 (C-3), 127.0 (C-9), 128.8 (C-10), 129.3 (C-11), 132.0 (C-5), 137.5 (C-4), 138.6 (C-2), 149.7 (C-6), 157.4 (C-8); MS $(ESI)^+$ m/z: 250 $(M+H)^+$. Data agrees with published results.[93]

## 6-monohydroxy-permethylated-β-cyclodextrin (11)

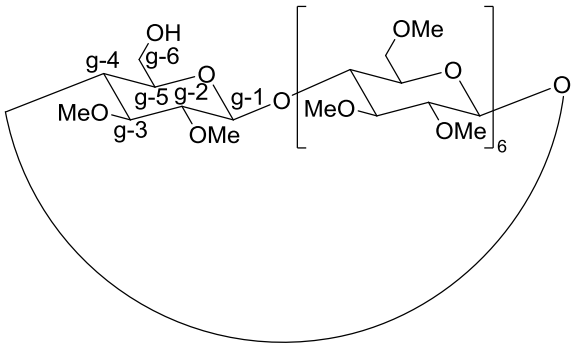


**6-monohydroxy-permethylated-β-cyclodextrin (11)** was synthesised in analogous fashion to a previously reported method.[32] β-cyclodextrin (8.03 g, 7.1 mmol) and imidazole (1.08 g, 15.9 mmol) were dissolved in dry DMF (150 mL), to which *tert*-butyldimethylsilyl chloride (2.26 g, 15.0 mmol) in dry DMF (50 mL) was added dropwise over 30 minutes. The mixture was then stirred for 2 hours, after which TLC analysis (5:4:3 n-butanol:water:ethanol) revealed three spots at $R_f$ 0.4, 0.6 and 0.8 which indicated silyl protection of the β-cyclodextrin. The mixture was then cooled to 0 °C, after which sodium hydride (21.0 g, 60% dispersion in mineral oil, 525.0 mmol) was added portionwise. Dry DMF (30 mL) was added to aid viscosity, and the mixture was stirred at 0 °C for 1 hour, followed by stirring at room temperature for 2 hours,

whereupon it was cooled to 0 °C. Methyl iodide (140.82 g, 988.9 mmol) was added dropwise over 30 minutes. The mixture was stirred at 0 °C for 1 hour, and then at room temperature overnight, after which time TLC analysis (9:1 ethyl acetate:methanol) revealed that full methylation had occurred. The mixture was cooled to 0 °C, and methanol (40 mL) was added. The mixture was then poured into ice-water (750 mL) and extracted with chloroform (6 × 250 mL). The combined organic extracts were washed with 3% aqueous sodium thiosulfate solution (200 mL) and water (200 mL), before drying ($MgSO_4$), and removing the solvent *in vacuo*. The brown residue was then dried *in vacuo* at 80 °C for 8 hours, after which the residue was dissolved in methanol (400 mL). Ammonium fluoride (4.82 g, 130.3 mmol) was added and the mixture heated to reflux overnight, after which TLC analysis (9:1 ethyl acetate:methanol) revealed the silyl groups had been removed. The solvent was removed *in vacuo* and the residue was dissolved in ethyl acetate (200 mL), filtered through celite and the solvent removed *in vacuo*. The orange residue was purified by column chromatography using Biotage or Grace Scientific prepacked silica columns, eluting isocratically at 4.8% methanol in ethyl acetate or on a gradient at 2-8% methanol in ethyl acetate to yield **6-monohydroxy-permethylated-β-cyclodextrin (11)** as a white solid (1.41 g, 1.0 mmol, 14%). $\delta_H$ (300 MHz, $CDCl_3$) 3.13-3.94 (103H, m, H-g-2,g-3,g-4,g-5,g-6,OMe), 5.05 (1H, d, J= 3.5, H-g-1), 5.12 (3H, d, J= 3.5, H-g-1), 5.16-5.20 (2H, m, H-g-1), 5.24 (1H, d, J= 3.9, H-g-1); $\delta_C$ (100 MHz, $CDCl_3$) 58.2, 58.3, 58.4, 58.5, 58.7, 58.8, 59.0, 59.1, 59.2, 61.1, 61.3, 61.6, 61.7, 70.9, 71.0, 71.2, 71.5, 71.6, 71.7, 78.5, 79.9, 80.0, 80.7, 81.2, 81.4, 81.6, 81.8, 81.9, 82.4, 98.8, 99.0; MS (MALDI, 2,5-dihydroxybenzoic acid)$^+$ 1438 $(M+Na)^+$, 1454 $(M+K)^+$. Data agrees with published results.[32, 70]

## 6-mono(5-methoxy-2,2′-bipyridyl)-permethylated-β-cyclodextrin (bpy-CD) (13)

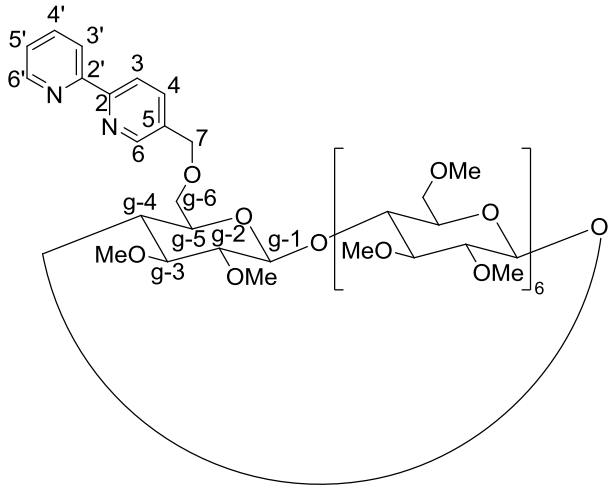


**bpy-CD (13)** was synthesised via a modification to a previously reported method.[70] 6-monohydroxy-permethylated-β-cyclodextrin (**11**, 0.20 g, 0.1 mmol), was dissolved in dry THF (8 mL), to which sodium hydride (60% dispersion in mineral oil, 0.10 g, 2.5 mmol) was added, and the mixture stirred at 60 °C for 1 hour. The mixture was then cooled to room temperature, and 5-bromomethyl-2,2′-bipyridine (**9**, 0.11 g, 0.4 mmol) in dry THF (5 mL) was added. The mixture was heated to reflux for 2 days, after which time the mixture was cooled to room temperature, and brine (5 mL) was added. The solvent was removed *in vacuo* and brine (5 mL) was added, before extraction with DCM (4 × 20 mL). The combined organic extracts were dried ($Na_2SO_4$), filtered, and the solvent removed *in vacuo*, before passing the brown residue through a short column of alumina eluting with 1:0.9 ethyl acetate:methanol to yield a pale yellow solid **bpy-CD** (**12**, 0.19 g, 0.1 mmol, 86%). $\delta_H$ (300 MHz, $CDCl_3$) 3.05-4.20 (m, H-g-2,g-3,g-4,g-5,g-6,OMe), 4.42-4.77 (2H, m, H-7), 4.91-5.18 (7H, m, H-g-1), 7.20-7.32 (1H, m, H-5′), 7.65-7.88 (2H, m, H-4,4′), 8.21-8.41 (2H, m, H-3,3′), 8.50-8.69 (2H, m, H-6,6′); $\delta_C$ (100 MHz, $CDCl_3$) 29.7, 58.1-59.0, 60.8-62.0, 69.3-72.0, 79.6-82.2, 99.0, 120.6, 121.0, 123.8, 133.8,

136.3, 136.9, 148.5, 149.2, 155.6, 155.8; MS (MALDI, 2,3-dihyroxybenzoic acid)$^+$ m/z: 1583 $(M+H)^+$, 1605 $(M+Na)^+$, 1621 $(M+K)^+$.

## 6-mono-(2-phenyl-5-methoxypyridine)-permethylated-β-cyclodextrin (ppy-CD) (13)

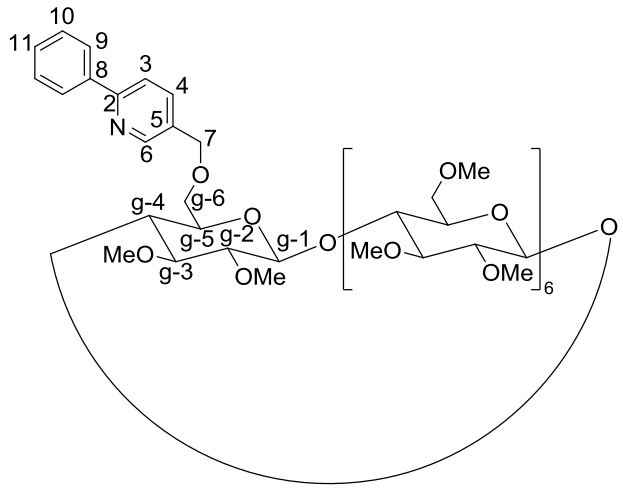


**ppy-CD (13)** was synthesised via a modification to a previously reported method.[70] 6-monohydroxy-permethylated-β-cyclodextrin (**11**, 0.40 g, 0.2 mmol), was dissolved in dry THF (8 mL), to which sodium hydride (60% dispersion in mineral oil, 50 mg, 1.3 mmol) was added, and the mixture stirred at 60 °C for 1 hour. The mixture was then cooled to room temperature, and 2-phenyl-5-bromomethylpyridine (**10**, 0.10 g, 0.4 mmol) in dry THF (5 mL) was added. The mixture was heated to reflux for 2 days, after which time the mixture was cooled to room temperature, and brine (2.5 mL) was added. The solvent was removed *in vacuo* and brine (5 mL) was added, before extraction with DCM (4 × 20 mL). The combined organic extracts were washed with water (20 mL), dried ($Na_2SO_4$), filtered, and the solvent removed *in vacuo*, before passing the brown residue through a short column of alumina eluting with 1:0.9 ethyl acetate:methanol to yield an off-white solid **ppy-CD** (**13**, 0.28 g, 0.2 mmol, 62%). $\delta_H$ (300 MHz, $CDCl_3$) 3.04-3.88 (m, H-g-2,g-3,g-4,g-5,g-6,OMe), 3.99 (1H, dd, J= 3.7, 10.7, H-g-6),

4.46-4.67 (2H, m, H-7), 4.95-5.20 (7H, m, H-g-1), 7.31-7.48 (3H, m, H-10,11), 7.66 (1H, d, J= 8.1, H-3), 7.73 (1H, dd, J= 1.4, 8.5, H-4), 7.87-7.97 (2H, m, H-9), 8.59 (1H, d, J= 1.4, H-6); $\delta_C$ (100 MHz, $CDCl_3$) 29.7, 57.8-59.3, 60.9-61.8, 69.3, 70.4-71.7, 79.6-82.3, 120.1, 126.8, 128.8, 129.1, 132.1, 136.5, 149.0; MS (MALDI, 2,3-dihydroxybenzoic acid)$^+$ m/z: 1604 $(M+Na)^+$, 1620 $(M+K)^+$.

## bis-[6-mono-(5-methoxy-2,2′-bipyridyl)-permethylated-β-cyclodextrin]ruthenium(II) dichloride ($Ru(bpy\text{-}CD)_2Cl_2$) (14)

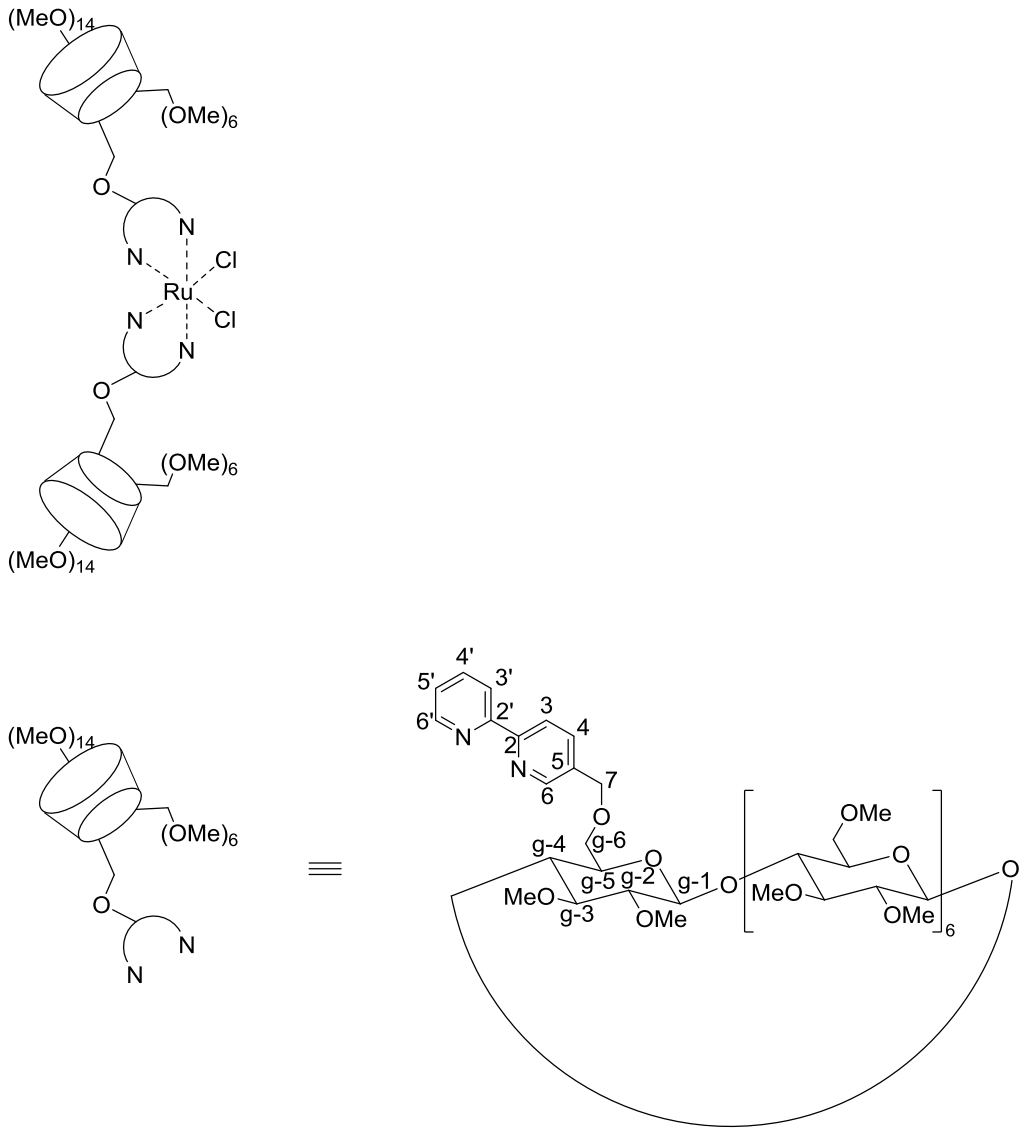


**$Ru(bpy\text{-}CD)_2Cl_2$ (14)** was synthesised via a modification to a previously reported method.[70] Dichloro(1,5-cyclooctadiene)ruthenium(II) polymer (29.2 mg, 0.10 mmol) and lithium chloride (175 mg, 4.17 mmol) were suspended in 2-methoxyethanol (10 mL) and the mixture degassed for 1 hour, before heating to reflux. When the mixture reached reflux, a degassed (1 hour) solution of **bpy-CD (12)** (150 mg, 0.09 mmol) in 2-methoxyethanol (3 mL) was added and the

mixture was maintained at reflux for 2.5 hours, at which point the resulting dark purple solution was cooled to room temperature, and the solvent removed *in vacuo*. DCM (20 mL) was then added, and the solution was filtered and the solvent removed *in vacuo*. The residue was then passed through Sephadex CM C-25 cation exchange resin eluting with 0.2 M NaCl and collecting the red/purple band, before removing the solvent *in vacuo*, dissolving in minimal DCM, filtering and removing the solvent *in vacuo* to yield **Ru(bpy-CD)$_2$Cl$_2$ (14)** as a dark purple solid which was used without further purification (25.0 mg, $7.5 \times 10^{-6}$ mol, 16%). $\delta_H$ (300 MHz, $CDCl_3$) 3.04-3.87 (m, H-g-2,g-3,g-4,g-5,g-6,OMe), 4.56-4.74 (4H, m, H-7), 4.91-5.20 (14H, m, H-g-1), 7.24-10.29 (14H, m, H-ar); MS (MALDI, norharmane)$^+$ m/z: 3421 $(M+2(MeCN)+H)^+$.

**tetrakis-[6-mono-(2-phenyl-5-methoxypyridine)-permethylated-β-cyclodextrin]-(μ-dichloro)-diiridium(III) ([Ir(ppy-CD)$_2$Cl]$_2$) (15)**

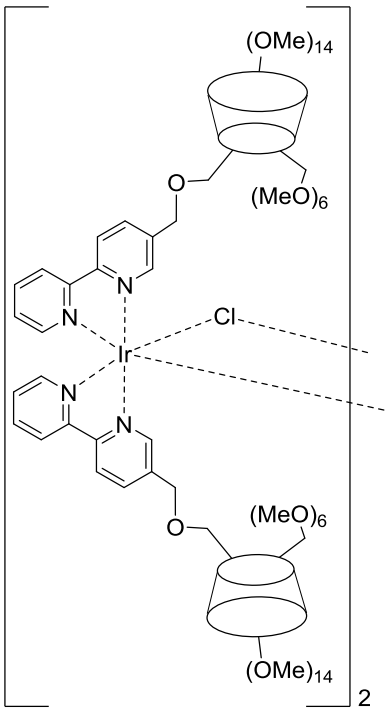


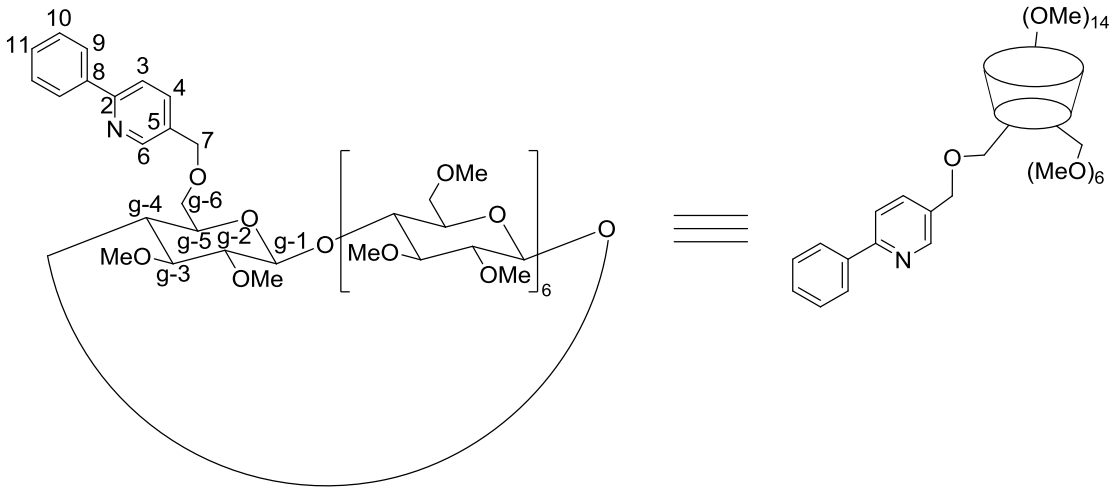


**[Ir(ppy-CD)$_2$Cl]$_2$ (15)** was synthesised by a modification to a previously reported method.[74] Iridium(III) chloride hydrate (6.1 mg, 0.05 mmol) and **ppy-CD (13)** (170 mg, 0.11 mmol) were suspended in a 3:1 mixture of 2-methoxyethanol and water (12 mL), and the mixture was degassed for 40 minutes. Following this, the mixture was heated to reflux in the dark for 3.5

hours, before cooling to room temperature and removing the solvent *in vacuo*. The residue was dissolved in minimal DCM, filtered and the solvent removed *in vacuo* to yield **[Ir(ppy-CD)$_2$Cl]$_2$ (15)** as a dark yellow/orange solid, which was used without further purification (110 mg, 0.03 mmol, 62%). $\delta_H$ (300 MHz, $CDCl_3$) 3.04-3.87 (m, H-g-2,g-3,g-4,g-5,g-6,OMe), 4.06-4.14 (m, H-g-6), 4.55-4.71 (8H, m, H-7), 4.98-5.12 (28H, m, H-g-1), 7.32-7.64 (m, H-10,11), 7.74-7.90 (6H, m, H-3,4), 7.92-8.08 (m, H-9), 8.66-8.75 (4H, m, H-6); MS (MALDI, norharmane)$^+$ m/z: 3355 (Ir(ppy-CD)$_2$)$^+$.

## [Ru(bpy-CD)$_2$(bpySS)]Cl$_2$ (16)

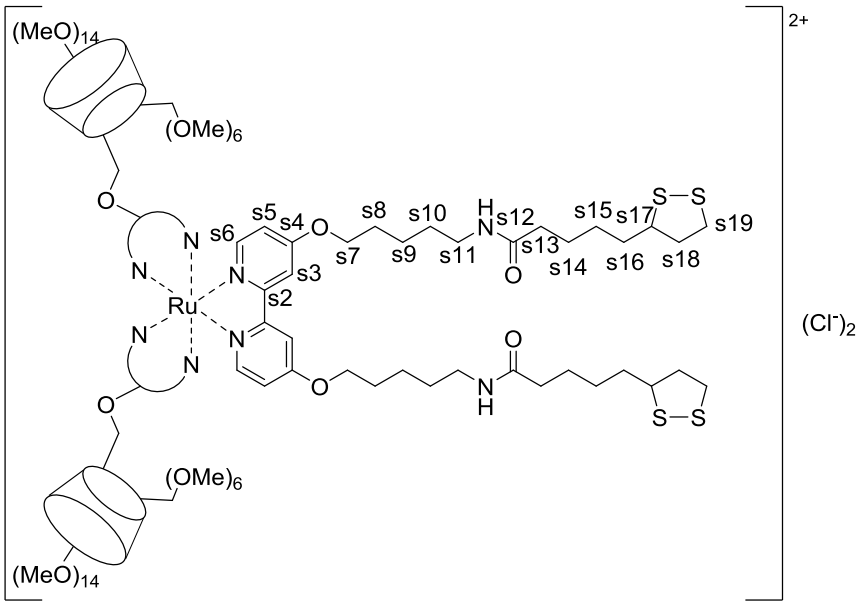


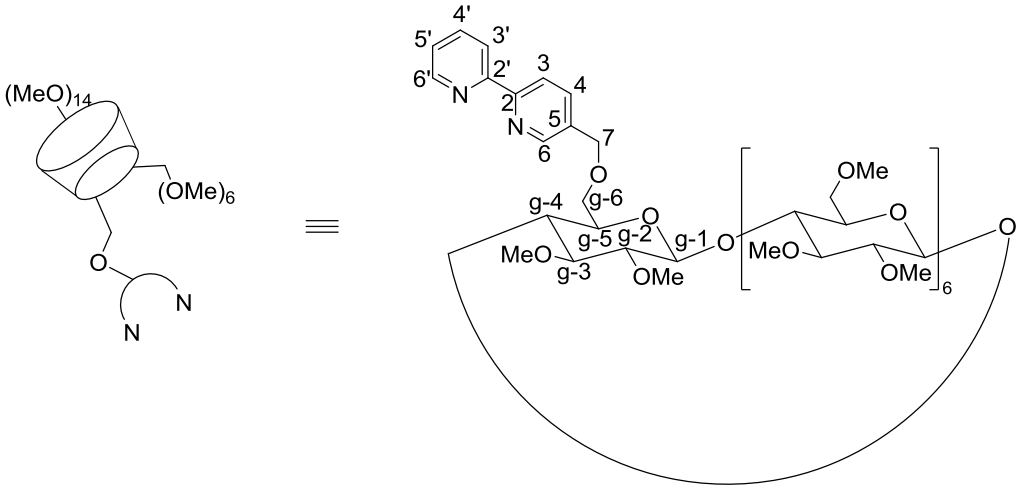


**[Ru(bpy-CD)$_2$(bpySS)]Cl$_2$** was synthesised via a modification to a previously reported method.[9] **Ru(bpy-CD)$_2$Cl$_2$ (14)** (25.0 mg, $7.5 \times 10^{-6}$ mol) and **bpySS** (6.6 mg, $9.0 \times 10^{-6}$ mol) were dissolved in 5% water in 2-methoxyethanol (10 mL) and heated to 110 °C for 4 hours, after which time the reaction mixture was cooled to room temperature and the solvent removed *in vacuo*. The residue was dissolved in water (20 mL), filtered and the solvent removed *in vacuo* to yield **[Ru(bpy-CD)$_2$(bpySS)]Cl$_2$ (16)** as a red solid (13.1 mg, $3.2 \times 10^{-6}$ mol, 43%). $\delta_H$ (500

MHz, $CDCl_3$) 1.19-1.76 (m, H-s8,s9,s14,s15,s16), 1.76-2.17 (m, H-s13,s18′), 2.22-2.51 (m, H-s18), 3.04-4.00 (m, H-g-2,g-3,g-4,g-5,g-6,OMe,s11,s17,s19), 4.10-4.52 (m, H-g-6,s7), 4.59-4.92 (4H, m, H-7), 4.97-5.27 (14H, m, H-g-1), 5.47-5.73 (2H, m, N*H*), 6.46-9.95 (20H, m, H-ar); MS $(ESI)^+$ m/z: 2002 $(M-2(Cl))^{2+}$.

## [Ir(ppy-CD)$_2$(bpySS)]Cl (17)

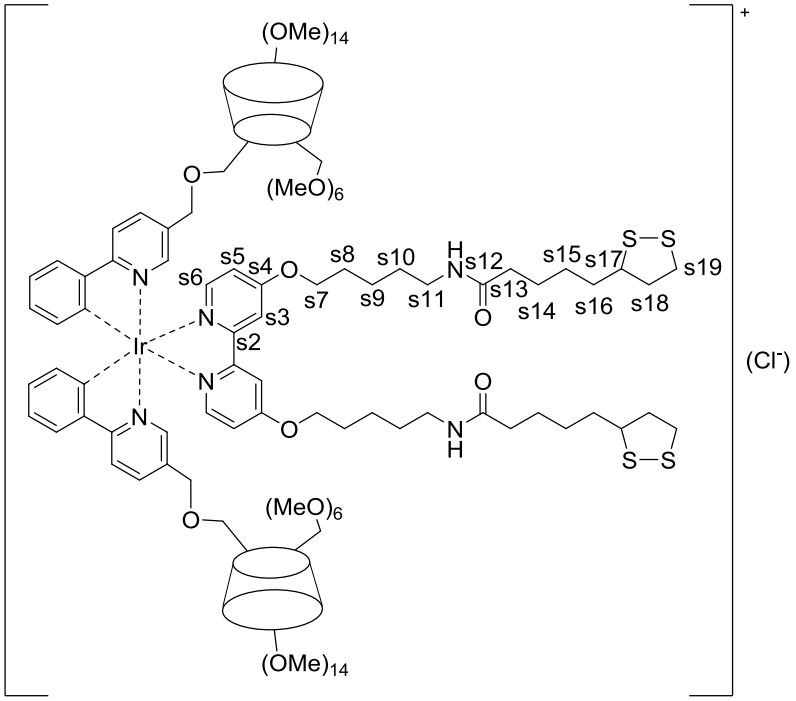


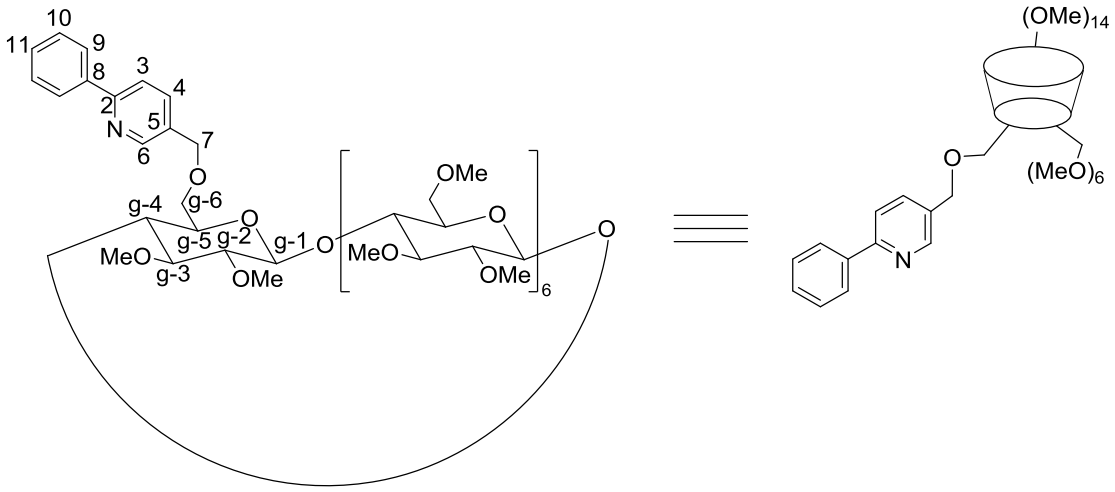


**[Ir(ppy-CD)$_2$(bpySS)]Cl (17)** was synthesised in a modification to a previously outlined method.[9] **[Ir(ppy-CD)$_2$Cl]$_2$ (15)** (0.11 g, 1.67 × $10^{-5}$ mol) and **bpySS** (30.7 mg, 4.17 × $10^{-5}$ mol) were suspended in 5% water in 2-methoxyethanol (10 mL) and heated to 130 °C for 4.5 hours, after which time the reaction mixture was cooled to room temperature and the solvent removed *in vacuo*. The yellow residue was taken up in minimal methanol and passed through

a column of Sephadex LH-20 collecting the yellow band to yield **[Ir(ppy-CD)$_2$(bpySS)]Cl (17)** as a yellow solid (59.8 mg, 1.45 × $10^{-5}$ mol, 43%). $\delta_H$ (300 MHz, $CDCl_3$) 1.31-1.68 (m, H-s8,s9,s14,s15,s16), 1.68-2.02 (m, H-s13,s18′), 2.04-2.45 (m, H-s18), 2.90-3.89 (H-g-2,g-3,g-4,g-5,g-6,OMe,s11,s17,s19), 3.92-4.13 (m, H-g-6,s7), 4.42-4.64 (4H, m, H-7), 4.90-5.13 (14H, m, H-g-1), 6.64-6.89 (m, H-s5), 6.89-6.99 (2H, t, J = 6.6, N*H*), 7.29-7.45 (m, H-10,11), 7.47-7.61 (m, H-s3), 7.64 (2H, d, J = 8.2, H-3), 7.70 (2H, dd, J = 2.1, 8.2, H-4), 7.78-7.84 (2H, s, H-s6), 7.87-7.93 (4H, m, H-9), 8.56 (2H, d, J = 1.4, H-6); $\delta_C$ (100 MHz, $CDCl_3$) 50.7, 53.5, 56.6, 58.5, 58.6, 59.0, 61.5, 61.6, 69.3, 70.6, 70.9, 71.4, 71.6, 80.2, 80.3, 80.4, 80.9, 81.7, 82.0, 98.9, 120.1, 126.8, 128.8, 129.0, 132.0, 136.4, 139.0, 149.1, 156.9; MS (MALDI, norharmane)$^+$ 4124 $(M+H)^+$.

**Ad-biotin (18)**

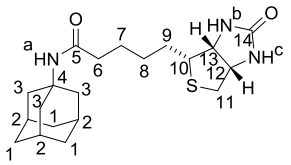


**Ad-biotin (18)** was synthesised via a modification to a previously outlined method.[75] Biotin (1.95 g, 8.2 mmol) and 1-hydroxybenzotriazole hydrate (1.11 g, 8.2 mmol) were suspended in DMF (40 mL) and cooled to 0-5 °C, and EDC.HCl (1.57 g, 8.2 mmol) was added. The mixture was stirred for 1 hour at this temperature until the EDC.HCl had dissolved, and subsequently allowed to warm to room temperature and stirred for a further hour. After this time, 1-adamantylamine (1.24 g, 8.2 mmol) and N-ethylmorpholine (0.94 g, 8.2 mmol) in DMF (15 mL) were added, and the mixture stirred at room temperature overnight. After this time, water (100 mL) was added and the mixture was extracted with chloroform (3 × 100 mL). The combined organic extracts were dried ($Na_2SO_4$) and the solvent removed *in vacuo*. The clear residue was dissolved in a minimal amount of DCM, to which hexane (50 mL) was added,

forming a white precipitate. The precipitate was filtered and washed with hexane and ethyl acetate to yield the title compound **Ad-biotin (18)** as a white solid (1.35 g, 3.4 mmol, 43%). $\delta_H$ (300 MHz, $CDCl_3$) 1.38-1.52 (2H, m, H-8), 1.58-1.83 (10H, m, H-1, 7, 9), 2.00 (6H, d, J= 2.86, H-3), 2.08 (3H, br s, H-2), 2.14 (2H, t, J= 7.4, H-6), 2.76 (1H, d, J= 12.9, H-11′), 2.93 (1H, dd, J= 5.0, 12.9, H-11), 3.17 (1H, td, J= 4.7, 7.4, H-10), 4.34 (1H, ddd, J= 0.9, 4.7, 7.9, H-13), 4.53 (1H, dd, J= 5.0, 7.9, H-12), 5.43 (2H, br s, H-a,c), 6.11 (1H, br s, H-b); $\delta_C$ (100 MHz, $CDCl_3$) 25.7 (C-7), 28.1 (C-8,9), 29.4 (C-2), 36.4 (C-1), 37.0 (C-6), 40.6 (C-11), 41.6 (C-3), 51.9 (C-4), 55.5 (C-10), 60.2 (C-12), 61.9 (C-13), 163.7 (C-14), 172.4 (C-5); m/z $(ESI)^+$ 378 $(M+H)^+$, 400 $(M+Na)^+$.

# 4.7 References


1. E. A. Meyer, R. K. Castellano and F. Diederich, *Angew. Chem. Int. Ed.*, 2003, **42**, 1210-1250.
2. M. F. Dunn, in *eLS*, John Wiley & Sons, Ltd, 2001.
3. A. K. Gupta and M. Gupta, *Biomaterials*, 2005, **26**, 3995-4021.
4. J. Homola, S. S. Yee and G. Gauglitz, *Sensor. Actuat. B-Chem.*, 1999, **54**, 3-15.
5. L. G. Fägerstam, Å. Frostell, R. Karlsson, M. Kullman, A. Larsson, M. Malmqvist and H. Butt, *J. Mol. Recognit.*, 1990, **3**, 208-214.
6. C. K. Ho, A. Robinson, D. R. Miller and M. J. Davis, *Sensors*, 2005, **5**, 4-37.
7. C. David, F. Hervé, B. Sébille, M. Canva and M.-C. Millot, *Sensor. Actuat. B-Chem.*, 2006, **114**, 869-880.
8. T. Mossman, *J. Immunol. Methods*, 1983, **65**, 55-63.
9. J. A. Faiz, R. M. Williams, M. Silva, L. De Cola and Z. Pikramenou, *J. Am. Chem. Soc.*, 2006, **128**, 4520-4521.
10. J. M. Haider, R. M. Williams, L. De Cola and Z. Pikramenou, *Angew. Chem. Int. Ed.*, 2003, **42**, 1830-1833.
11. M. Felici, P. Contreras-Carballada, J. M. M. Smits, R. J. M. Nolte, R. M. Williams, L. De Cola and M. C. Feiters, *Molecules*, 2010, **15**, 2039-2059.
12. J. Muldoon, A. E. Ashcroft and A. J. Wilson, *Chem. Eur. J.*, 2010, **16**, 100-103.
13. M.-X. Zhao, M. Zhao, E.-Z. Zeng, Y. Li, J.-M. Li, Q. Cao, C.-P. Tan, L.-N. Ji and Z.-W. Mao, *J. Inorg. Biochem.*, 2014, **137**, 31-39.
14. M. Slim and H. F. Sleiman, *Bioconjugate Chem.*, 2004, **15**, 949-953.
15. P. D. Beer and P. A. Gale, *Angew. Chem. Int. Ed.*, 2001, **40**, 486-516.
16. X. Zhang, H. Chen and H. Zhang, *Chem. Commun.*, 2007, 1395-1405.
17. A. Friggeri, F. C. J. M. van Veggel, D. N. Reinhoudt and R. P. H. Kooyman, *Langmuir*, 1998, **14**, 5457-5463.
18. B. Genorio, T. He, A. Meden, S. Polanc, J. Jamnik and J. M. Tour, *Langmuir*, 2008, **24**, 11523-11532.
19. F. Tian, M. Czifersky, D. Jiao, K. Wahlström, J. Geng and O. A. Scherman, *Langmuir*, 2011, **27**, 1387-1390.
20. F. Tian, D. Jiao, F. Biedermann and O. A. Scherman, *Nat. Commun.*, 2012, **3**, 1207.
21. H. Tian and Q.-C. Wang, *Chem. Soc. Rev.*, 2006, **35**, 361-374.
22. I. Willner, V. Pardo-Yissar, E. Katz and K. T. Ranjit, *J. Electroanal. Chem.*, 2001, **497**, 172-177.
23. M. T. Rojas, R. Koeniger, J. F. Stoddart and A. E. Kaifer, *J. Am. Chem. Soc.*, 1995, **117**, 336-343.
24. G. Nelles, M. Weisser, R. Back, P. Wohlfart, G. Wenz and S. Mittler-Neher, *J. Am. Chem. Soc.*, 1996, **118**, 5039-5046.
25. M. Weisser, G. Nelles, P. Wohlfart, G. Wenz and S. Mittler-Neher, *J. Phys. Chem.*, 1996, **100**, 17893-17900.
26. M. W. J. Beulen, J. Bügler, B. Lammerink, F. A. J. Geurts, E. M. E. F. Biemond, K. G. C. van Leerdam, F. C. J. M. van Veggel, J. F. J. Engbersen and D. N. Reinhoudt, *Langmuir*, 1998, **14**, 6424-6429.
27. M. W. J. Beulen, J. Bügler, M. R. de Jong, B. Lammerink, J. Huskens, H. Schönherr, G. J. Vancso, B. A. Boukamp, H. Wieder, A. Offenhäuser, W. Knoll, F. C. J. M. van Veggel and D. N. Reinhoudt, *Chem. Eur. J.*, 2000, **6**, 1176-1183.

28. S. Onclin, A. Mulder, J. Huskens, B. J. Ravoo and D. N. Reinhoudt, *Langmuir*, 2004, **20**, 5460-5466.
29. S. H. Toma, J. A. Bonacin, K. Araki and H. E. Toma, *Surf. Sci.*, 2006, **600**, 4591-4597.
30. J. Faiz, A. I. Philippopoulos, A. G. Kontos, P. Falaras and Z. Pikramenou, *Adv. Funct. Mater.*, 2007, **17**, 54-58.
31. A. Biwer, G. Antranikian and E. Heinzle, *Appl. Microbiol. Biot.*, 2002, **59**, 609-617.
32. Z. Chen, J. S. Bradshaw and M. L. Lee, *Tetrahedron Lett.*, 1996, **37**, 6831-6834.
33. W. C. E. Schofield and J. P. S. Badyal, *ACS Appl. Mater. Interfaces*, 2011, **3**, 2051-2056.
34. M. Yu, S.-Z. Zu, Y. Chen, Y.-P. Liu, B.-H. Han and Y. Liu, *Chem. Eur. J.*, 2010, **16**, 1168-1174.
35. O. Crespo-Biel, B. Dordi, D. N. Reinhoudt and J. Huskens, *J. Am. Chem. Soc.*, 2005, **127**, 7594-7600.
36. X. Y. Ling, D. N. Reinhoudt and J. Huskens, *Chem. Mater.*, 2008, **20**, 3574-3578.
37. O. Crespo-Biel, C. W. Lim, B. J. Ravoo, D. N. Reinhoudt and J. Huskens, *J. Am. Chem. Soc.*, 2006, **128**, 17024-17032.
38. M. J. W. Ludden, A. Mulder, K. Schulze, V. Subramaniam, R. Tampé and J. Huskens, *Chem. Eur. J.*, 2008, **14**, 2044-2051.
39. Q. Chen, H. Chen, Y. Zhao, F. Zhang, F. Yang, J. Tang and P. He, *Biosens. Bioelectron.*, 2014, **54**, 547-552.
40. M. Frasconi and F. Mazzei, *Nanotechnology*, 2009, **20**, 285502.
41. A. D'Annibale, R. Regoli, P. Sangiorgio and T. Ferri, *Electroanalysis*, 1999, **11**, 505-510.
42. I. A. Banerjee, L. Yu and H. Matsui, *J. Am. Chem. Soc.*, 2003, **125**, 9542-9543.
43. Y.-f. Chen, I. A. Banerjee, L. Yu, R. Djalali and H. Matsui, *Langmuir*, 2004, **20**, 8409-8413.
44. M. J. W. Ludden, M. Péter, D. N. Reinhoudt and J. Huskens, *Small*, 2006, **2**, 1192-1202.
45. M. J. W. Ludden, X. Li, J. Greve, A. van Amerongen, M. Escalante, V. Subramaniam, D. N. Reinhoudt and J. Huskens, *J. Am. Chem. Soc.*, 2008, **130**, 6964-6973.
46. M. J. W. Ludden, J. K. Sinha, G. Wittstock, D. N. Reinhoudt and J. Huskens, *Org. Biomol. Chem.*, 2008, **6**, 1553-1557.
47. A. Fragoso, J. Caballero, E. Almirall, R. Villalonga and R. Cao, *Langmuir*, 2002, **18**, 5051-5054.
48. Z. Zhang, J. Wang, X. Wang, Y. Wang and X. Yang, *Talanta*, 2010, **82**, 483-487.
49. L. Wang, J. Lei, R. Ma and H. Ju, *Anal. Chem.*, 2013, **85**, 6505-6510.
50. N. Hayashi, R. Chen, M. Hiraoka, T. Ujihara and H. Ikezaki, *J. Agric. Food Chem.*, 2010, **58**, 8351-8356.
51. T. Ikunaga, H. Ikeda and A. Ueno, *Chem. Eur. J.*, 1999, **5**, 2698-2704.
52. M. Holzinger, M. Singh and S. Cosnier, *Langmuir*, 2012, **28**, 12569-12574.
53. J. Hyun, S. J. Ahn, W. K. Lee, A. Chilkoti and S. Zauscher, *Nano Lett.*, 2002, **2**, 1203-1207.
54. T. Hoshi, J.-i. Anzai and T. Osa, *Anal. Chem.*, 1995, **67**, 770-774.
55. H. C. Yoon, M.-Y. Hong and H.-S. Kim, *Langmuir*, 2001, **17**, 1234-1239.
56. D. S. Turygin, M. Subat, O. A. Raitman, S. L. Selector, V. V. Arslanov, B. König and M. A. Kalinina, *Langmuir*, 2007, **23**, 2517-2524.
57. Z. Pikramenou and D. G. Nocera, *Inorg. Chem.*, 1992, **31**, 532-536.
58. S. Weidner and Z. Pikramenou, *Chem. Commun.*, 1998, 1473-1474.

59. J. M. Haider, M. Chavarot, S. Weidner, I. Sadler, R. M. Williams, L. De Cola and Z. Pikramenou, *Inorg. Chem.*, 2001, **40**, 3912-3921.
60. J. A. Faiz, R. M. Williams, M. J. J. P. Silva, L. De Cola and Z. Pikramenou, *J. Am. Chem. Soc.*, 2006, **128**, 4520-4521.
61. C. T. Mallon, R. J. Forster, A. McNally, E. Campagnoli, Z. Pikramenou and T. E. Keyes, *Langmuir*, 2007, **23**, 6997-7002.
62. M. R. de Jong, J. Huskens and D. N. Reinhoudt, *Chem. Eur. J.*, 2001, **7**, 4164-4170.
63. L. E. P. Kyllonen, V. Chinuswamy, D. Maffeo, E. T. Kefalas, J. M. Haider, Z. Pikramenou, I. Mavridis, K. Yannakopolou and N. Glezos, *J. Phys. Org. Chem.*, 2012, **25**, 198-206.
64. D. Velessiotis, D. Maffeo, C. Millios, E. Makarona, C. Viswanathan, K. Yannakopolou, I. Mavridis, Z. Pikramenou and N. Glezos, *Phys. Stat. Sol.*, 2008, **205**, 2532-2535.
65. L. Chaiet and F. J. Wolf, *Arch. Biochem. Biophys.*, 1964, **106**, 1-5.
66. A. Michalke, A. Janshoff, C. Steinem, C. Henke, M. Sieber and H.-J. Galla, *Anal. Chem.*, 1999, **71**, 2528-2533.
67. P. F. H. Schwab, F. Fleischer and J. Michl, *J. Org. Chem*, 2002, **67**, 443-449.
68. S. Gowrisankar, A. G. Sergeev, P. Anbarasan, A. Spannenberg, H. Neumann and M. Beller, *J. Am. Chem. Soc.*, 2010, **132**, 11592-11598.
69. U. S. Schubert, C. Eschbaumer and M. Heller, *Org. Lett.*, 2000, **2**, 3373-3376.
70. J. A. Faiz, *PhD. Thesis - University of Birmingham*, 2005.
71. E. T. Kefalas, *PhD. Thesis - University of Birmingham*, 2004.
72. M. Heller and U. S. Schubert, *J. Org. Chem*, 2002, **67**, 8269-8272.
73. C. J. Moulton and B. L. Shaw, *J. Chem. Soc., Dalton Trans.*, 1976, 1020-1024.
74. S. Sprouse, K. A. King, P. J. Spellane and R. J. Watts, *J. Am. Chem. Soc.*, 1984, **106**, 6647-6653.
75. S. J. Adams, D. J. Lewis, J. A. Preece and Z. Pikramenou, *ACS Appl. Mater. Interfaces*, 2014, **6**, 11598-11608.
76. A. Juris, V. Balzani, F. Barigelletti, S. Campagna, P. Belser and A. von Zelewsky, *Coord. Chem. Rev.*, 1988, **84**, 85-277.
77. H. F. M. Nelissen, A. F. J. Schut, F. Veneman, M. C. Feiters and R. J. M. Nolte, *Chem. Commun.*, 2000, 577-578.
78. K. Nakamaru, *Bull. Chem. Soc. Jpn.*, 1982, **55**, 2697-2705.
79. K. A. King and R. J. Watts, *J. Am. Chem. Soc.*, 1987, **109**, 1589-1590.
80. M. G. Colombo, A. Hauser and H. U. Güdel, *Inorg. Chem.*, 1993, **32**, 3088-3092.
81. J. D. Slinker, A. A. Gorodetsky, M. S. Lowry, J. Wang, S. Parker, R. Rohl, S. Bernhard and G. G. Malliaras, *J. Am. Chem. Soc.*, 2004, **126**, 2763-2767.
82. C. J. Timpson, C. C. Carter and J. Olmsted, *J. Phys. Chem.*, 1989, **93**, 4116-4120.
83. P. Bortolus, G. Marconi, S. Monti, B. Mayer, G. Köhler and G. Grabner, *Chem. Eur. J.*, 2000, **6**, 1578-1591.
84. J. A. Faiz, L. E. P. Kyllonen, P. Contreras-Carballada, R. M. Williams, L. De Cola and Z. Pikramenou, *Dalton Trans.*, 2009, 3980-3987.
85. J.-P. Sauvage, J.-P. Collin, J.-C. Chambron, S. Guillerez, C. Coudret, V. Balzani, F. Barigelletti, L. De Cola and L. Flamigni, *Chem. Rev.*, 1994, **94**, 993-1019.
86. H.-F. Dai, W.-X. Chen, L. Zhao, F. Xiong, H. Sheng and F.-E. Chen, *Adv. Synth. Catal.*, 2008, **350**, 1635-1641.
87. W. A. Hendrickson, A. Pähler, J. L. Smith, Y. Satow, E. A. Merritt and R. P. Phizackerley, *Proc. Natl. Acad. Sci.*, 1989, **86**, 2190-2194.
88. J. Homola, *Chem. Rev.*, 2008, **108**, 462-493.

89. J. A. de Feijter, J. Benjamins and F. A. Veer, *Biopolymers*, 1978, **17**, 1759-1772.
90. C. L. Yeung, P. Iqbal, M. Allan, M. Lashkor, J. A. Preece and P. M. Mendes, *Adv. Funct. Mater.*, 2010, **20**, 2657-2663.
91. A. Gagnon and P. Petiot, *Eur. J. Org. Chem.*, 2013, **24**, 5282-5289.
92. R. Heck, F. Dumarcay and A. Marsura, *Chem. Eur. J.*, 2002, **8**, 2438-2445.
93. U. d. Saarlandes, R. Hartmann, U. Hille, C. Zimmer, C. A. Vock and Q. Hu, WO2012/52540, 2012.

# 4.8 Appendix

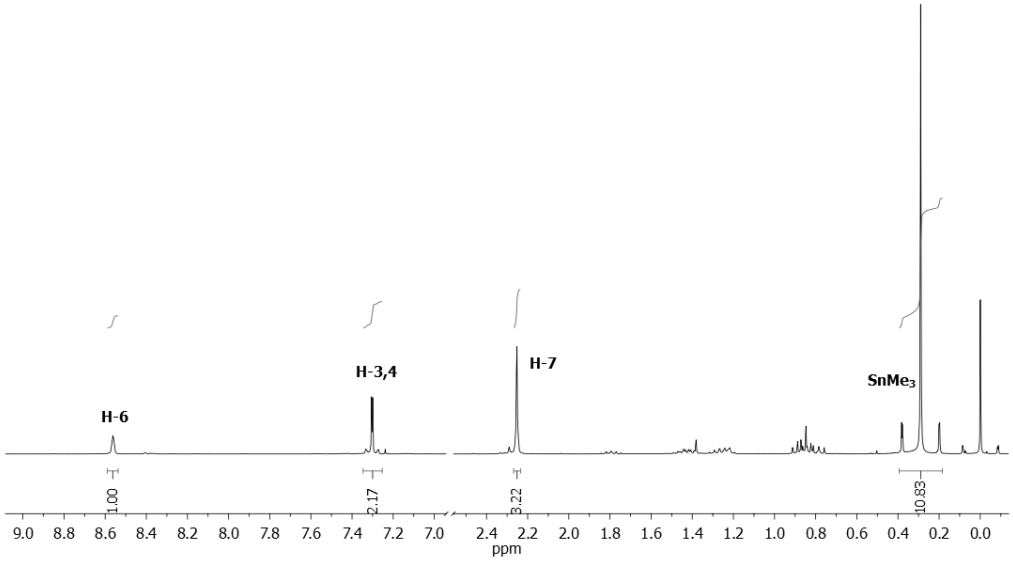


**Figure 4.A1.** $^{1}$H NMR spectrum of **2-trimethylstannyl-5-methylpyridine (6)** in $CDCl_3$.

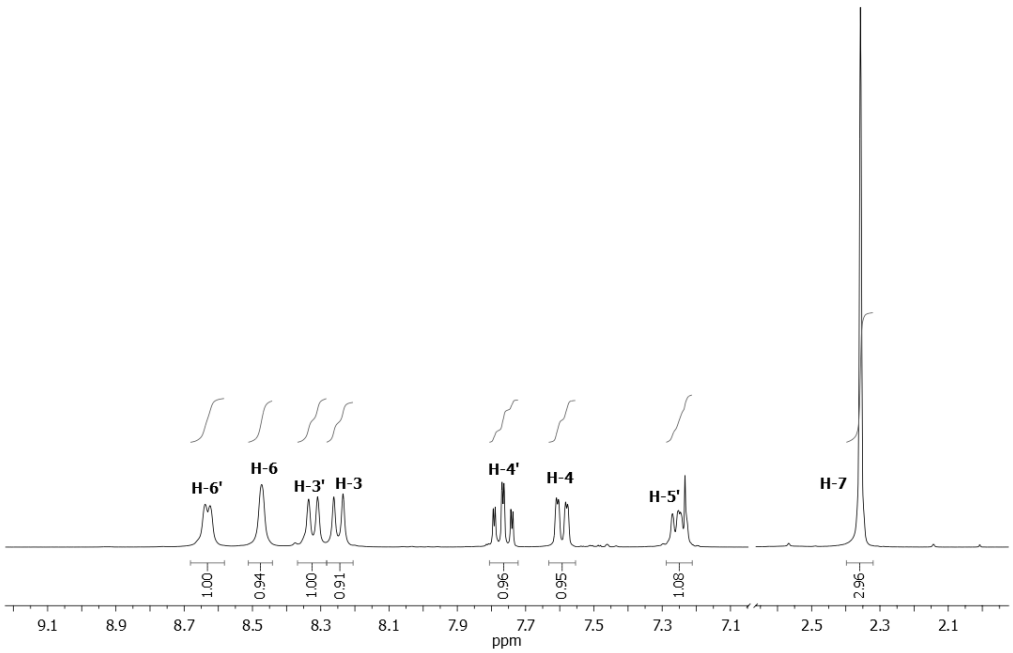


**Figure 4.A2.** $^{1}$H NMR spectrum of **Me-bpy (7)** in $CDCl_3$.

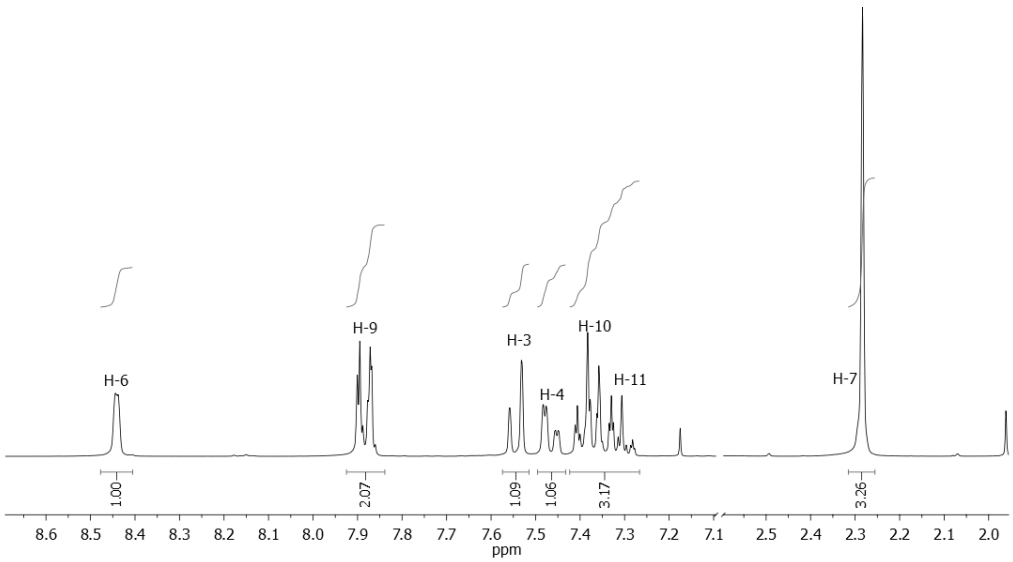


**Figure 4.A3.** $^{1}$H NMR spectrum of **Me-ppy (8)** in $CDCl_3$.

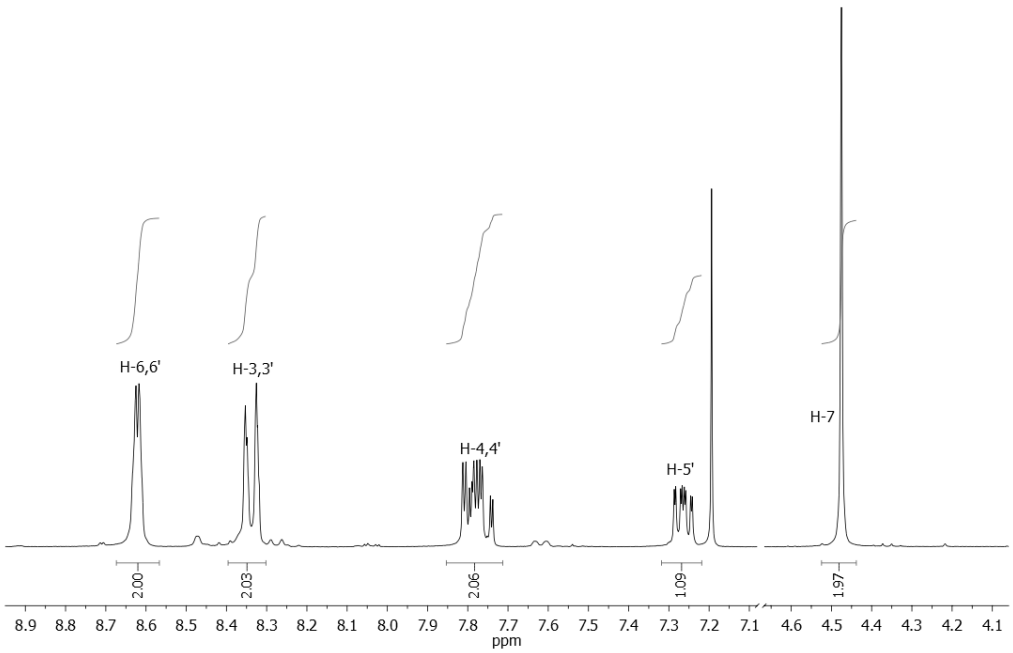


**Figure 4.A4.** $^{1}$H NMR spectrum of **Br-bpy (9)** in $CDCl_3$.

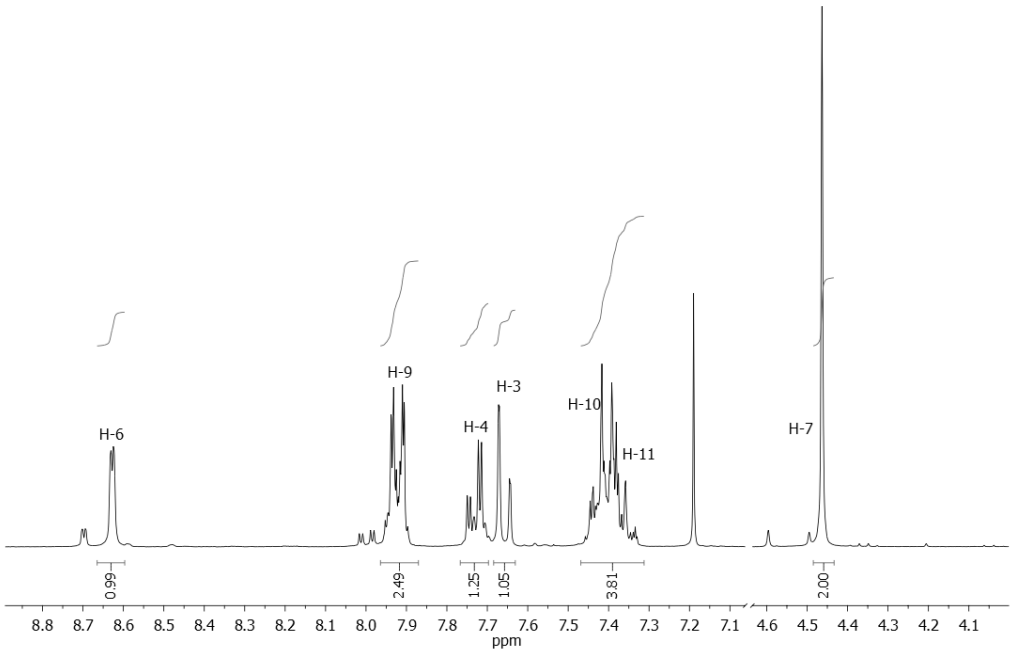


**Figure 4.A5.** $^{1}$H NMR spectrum of **Br-ppy (10)** in $CDCl_3$.

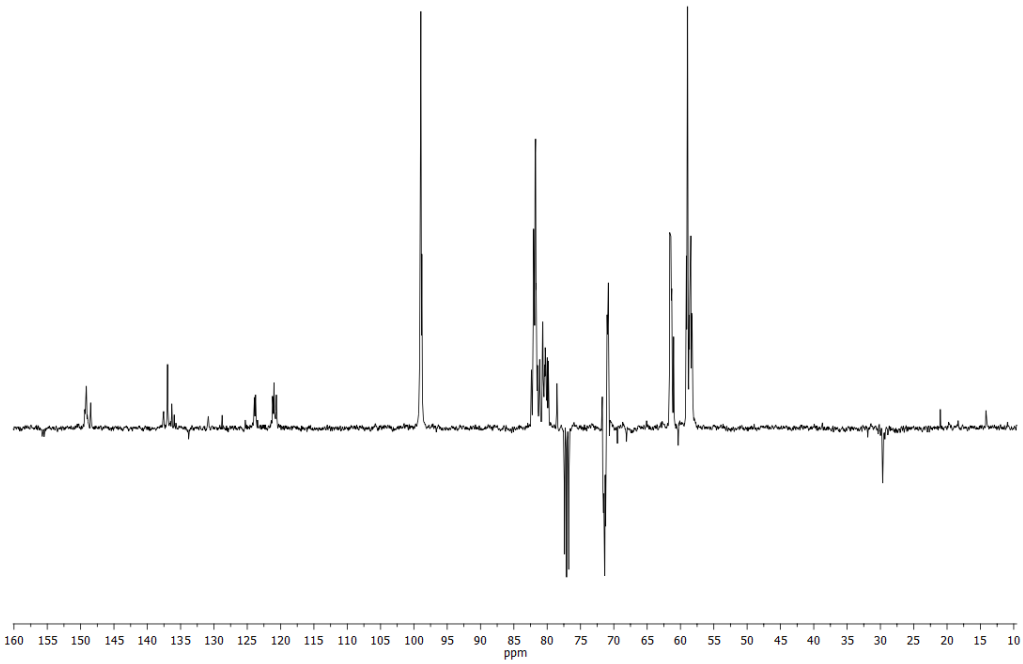


**Figure 4.A6.** $^{13}C$ NMR spectrum of **bpy-CD (12)** in $CDCl_3$.

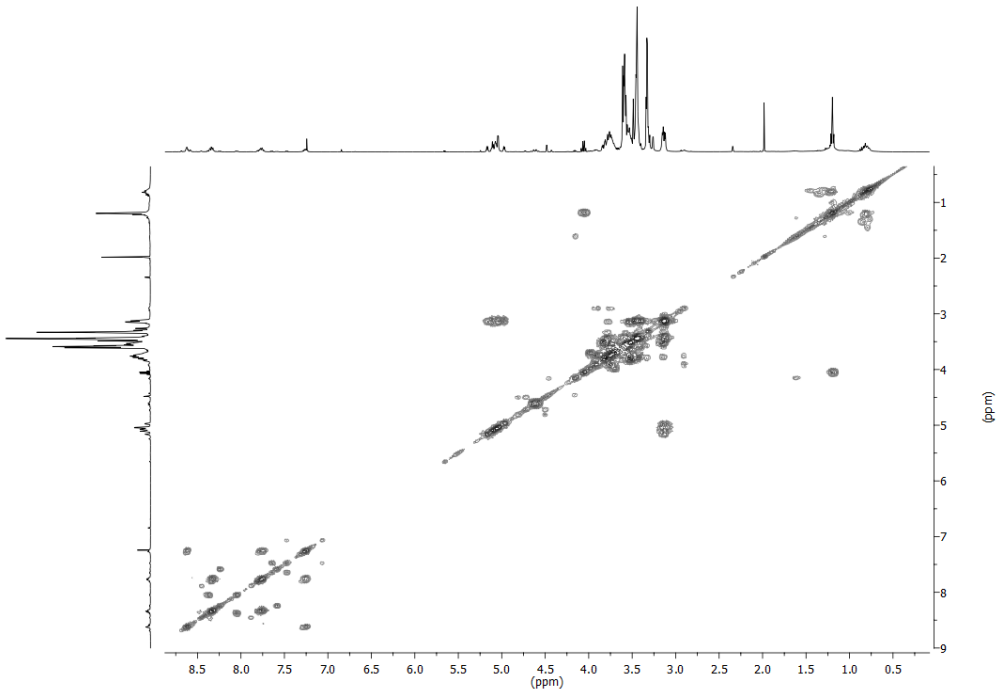


**Figure 4.A7.** COSY spectrum of **bpy-CD (12)** in $CDCl_3$.

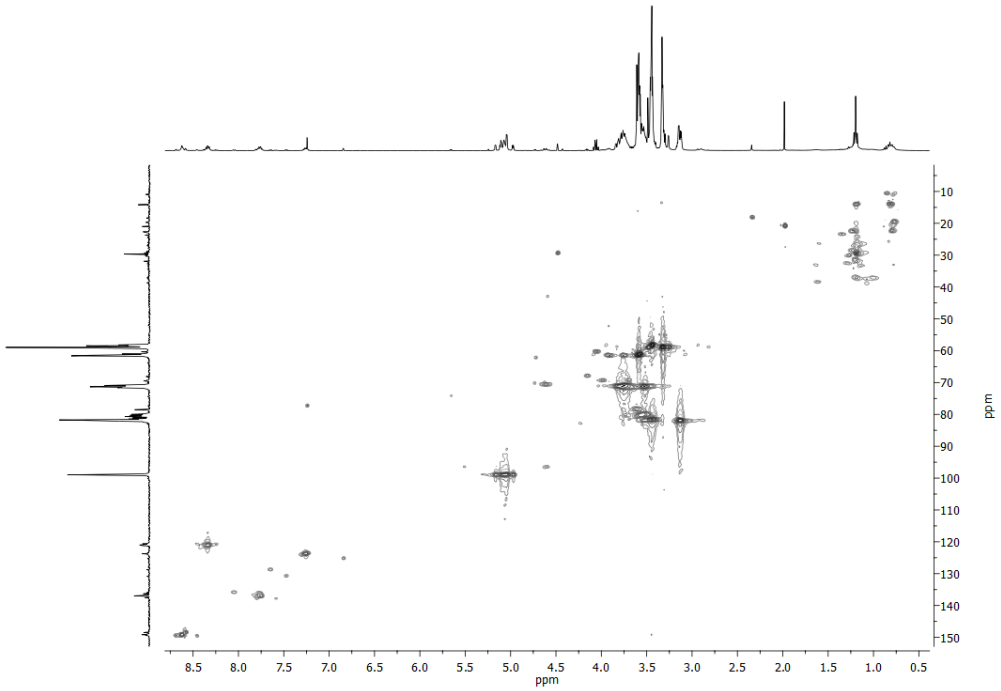


**Figure 4.A8.** HSQC spectrum of **bpy-CD (12)** in $CDCl_3$.

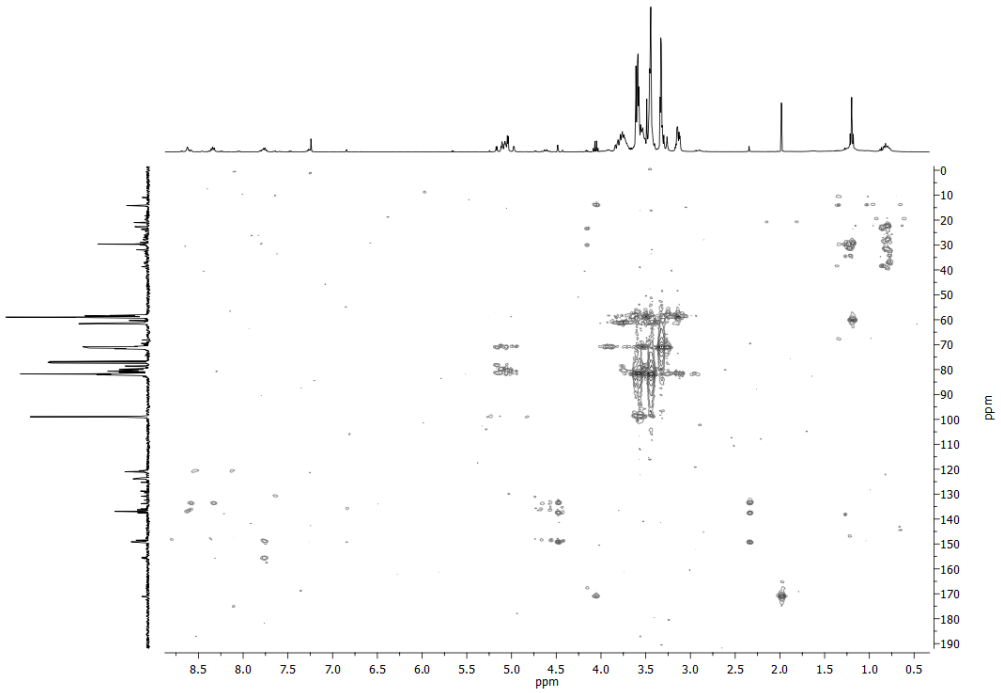


**Figure 4.A9.** HMBC spectrum of **bpy-CD (12)** in $CDCl_3$.

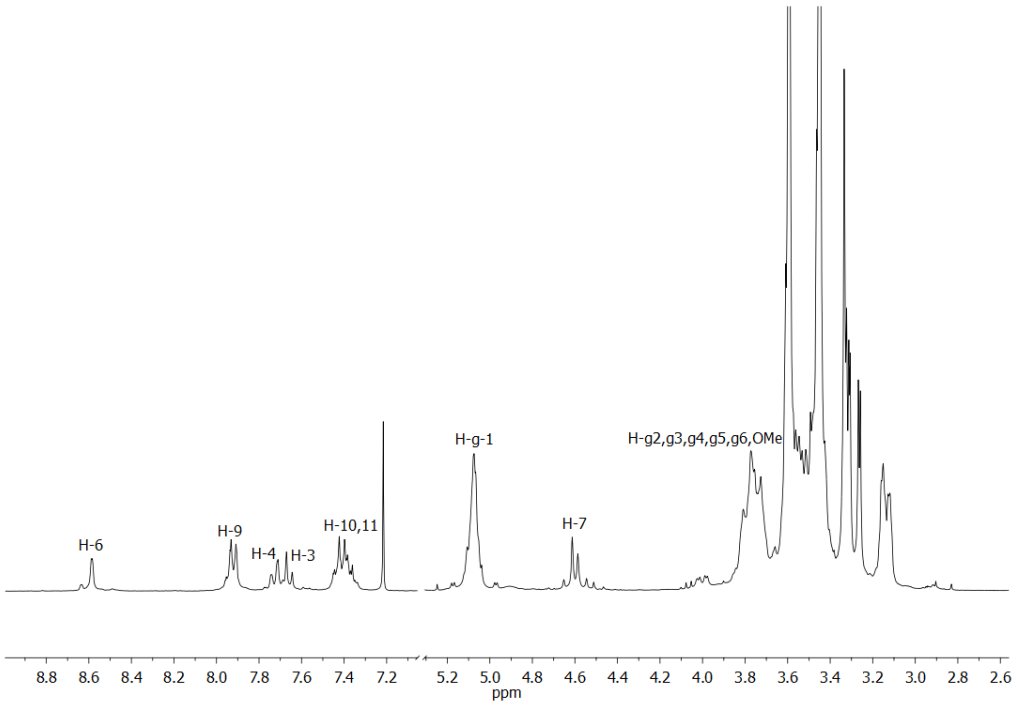


**Figure 4.A10.** $^{1}$H NMR spectrum of **ppy-CD (13)** in $CDCl_3$.

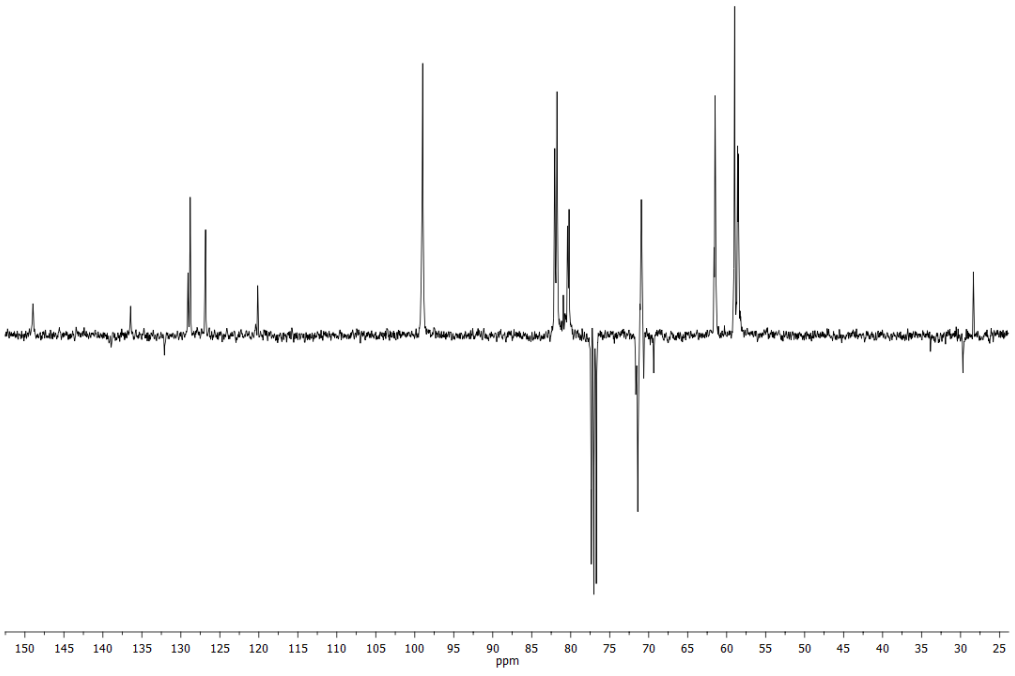


**Figure 4.A11.** $^{13}$C NMR spectrum of **ppy-CD (13)** in $CDCl_3$.

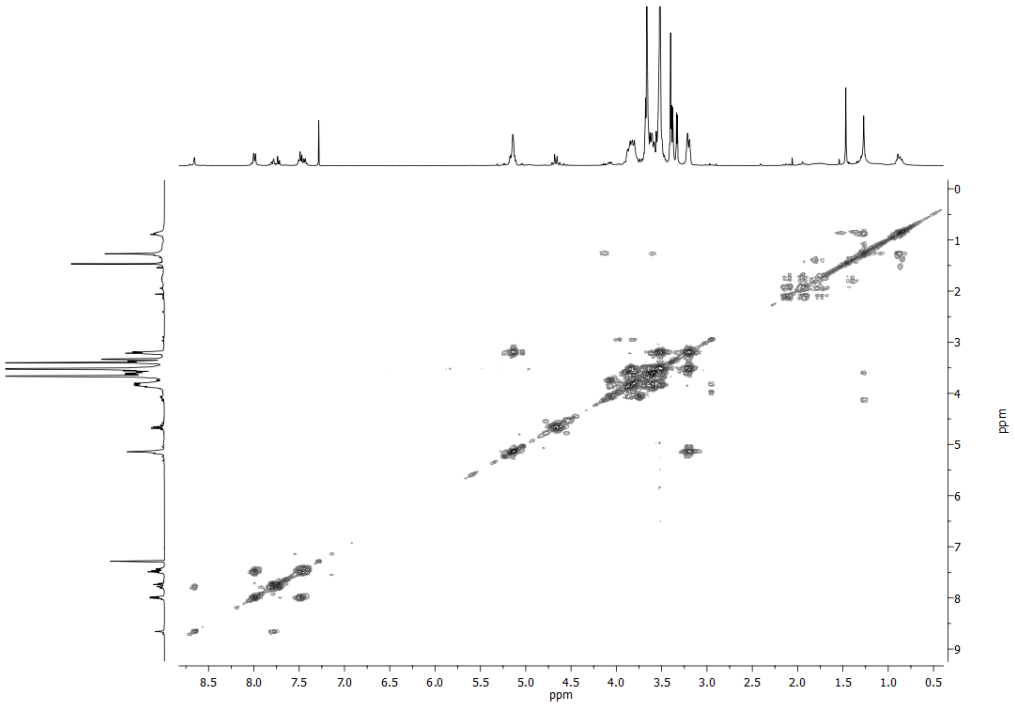


**Figure 4.A12.** COSY spectrum of **ppy-CD (13)** in $CDCl_3$.

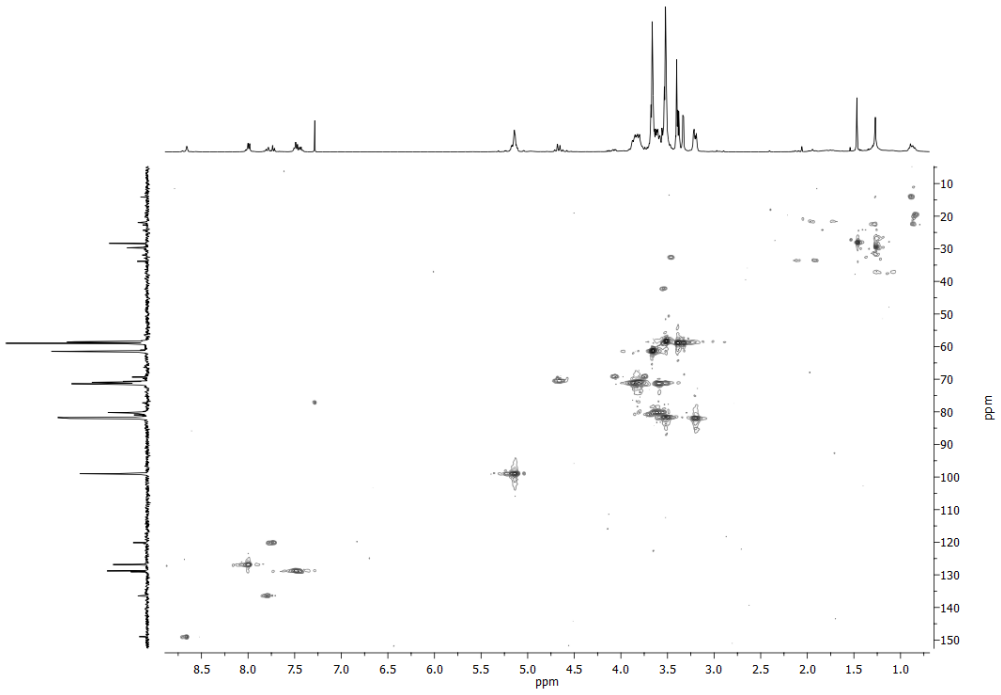


**Figure 4.A13.** HSQC spectrum of **ppy-CD (13)** in $CDCl_3$.

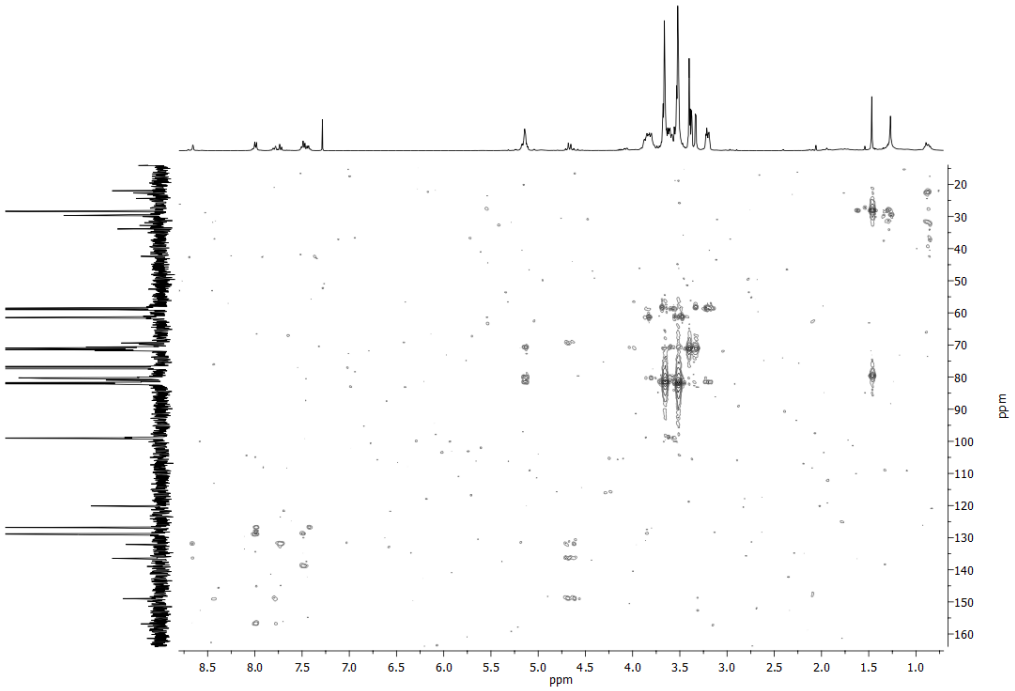


**Figure 4.A14.** HMBC spectrum of **ppy-CD (13)** in $CDCl_3$.

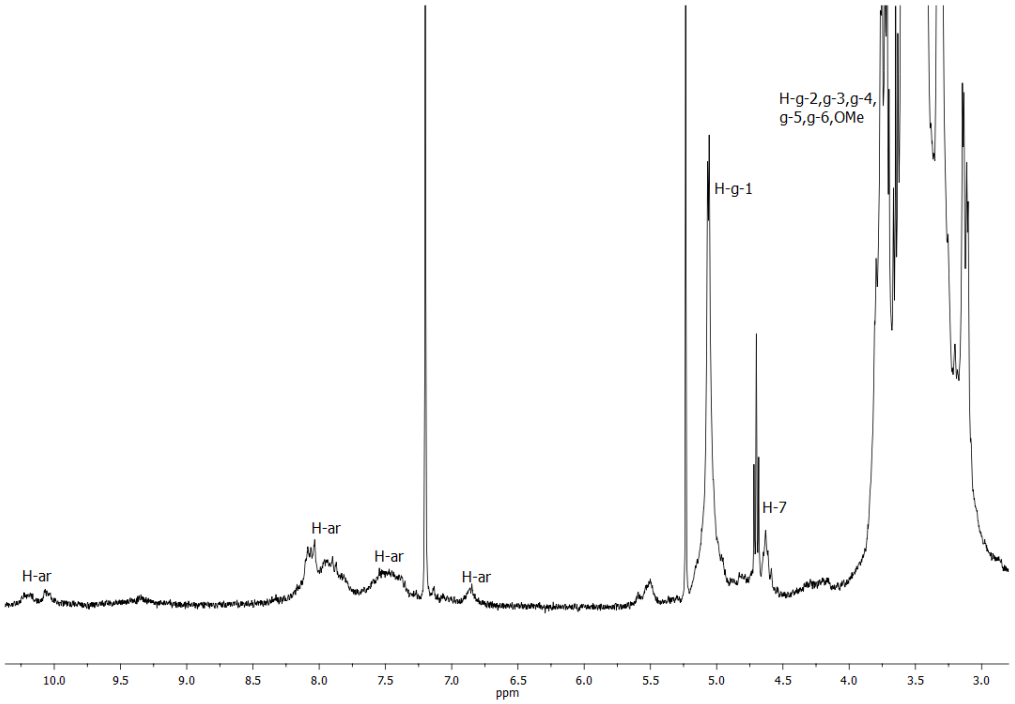


**Figure 4.A15.** $^1$H NMR spectrum of **$Ru(bpy\text{-}CD)_2Cl_2$ (14)** in $CDCl_3$

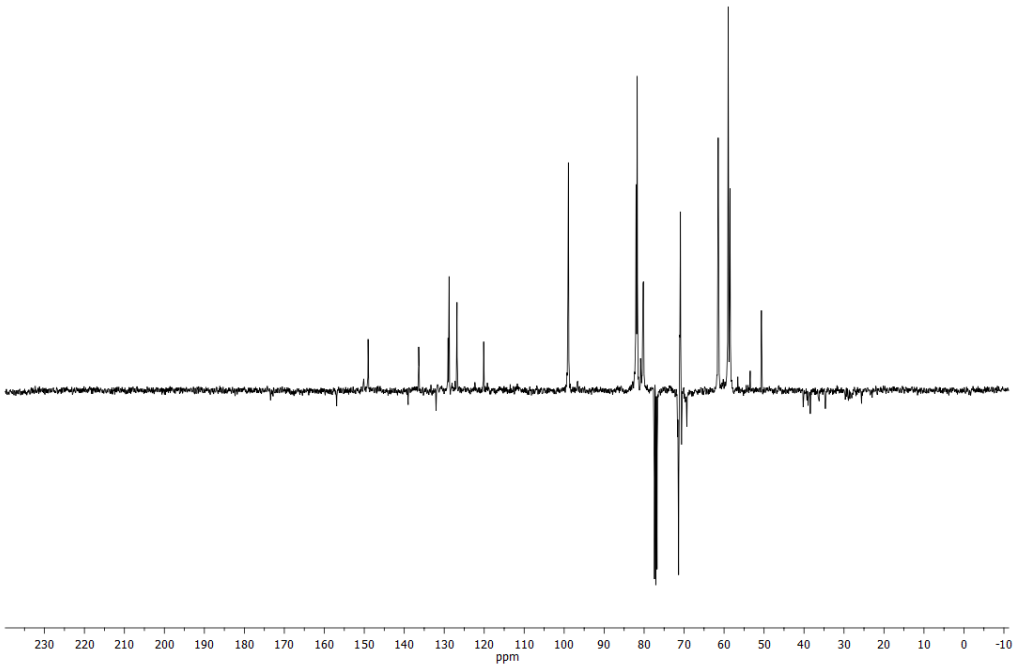


**Figure 4.A16.** $^{13}C$ NMR spectrum of **Ir(ppy-CD)$_2$(bpySS) (17)** in $CDCl_3$.

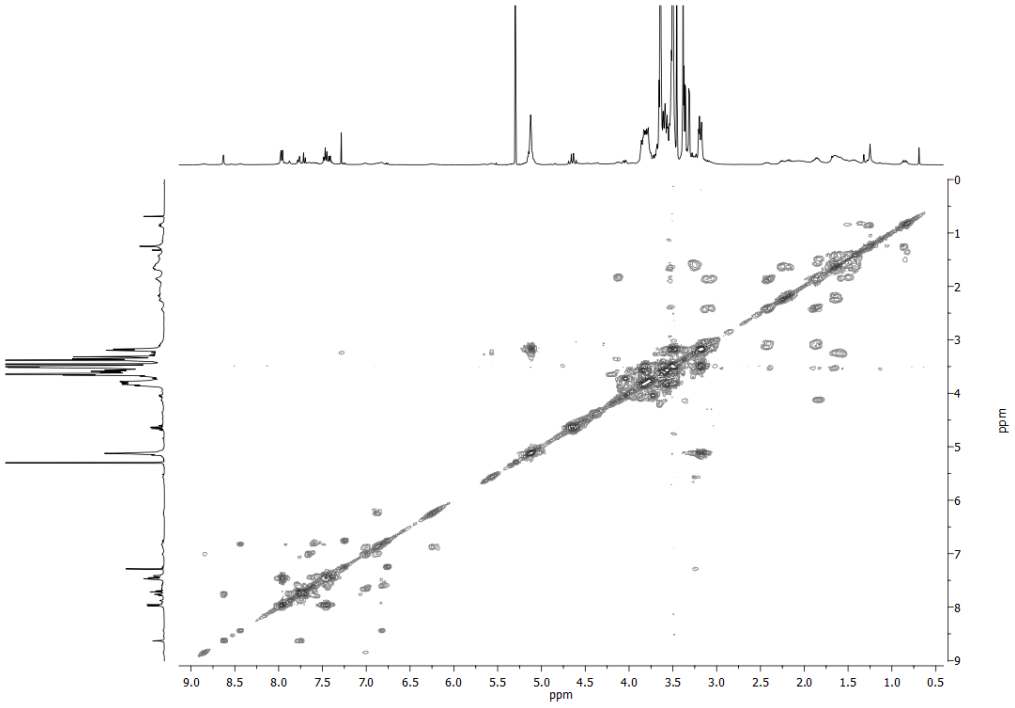


**Figure 4.A17.** COSY spectrum of **Ir(ppy-CD)$_2$(bpySS) (17)** in $CDCl_3$.

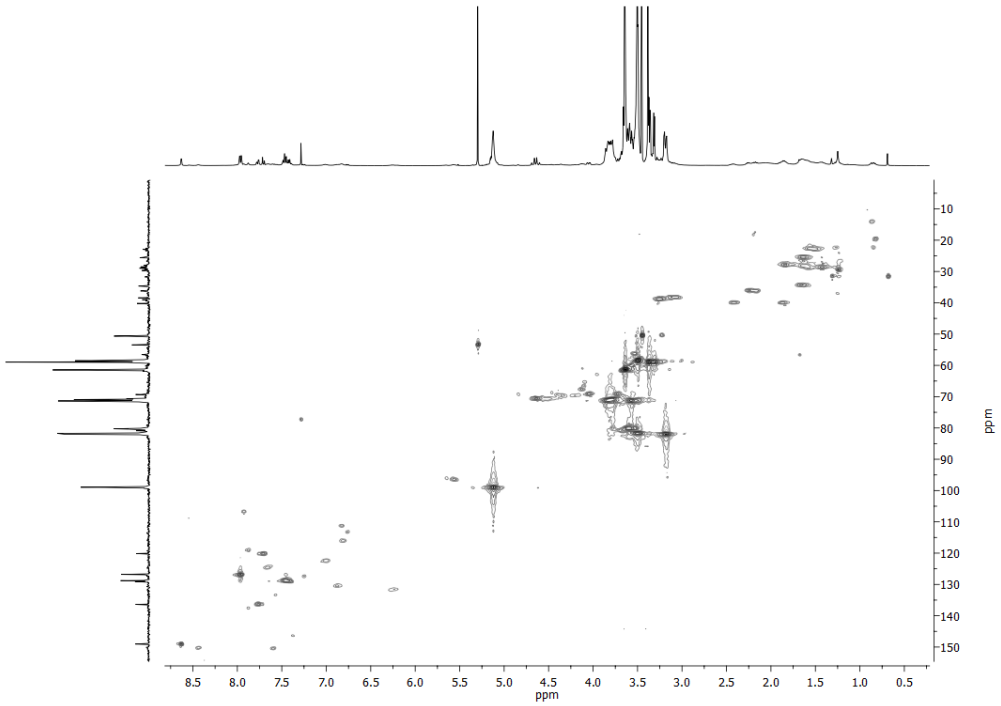


**Figure 4.A18.** HSQC spectrum of **Ir(ppy-CD)$_2$(bpySS) (17)** in $CDCl_3$.

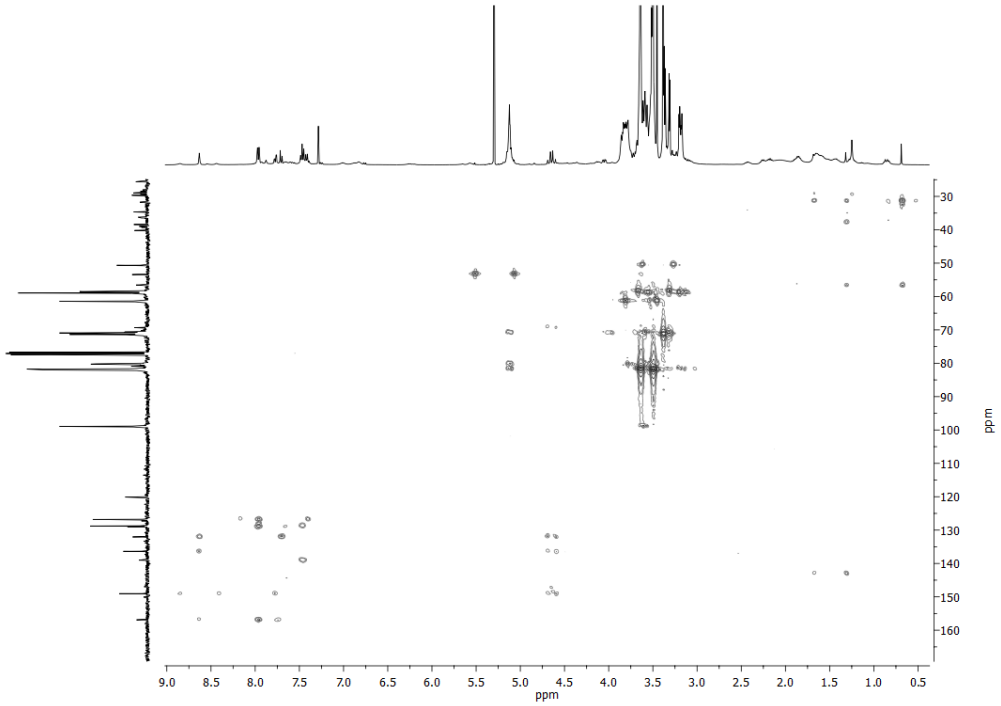


**Figure 4.A19.** HMBC spectrum of **Ir(ppy-CD)$_2$(bpySS) (18)** in $CDCl_3$.

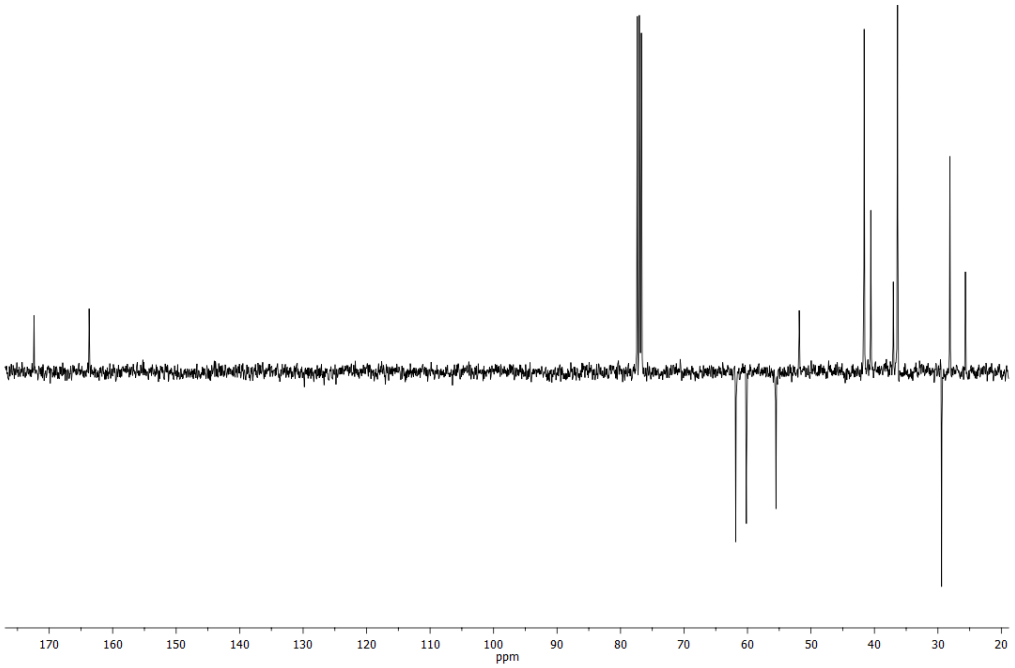


**Figure 4.A20.** $^{13}C$ NMR spectrum of **Ad-Biotin (18)** in $CDCl_3$.

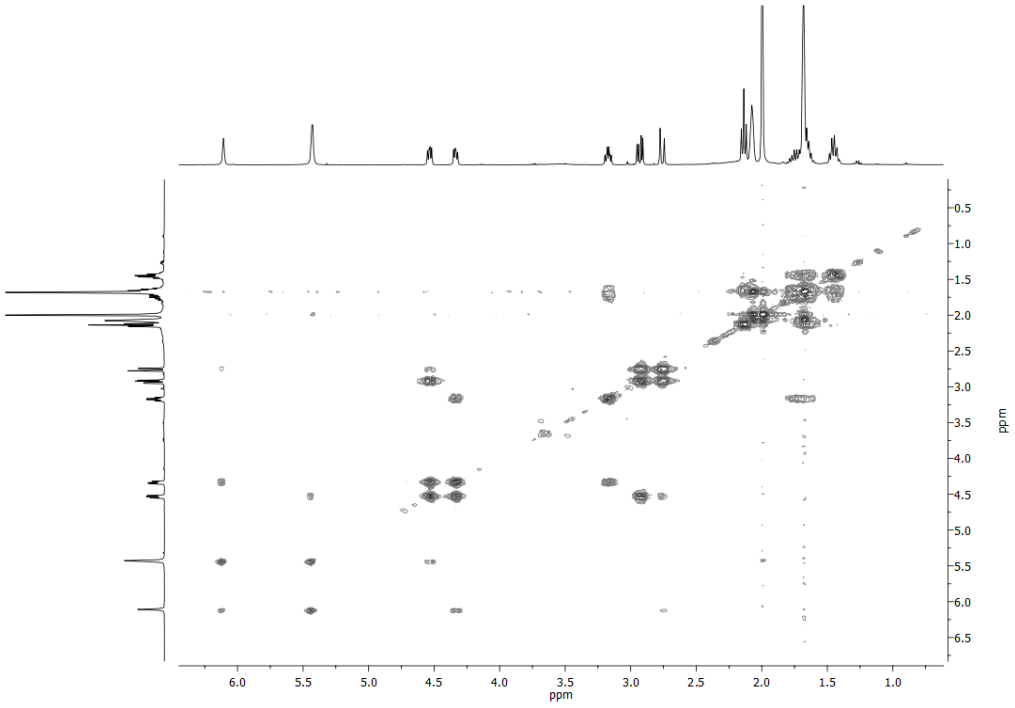


**Figure 4.A21.** COSY spectrum of **Ad-Biotin (18)** in $CDCl_3$.

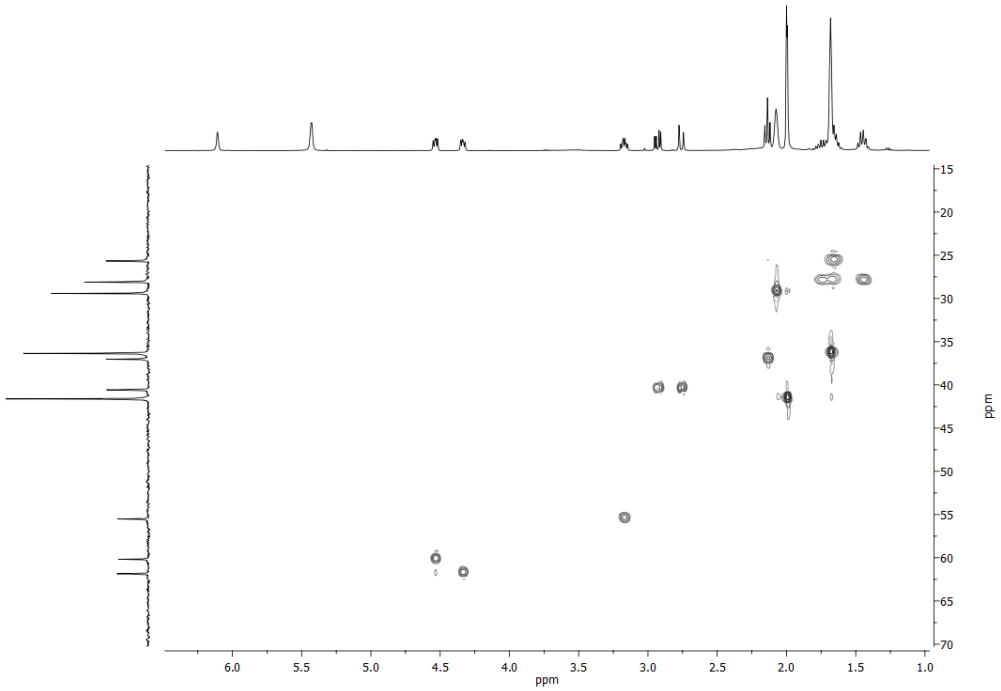


**Figure 4.A22.** HSQC spectrum of **Ad-Biotin (18)** in $CDCl_3$.

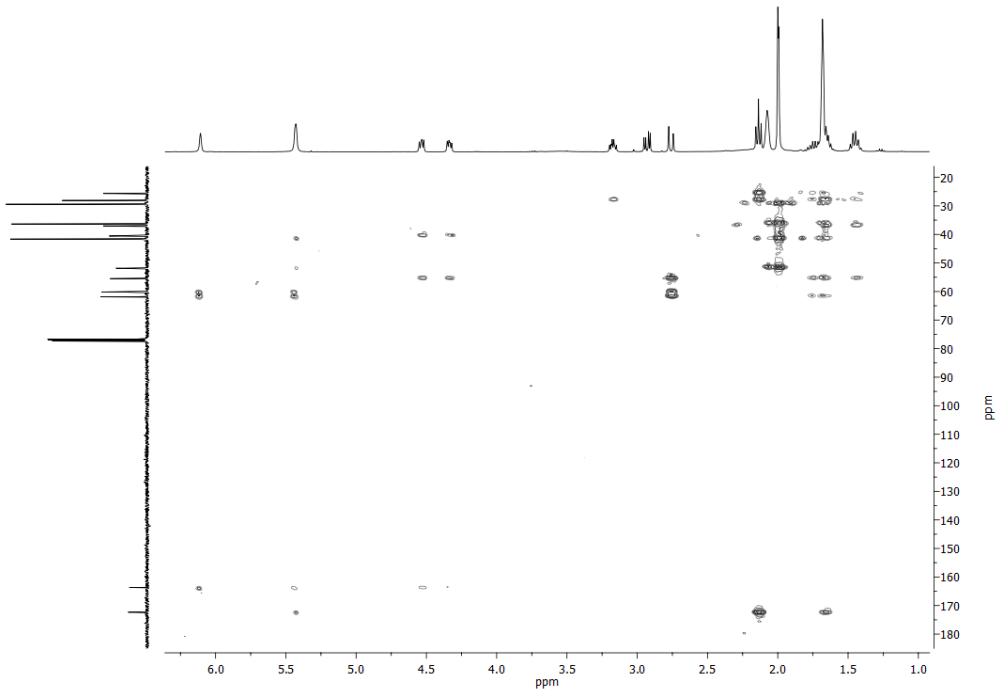


**Figure 4.A23.** HMBC spectrum of **Ad-Biotin (18)** in $CDCl_3$.

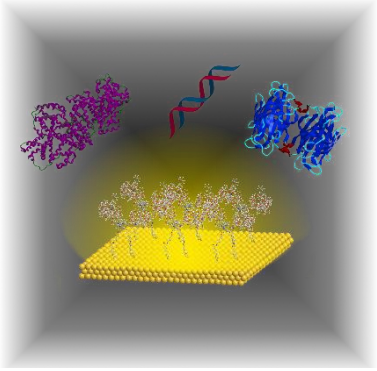

# Chapter Five

## General Conclusions

In this thesis the use of transition metal complexes as architectures for sensing at surfaces has been explored. Through the use of saturated long chain surface-active ligands, the luminescence quenching on metal surfaces associated with other metal complexes is mitigated, and for all ruthenium(II) and iridium(III) complexes reported, an enhancement of luminescence lifetime on gold surfaces is recorded compared with aerated solution. Through this, it has been shown that transition metal complexes offer a desirable platform for luminescent sensing devices across the visible spectrum, with greater longevity than their organic counterparts due to the inherent photostability and longer luminescence lifetimes afforded by luminescent transition metal complexes.

The design of metal complexes to incorporate cyclodextrin moieties has allowed the creation of metal complexes capable of facile directed assembly at surfaces through supramolecular linkages, increasing the scope and application for potential optical or optoelectronic device formation. Cyclodextrin containing transition metal complexes also afford a luminescent architecture that can, through supramolecular chemistry, allow multimodal sensing platforms to be constructed. Through careful choice of guest for the cyclodextrin moiety, and binding site for an analyte of choice, a selective, non-chemically bound sensing platform can be achieved. Indeed, through SPR spectroscopy this has been achieved for the selective recognition of streptavidin utilising such a sensing platform.

The scope of this system affords the possibility of reusability and a broad spectrum of potential sensing motifs, thus future work will invariably be focused on the improvement of these systems to allow total reusability through washing of the surfaces to leave only the metal complex. Sequential sensing experiments will also be valuable in order to examine the cycling ability of the platform, and its ability to sense for more than one analyte, with a view to creating a ‘one-size-fits-all’ multimodal sensor capable of detecting changes through SPR response,

luminescence lifetime and emission maxima. In order to achieve this, potential improvements to the surface coverage of the transition metal complexes will need to be examined and evaluated, such as stepwise assembly of the complex through simpler organic monolayers and chemical reactions at the interface. Improvements to the supramolecular architecture will also need to be considered, in order to ensure that supramolecular linkages can be made efficiently. The examination of the monolayers through surface techniques such as infrared spectroscopy and also modelling to determine the orientation of the tori of the cyclodextrin would also be beneficial.

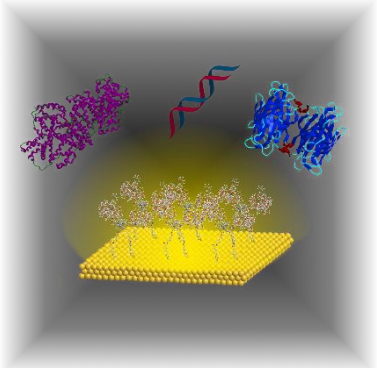

# Chapter Six

## General Experimental

# 6.1 Materials and Methods

Starting materials were obtained from Sigma Aldrich, Fluka, Fisher Scientific or Acros Chemicals and used without any further purification. DMF was obtained from AGTC Bioproducts Ltd. or Sigma Aldrich and dried with 3 or 4 Å molecular sieves for at least 24 hours before use. Gold substrates (30 nm on silicon with 5 nm Ti priming layer) were purchased from Georg Albert PVD, Germany. A Sylgard 184 elastomer kit (Dow-Corning) was used to create polydimethoxysiloxane (PDMS) stamps. Flash column chromatography was performed using silica gel LC60A (particle size 40-63 µm) purchased from FluoroChem or neutral alumina (activated, Brockmann I) purchased from Sigma Aldrich. Automated flash column chromatography was performed using either a Biotage Flash 40 system using Biotage SNAP silica cartridges or a Grace Scientific Reveleris X2 flash purification system using Reveleris flash cartridges. Deionised water was obtained using an Elga 3 Option water purifier, ultrapure water was obtained using a Millipore Milli-Q Integral Water Purification System. $Ru(bpy)_2Cl_2$ was synthesised *via* a method outlined by Pikramenou and Rogers,[1] $Os(bpy)_2Cl_2$ was synthesised *via* the method outlined by Kober *et al.*,[2] $[Ir(ppy)_2Cl]_2$ was synthesised *via* the method outlined by Sprouse *et al.*[3]

$^1H$ NMR spectroscopy was carried out on a Brüker AVIII300 spectrometer or a Brüker DRX500 spectrometer where stated. $^{13}C$ and 2D NMR spectroscopy were carried out on a Brüker AVIII400 spectrometer. Electrospray mass spectrometry was carried out on a Micromass LC-TOF. MALDI mass spectrometry was carried out for some of the cyclodextrin containing compounds (chapters two and three) on a Micromass MX MALDI-TOF. UV−vis spectroscopy was carried out on a Varian Cary 50 or Cary 5000 spectrophotometer. UV−vis spectra were collected using 1 cm path length quartz cuvettes. Luminescence spectroscopy was carried out on an Edinburgh Instruments FLS920 steady state and time-resolved spectrometer fitted with

an Olympus IX71 inverted microscope. The detection system used incorporated R928 (visible) and R5509-72 (NIR) Hamamatsu photomultiplier tubes. The emission monochromator is fitted with two interchangeable gratings blazed at 500 and 1200 nm. F900 spectrometer analysis software was used to record the data. Luminescence lifetime experiments were carried out using an Edinburgh Instruments EPL-445 or EPL-375 laser as the excitation source. Lifetimes were fitted using Edinburgh Instruments F900 or FAST software, with errors of ±10%. Luminescence experiments were carried out using 1 cm path length quartz cuvettes with four transparent polished faces. Degassed samples were obtained by bubbling nitrogen through the cuvettes for 30−40 min. Circular dichroism experiments (chapter two) were carried out on a Jasco J-810 spectropolarimeter using 1 cm path length quartz cuvettes. Surface plasmon resonance studies were carried out on a Reichert SR7500DC surface plasmon resonance (SPR) system at 15 °C. Microwave reactions were performed in a CEM Discovery SP Microwave under open vessel conditions unless otherwise stated. Ellipsometry measurements were taken using a Jobin-Yvon UVISEL ellipsometer with a He-Ne laser light source at a controlled angle of incidence of 70 °C using a wavelength range of 280–800 nm. Layer thicknesses were calculated using the Drude model using collected blank gold data as the background. A minimum of three measurements were taken per substrate and the average value stated.

## 6.2 General Surface Studies

Gold substrates (30 nm on silicon) were cleaned by UVO cleaner (1 hour) and immersed in the applicable solvent for at least 10 minutes before use.

Slides were immersed in a *ca.* 1 mM solution of compound in applicable solvent and sealed from the outside atmosphere to prevent solvent evaporation. The slides were left immersed for a stipulated amount of time, before immersion in clean solvent, and dried under $N_2$.

For micropatterning, gold slides were cleaned by the general method described above. Stamps were made as per the method outlined by Kumar *et al.*[4] from PDMS (Dow Corning). PDMS:PDMS curing agent (9:1) were mixed for 10 minutes and poured onto silicon masters. The mixture was allowed to cure at room temperature for 1 hour, and the bubbles that formed on the top of the mixture were popped. The mixture was then cured in the oven at 60 °C for 1 hour. The PDMS stamps were peeled away from the masters and cut into shape. The stamps were inked by immersing the stamps in a 1-10 mM solution of compound in applicable solvent for 20 minutes, before removing and carefully drawing away any excess liquid from the stamp with a tissue. The stamps were placed firmly on the clean gold slides and left with a small weight (ca. 30 g) on top of the stamp (unless otherwise stated) for an allotted time before peeling the stamp away to leave the micropatterned surface. The slides were then washed by immersion in clean solvent and dried under $N_2$.

## 6.3 SPR Studies

Gold substrates (50 nm on glass, Reichert) were cleaned in Piranha solution (CARE! Piranha solution reacts violently with organic material) for 10 minutes, before washing with ultrapure water and storage in ethanol until use. Before use, the substrates were dried in nitrogen stream. Two general methods of data collection were employed:

**Method 1.** Substrates were equilibrated in the instrument at a flow rate of 50 µL $min^{-1}$ for 10 minutes. The sample was then injected over the substrate at a rate of 1500 µL $min^{-1}$ for 10 seconds, before reducing the flow rate to 10 µL $min^{-1}$ for 30 minutes to allow binding to occur. After this time, the substrates were washed with clean solvent at a rate of 1500 µL $min^{-1}$ for 2 minutes, followed by a further wash period of 10 minutes at 50 µL $min^{-1}$.

**Method 2.** Substrates were equilibrated in the instrument at a flow rate of 50 µL $min^{-1}$ for 10 minutes. The sample was then injected at a flow rate of 50 µL $min^{-1}$ for 30 minutes, followed by washing the substrate at a flow rate of 50 µL $min^{-1}$ for 10 minutes.

After data collection the units of data were converted from µRIU units to degrees as per studies outlined by Whitesides and coworkers.[5] Biomolecule surfaces concentrations were estimated as per the study outlined by Urbanickzy and colleagues.[6]

# 6.4 Acknowledgements

With thanks to Dr. Jon Faiz for the provision of **Osbiptpy**. Thanks to Dr Neil Spencer and Peter Ashton for assistance with obtaining NMR and mass spectral data and discussions of results.

Some of the spectrometers used in this research were obtained, through Birmingham Science City: Innovative Uses for Advanced Materials in the Modern World (West Midlands Centre for Advanced Materials Project 2), with support from Advantage West Midlands (AWM) and part funded by the European Regional Development Fund (ERDF).

# 6.5 References

1. Z. Pikramenou and N. J. Rogers, WO2013004989 A1, 2013.
2. E. M. Kober, J. V. Caspar, P. B. Sullivan and T. J. Meyer, *Inorg. Chem.*, 1988, **27**, 4587-4598.
3. S. Sprouse, K. A. King, P. J. Spellane and R. J. Watts, *J. Am. Chem. Soc.*, 1984, **106**, 6647-6653.
4. A. Kumar, H. A. Biebuyck and G. M. Whitesides, *Langmuir*, 1994, **10**, 1498-1511.
5. J. Lahiri, L. Isaacs, J. Tien and G. M. Whitesides, *Anal. Chem.*, 1999, **71**, 777-790.
6. E. Stenberg, B. Persson, H. Roos and C. Urbaniczky, *J. Colloid Interf. Sci.*, 1990, **143**, 513-526.